Georgia Water Resources Institute
Annual Technical Report
FY 2011

Introduction

INTRODUCTION The Georgia Water Resources Institute (GWRI) aims to provide interdisciplinary research, education, technology transfer, and information dissemination, and works collaboratively with various local, state, and federal agencies. At the state and local levels, GWRI collaborates with and supports the Georgia Environmental Protection Division/Georgia Department of Natural Resources, water and power utilities, environmental organizations and citizen groups, and lake associations. At the national level, GWRI has collaborative efforts with the California Energy Commission, California Department of Water Resources, National Oceanic and Atmospheric Administration, U.S. Army Corps of Engineers, U.S. Bureau of Reclamation, U.S. Geological Survey, and the U.S. Environmental Protection Agency. Finally, GWRI has significant international involvement in China, Africa, and Europe with support from the U.S. Agency for International Development, World Bank, Food and Agriculture Organization of the United Nations, and other international organizations. In all initiatives, the Institute strives to bring to bear expertise from a variety of disciplines, including civil and environmental engineering, atmospheric sciences, agriculture, oceanography, forestry, ecology, economics, and public policy.

This year's funded activities include:

RESEARCH PROJECTS

(1) Multi-Scale Investigation of Seawater Intrusion and Application in Coastal Georgia, Jian Luo PI, Georgia Institute of Technology, sponsored by USGS under grant # 2006P17 (Fund #R9261).

(2) Flood Risk and Homeowners' Flood Risk Perceptions: Evidence from Property Prices in Georgia" USGS 104B/GWRI Project, Susanna Ferriera # 2011GA275B #1266663

(3) Impact of Upstream Water Use on Salinity and Ecology of Apalachicola Bay, Beatriz Villegas and Philip J. W. Roberts, sponsored by USGS under grant #1266663 (Fund R7113).

(4) Assessment of Endocrine Disruption in Fish and Estrogenic Potency of Waters in Georgia, Robert Bringolf, University of Georgia, sponsored by USGS under grant #1266663 (Fund R7113).

(5) Integrated Forecast and Reservoir Management (INFORM) for Northern California, Phase II: Operational Implementation, Aris Georgakakos PI, Georgia Institute of Technology, sponsored by California-Nevada River Forecast Center, California Department of Water Resources, California Energy Commission under grant #2006Q15.

(6) Upstream Regulation (INFORM) for Northern California, Aris Georgakakos PI, Georgia Institute of Technology, sponsored by California-Nevada River Forecast Center, California Department of Water Resources, California Energy Commission under grant #2006S61.

(7) Climate Change Scenario Assessment for ACF, OOA, SO, ACT, TN, and OSSS Basins in Georgia, Aris Georgakakos PI, Georgia Institute of Technology, sponsored by Georgia Department of Natural Resources/ Environmental Protection Division under grant #2006R69.

EDUCATIONAL INITIATIVES

GWRI is developing a graduate level water resources network in Africa. This year’s efforts concentrated in Kenya. Discussions are on-going with the Jomo Kenyata University for Agricultural Technology (JKUAT) for the establishment of a joint Master’s degree program.

PROFESSIONAL AND POLICY IMPACT

Georgia: GWRI continues to provide technical assistance to the Georgia Department of Natural Resources in relation to the state water planning process. The emphasis this year was on climate change assessments. GWRI performed comprehensive assessments for all major Georgia Basins. The results indicate that droughts will most likely intensify having serious implications on water supply, energy generation, and ecological flows. As part of this study, GWRI developed and made available to Georgia DNR multi-ensemble sequences of unimpaired flows at more than 25 key locations in Georgia. The study findings and this information is now being considered as part of the state water resources planning. California: Similar work, collaboratively with the Hydrologic Research Center in San Diego, has focused on climate change impacts on the Northern California water resources system (including the Sacramento and San Joaquin River basins). While the nature of the changes is different, due to hydrologic significance of snow melt, the findings are equally important regarding the need for mitigation and adaptation measures. With funding from the California Energy Commission and the Department of Water Resources, GWRI and HRC have just initiated a second project phase which aims at finalizing and transferring the forecast-decision tools and evaluating alternative climate and demand change mitigation measures. US: GWRI is involved in the on-going National Climate Assessment (NCA), and is leading the development of the Water Sector Chapter. In addition, GWRI made several contributions to the NCA:

(1) Federal Agency Water Resources Sector Technical Input in Support of the US Global Change Research Program, 2012 National Climate Assessment, 2013.

(2) Southeast Water Resources Sector Technical Input to the National Climate Assessment, 2012.

(3) Georgakakos, K.P., Graham, N.H., Cheng, F.-Y., Spencer, C., Shamir, E., Georgakakos, A.P, Yao, H., and Kistenmacher, M., "Value of Adaptive Water Resources Management in Northern California under Climatic Variability and Change: Dynamic Hydroclimatology," J. Hydrology, in press, on line reference doi:10.1016/j.jhydrol.2011.04.032, 2011.

(4) Georgakakos, A.P, Yao, H., Kistenmacher, M., Georgakakos, K.P., Graham, N.H., Cheng, F.-Y., Spencer, C., Shamir, E., "Value of Adaptive Water Resources Management in Northern California under Climatic Variability and Change: Reservoir Management," J. Hydrology, in press, on line reference doi:10.1016/j.jhydrol.2011.04.038, 2011.

(5) Zhang, F. and A. P. Georgakakos, "Joint Variable Spatial Downscaling," Climatic Change, in press, on line reference doi.org/10.1007/s10584-011-0167-9, 2011.

(6) Georgakakos, A., F. Zhang, and H. Yao, (2010). Climate Variability and Change Assessment for the ACF River Basin, Southeast US. Georgia Water Resources Institute (GWRI) Technical Report sponsored by NOAA, USGS, and Georgia EPD, Georgia Institute of Technology, Atlanta, Georgia, 321 pp. (7) Georgakakos, A. and F. Zhang, (2011a): Climate Change Scenario Assessment for ACF, OOA, SO, ACT, TN, and OSSS Basins in Georgia. Georgia Water Resources Institute (GWRI) Technical Report sponsored by NOAA, USGS, and the Georgia EPD; Georgia Institute of Technology, Atlanta, Georgia, USA, 229 pp.

CONFERENCE ORGANIZATION AND TECHNOLOGY TRANSFER

GWRI helped co-organize and co-chair the Georgia Water Resources Conference, University of Georgia, Athens, Georgia, 12-13 April 2011. GWRI also organized a session in the American Geophysical Union Meeting in San Francisco, California, on the "Hydro-climatic Forecasts and Real-Time Operation of Water Resources Systems," 5-9 December 2011.

Journal Publications 1. Lu, C., Du, P., Chen, Y., Luo, J. (2011), Recovery efficiency of aquifer storage and recovery (ASR) with mass transfer limitation, Water Resour. Res.,47, W08529, doi:10.1029/2011WR010605.

2. Lu, C., Luo, J. (2012), Boundary condition effects on estimating maximum groundwater withdrawal in coastal aquifers, Ground Water, in press.

3. Chen, Y., Lu, C., Luo, J. (2012), Solute transport in transient divergent flow, Water Resour. Res., 48, W02510, doi:10.1029/2011WR010692.

4. Lu, C., Chen, Y., Zhang, C., Luo, J. (2012), Freshwater-seawater mixing zone in stratified coastal aquifers, Water Resour. Res., submitted.

5. Atreya, A., S. Ferreira and W. Kriesel (2012) "Forgetting the Flood? Changes in Flood risk Perceptions over Time",University of Georgia, Athens, GA. Presented at UGA Department of Agricultural and Applied Economics Seminar Series, Athens, August 17, 2011.

6. Atreya, A., S. Ferreira and W. Kriesel (2012) "Forgetting the Flood? Changes in Flood risk Perceptions over Time",University of Georgia, Athens, GA. Presented at UNICT- EAERE- FEEM Belpasso International Summer School on Environmental and Resource Economics, Belpasso, Sicily, Italy, Sept 4-10, 2011.

7. Atreya, A. and S. Ferreira (2012) "Analysis of Spatial Variation in Flood Risk Perception" Presented at UGA Department of Agricultural and Applied Economics Seminar Series, Athens, January 18, 2012.

8. Atreya, A. and S. Ferreira (2011) "Flood Risk and Risk Perception: Evidence from Property Prices in Fulton County, Georgia" Presented at CIMR- Climate Information for Managing Risk, Local to Regional Adaptation and Mitigation Strategies, An International Symposium, Orlando Florida, May 24-27, 2011.

9. Atreya, A. and S. Ferreira (2012) "Variation in Flood Risk Perception: Does Scale Matter?" Presented at ICARUS- Initiative on Climate Adaptation Research and Understanding through the Social Sciences, Columbia University, New York, May 18-20, 2012.

10. Atreya, A. and S. Ferreira (2012) "Spatial Variation in Flood Risk Perception: A Spatial Econometric Approach" To be presented Agricultural and Applied Economics Association 2012 Annual Meeting, Seattle, Washington, August 12-14, 2012.

11. Atreya, A., S. Ferreira and W. Kriesel (2012) "Forgetting the Flood? Changes in Flood risk Perceptions over Time" Submitted to Land Economics.Kellock, K., B. Trushel, P. Ely, C. Jennings and R.B. Bringolf. High rate of intersex in bass from small impoundments. Journal of Aquatic Animal Health: to be submitted June 2012.

12. Kellock, K. and R.B. Bringolf. 2011. Assessment of endocrine disruption in fish and estrogenic potency of waters in Georgia. Proceedings of the 2011 Georgia Water Resources Conference, Athens, GA, April 11–13, 2011.

13. Intersex fish in small impoundments: why won't the boys be boys? Iowa State University, Department of Natural Resource Ecology and Management. Ames, IA. May 4, 2012.

14. Intersex fish in Georgia. University of Georgia Fisheries Society. Athens, GA. February 16, 2012.

15. A survey of intersex bass in Georgia: Serendipity strikes again? University of Georgia, Warnell School of Forestry & Natural Resources. Athens, GA. September 22, 2011.

16. Intersex fish: not just in Wastewater anymore. Auburn University, Department of Fisheries and Allied Aquaculture. Auburn, AL. September 16, 2011.

17. K. Kellock, C. Jennings, P. Ely, B. Trushel, and R.B. Bringolf. Intersex fish: Not just in wastewater anymore. Presented at the 2012 Southeast Regional Chapter of the Society of Environmental Toxicology and Chemistry. Pensacoala, FL. Mar. 16-17, 2012.

18. Kellock, K.A., C.A. Jennings, P. Ely, B. Trushel, and R.B. Bringolf. Intersex fish influenced by factors other than municipal wastewater effluent. Presented at the 2012 annual meeting of the Georgia Chapter of the American Fisheries Society. Macon, GA. Feb. 7-9, 2012.

19. Bringolf, R.B., K. Kellock, B. Trushel, P. Ely, and C. Jennings. Intersex fish: Not just in wastewater anymore. Presented at the 2012 annual meeting of the Southern Division of American Fisheries Society. Biloxi, MS. Jan. 26-29, 2012.

20. Kellock, K. and R.B. Bringolf. Intersex fish influenced by factors other than municipal wastewater effluent. Presented at the 2011 Society of Environmental Toxicology and Chemistry North America Meeting. Boston, MA. Nov. 7-12, 2011.

21. Kellock, K. and R.B. Bringolf. Assessment of endocrine disruption in fish and estrogenic potency of waters in Georgia. Presented at the 2011 Georgia Water Resources Conference, Athens, GA, April 11–13, 2011. Awarded Best Student Presentation.

22. Bringolf, R.B., K. Kellock, B. Trushel, P. Ely and C. Jennings. Survey of intersex bass and estrogens in GA waters. Presented at the 2011 Meeting of the Georgia Chapter of the American Fisheries Society. Perry, GA. Feb. 2-3, 2011.

23. Georgakakos, K.P., Graham, N.H., Cheng, F.-Y., Spencer, C., Shamir, E., Georgakakos, A.P, Yao, H., and Kistenmacher, M., "Value of Adaptive Water Resources Management in Northern California under Climatic Variability and Change: Dynamic Hydroclimatology," J. Hydrology, in press, on line reference doi:10.1016/j.jhydrol.2011.04.032, 2011.

24. Georgakakos, A.P, Yao, H., Kistenmacher, M., Georgakakos, K.P., Graham, N.H., Cheng, F.-Y., Spencer, C., Shamir, E., "Value of Adaptive Water Resources Management in Northern California under Climatic Variability and Change: Reservoir Management," J. Hydrology, in press, on line reference doi:10.1016/j.jhydrol.2011.04.038, 2011.

25. Zhang, F. and A. P. Georgakakos, "Joint Variable Spatial Downscaling," Climatic Change, in press, on line reference doi.org/10.1007/s10584-011-0167-9, 2011.

Research Program Introduction

None.

Multi-Scale Investigation of Seawater Intrusion and Application in Coastal Georgia

Basic Information

Title:	Multi-Scale Investigation of Seawater Intrusion and Application in Coastal Georgia
Project Number:	2007GA165G
Start Date:	4/1/2008
End Date:	9/30/2011
Funding Source:	104G
Congressional District:	5th
Research Category:	Ground-water Flow and Transport
Focus Category:	Groundwater, Hydrology, Models
Descriptors:	
Principal Investigators:	Jian Luo, Jian Luo

Publications

1. Lu, C., Kitanidis, P.K., Luo, J. (2009), Effects of kinetic mass transfer and transient flow conditions on widening mixing zones in coastal aquifers, Water Resour. Res., 45, W12402, doi:10.1029/2008WR007643.
2. Lu, C., Gong, R., Luo, J. (2009), Analysis of stagnation points for a pumping well in recharge areas, J. Hydrol., 373, 442-452.
3. Lu, C., Luo, J. (2010), Boundary condition effects on estimating maximum groundwater withdrawal in coastal aquifers, J. Hydrol., submitted.
4. Lu, C., Luo, J. (2010), Dynamics of freshwater-seawater mixing zone development in dual-domain formations, Water Resour. Res., submitted.
5. Lu, C., Kitanidis, P.K., Luo, J., Mixing enhanced by kinetic mass transfer and dynamic forces in coastal aquifers, Eos Trans. AGU, 90(52), Fall Meet. Suppl., Abstract H32C-05, San Francisco, CA, Dec. 14-18, 2009
6. Lu, C., Kitanidis, P.K., Luo, J. (2009), Effects of kinetic mass transfer and transient flow conditions on widening mixing zones in coastal aquifers, Water Resour. Res., 45, W12402, doi:10.1029/2008WR007643.
7. Lu, C., Gong, R., Luo, J. (2009), Analysis of stagnation points for a pumping well in recharge areas, J. Hydrol., 373, 442-452.
8. Lu, C., Luo, J. (2010), Boundary condition effects on estimating maximum groundwater withdrawal in coastal aquifers, J. Hydrol., submitted.
9. Lu, C., Luo, J. (2010), Dynamics of freshwater-seawater mixing zone development in dual-domain formations, Water Resour. Res., submitted.
10. Lu, C., Kitanidis, P.K., Luo, J., Mixing enhanced by kinetic mass transfer and dynamic forces in coastal aquifers, Eos Trans. AGU, 90(52), Fall Meet. Suppl., Abstract H32C-05, San Francisco, CA, Dec. 14-18, 2009
11. Lu, C., Du, P., Chen, Y., Luo, J. (2011). Recovery Efficiency of Aquifer Storage and Recovery (ASR) with Mass Transfer Limitation, Water Resources Res., (in revision)
12. Chen, Y., Lu, C., Luo, J. (2011). Solute Transport in Transient Divergent Flow, Water Resources Res., (in review).
13. Lu, C., Luo, J., Effects of Aquifer Stratification on Freshwater-Seawater Mixing-Zone Development, EOS Trans., AGU, Fall Meet. Suppl., Abstract H43A-1206, San Francisco, CA, Dec. 13-17, 2010.

14. Lu, C., Kitanidis, P.K., Luo, J. (2009), Effects of kinetic mass transfer and transient flow conditions on widening mixing zones in coastal aquifers, Water Resour. Res., 45, W12402, doi:10.1029/2008WR007643.
15. Lu, C., Gong, R., Luo, J. (2009), Analysis of stagnation points for a pumping well in recharge areas, J. Hydrol., 373, 442-452.
16. Lu, C., Luo, J. (2010), Boundary condition effects on estimating maximum groundwater withdrawal in coastal aquifers, J. Hydrol., submitted.
17. Lu, C., Luo, J. (2010), Dynamics of freshwater-seawater mixing zone development in dual-domain formations, Water Resour. Res., submitted.
18. Lu, C., Kitanidis, P.K., Luo, J., Mixing enhanced by kinetic mass transfer and dynamic forces in coastal aquifers, Eos Trans. AGU, 90(52), Fall Meet. Suppl., Abstract H32C-05, San Francisco, CA, Dec. 14-18, 2009
19. Lu, C., Du, P., Chen, Y., Luo, J. (2011). Recovery Efficiency of Aquifer Storage and Recovery (ASR) with Mass Transfer Limitation, Water Resources Res., (in revision)
20. Chen, Y., Lu, C., Luo, J. (2011). Solute Transport in Transient Divergent Flow, Water Resources Res., (in review).
21. Lu, C., Luo, J., Effects of Aquifer Stratification on Freshwater-Seawater Mixing-Zone Development, EOS Trans., AGU, Fall Meet. Suppl., Abstract H43A-1206, San Francisco, CA, Dec. 13-17, 2010.
22. Lu, C., Luo, J. (2010), Dynamics of freshwater-seawater mixing zone development in dual-domain formations, Water Resour. Res., 46, W11601, doi:10.1029/2010WR009344.
23. Lu, C., Du, P., Chen, Y., Luo, J. (2011), Recovery efficiency of aquifer storage and recovery (ASR) with mass transfer limitation, Water Resour. Res.,47, W08529, doi:10.1029/2011WR010605..
24. Lu, C., Luo, J. (2012), Boundary condition effects on estimating maximum groundwater withdrawal in coastal aquifers, Ground Water, in press.
25. Chen, Y., Lu, C., Luo, J. (2012), Solute transport in transient divergent flow, Water Resour. Res., 48, W02510, doi:10.1029/2011WR010692.
26. Lu, C., Chen, Y., Zhang, C., Luo, J. (2012), Freshwater-seawater mixing zone in stratified coastal aquifers, Water Resour. Res., submitted.

Report for 2007GA165G: " Multi-Scale Investigation of Seawater Intrusion and Application in Coastal Georgia"

Students Supported

Lu, Chunhui, Ph.D., degree earned Apr. 2011.
Yiming Chen, Ph.D. student

Journal Publications

Lu, C., Kitanidis, P.K., Luo, J. (2009), Effects of kinetic mass transfer and transient flow conditions on widening mixing zones in coastal aquifers, *Water Resour. Res.*, 45, W12402, doi:10.1029/2008WR007643.

Lu, C., Gong, R., Luo, J. (2009), Analysis of stagnation points for a pumping well in recharge areas, *J. Hydrol.*, 373, 442-452.

Lu, C., Luo, J. (2010), Dynamics of freshwater-seawater mixing zone development in dual-domain formations, *Water Resour. Res.*, 46, W11601, doi:10.1029/2010WR009344.

Lu, C., Du, P., Chen, Y., Luo, J. (2011), Recovery efficiency of aquifer storage and recovery (ASR) with mass transfer limitation, *Water Resour. Res.*,47, W08529, doi:10.1029/2011WR010605..

Lu, C., Luo, J. (2012), Boundary condition effects on estimating maximum groundwater withdrawal in coastal aquifers, *Ground Water*, in press.

Chen, Y., Lu, C., Luo, J. (2012), Solute transport in transient divergent flow, *Water Resour. Res.*, 48, W02510, doi:10.1029/2011WR010692.

Lu, C., Chen, Y., Zhang, C., Luo, J. (2012), Freshwater-seawater mixing zone in stratified coastal aquifers, *Water Resour. Res.*, submitted.

Conference

Lu, C., Kitanidis, P.K., Luo, J., Mixing enhanced by kinetic mass transfer and dynamic forces in coastal aquifers, *Eos Trans. AGU*, 90(52), Fall Meet. Suppl., Abstract H32C-05, San Francisco, CA, Dec. 14-18, 2009.

Lu, C., Luo, J., Effects of aquifer stratification on freshwater-seawater mixing- zone development, *EOS Trans. AGU*, Fall Meet. Suppl., Abstract H43A-1206, San Francisco, CA, Dec. 13-17, 2010.

Report Follows

In the following report, the research conducted in FY2011 is presented. Research completed or published in previous years are not included.

Chap. 1

Boundary condition effects on estimating maximum groundwater withdrawal in coastal aquifers **2**

Chap. 2

Solute transport in divergent radial flow with multistep pumping **23**

Chap. 3

Freshwater-seawater mixing zone in stratified coastal aquifers **44**

Chap. 1

Boundary condition effects on estimating maximum groundwater withdrawal in coastal aquifers

Abstract

Prevention of seawater intrusion in coastal aquifers subject to groundwater withdrawal requires optimization of well pumping rates to maximize the water supply while avoiding seawater intrusion. Boundary conditions and the aquifer domain size have significant influences on simulating flow and concentration fields and estimating maximum pumping rates. In this study, an analytical solution is derived based on the potential-flow theory for evaluating maximum groundwater pumping rates in a domain with a constant hydraulic head landward boundary. An empirical correction factor, which was introduced by Pool and Carrera (2011) to account for mixing in the case with a constant recharge rate boundary condition, is found also applicable for the case with a constant hydraulic head boundary condition, and therefore greatly improves the usefulness of the sharp-interface analytical solution. Comparing with the solution for a constant recharge rate boundary, we find that a constant hydraulic head boundary often yields larger estimations of the maximum pumping rate and when the domain size is five times greater than the distance between the well and the coastline, the effect of setting different landward boundary conditions becomes insignificant with a relative difference between two solutions less than 2.5%. These findings can serve as a preliminary guidance for conducting numerical simulations and designing tank-scale laboratory experiments for studying groundwater withdrawal problems in coastal aquifers with minimized boundary condition effects.

Introduction

Groundwater is a vital resource providing water supplies for public potable water, agriculture and industry in coastal areas. To satisfy the increasing demand for freshwater, excessive groundwater withdrawals have upset the long established balance between freshwater and seawater potentials, causing encroachment of seawater into freshwater aquifer, resulting in well-known seawater intrusion problems (Bear 1972). Once seawater has intruded into coastal aquifer to an intolerable distance, the deterioration of the groundwater quality significantly threatens the sustainability of coastal communities and further development of coastal areas. Restoration of groundwater quality in the invaded zones is generally an expensive and ineffective proposition (Bear et al. 1999). Therefore, prevention is considered the most effective approach from the perspective of implementing an integrative groundwater management strategy in coastal areas. One of the most cost-effective prevention strategies is to optimize withdrawal rates, i.e., the management of groundwater extraction in coastal aquifers to maximize the water supply while avoiding seawater intrusion (e.g., Das and Datta 1999a, 1999b; Cheng et al. 2000; Park and Aral 2004; Mantoglou et al. 2004; Bhattacharjya and Datta 2005).

Two types of conceptual models have been used in estimating maximum groundwater withdrawal rates in coastal aquifers: the sharp-interface approximation and the miscible flow transport model. By assuming a steady flow in a hydrologically homogeneous porous medium, as well as a sharp interface between the freshwater and the seawater,

analytical solutions can be derived for simplified conceptual models by applying potential-flow theories (e.g. Bear and Dagan 1964; Ozturk 1970; Strack 1989; Dagan and Zeitoun 1998; Naji et al. 1998; Kacimov and Obnosov 2001; Bakker 2000 and 2006; Kacimov and Sherif 2006). By contrast, an approach to modeling based on miscible flow assumptions is more realistic by incorporating a system of variable-density flow equation and the advection-dispersion equation (e.g., Henry 1964; Voss and Souza 1987; Galeati et al. 1992; Croucher and O'Sullivan 1995; Ackerer et al. 1999; Diersch and Kolditz 2002; Simpson and Clement 2003; Simmons 2005; Langevin and Guo 2006). In this context, a variable-density mixing zone with a certain thickness, rather than a sharp interface, can be generated, consistent with field observations in coastal aquifers (Barlow 2003, Cherry 2006).

Solutions to both sharp-interface and miscible-flow models are influenced by boundary conditions. For the seaward boundary, constant hydraulic heads are usually imposed (e.g., Cheng et al. 2000; Park and Aral 2004; Lu et al., 2009), while there are two types of boundary conditions, constant hydraulic head and constant recharge rate, available at the landward boundary (Werner and Simmons 2009). Conditions of constant recharge are often used by sharp-interface models, which implicitly assume an infinite large simulation domain (Strack 1976, 1989; Cheng et al. 2000). By contrast, miscible flow models generally define a sufficiently large domain so that the flow field is not affected by the landward boundary condition. However, no general solution has been given regarding the domain size required for eliminating the boundary condition effects. Moreover, such information is particularly useful for designing tank-scale laboratory experiments to investigate upconing problems, which are sensitive to boundary conditions due to limited equipment size. The present work aims to resolve this issue by investigating the effects of different boundary conditions on estimating the maximum groundwater withdrawal rates from an extraction well in coastal aquifers. In specific, we first derive an analytical solution for the flow field and the maximum groundwater withdrawal rate in a homogeneous domain with landward boundary conditions being constant hydraulic head. The derived solutions are then compared with those obtained in a domain with constant recharge rate boundaries to evaluate the effects of different boundary conditions and the domain size required for minimizing the solution variations. This comparison can provide fundamental understanding of the relationships between the rate of freshwater flow or the water table elevations in the vicinity of the coast and the length of the intruding seawater wedge. Finally, we numerically examine the applicability of the derived solutions and results in cases with dispersive mixing by including a correction factor recently proposed by Pool and Carrera (2011).

Mathematical Models

Conceptual Model

Consider a fully-penetrating pumping well in a homogeneous, isotropic coastal aquifer. Figure 1 shows the plan view and cross section of the conceptual model in an unconfined aquifer. The freshwater area within the aquifer is bounded above by a phreatic surface and below by either an interface that separates the freshwater from seawater at rest (Zone 1), or an impermeable bed (Zone 2). The horizontal bed of the aquifer is at depth D below the mean sea level. The distance between the phreatic surface and the impermeable bed

is h_f. The interface is located at a distance d below the mean sea level. q_{x0} is a uniform flow rate of the regional flow to the sea. A similar conceptual model can be developed for a confined aquifer with a uniform aquifer thickness, B.

Two types of boundary conditions are considered for the landward boundary: constant recharge rate q_{x0} and constant hydraulic head. Analytical solutions have been derived for the former boundary condition (Strack 1989), which implicitly assumes an infinite domain. For the latter, we assume that a constant head boundary is located at a distance of L from the coastline, which can generate the same influx flow rate q_{x0} in the absence of a pumping well. This boundary condition can also describe coastal hydrogeologic systems containing a surface freshwater body, such as rivers, streams or canals, in coastal regions (Kondolf and Matthews 1986; Sahoo and Smith 2009). Such water bodies, especially those parallel to the coastline, may serve as a barrier for preventing seawater intrusion. For example, at Great Yarmouth, UK, the river Yare flows parallel to the coastline for several miles with most of the town, sandwiched between the sea and the Yare. Bailey and Lear (2006) also indicated that it is common that a river in coastal areas flows approximately parallel to the sea for some distance before joining it. Therefore, under these field conditions, it is necessary to define a constant hydraulic head boundary for a pumping well located between the sea and the surface water body, and it is important to know how the surface water body affects the maximum allowed groundwater pumping rate. This scenario is also similar to the case with a pumping well located between two parallel rivers (Wilson 1993; Intaraprasong and Zhan 2007). However, in coastal aquifers a constraint that saltwater is not allowed to be extracted must be applied for preventing upconing and seawater intrusion.

Potential-Flow Theory

To apply the potential-flow theory to solve the flow field (Strack, 1976), several assumptions are made: (1) the seawater-freshwater interface is a sharp interface instead of a variable-density transition zone; (2) the sea level is constant; (3) the Dupuit-Forchheimer assumption is applied to neglect the vertical flow; and (4) the Ghyben-Herzberg formula is employed to locate the interface position. In the absence of a pumping well located in coastal aquifers, a potential, ϕ, can be defined for Zones 1 and 2 as (Strack 1976; Cheng et al. 2000):

Unconfined:

Zone 1: $\phi = \frac{\varepsilon + 1}{2\varepsilon}\left(h_f - D\right)^2$

(1a)

Zone 2: $\phi = \frac{1}{2}\left(h_f^2 - (\varepsilon + 1)D^2\right)$

(1b)

Confined:

Zone 1: $\phi = \frac{1}{2\varepsilon}\left(h_f + \varepsilon B - (\varepsilon + 1)D\right)^2$

(2a)

Zone 2: $\phi = Bh_f + \frac{1}{2}\varepsilon B^2 - (\varepsilon + 1)BD$

(2b)

where ε is the seawater and freshwater density ratio $(\rho_s - \rho_f)/\rho_f$. The sharp interface location can be evaluated based on both the potentials in zones 1 and 2 satisfying the Laplace's equation $\nabla\phi^2 = 0$ and the condition of continuity of flow (Strack 1989). The potential at the toe of saltwater wedge is (Cheng et al. 2000):

Unconfined: $\phi_{toe} = \frac{\varepsilon(\varepsilon+1)}{2}D^2$

(3)

Confined: $\phi_{toe} = \frac{\varepsilon}{2}B^2$

(4)

For a pumping well located between two parallel surface water bodies with constant head, the freshwater discharge potential can be evaluated by superposing an infinite series of imaginary wells, which yields:

$$\phi = \frac{q_{x0}}{K}x + \frac{Q}{4\pi K}\sum_{n=-\infty}^{\infty}\ln\left[\frac{(x-(x_w+2nL))^2 + y^2}{(x+(x_w-2nL))^2 + y^2}\right]$$

(5)

in which n is the number of image wells, Q is the pumping rate, x_w is the distance between pumping well and the sea, K is hydraulic conductivity, and L is the distance between two parallel surface water bodies.

Maximum Pumping Rate

In water resources management, it is of practical interest to predict the maximum pumping rate for a well or to design the well location for required pumping rates. In cases where the saltwater does not reach the pumping well, the flow field in Zone 1 is a one-fluid flow system, while in cases with saltwater pumped by the well it becomes a two-fluid flow system. The critical case between these two occurs when the stagnation point created by the pumping well and the toe position of saltwater wedge coincide (Strack 1976). The seawater-freshwater interface in this critical case is unstable because an infinitesimal increase of the pumping rate may lead to saltwater upconing. Based on the potential theory, the implicit analytical solution for the maximum pumping rate for the constant recharge boundary condition is given by (Strack 1976):

$$\phi_{toe}^* = x_w^*\left[\left(1-\frac{2Q^*}{\pi x_w^*}\right)^{1/2} + \frac{Q^*}{\pi x_w^*}\ln\left[\frac{1-\left(1-\frac{2Q^*}{\pi x_w^*}\right)^{1/2}}{1+\left(1-\frac{2Q^*}{\pi x_w^*}\right)^{1/2}}\right]\right]$$

(6)

in which the dimensionless variables are defined as

$$x_w^* = \frac{x_w}{L} \quad , \quad Q^* = \frac{Q}{2q_{x0}L} \quad , \quad \phi_{toe}^* = \frac{\varepsilon(\varepsilon+1)}{2q_{x0}L}KD^2 \text{ (unconfined), and } \phi_{toe}^* = \frac{\varepsilon}{2q_{x0}L}KB^2 \text{ (confined)} \quad (7)$$

Note that the parameter L is not shown in Strack's solution, and is included here for the sake of comparison with analytical solutions of the case with constant head boundary conditions.

For constant head boundary conditions, Eq. (5) can be rewritten as (see Appendix):

$$\phi^* = x^* + \frac{Q^*}{2\pi}\ln\left[\frac{\cosh(\pi y^*) - \cos\left(\pi(x^* - x_w^*)\right)}{\cosh(\pi y^*) - \cos\left(\pi(x^* + x_w^*)\right)}\right] \quad (8)$$

where x^* and y^* are dimensionless coordinates normalized by domain length L. By taking the first derivative with respect to x^* and setting it to be zero, the dimensionless x-coordinate of the stagnation point is given by:

$$x_s^* = \frac{1}{\pi}\cos^{-1}(\cos(\pi x_w^*) + Q^*\sin(\pi x_w^*)) \quad (9)$$

which can be expressed as

$$\cos(\pi x_s^*) = \cos(\pi x_w^*) + Q^*\sin(\pi x_w^*) \quad (10)$$

Eq. (10) implicitly requires that

$$-1 \le \cos(\pi x_w^*) + Q^*\sin(\pi x_w^*) \le 1 \quad (11)$$

Note that $Q^*\sin(\pi x_w^*)$ is non-negative because Q^* is non-negative and $0 < x_w^* \le 1$. The monotonically decreasing property of cosine function within the range $[0,\pi]$ indicates that $x_s^* \le x_w^*$, i.e., the stagnation point only exists between the well and the sea. The derivation of Eq. (8) and the analysis of stagnation points are essentially the same as those in Intaraprasong and Zhan (2007).

As discussed above, the critical pumping rate, i.e., the maximum pumping rate that does not cause seawater intrusion, can be evaluated when the stagnation point and the toe of saltwater wedge coincide. By substituting the stagnation point coordinate $(x_s^*, 0)$ given by Eq. (9) and the potential at the toe in Eq. (7) into Eq. (8), we obtain:

$$\phi_{toe}^* = \frac{1}{\pi}\cos^{-1}(\cos(\pi x_w^*) + Q_{\max}^*\sin(\pi x_w^*)) + \frac{Q_{\max}^*}{2\pi}\ln\left[\frac{1-\cos(\cos^{-1}(\cos(\pi x_w^*) + Q_{\max}^*\sin(\pi x_w^*)) - \pi x_w^*)}{1-\cos(\cos^{-1}(\cos(\pi x_w^*) + Q_{\max}^*\sin(\pi x_w^*)) + \pi x_w^*)}\right] \quad (12)$$

where $Q^*_{\max}$ is the dimensionless maximum pumping rate. Eq. (12) is an implicit analytical solution for the maximum pumping rate for the constant head boundary condition, which can also be used to determine where the pumping well should be placed given a withdrawal rate.

Adjusted Maximum Pumping Rate with Dispersive Mixing

The sharp-interface analytical solutions neglect the mixing between freshwater and seawater, which are conservative in the assessment of maximum pumping rate (Dausman et al., 2010). To overcome this issue, an empirical correction factor was recently introduced by Pool and Carrera (2011), who found that Strack's equations can be extended to the variable density flow case if the density factor is multiplied by a corrector factor, $\left[1-\left(\frac{\alpha_T}{B}\right)^{1/6}\right]$, where α_T is the transverse dispersivity. This correction factor was obtained based on numerical simulations with a constant recharge rate boundary at the landward side. By conducting systematic numerical simulations, we found that this correction factor is also applicable to the analytical solution for the constant head boundary condition. This finding simplifies the analysis for comparing the differences between the two boundary conditions for cases with dispersive mixing and can significantly improve the usefulness of the sharp-interface analytical solution.

Results and Discussion

Stagnation-Point Location

Figure 2 shows the position of the stagnation point as a function of the pumping rate and well location. Figure 2a shows that for a given well location the stagnation point moves towards the sea as the pumping rate increases. A maximum pumping rate may be obtained for x^*_s approaching zero, i.e., the stagnation point reaches the coastline. Certainly, this pumping rate is not the maximum pumping rate allowed in the coastal aquifer because the stagnation point has passed the toe of saltwater wedge. The maximum allowed pumping rate should be less than this rate. Figure 2b shows that for a given pumping rate the stagnation point moves with the pumping well toward the same direction. Similarly, the well location when x^*_s approaches zero is not the desirable location to place a pumping well for a given pumping rate. The pumping well should be placed further away from the coastline.

Implications for Model Design

Figure 3 shows the analytical solutions given by Eqs. (5) and (11) for the two different boundary conditions. The essential difference between these two is that the constant recharge rate boundary implicitly assumes a sufficiently large aquifer domain so that only one imaginary well needs to be considered to create the seaward boundary. It is shown for both boundary conditions that with the increase of the potential at the toe, i.e., a larger K or/and B (D for unconfined aquifer), or/and a smaller $q_{x0,}$ less water can be extracted from the pumping well because the potential increase results in landward movement of the toe position; and with the increase of x^*_w, i.e., the pumping well is located further

from the coastline, more water can be extracted from the pumping well as a result of landward movement of the stagnation point.

In addition, it clearly shows that constant hydraulic head boundary often results in enhanced maximum pumping rates for a large x_w^* . The deviation becomes more pronounced for a lower ϕ_{toe}^*, which can be resulted from a smaller *K* or/and *B* (*D* for unconfined aquifer), or/and a larger *L*. Here, we define a parameter to quantitatively compare the maximum pumping rates between two boundary conditions:

$$\eta = \frac{\overline{Q_{\max}^*(h)} - \overline{Q_{\max}^*(d)}}{\overline{Q_{\max}^*(d)}} \times 100\% \quad (13)$$

where $\overline{Q_{\max}^*(h)}$ and $\overline{Q_{\max}^*(d)}$ are the toe potential averaged maximum pumping rates for constant head boundary condition and constant discharge boundary condition, respectively. The calculated η with the locations of pumping well are shown in Figure 4. It is shown that for $x_w^* > 0.5$, η > 20%, indicating that highly different results are obtained from two different boundary conditions. However, when $x_w^* < 0.2$, the differences between the two cases with different boundary conditions are not significant (η < 2.5%). Certainly, this criterion is adjustable with an altered requirement in accuracy.

These findings have very important implications for numerical and experimental endeavors for investigating groundwater withdrawal in coastal aquifers. For a fixed domain, the pumping well should be located at $x_w^* < 0.2$ in order to minimize the boundary condition effects. Otherwise, a constant hydraulic head boundary always predicts larger maximum pumping rates allowed for avoiding seawater intrusion than a constant discharge boundary. Similarly, for a fixed well location, the domain size must satisfy $L > 5x_w$ to minimize the boundary condition effects. These findings give experimentalists and modelers a preliminary guidance for designs of numerical models and laboratory experiments for studying groundwater withdrawal in coastal aquifers with minimized boundary condition effects (Werner et al. 2009).

Case Study with Dispersive Mixing

To demonstrate the applicability of the conclusion above, a numerical case with dispersive mixing is designed to estimate maximum pumping rates under two different boundary conditions. Parameters used in the case study are listed in Table 1. The pumping well is fixed at the location x_w = 250 m. Three domain lengths *L* = 1000, 1250, and 1500 m are considered for the cases with different boundary conditions, leading to x_w^* = 0.25, 0.2, and 0.17, respectively. Adjusted maximum pumping rates for the two boundary conditions are calculated using the sharp-interface analytical solutions and the correction factor. Figure 5 shows the effects of domain length and transverse dispersivity on the relative maximum pumping rate difference. As shown, as $x_w^* \le 0.2$, η is less than 2.5%, which is reasonably in agreement with the results of the sharp-interface analytical solutions. On the other hand, η slightly increases with the increase of α_T , showing that

the effect of local α_T on η is relatively stable. Our sharp-interface analytical solutions provide a good approximation and show great potential in numerical and experimental studies on groundwater withdrawal in coastal aquifers.

Conclusion

Optimization of groundwater withdrawal to avoid upconig or seawater intrusion is the most effective prevention strategy for groundwater resources management in coastal aquifers. Boundary conditions and the system domain size have significant influences on simulating the flow and concentration fields and estimating the maximum pumping rates. In this study, we apply the potential-flow theory to investigate the effects of constant hydraulic head and constant recharge rate boundary conditions at the landward boundary. An analytical solution is derived for the flow field and the maximum groundwater withdrawal rate in a domain with a constant hydraulic head landward boundary condition, which is also capable of simulating coastal hydrogeologic systems involving a surface freshwater body. An empirical correction factor, which was originally introduced for the case with constant recharge rate boundary condition to take mixing into account, is found also applicable for the case with constant head boundary condition. This finding greatly improves the usefulness of the derived analytical solutions.

Comparing with the solution for a constant recharge rate boundary, we find that (1) a constant hydraulic head boundary often yields significantly larger maximum pumping rates for $x_w^* > 0.5$, where x_w^* is a dimensionless well location normalized by the domain length, than a constant recharge boundary condition, and the difference becomes more significant for lower potentials at the toe of saltwater wedge; and (2) for $x_w^* < 0.2$, the differences between the two boundary cases are not significant ($\eta < 2.5\%$).

Our findings can serve as a preliminary guidance for conducting numerical simulations and designing tank-scale laboratory experiments for studying groundwater withdrawal problems in coastal aquifers. One may use the findings to choose the domain size and well locations to minimize the boundary condition effects. For example, in laboratory experiments, it is more convenient to control a constant hydraulic head boundary than a constant recharge rate boundary. By locating the well at $x_w^* < 0.2$, the boundary condition effect may be minimized and there is no need to construct an expensive, large tank-scale equipment. Similarly, with a given well location, modelers may only need to define a domain size satisfying $L > 5x_w$ instead of a much larger simulation domain to minimize the boundary condition effects. The criterion above is adjustable depending on the requirement in accuracy.

Appendix. Derivation of Eq. (8) (Zhan 1999; Intaraprasong and Zhan 2007)

The complex potential for the flow field is defined as (Bear, 1972):

$$\Omega(z) = \phi + i\psi \tag{A.1}$$

where Ω is the complex potential, ϕ and ψ are real and imaginary parts describing potential and stream functions, respectively, $z = x + iy$ is the complex argument, and $i = \sqrt{-1}$ is the sign of complex.

For a pumping well located between two parallel water bodies with constant head, the dimensionless complex potential is given as

$$\Omega^*(z^*) = Q^* \sum_{n=-\infty}^{\infty} \left[\ln[z^* - (x_w^* + 2n) - \ln[z^* - (-x_w^* + 2n)] \right] + z^*$$

(A.2)

In which $\Omega^* = \dfrac{\Omega}{2q_{x0}L}$ and $z^* = \dfrac{z}{L}$.

Since $$\sum_{n=-\infty}^{\infty} \ln\left[(z^* - x_w^*) - 2n)\right] = \ln\left[\sin(\frac{\pi(z^* - x_w^*)}{2}) \right],$$

(A. 3)

Eq. (A.2) can be simplified as

$$\Omega^*(z^*) = Q^* \ln\left[\frac{\sin\left(\pi(z^* - x_w^*)/2\right)}{\sin\left(\pi(z^* + x_w^*)/2\right)} \right] + z^*$$

(A. 4)

Note that the derivation of Eq. (A.3) can be found in Zhan (1999). By using the equation $\exp(\phi + \psi i) = \exp(\phi)\left(\cos(\psi) + i\sin(\psi)\right)$ and separating the real part from the imaginary part, Eq. (8) can be easily obtained.

Acknowledgements

This research was sponsored by U.S. Geological Survey (USGS) under project ID 2007GA165G. We would like to thank the comments from anonymous reviewers, which significantly help us improve the manuscript quality.

References

Ackerer, P., A. Younes, and R. Mose. 1999. Modeling variable density flow and solute transport in porous medium: 1. Numerical model and verification. *Transport in Porous Media* 35, no. 3: 345-373.

Bailey, T.R., and C.H. Lear. 2006. Testing the effect of carbonate saturation on the Sr/Ca of biogenic aragonite: A case study from the River Ehen, Cumbria, UK. *Geochemistry Geophysics Geosystems* 7: Q03019. doi: 10.1029/2005GC001084.

Bakker, M. 2000. The size of the freshwater zone below an elongated island with infiltration. *Water Resources Research* 36, no. 1: 109-117.

Bakker, M. 2006. Analytical solution for interface flow in combined confined and semi-confined, coastal aquifers. *Advances in Water Resources* 29, no 3: 417-425.

Barlow, P.M. 2003. Ground water in freshwater-saltwater environments of the Atlantic coast: U.S. *Geological Survey Circular* 1262.

Bear, J. 1972. Dynamics of Fluids in Porous Media. American Elsevier, New York.

Bear, J., A.H.D. Cheng, S. Sorek, D. Ouazar and I. Herrera. 1999. Seawater Intrusion in Coastal Aquifers- Concepts, Methods and Practices. Springer, New York.

Bear, J., and G. Dagan. 1964. Some exact solutions of interface problems by means of hodograph method. *Journal of Geophysical Research* 69, no. 8: 1563-1572.

Bhattacharjya, R., and B. Datta. 2005. Optimal management of coastal aquifers using linked simulation optimization approach. *Water Resources Management* 19, no. 3: 295-320.

Cherry, G.S. 2006. U.S. Geological Survey Georgia Water Science Center and City of Brunswick-Glynn County Cooperative Water Program - Summary of Activities, July 2005 through June 2006, U.S.G.S. Open-File Report 2006-1368.

Cheng A.H.D., D. Halhal, A. Naji, and D. Ouazar. 2000. Pumping optimization in saltwater-intruded coastal aquifers. *Water Resources Research* 36, no. 8: 2155-2165.

Croucher, A.E., and M.J. O'Sullivan. 1995. The Henry problem for saltwater intrusion. *Water Resources Research* 31, no. 7: 1809-1814.

Dagan, G., and D.G. Zeitoun. 1998. Seawater-freshwater interface in a stratified aquifer of random permeability distribution. *Journal of Contaminant Hydrology* 29, no. 3: 185-203.

Das, A., and B. Datta. 1999a. Development of management models for sustainable use of coastal aquifers. *Journal of Irrigation and Drainage Engineering-ASCE* 125, no. 3: 112-121.

Das, A., and B. Datta. 1999b. Development of multi-objective management models for coastal aquifers. *Journal of Water Resources Planning and Management-ASCE* 125, no. 2: 76-87.

Dausman, A., C. Langevin, M. Bakker, and F. Schaars. 2010. A comparison between SWI and SEAWAT-The importance of dispersion, inversion and vertical anisotropy, paper presented at the 21st Salt Water Intrusion Meeting, Gov. of Azores, Azores.

Diersch, H.J.G., and O. Kolditz. 2002. Variable-density flow and transport media: approach and challenges. *Advances in Water Resources* 25, no. 8-12: 899-944.

Galeati, G., G. Gambolati, and S.P. Neuman. 1992. Coupled and partially coupled Eulerian-Lagrangian model of freshwater-seawater mixing zone. *Water Resources Research* 28, no. 1: 149-165.

Henry, H.R. 1964. Effects of dispersion on salt encroachment in coastal aquifers. Water-Supply Paper 1613-C. US Geological Survey.

Intaraprasong, T., and H. Zhan. 2007. Capture zone between two streams. *Journal of Hydrology* 338, no. 3-4: 297-307.

Kacimov, A.R., and Y. Obnosov. 2001. Analytical solution for a sharp interface problem in sea water intrusion into a coastal aquifer. *Proceedings of the Royal Society A* 457, no. 2016: 3032-3038.

Kacimov, A.R., and M.M. Sherif. 2006. Sharp interface, one-dimensional seawater intrusion into a confined aquifer with controlled pumping: analytical solution. *Water Resources Research* 42: W06501. doi:10.1029/2005WR004551.

Kondolf, G.M., and W.V.G. Matthews. 1986. Transport of tracer gravels on a coastal California River. *Journal of Hydrology* 85, no. 3-4: 265-280.

Langevin, C.D., and W. Guo. 2006. MODFLOW/MT3DMS-based simulation of variable-density ground water flow and transport. *Ground Water* 44, no. 3: 339-351.

Lu, C., P.K. Kitanidis, and J. Luo. 2009. Effects of mass transfer and transient flow conditions on widening mixing zones in coastal aquifers. *Water Resources Research* 45: W12402. doi:10.1029/2008WR007643.

Mantoglou, A., M. Papantoniou, and P. Giannoulopoulos. 2004. Management of coastal aquifers based on nonlinear optimization and evolutionary algorithms. *Journal of Hydrology* 297, no. 1-4: 209-228.

Naji, A., A.H.D. Cheng, and D. Ouazar. 1998. Analytical stochastic solutions of saltwater/freshwater interface in coastal aquifers. *Stochastic Hydrology and Hydraulics* 12, no. 6: 413-430.

Ozturk, Y.F. 1970. Seawater intrusion length in stratified estuaries. *Water Research* 4, no. 7: 477-484.

Park, C.H., and M.M. Aral. 2004. Multi-objective optimization of pumping rates and well placement in coastal aquifers. *Journal of Hydrology* 290, no. 1-2: 80-99.

Pool M. and J. Carrera. 2011. A correction factor to account for mixing in Ghyben-Herzberg and critical pumping rate approximations of seawater intrusion in coastal aquifers. *Water Resource Research* 47: W05506. doi: 10.1029/2010WR010256.

Sahoo, D., and P.K. Smith., 2009. Hydroclimatic trend detection in a rapidly urbanizing semi-arid and coastal river basin. *Journal of Hydrology* 367, no. 3-4: 217-227.

Simmons, C.T. 2005. Variable density groundwater flow: From current challenges to further possibilities. *Hydrogeology Journal* 13, no. 1: 116-119.

Simpson, M.J., and T.P. Clement. 2003. Theoretical analysis of the worthiness of Henry and Elder problems as benchmarks of density-dependent groundwater flow models. *Advances in Water Resources* 26, no. 1: 17-31.

Strack, O.D.L. 1976. A single-potential solution for regional interface problems in coastal aquifers. *Water Resources Research* 12, no. 6: 1165-1174.

Strack, O.D.L. 1989. Groundwater Mechanics. Englewood Cliffs, NJ: Prentice-Hall.

Voss, C.I. and W.R. Souza. 1987. Variable density flow and solute transport simulation of regional aquifers containing a narrow freshwater-seawater mixing zone. *Water Resources Research* 23, no. 10: 1851-1866.

Werner, A.D., D. Jakovovic, and C.T. Simmons. 2009. Experimental observations of saltwater up-coning. *Journal of Hydrology* 373, no. 1-2: 230-241.

Werner, A.D., and C.T. Simmons. 2009. Impact of sea-level rise on sea water intrusion in coastal aquifers. *Ground Water* 47, no. 2: 197-204.

Wilson, J. 1993. Induced infiltration in aquifers with ambient flow. *Water Resources Research* 29, no. 10: 3503-3512.

Table 1. Parameters Used in the Case Study

Parameter	Symbol	Value	Unit
Domain length	L	1000, 1250, 1500	m
Aquifer thickness	B	20	m
Hydraulic conductivity	K	10	m d^{-1}
freshwater influx	q_{x0}	0.24	m^2 d^{-1}
Transverse dispersivity	α_T	0.1-2	m
Freshwater density	ρ_f	1000	kg m^{-3}
Seawater density	ρ_s	1025	kg m^{-3}
Well location	x_w	250	m

Figure Captions

Figure 1. Plan view and cross section of the conceptual model for a pumping well located in a homogeneous, isotropic, unconfined coastal aquifer.

Figure 2. Location of stagnation points for a pumping well in coastal aquifers with constant hydraulic head landward boundary. (a) stagnation point vs. pumping rate; and (b) stagnation point vs. well location.

Figure 3. Comparison of maximum pumping rates for avoiding seawater intrusion in coastal aquifers with different boundary condition settings.

Figure 4. Relative maximum pumping rate difference as a function of the location of the pumping well.

Figure 5. Effects of the well location and transverse dispersivity on the relative maximum pumping rate difference.

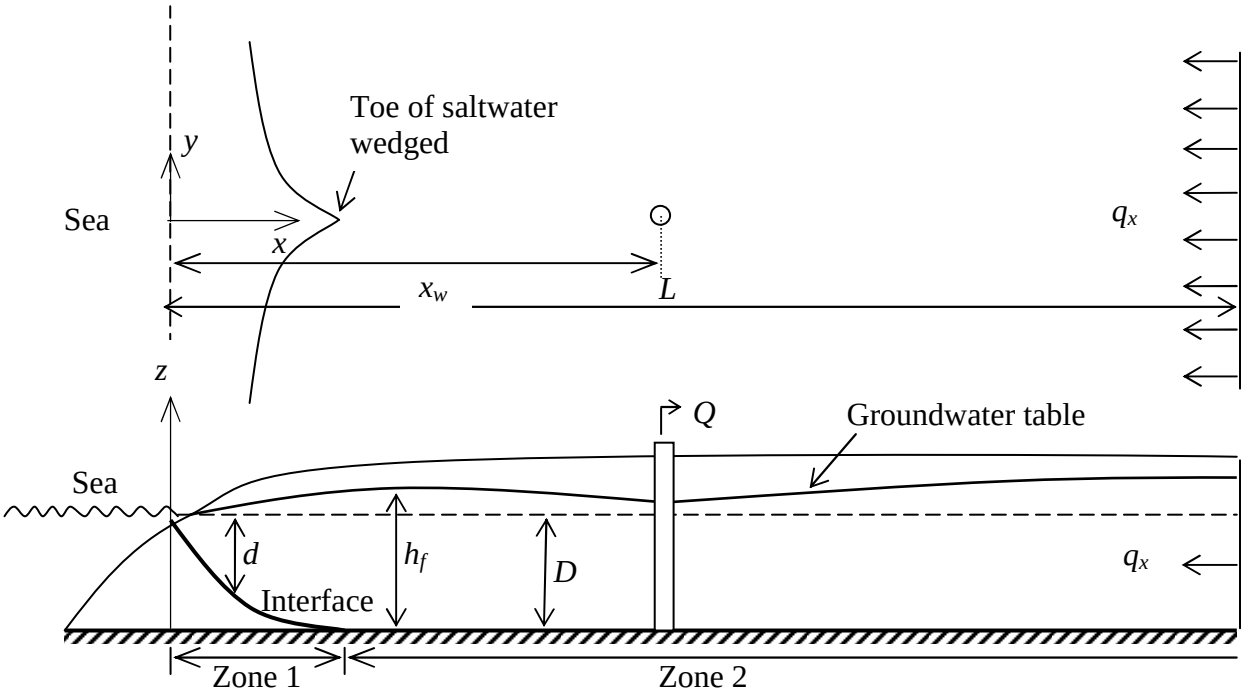

Figure 1. Plan view and cross section of the conceptual model for a pumping well located in a homogeneous, isotropic, unconfined coastal aquifer.

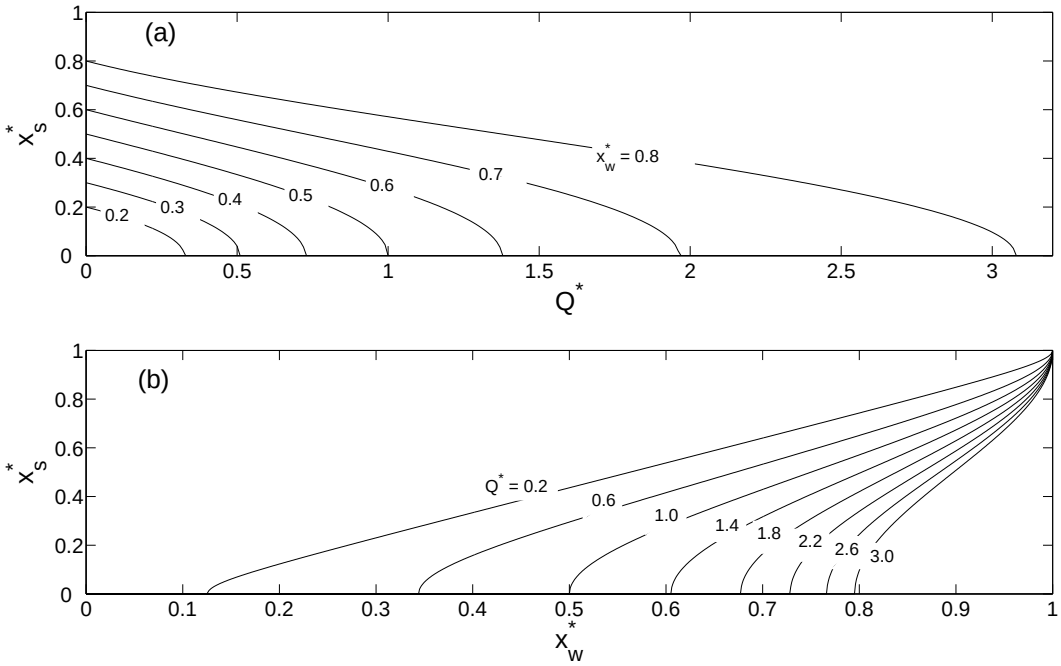

Figure 2. Location of stagnation points for a pumping well in coastal aquifers with constant hydraulic head landward boundary. (a) Stagnation point vs. pumping rate; and (b) stagnation point vs. well location.

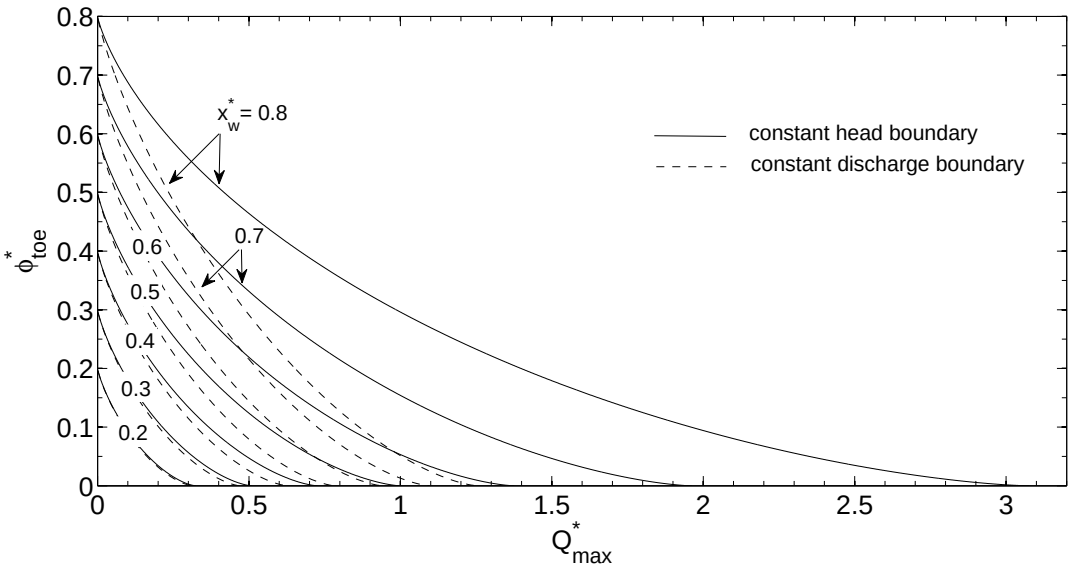

Figure 3. Comparison of the maximum pumping rates for avoiding seawater intrusion in coastal aquifers with different boundary condition settings.

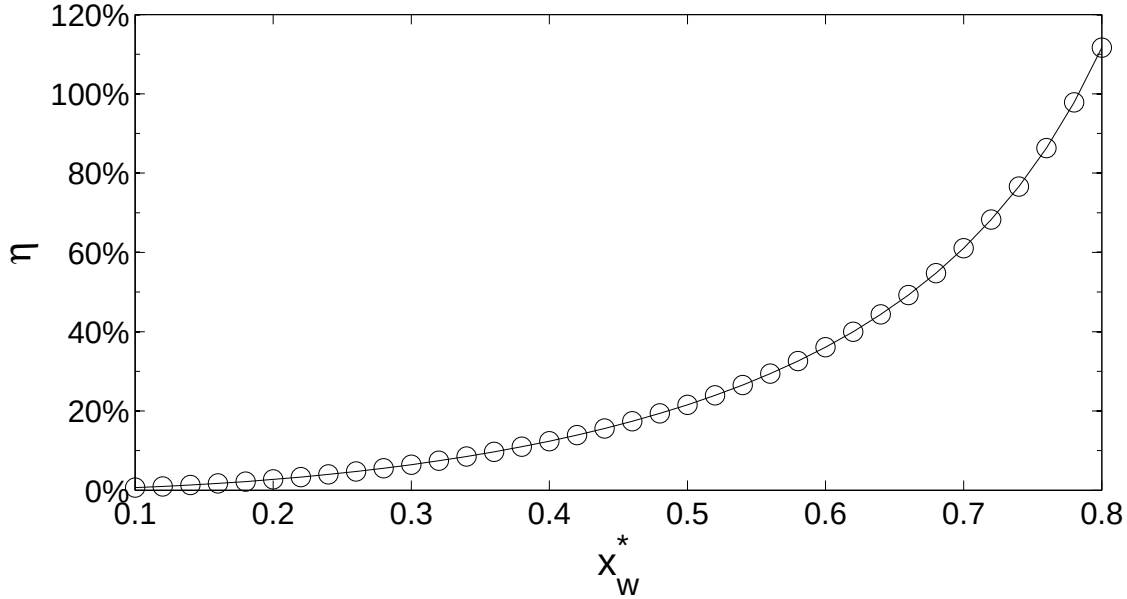

Figure 4. Relative maximum pumping rate difference with the locations of pumping well.

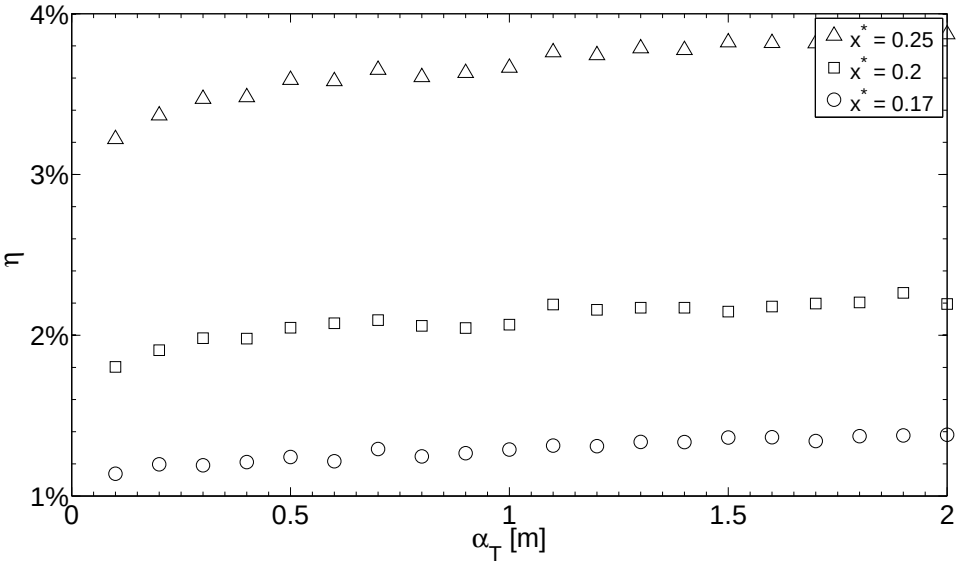

Figure 5. Effects of the well location and transverse dispersivity on the relative maximum pumping rate difference.

Chap. 2

Solute transport in divergent radial flow with multistep pumping

Abstract

An efficient approach is developed to analytically evaluate solute transport in a horizontal, divergent radial flow field with a multistep injection flow rate and an arbitrary input concentration history. By assuming a piecewise steady-state flow and transforming the time domain to the cumulative injected flow domain, the concentration distribution is found to be completely determined by the total volume of injected flow and independent of specific flow rates. Thus, on the cumulative flow domain, the transport problem with a temporally varying velocity field can be transformed into a steady-state flow problem. Linear convolution can then be applied on the cumulative injected flow domain to evaluate the solution for an arbitrarily time-dependent input concentration. Solutions on the regular time domain can be conveniently obtained by mapping the solution on the cumulative injected flow domain to the time domain. Furthermore, we theoretically examine the conditions for the assumption of piecewise steady-state flow to be valid. Based on the critical timescale of the "peudo-steady state condition", defined when velocity changes accomplish 99% of their steady-state differences, and the relative error in the mean travel time of plume front, we obtain conditions for neglecting the transitional period between two pumping steps. Such conditions include (1) the duration of a pumping step, t_p, must be longer than the critical timescale, t_c, i.e., $t_p \geq t_c = 25r^2S/T$, where r is the radial distance, S is the storage coefficient, and T is the transmissivity; or similarly, a maximum problem domain needs to be defined for a given pumping strategy; and (2) the maximum well pumping rate, $q_{\max}$, should satisfy $q_{\max} \leq \pi\theta T/25S$, where θ is the effective porosity. When both conditions are satisfied, transitional periods may be neglected.

Introduction

Significant contributions have been made to evaluate analytical solutions to the problem of advection and dispersion in a homogeneous aquifer due to well injection or extraction in a horizontal, radially divergent or convergent flow field [e.g., *Ogata*, 1958; *Tang and Babu*, 1979; *Moench and Ogata*, 1981; *Chen*, 1985, 1986, 1987; *Hsieh*, 1986; *Chen and Woodside*, 1988; *Moench*, 1989, 1995; *Goltz and Oxley*, 1991; *Tomasko et al.*, 2001; *Huang and Goltz*, 2006; *Huang et al.*, 2010]. Such solutions have important applications in groundwater practice whenever well pumping is involved, such as tracer tests in convergent and divergent radial flow fields [e.g., *Novakowski*, 1992; *Moench*, 1995; *Becker and Charbeneau*, 2000], decontamination by pumping with rate-limited sorption or mass transfer [e.g., *Goltz and Oxley*, 1991; *Harvey et al.*, 1994], and single-well push-pull tracer tests [*Huang et al.*, 2010], etc. First-order analysis and macrodispersion theory have also been applied for solute transport in divergent radial flow in heterogeneous porous media [e.g., *Indelman and Dagan*, 1999; *Neuweiler et al.*, 2001]. One major assumption for these analytical solutions and analyses is that the radial flow field is steady state, i.e., the velocity field is a spatial function of the distance to the pumping well, but not a temporal function. In this work, we present a novel, efficient approach to

evaluate solute transport in divergent radial flow fields created by multistep pumping with an arbitrarily time-dependent input concentration. The major assumption of this approach is that the transitional period between two pumping steps can be neglected. Such an assumption was accepted in all the available analytical solutions, i.e., solute transport starts when the radial field reaches the steady state. This work also presents theoretical analyses to investigate the conditions for such an assumption to be valid.

Governing Equation

Consider a recharge well that fully penetrates a homogeneous, confined aquifer of uniform thickness and infinite lateral extent. The transport problem can be described by the radially advective-dispersive equation in cylindrical coordinates as the following by neglecting molecular diffusion [e.g., *Hoopes and Harleman*, 1967; *Hsieh*, 1986]:

$$\theta \tfrac{\partial c}{\partial t} = -\theta v \tfrac{\partial c}{\partial r} + \tfrac{1}{r}\tfrac{\partial}{\partial r}\left(\theta r \alpha_L |v| \tfrac{\partial c}{\partial r}\right), \quad r > r_w$$

where t [T] is the time; r [L] is the radial distance from the well center; r_w [L] is the well radius; c [M/L^3] is the dissolved solute concentration; θ [$-$] is the effective porosity; α_L [L] is the longitudinal dispersivity; v [L/T] is the pore fluid velocity; and $|v|$ represents the absolute magnitude of v .

When the well injection rate is constant, the steady-state velocity field is only a spatial function of r ,

$$v(r) = \frac{q}{2\pi\theta r}, \quad r > r_w$$

where q [L^2/T] is the specific injection rate, defined as the flow recharge rate per unit length of aquifer thickness, and r_w is the well radius. The initial condition is:

$$c(r, t = 0) = 0$$

and the boundary condition with a constant injection concentration is:

$$c(r \to \infty, t) = 0, \quad c(r = r_w, t) = c_0$$

The above equations represent a typical model setup for describing solute transport in a steady-state divergent radial flow field with a constant solute input concentration at the injection well. In practice, however, one may adjust the pumping rate and input concentration during experiments to create favorable subsurface flow fields and conditions, i.e., both the pumping rate q and input concentration c_0 may vary with time. For example, a multistep pumping strategy consisting of a series of rate increases may be applied to increase the sensitivity of drawdown to zonal properties and to estimate well loss parameters [e.g., *Butler and McElwee*, 1990; *Singh*, 2002], and mixing within the injection well may generate a gradually increasing input concentration history for a step injection [*Luo et al.*, 2006].

For a multistep pumping rate $q(t)$, we assume that the velocity field varies with the well pumping rate and the velocity field is a function of both r and t , i.e.,

$$v(r,t) = \frac{q(t)}{2\pi\theta r}, \quad r > r_w$$

and for a time-dependent input concentration, the boundary condition is:

$$c(r \to \infty, t) = 0, \quad c(r = r_w, t) = c_0(t)$$

Eq. (velocity2) neglects the transitional period between two well pumping rates and assumes a steady-state velocity for each pumping rate. Such an assumption has been widely accepted in the summarized analytical solutions. *Harvey et al.* [1994] showed that velocities approach steady state rapidly (exponentially decay with the increase of time) for changing pumping rates. In a typical mixed-sand aquifer, velocities may take only minutes to couple of days to reach 99% of steady state for a scale up to 100 meters. Thus, Eq. (velocity2) approximates a piecewise steady-state velocity field in aquifers with short transitional periods to reach steady state. The conditions for such an assumption to be valid will be further discussed in later sections.

As indicated in the introduction, a series of analytical solutions were derived for solute transport in a steady-sate divergent radial flow field with a constant input concentration. To evaluate solute transport in a piecewise steady-state radial flow field, we may discretize the time-dependent function, $q(t)$, into a number of small intervals, $q(t_0), q(t_1), \ldots$, and assume a steady-state flow field within each time interval $t_{n-1} \le t < t_n$. For the first time interval, the transport problem has a zero initial condition and can be conveniently solved by available analytical solutions. For all subsequent time intervals, the transport problem can be described by Eq. (pumping) with a steady-state velocity field but with a non-zero initial condition. Laplace transform of such a problem leads to an inhomogeneous differential equation, which may be solved by the much more complicated Green's function approach [e.g., *Chen and Woodside*, 1988]. Furthermore, such problems can also be solved numerically by taking the solution of the previous time step as the initial condition for the next time step. However, with an arbitrarily time-dependent input concentration history, these methods are computationally complicated and the accuracy relies on the temporal discretization of both q and c_0 and the spatial discretization of travel distance. For example, for a multistep pumping profile and a continuous temporal function of input concentration history, a finer time discretization than the pumping steps is necessary to characterize both q and c_0. In addition, for analyzing tracer tests, one may be interested in concentration profiles at specific sampling locations for parameter estimation. However, numerical models have to solve the extire spatial domain to evaluate concentration profiles at certain locations, causing inefficient inverse modeling and parameter estimation. In the following, we present an efficient approach to solve transport in a multistep pumping field, which is completely based on the available analytical solutions and does not require advanced numerical methods.

Analytical Solutions

Steady-state flow with a constant input concentration

For the sake of completeness, we first summarize the analytical solution in a steady-state flow field with a constant input concentration, which will be used later to evaluate the

solution in a transient flow field. We denote c_s as the solution in a steady-state flow field. By introducing the following dimensionless groups:

$$c_s^* = \frac{c_s}{c_0}, R = \frac{r}{\alpha_L}, R_0 = \frac{r_w}{\alpha_L}, \tau = \frac{qt}{2\pi\theta\alpha_L^2}$$

Eq. (pumping) can be transformed into:

$$\frac{\partial c_s^*}{\partial \tau} = \frac{1}{R}\left(-\frac{\partial c_s^*}{\partial R} + \frac{\partial^2 c_s^*}{\partial R^2}\right)$$

The analytical solution on the Laplace domain is given by [*Moench and Ogata*, 1981]:

$$\overline{c_s^*}(R, p) = \frac{1}{p}\exp\left(\frac{R - R_w}{2}\right)\frac{\mathbf{Ai}(Y)}{\mathbf{Ai}(Y_w)}$$

where p is the Laplace coordinate, Ai (z) is an Airy function, and

$$Y = \frac{4Rp + 1}{4p^{2/3}}$$

$$Y_w = \frac{4R_w p + 1}{4p^{2/3}}$$

The time-domain solution can be evaluated numerically by inverse Laplace algorithms [e.g., *de Hoog et al.*, 1982] or analytically by [*Moench and Ogata*, 1981]:

$$c_s^*(R, \tau) = 1 - \int_0^\infty F(\upsilon)\, d\upsilon$$

where

$$F(\upsilon) = \frac{2\exp\left[-\upsilon^2\tau + (R - R_w)/2\right]}{\pi\upsilon}\frac{\mathbf{Ai}(y)\mathbf{Bi}(y_w) - \mathbf{Ai}(y_w)\mathbf{Bi}(y)}{[\mathbf{Ai}(y_w)]^2 + [\mathbf{Bi}(y_w)]^2}$$

$$y = \frac{1 - 4R\upsilon^2}{4\upsilon^{4/3}}$$

$$y_w = \frac{1 - 4R_w\upsilon^2}{4\upsilon^{4/3}}$$

and Ai and Bi are independent Airy functions of first and second order, respectively.

Steady-state flow with a time-dependent input concentration

For a steady-state divergent flow field with a time-dependent injection history at the pumping well, $c_0(t)$, the solution can be conveniently evaluated by linear convolution:

$$c(R,\tau)=\int_0^{\tau} c_0(\tau')\,g(\tau-\tau')\,d\tau'$$

where g is known as the transfer function or impulse response function corresponding to a unit impulse input function at the pumping well. g can be evaluated by taking inverse Laplace transform of:

$$\bar{g}(R,p)=\exp\left(\frac{R-R_w}{2}\right)\frac{\mathbf{Ai}(Y)}{\mathbf{Ai}(Y_w)}$$

or by taking the first derivative of Eq. (steady solution) with respect to τ :

$$g(R,\tau)=\int_0^{\infty} \upsilon^2 F(\upsilon)\,d\upsilon$$

Because there is a scaling factor between t and τ according to the definition of dimensionless groups, g on the time domain is given by:

$$g(r,t)=\frac{q}{2\pi\theta\alpha_L^2}\,g(R,\tau)$$

Multistep pumping with a constant input concentration

We notice that Eq. (steady solution) is a general solution on the transformed time domain τ for a steady-state flow field with an arbitrary well pumping rate. For the solution on the regular time domain t , one only needs to scale τ according to the definition of dimensionless parameters, i.e.,

$$c^*(r,t)=c_s^*\left(\frac{r}{\alpha_L},\frac{qt}{2\pi\theta\alpha_L^2}\right)$$

We define:

$$Q(t)=qt$$

which represents the cumulative amount of injected water. Eq. (c trans) can then be written as:

$$c^*(r,t)=c_s^*\left(\frac{r}{\alpha_L},\frac{Q(t)}{2\pi\theta\alpha_L^2}\right)$$

For any two steady-state flow fields with different well flow rates, q_1 and q_2 , we have:

$$c_{s1}^*(r,Q;q_1)=c_{s2}^*(r,Q;q_2)$$

which implies that the concentration distribution is independent of specific flow rate q given a constant total injected flow Q .

Eq. (q1q2) leads to an efficient approach to transform a multistep pumping history $q(t)$ to a constant pumping rate by working on the Q domain instead of the regular time

domain t . Consider a simple $q(t)$ with a two-step injection: $q_1(0 \le t < t_1)$ and $q_2(t_1 \le t < t_2)$. At the end of the first pumping period, the concentration is given by:

$$c^*(r, t_1; q_1) = c_s^*(r, Q_1; q_1) = c_s^*(r, Q_1; q_2)$$

where Q_1 is the total injected flow amount during the first injection period, i.e., $Q_1 = q_1 t_1$. Eq. (cts) implies that the initial concentration for the second period may be considered as a result of the pumping rate q_2 for a total injected flow of Q_1 . Thus, the piecewise steady-state flow field created by a two-step injection can be transformed into a steady-state flow field with a constant injection rate. The solution at t_2 can then be conveniently evaluated by:

$$c^*(r, t_2; q_2) = c_s^*(r, Q_1 + Q_2; q_2)$$

Eq. (Eq q1 q2) can be generalized to an arbitrarily discretized pumping history, $q_1(t_1), q_2(t_2), \ldots, q_n(t_n)$:

$$c^*(r, t_i; q_i) = c_s^*\left(r, \sum_{j=1}^{i} Q_j; q_i\right) = c_s^*\left(r, \sum_{j=1}^{i} Q_j; q'\right)$$

where q' represents an arbitrary, constant specific flow rate.

Essentially, Eq. (discrete) evaluates the solution on the domain of the cumulative injection flow volume, Q , instead of the time domain. Eq. (cQ) may be considered as the solution for a unit step injection flow rate on the Q domain. Thus, the transient flow is transformed into the steady-state flow on the Q domain. To obtain the time-domain solution, one only needs to map the solution to the time domain according to the relation between t and $Q(t)$. The fundamental physical principle is that the concentration distribution is completely determined by the total volume of injected water but independent of specific flow rates. We shall notice that the cumulative flow or mass concept has been widely used in analyzing column studies, in which the cumulative mass is usually expressed as pore volume [e.g., *Shackelford*, 1995]. The general procedure to analytically evaluate the concentration solution in a divergent flow field with a multistep pumping history and a constant injection concentration can be summarized as follows:

- Calculate the analytical solution for a steady-state flow field $c^*(R, \tau)$;
- Transform $c^*(R, \tau)$ into $c^*(r, Q)$ according to the definition of dimensionless groups, i.e., $r = \alpha_L R$ and $Q = 2\pi\theta\alpha_L^2\tau$;
- Evaluate the cumulative pumping function $Q(t) = \int_0^t q dt$;
- Map $c^*(r, Q)$ onto the time domain, $c^*(r, t)$.

The above algorithm is essentially identical to defining the dimensionless time, τ , by:

$$\tau = \frac{1}{2\pi\theta\alpha_L^2}\int_0^t q(t')dt'$$

which removes $q(t)$ from the transport equation and results in the same dimensionless transport equation in a steady-state flow field. Analytical solutions can then be applied and the mapping between t and τ yields the solution on the time domain, similar to the mapping between t and Q. For a known $q(t)$, the mapping can be implemented by numerical methods with very fine discretization in time and linear interpolation. In addition, the developed approach is similar to the time transformation to evaluate concentrations in transient uniform flow fields [*Carlier*, 2008]. However, our algorithm evaluates concentrations on the cumulative flow domain, and time mapping only applies in the end to obtain the regular time solution. This algorithm is more efficient and straightforward and can be conveneintly extended to cases with time-dependent input concentrations (next section).

Multistep pumping with a time-dependent input concentration

For both a multistep well flow rate, $q(t)$, and a time-dependent input concentration, $c_0(t)$, we may discretize the functions into $q(t_0), q(t_1),...$ and $c_0(t_0), c_0(t_1),...$. Consider the simple case with the first two steps: $q_1(0 \le t < t_1), c_1(0 \le t < t_1)$ and $q_2(t_1 \le t < t_2), c_2(t_1 \le t < t_2)$. Following the procedure describe in the previous section, the solution at t_1 is given by:

$$c(r, t_1; q_1, c_1) = c_s(r, Q_1; q_1, c_1) = c_s(r, Q_1; q_2, c_1)$$

That is, the initial solution for the second period can be regarded as a result of the pumping rate q_2 for a total injected flow Q_1 at a constant input concentration c_1. Thus, for the second period, the problem becomes a steady-state flow with a time-dependent input history at the pumping well, which can be solved by linear convolution,

$$c(r, t_2; q_2, c_2) = g(r, Q_1 + Q_2)c_1 + g(r, Q_1)c_2$$

where the transfer function $g(r,Q)$ is given by

$$g(r,Q) = \frac{g(r,t)}{2\pi\theta\alpha_L^2}$$

The general solution on the Q domain is given by:

$$c(r, Q; q(t), c_0(t)) = \int_0^Q g(r, Q')c_0(Q - Q')dQ'$$

where the input concentration is written as a function of Q instead of t. Thus, the procedure to analytically evaluate solute transport in a multistep divergent flow field with a time-dependent input concentration can be summarized as follows:

- Calculate the transfer function $g(r,t)$ in a steady-state flow field;
- Transform $g(r,t)$ into $g(r,Q)$ according to the definition of dimensionless groups;

- Evaluate the cumulative pumping function $Q(t)=\int_0^t q dt$;
- Transform the input concentration history $c_0(t)$ into $c_0(Q)$;
- Evaluate the linear convolution, Eq. (conv);
- Map $c(r,Q)$ onto the time domain, $c(r,t)$.

An Alternative Approach

For an impulse or step concentration input function, the concentration distribution may be written as:

$$c(r,t;q(t))=c\left(r,\int_0^t q dt;q'\right)=c(r,t;\bar{q})$$

where $\bar{q}$ is the mean pumping rate

$$\bar{q}(t)=\frac{1}{t}\int_0^t q dt$$

Thus, the concentration distribution at a time moment is the same to that created by the mean pumping rate within the same time frame. This means one can always assume an effective, constant pumping rate, i.e., the mean pumping rate, in the transport model to describe the spatial concentration distribution at a time moment. To describe concentration distributions at different time moments or concentration breakthrough curves at monitoring points, one needs to use the time-dependent mean flow rate. This provides an alternative approach to evaluate the transport problem: given the q function, one may first evaluate the time-dependent $\bar{q}$ function and the concentration at a time moment t can then be calculated using the analytical solutions by assuming the constant $\bar{q}(t)$. This approach is equivalent to the above approach on the cumulative flow domain because the mean flow rate function essentially reproduces the cumulative flow within the same time frame. In addition, this approach does not require time transformation or mapping because it deals with the problem in the original time frame. However, the alternative approach may not be as convenient as the proposed approach on the cumulative flow domain for a variable input concentration because the transfer function changes with time.

Case Study

In this section, we present two synthetic cases to validate the developed algorithms describe in the previous section. Consider a discrete function for $q(t)$:

$$q(t)=\begin{cases}10\,m^2/d, & 0\le t<20d\\ 8\,m^2/d, & 20d\le t<30d\\ 5\,m^2/d, & 30d\le t<40d\\ 2\,m^2/d, & 40d\le t<50d\\ 10\,m^2/d, & t\ge 50d\end{cases}$$

Associated with the well flow rate, we consider two input concentration profiles at the injection well: one has a discrete concentration history:

$$c_0^*(t) = \begin{cases} 1, & 0 \le t < 20d \\ 0.5, & 20d \le t < 30d \\ 0.2, & 30d \le t < 40d \\ 1, & 40d \le t < 50d \\ 0, & t \ge 50d \end{cases}$$

and the other has a continuous concentration history:

$$c_0^*(t) = 1 + 0.1\sin\left(\frac{\pi t}{10} + \frac{\pi}{2}\right)$$

which represents an input concentration fluctuating around 1. Other parameters include: $r_w = 0.5m$, $\alpha_L = 1m$, and $\theta = 0.3$.

Figure 1 shows the well flow rate history (Figure 1a) and the two input concentration profiles (Figure 1b and 1c). Figure 1d shows the cumulative injected flow, Q , which is the integral function of the multistep pumping rate shown in Figure 1a. Figures 1e and 1f show the input concentration as a function of Q by mapping $c_0^*(t)$ shown in Figures 1b and 1c onto the Q domain.

Figure 2 compares the results of the proposed algorithms with numerical solutions evaluated by the Matlab built-in *ode* solver. The cases compared include: (a) steady-state flow for a constant well injection rate, $q = 10m^2/d$, and a constant input concentration, $c_0^* = 1$, throughout the pumping history; (b) steady-state flow, $q = 10m^2/d$, and the discrete input concentration history described by Eq. (c0t); (c) steady-state flow, $q = 10m^2/d$, and the continuous input concentration history described by Eq. (c0t'); (d) multistep pumping flow created by the pumping history, Eq. (qt), and a constant input concentration, $c_0^* = 1$; (e) multistep pumping flow with the discrete input concentration history; and (f) multistep pumping flow with the continuous input concentration history. For the discrete input concentration case, numerical methods may be conveniently applied by dividing the time into several time intervals with a step of 10 days so that within each time interval the problem becomes a steady-state flow with a constant input concentration. However, for the continuous input concentration, numerical methods are required to divide the time into much smaller intervals to reproduce the continuous function although there are only several steps of pumping. Thus, the continuous case requires more considerations in terms of the spatial and temporal discretization to satisfy the accuracy requirement and to characterize the continuous input function well. The developed algorithms on the basis of the analytical solutions have no such concerns and are much more efficient. Figure 2 shows that the developed algorithms and numerical solutions match very well for all cases.

Figure 3 illustrates the developed algorithms using two cases presented above: one is the multistep pumping with a constant input concentration (Figure 3a-3d), and the other is the multistep pumping with the discrete input concentration described by Eq. (c0t) (Figure 3e-3i). Figure 3a shows the analytical solution in a steady-state radial divergent flow field, i.e., Eq. (Laplace solution) or (steady solution). Such a solution can be conveniently expressed a function of the cumulative injected water, Q , which is a linear function of time (Figure 3b). The solution for the multistep pumping (Figure 3d) is then evaluated by simply mapping Figure 3b from the Q domain to the time domain according to the function of the cumulative injected water (Figure 3c). We shall notice that Figure 3b works for any pumping strategy with a constant input concentration. One only needs to update the mapping function, i.e., Q (Figure 3c), for other pumping strategies. For the case with both time-dependent pumping and input concentrations, Figure 3e provides the transfer functions as a function of Q , which can be analytically evaluated by Eq. (gQ) or numerically by taking the first derivative of Figure 1b. The solution on the Q domain (Figure 1g) is evaluated by the convolution of the transfer function (Figure 3e) with the input concentration function on the Q domain (Figure 3f). The solution on the time domain (Figure 3i) is then evaluated by mapping Figure 1g to the time domain according to the Q function (Figure 1h). Unlike the constant input concentration case, Figure 1g changes with the pumping strategy because the input concentration profile (Figure 1f) changes. Thus, for different pumping strategies, one needs to update Figure 3f and the mapping function (Figure 3h). We can see from the presented case that the developed algorithms completely rely on the available analytical solutions and are very efficient and straightforward.

Transitional Period

The major assumption for the developed approach is that the flow field created by multistep pumping is piecewise-steady state, i.e., the velocity field reaches steady state instantaneously with the pumping rate and the transitional period between two steady-state flow fields can be neglected. In the following, we discuss the conditions for this assumption to be valid from two aspects: one is the critical timescale to reach a "peudo-steady state condition", and the other is mean travel time from the pumping well to a certain point.

Critical Timescale

The velocity $v(r,t)$ for an arbitrary pumping history $q(t)$ can be computed from the velocity $v_\delta(r,t)$, valid for instantaneous pumping of a unit volume, by convolution:

$$v(r,t)=\int_0^t v_\delta(r,t-t')q(t')dt'$$

In an infinite horizontal confined aquifer with an isotropic, homogeneous hydraulic conductivity, the Theis solution yields:

$$v_\delta(r,t)=\frac{rS}{8\pi\theta Tt^2}\exp\left(-\frac{r^2S}{4Tt}\right)$$

where S is the storage coefficient [-], and T is the aquifer transmissivity [L^2/T]. For a one-step pumping case from the static state, the transient velocity is given by:

$$v(r,t) = \frac{q}{2\pi\theta r}\exp\left(-\frac{r^2 S}{4Tt}\right)$$

A "peudo-steady state condition" is defined when velocities reach 99% of their steady-state values, which requires $\left(r^2 S/4Tt\right) \le 0.01$ [*Chen*, 1985]. We may define a critical timescale for velocities to reach the "peudo-steady state condition", t_c ,

$$t_c(r) = \frac{25 r^2 S}{T}$$

which indicates that the critical timescale increases with the radial distance and storage coefficient and decreases with the transmissivity. In order to assume a steady-state flow field, the pumping duration must be longer than the critical timescale [*Harvey et al.*, 1994].

For a multistep pumping profile, we consider the fundamental two-step pumping: $q_1(0 \le t < t_1)$ and $q_2(t_1 \le t)$. When $q_1 = 0$, the two-step pumping reduces to the single-step pumping presented above. The velocity field for the two-step pumping is given by:

$$v(r,t) = \begin{cases} q_1 \int_0^t v_\delta(r,t')dt', & 0 \le t < t_1 \\ q_1 \int_0^t v_\delta(r,t')dt' + \Delta q \int_0^{t-t_1} v_\delta(r,t')dt', & t_1 \le t \end{cases}$$

where $\Delta q = q_2 - q_1$ is the increment of the pumping rate. We assume at the end of the first pumping step the velocity has reached the peudo-steady state and can be approximated by the steady-state velocity, i.e., the pumping duration of the first step is longer than the critical timescale given by Eq. (ts). Thus, the velocity during the transitional period within the second pumping step is approximated by:

$$\begin{aligned} v(r,t) &= \frac{q_1}{2\pi\theta r} + \Delta q \int_0^{t-t_1} v_\delta(r,t')dt' \\ &= \frac{q_1}{2\pi\theta r} + \frac{\Delta q}{2\pi\theta r}\exp\left[-\frac{r^2 S}{4T(t-t_1)}\right], \quad t_1 \le t \end{aligned}$$

We define the critical timescale of the "peuso-steady state condition" for the two-step pumping as the time required for the velocity field to accomplish 99% of the change between two steady-state flow fields, i.e.,

$$\frac{\Delta q}{2\pi\theta r}\exp\left[-\frac{r^2 S}{4T(t-t_1)}\right] = 0.99\frac{\Delta q}{2\pi\theta r}$$

which yields the same critical timescale given by Eq. (ts). Thus, a necessary condition for a multistep pumping field to assume the "peuso-steady state condition" is that the duration of each pumping step, t_p , must be greater than the critical timescale:

$$t_p \geq t_c = \frac{25r^2 S}{T}$$

which can be written as:

$$r \leq \sqrt{\frac{t_p T}{25S}} \textbf{ or } r_{\max} = \sqrt{\frac{t_p T}{25S}}$$

Eq. (rrp) defines the maximum spatial distance for a given pumping period or the maximum domain from the pumping well where the transitional period is possible to be neglected. In addition, we should notice that a very small constant time step or a variable time step may be required to characterize the transitional period within the critical timescale at all locations because the critical timescale varies spatially and is very small near the pumping well.

Mean Travel Time

The above condition in terms of the critical timescale and pumping duration is not sufficient to assume the "peuso-steady state" for transport because it does not directly evaluate the error for solute transport. Here, we further examine the relative error of the mean travel time between the transient and steady-state case to quantify the impact of the transitional period on transport. For a tracer released in the injection well at the moment of pumping change, the relative error of the mean travel time for the tracer plume reaching a certain location is given by:

$$\varepsilon_\tau(r) = \frac{|\tau_t(r) - \tau_s(r)|}{\tau_t(r)}$$

where τ_t and τ_s represent the mean travel time for the transient and steady-state case, respectively. Consider the two-step pumping with pumping rates q_1 and q_2. By integrating the steady-state velocity, Eq. (velocity1), we have:

$$\tau_s(r) = \frac{\pi\theta r^2}{q_2}$$

For the transient case, we have:

$$\frac{dr}{dt} = \frac{q_1}{2\pi\theta r} + \frac{\Delta q}{2\pi\theta r}\exp\left(-\frac{r^2 S}{4Tt}\right)$$

which applies Eq. (vrt2) with the time reset at the end of the first pumping step, t_1. Integrating Eq. (rt) yields the mean travel time for the transient case:

$$\tau_t(r) = r^2\left\{\frac{q_1}{\pi\theta} + \frac{4T}{S}W\left[\frac{S\Delta q}{4\pi\theta T}\exp\left(-\frac{Sq_1}{4\pi\theta T}\right)\right]\right\}^{-1}$$

where $W(\cdot)$ is the Lambert W function [*Corless et al.*, 1996]. Substituting Eqs. (taus) and (taut) into (error), the relative error of the mean travel time, ε_τ, can be evaluated as:

$$\varepsilon_\tau = \frac{\left|\left\{q_1 + \frac{4\pi\theta T}{S} W\left[\frac{S\Delta q}{4\pi\theta T}\exp\left(-\frac{Sq_1}{4\pi\theta T}\right)\right]\right\}^{-1} - q_2^{-1}\right|}{\left\{q_1 + \frac{4T\pi\theta}{S} W\left[\frac{S\Delta q}{4\pi\theta T}\exp\left(-\frac{Sq_1}{4\pi\theta T}\right)\right]\right\}^{-1}}$$

which is not a function of r, indicating that the assumption of a steady-state velocity results in the same relative error of the mean travel time to any locations. Similar to the "peuso-steady state condition", we may require:

$$\varepsilon_\tau \le 0.01$$

Figure 4 shows the relative error of the mean travel time as a function of transmissivity and storage coefficient for a single-step pumping with $q_1 = 0$, $\Delta q = q_2 = 1$ m ^{2} /s and $\theta = 0.3$. The examined range for S is $[10^{-2}, 10^{-6}]$, and for T is $\left[10^{-2}, 10^{-6}\right]$. The contour line in Figure 4a delineates the ranges of T and S for $\varepsilon_\tau \le 0.01$. Figures 4b and 4c show that ε_τ decreases with the increase of T and the decrease of S. Thus, to make the assumption of piecewise steady-state flow fields for a multistep pumping profile, the aquifer should have a large hydraulic conductivity and a small storage coefficient, which essentially decrease the critical timescale defined by Eq. (ts). In fact, for a very small S and a very large T, we have:

$$\lim_{S\to 0, T\to\infty} \varepsilon_\tau = \frac{\left|\left[q_1 + \frac{4\pi\theta T}{S}\left(\frac{S\Delta q}{4\pi\theta T}\right)\right]^{-1} - \left(q_1 + \Delta q\right)^{-1}\right|}{\left[q_1 + \frac{4T\pi\theta}{S}\frac{S\Delta q}{4\pi\theta T}\right]^{-1}} = 0$$

Although Eq. (errortau) and inequality (error0.01) accurately define the conditions for the "peuso-steady state condition", they are not convenient to use. Here, we may compare the critical timescale and the mean travel time in the steady-state flow field to identify an empirical relation for the piecewise steady-state flow field to be valid:

$$\tau_s(r) \ge t_c(r)$$

which implies that the velocity at a certain travel distance has reached the "peudo-steady state condition" before the solute plume arrives at the point. Thus, the plume always moves with a nearly steady-state velocity from the pumping well. Because a multistep pumping profile may involve both positive and negative increment in pumping rates, we may use the maximum pumping rate to evaluate inequality (compare):

$$\frac{\pi\theta r^2}{q_{\max}} \ge \frac{25 r^2 S}{T}$$

Because $q_{\max}$ corresponds to the minimum travel time, inequality (qmax) assures the validity of (compare) for all pumping steps. Thus, we have:

$$\frac{T}{S} \ge \frac{25 q_{\max}}{\pi\theta}$$

Inequality (TS) gives a simple relation to determine whether an aquifer appropriate or not for assuming the "peudo-steady state condition" with a given pumping strategy. We

may write inequality (TS) as:

$$q_{\max} \le \frac{\pi\theta T}{25S}$$

which defines the maximum well pumping rate allowed to satisfy the "peuso-steady state condition" at a given site, i.e., T and S are constant. A larger q implies a shorter travel time to a certain point, while the critical timescale does not change. Therefore, the piecewise-steady state assumption is not valid. Contrarily, a smaller q implies a longer travel time to a certain point than the critical timescale so that the "peuso-steady state condition" is always satisfied. The contour line in Figure 4a and the circles in the bottom of Figures 4b and 4c show the critical cases with $T/S = 25q_2/\pi\theta$ and $\varepsilon_\tau \approx (1/0.99q_2 - 1/q_2)/(1/0.99q_2) = 0.01$. In addition, for a larger acceptable error, one may conveniently modify the critical timescale accordingly to identify appropriate conditions. For example, for a 5% error, $t_c(r) = 4.87r^2S/T$ and $q_{\max} \le \pi\theta T/4.87S$; and for a 10% error, $t_c(r) = 2.37r^2S/T$ and $q_{\max} \le \pi\theta T/2.37S$, which indicate that a larger error allowed, a shorter pumping duration or a larger domain and a larger pumping rate accepted, also shown in Figure 4.

Conclusion

We develop a novel, efficient approach to evaluate solute transport in divergent radial flow fields created by multistep pumping and with an arbitrary input concentration function. By working on the cumulative injected flow domain, $Q(t) = \int_0^t q(t')dt'$, instead of the time domain, the transport problem with a temporally varying velocity field can be transformed into a steady-state flow problem. The fundamental physical principle is that the concentration distribution is completely determined by the total volume of injected water but independent of specific flow rates, i.e., given a constant total injection volume, the final concentration distribution does not change with different pumping strategies. By directly mapping the available analytical solutions in steady-state flow fields according to the relation between the cumulative injected flow and time, one can conveniently evaluate the solution in multistep pumping flow fields. For time-dependent input concentrations, linear convolution can be applied on the Q domain and the solution on the time domain can be obtained by direct mapping. The proposed algorithms are very efficient and accurate because they are completely based on analytical solutions and no spatial and temporal discretization is required. An alternative approach is also proposed by working with the time-dependent mean well pumping rate for an impulse and step input function, which does not require mapping between the cumulative flow and time.

The primary assumption of the developed approach is the piecewise steady-state flow for each pumping rate, i.e., the transitional period between two pumping rates is neglected. We derive important conditions accurately determining the appropriate aquifer properties and pumping operations for the assumption to be valid. The analysis uses the Theis solution to evaluate the critical timescale of "peuso-steady state condition", defined when velocity changes reach 99% of their steady-state differences, and to evaluate the mean travel time of the solute plume from the pumping well for both steady and transient cases.

Simplified but more practical conditions are obtained, which are:

- $t_p \geq 25r^2 S/T$ or $r \leq \sqrt{t_p T/25S}$, where t_p is the pumping duration of a pumping step, r is the radial distance to the pumping well, S is the storage coefficient, and T is the transmissivity.
- $q_{\max} \leq \pi\theta T/25S$, where θ is the effective porosity and $q_{\max}$ is the maximum well pumping rate.

The first condition yields the minimum pumping duration or the maximum problem domain, which essentially implies that the transitional period may be negligible when the pumping periods are much longer than the critical timescale to reach steady state or in the vicinity of the pumping well. The second condition defines the maximum pumping rate allowed in a site for a multistep pumping strategy. When both conditions are satisfied, one may neglect the transitional periods between pumping steps and assume a piecewise steady-state flow field. Furthermore, if one considers T as the single parameter that varies most in natural aquifers, the two conditions imply that the "peuso-steady state" is more likely to be satisfied in high-conductivity aquifers or more likely to fail in low-conductivity aquifers.

Acknowledgement

This research was sponsored by the National Institutes of Water Resources (NIWR) and U.S. Geological Survey (USGS) under project ID 2007GA165G. We would like to thank three anonymous reviewers for their constructive comments.

References:

Becker, M.W., and R.J. Charbeneau (2000), First-passage-time transfer functions for groundwater tracer tests conducted in radially convergent flow, *J. Contam. Hydrol.*, *40*, 299-310.

Butler, J., Jr., and C. McElwee (1990), Variable-Rate Pumping Tests for Radially Symmetric Nonuniform Aquifers, Water Resour. Res., 26(2), 291-306.

Carlier, E. (2008), Analytical solutions of the advection-dispersion equation for transient groundwater flow. A numerical validation, *Hydrol. Process.*, *22*, 3500-3506.

Chen, C.-S. (1985), Analytical and approximate solutions to radial dispersion from an injection well to a geological unit with simultaneous diffusion into adjacent strata, *Water Resour. Res.*, *21*, 1069-1076.

Chen, C.-S. (1986), Solutions for radionuclide transport from an injection well into a single fracture in a porous formation, *Water Resour. Res.*, *22*, 508-518.

Chen, C.-S. (1987), Analytical solutions for radial dispersion with Cauchy boundary at injection well, *Water Resour. Res.*, *23*, 1217-1224.

Chen, C.-S., and G.D. Woodside (1988), Analytical solution for aquifer decontamination by pumping, *Water Resour. Res.*, *24*, 1329-1338.

Corless, R.M., G.H. Gonnet, D.E.G. Hare, D. J. Jeffrey, and D. E. Knuth (1996), On the

Lambert W Function, *Adv. Comp. Math.*, *5*, 329-359.

de Hoog, F. R., J. H. Knight, and A. N. Stokes (1982), An improved method for numerical inversion of Laplace transforms, *SIAM J. Sci. Stat. Comput.*, *3*, 357-366.

Goltz, M.N., and M.E. Oxley (1991), Analytical modeling of aquifer decontamination by pumping when transport is affected by rate-limited sorption, *Water Resour. Res.*, *27*, 547-556.

Harvey, C.F., R. Haggerty, and S.M. Gorelick (1994), Aquifer remediation: a method for estimating mass transfer rate coefficients and evaluation of pulsed pumping, *Water Resour. Res.*, *30*, 1979--1991.

Hoopes, J. A., and D. R. F. Harleman (1967), Dispersion in radial flow from a recharge well, *J. Geophys. Res.*, *72*, 3595-3607.

Hsieh, P. A. (1986), A new formula for the analytical solution of the radial dispersion problem, *Water Resour. Res.*, *22*, 1597-1605.

Huang, J., J.A. Christ, and M.N. Goltz (2010), Analytical solutions for efficient interpretation of single-well push-pull tracer tests, *Water Resour. Res.*, *46*, W08538.

Huang, J., and M.N. Goltz (2006), Analytical solutions for solute transport in a spherically symmetric divergent flow field, *Trans. Porous Media*, *63*, 305-321.

Indelman, P., Dagan, G. (1999), Solute transport in divergent radial flow through heterogeneous porous media, *J. Fluid. Mech.* 384, 159-182.

Luo, J., O.A. Cirpka, M.N. Fienen, W.-M. Wu, T.L. Mehlhorn, J. Carley, P.M. Jardine, C.S. Criddle, and P.K. Kitanidis (2006), A parametric transfer function methodology for analyzing reactive transport in nonuniform flow, *J. Contam. Hydrol.*, *83*, 27-41.

Moench, A.F. (1995), Convergent radial dispersion in a double-porosity aquifer with fracture skin: Analytical solution and application to a field experiment in fractured chalk, *Water Resour. Res.*, *31*, 1823-1835.

Moench, A.F. (1989), Convergent radial dispersion: A Laplace transform solution for aquifer tracer testing, *Water Resour. Res.*, *25*, 439-447.

Moench, A, F., and A. Ogata (1981), A numerical inversion of the Laplace transform solution to radial dispersion in a porous medium, *Water Resour. Res.*, *17*, 250-252.

Neuweiler I, Attinger S, Kinzelbach W (2001), Macrodispersion in a radially diverging flow field with finite Peclet numbers 1. Perturbation theory approach, *Water Resour. Res.*, 37, .

Novakowski, K.S. (1992), The analysis of tracer experiments conducted in divergent radial flow fields, *Water Resour. Res.*, *28*, 3215-3225.

Singh, S.K. (2002), Well loss estimation: Variable pumping replacing step drawdown test, *J. Hydraul. Engr.-ASCE*, 128, 343-348.

Shackelford, C.D. (1995), Cumulative mass approach for column testing, *J. Geotech. Engr.-ASCE*, 121, 696-703.

Tang, D. H., and D. K. Babu (1979), Analytical solution of a velocity dependent

dispersion problem, *Water Resour. Res.*, *15*, 1471-1478.

Tomasko, D., G.P. Williams, and K. Smith (2001), An analytical model for simulating step-function injection in a radial geometry, *Math. Geol.*, 33, 155-165.

Figure 1

Numerical cases for testing developed algorithms for analytically evaluating solute transport in divergent radial flow with multistep pumping and time-dependent input concentrations. (a) well flow rate; (b) a discrete input concentration profile; (c) a continuous input concentration profile; (d) cumulative injected flow; (e) the discrete input concentration as a function of cumulative injected water; and (f) the continuous input concentration as a function of cumulative injected water.

Figure 2

Comparison of analytical solutions with numerical solutions for multistep pumping and time-dependent input concentrations. (a) steady-state flow and a constant input concentration; (b) steady-state flow and discrete input concentrations; (c) steady-state flow and continuous input concentrations; (d) multistep pumping flow and a constant input concentration; (e) multistep pumping flow and discrete input concentrations; and (f) multistep pumping flow and continuous input concentrations.

Figure 3

Illustration of developed algorithms: (a) - (d) multistep pumping with a constant input concentration; and (e) - (i) multistep pumping with the discrete input concentration history. (a) concentration profiles for a unit step pumping and a constant input concentration; (b) concentration profiles as a function of Q ; (c) function of the cumulative injected water for the multistep pumping case; (d) concentration profiles mapped from (b) according to (c); (e) concentration transfer functions as a function of Q ; (f) input concentration as a function of Q ; (g) concentration profiles on the Q domain evaluated by the convolution of (e) and (f); (h) function of the cumulative injected water for the multistep pumping case, the same as (c); and (i) concentration profiles mapped from (g) according to (h).

Figure 4

Relative error in the mean travel time, ε_τ , between the steady-state and transient flow field for a single-step pumping with a pumping rate of 1m ^{2} /s and θ = 0.3. (a) ε_τ as a function of both T and S and the contour lines of 0.01, 0.05 and 0.1; (b) ε_τ as a function of T for fixed S ; and (c) ε_τ as a function of S for fixed T . The circles in (b) and (c) represent the cases with relative errors of 0.01, 0.05 and 0.1.

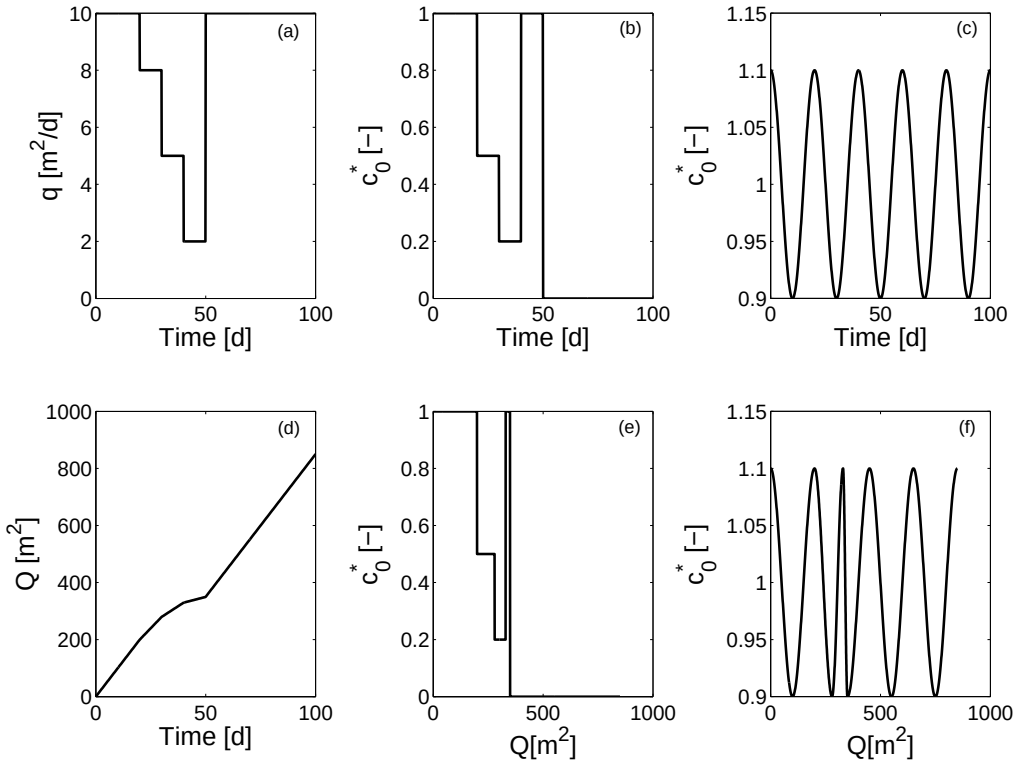

Figure 1

Numerical cases for testing developed algorithms for analytically evaluating solute transport in divergent radial flow with multistep pumping and time-dependent input concentrations. (a) well flow rate; (b) a discrete input concentration profile; (c) a continuous input concentration profile; (d) cumulative injected flow; (e) the discrete input concentration as a function of cumulative injected water; and (f) the continuous input concentration as a function of cumulative injected water.

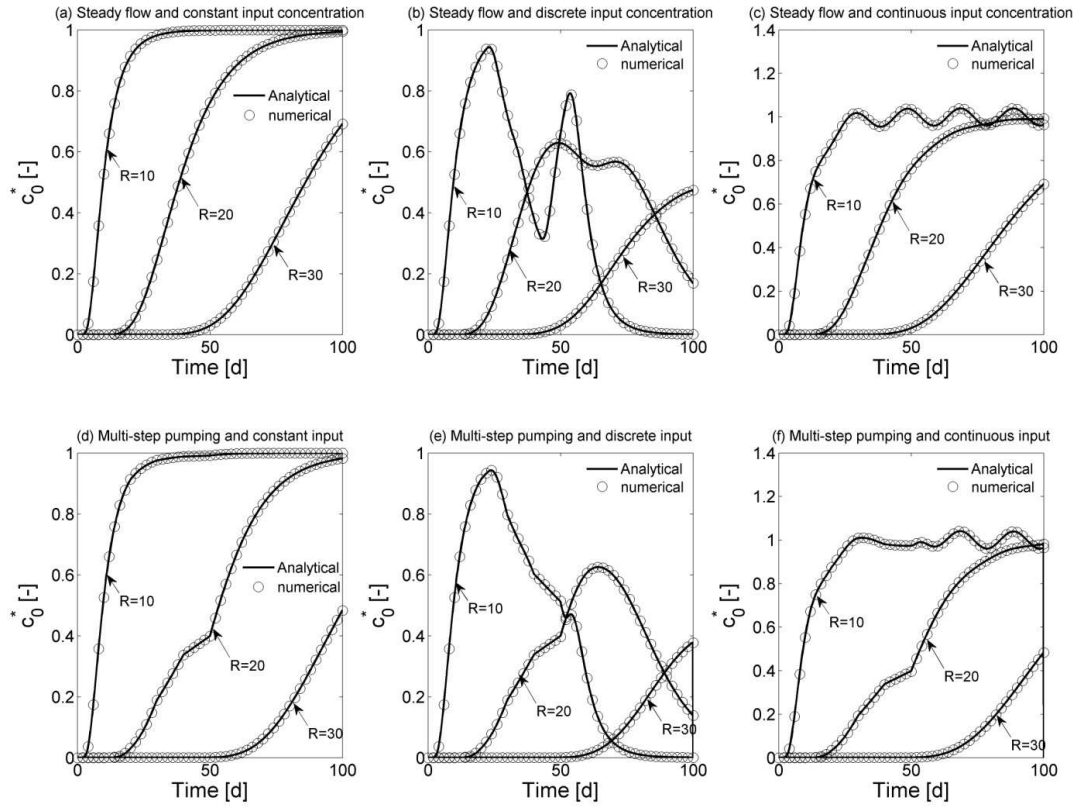

Figure 2

Comparison of analytical solutions with numerical solutions for multistep pumping and time-dependent input concentrations. (a) steady-state flow and a constant input concentration; (b) steady-state flow and discrete input concentrations; (c) steady-state flow and continuous input concentrations; (d) multistep pumping flow and a constant input concentration; (e) multistep pumping flow and discrete input concentrations; and (f) multistep pumping flow and continuous input concentrations.

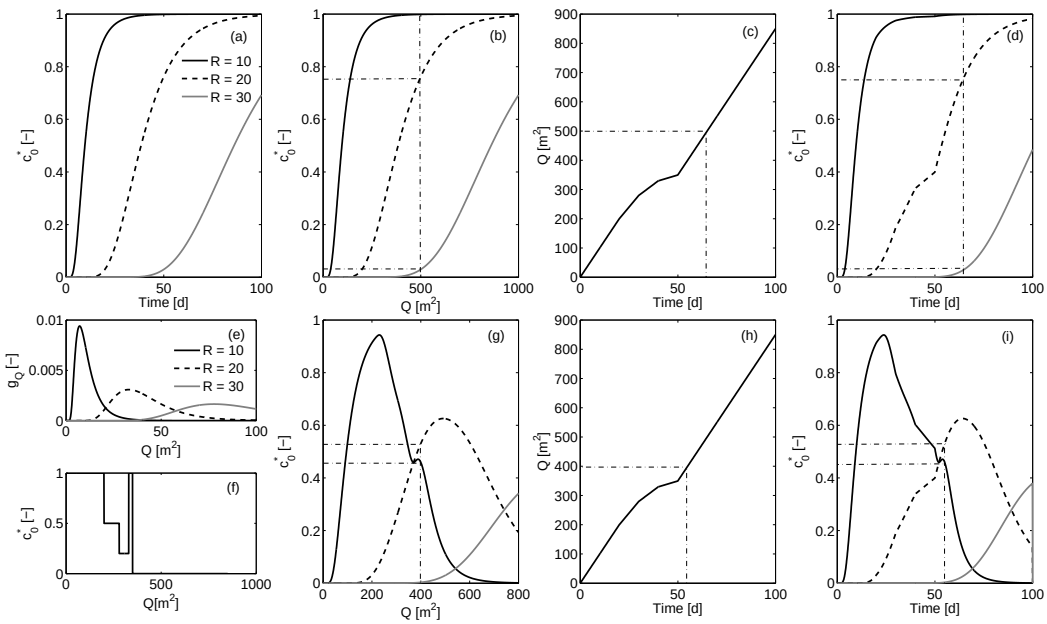

Figure 3

Illustration of developed algorithms: (a) - (d) multistep pumping with a constant input concentration; and (e) - (i) multistep pumping with the discrete input concentration history. (a) concentration profiles for a unit step pumping and a constant input concentration; (b) concentration profiles as a function of Q; (c) function of the cumulative injected water for the multistep pumping case; (d) concentration profiles mapped from (b) according to (c); (e) concentration transfer functions as a function of Q; (f) input concentration as a function of Q; (g) concentration profiles on the Q domain evaluated by the convolution of (e) and (f); (h) function of the cumulative injected water for the multistep pumping case, the same as (c); and (i) concentration profiles mapped from (g) according to (h).

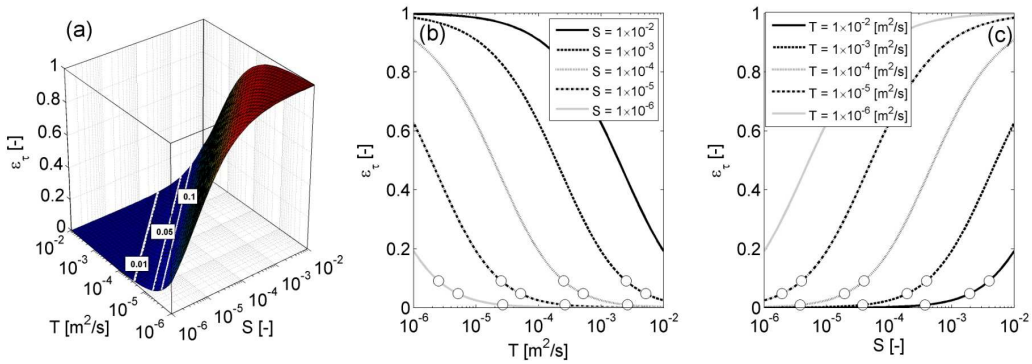

Figure 4

Relative error in the mean travel time, ε_τ , between the steady-state and transient flow field for a single-step pumping with a pumping rate of 1m ^{2} /s and θ = 0.3. (a) ε_τ as a function of both T and S and the contour lines of 0.01, 0.05 and 0.1; (b) ε_τ as a function of T for fixed S ; and (c) ε_τ as a function of S for fixed T . The circles in (b) and (c) represent the cases with relative errors of 0.01, 0.05 and 0.1.

Chap. 3

Freshwater-Seawater Mixing Zone in Stratified Coastal Aquifers

Abstract

Laboratory experiments and numerical simulations were conducted to show that aquifer stratification has significant impact on the distribution of the freshwater-seawater mixing-zone in coastal aquifers. When an aquifer layer with a lower hydraulic conductivity overlies a layer with a higher conductivity, slanting upward flow of diluted saltwater and circulated seawater flow are refracted at the interface between layers, resulting in streamline separation and a broad mixing zone in the lower hydraulic conductivity layer. By contrast, the mixing zone in a high conductivity layer is narrowed when it overlies a layer with a lower conductivity because flow refraction squeezes the streamlines within the mixing zone. Sensitivity analysis shows that increasing the magnitude of stratified heterogeneity would lead to the retreat of the toe and first increase and then decrease of the mixing-zone thickness, indicating that the neglect of aquifer stratification would overestimate seawater intrusion. Our results have demonstrated the significant impact of aquifer stratification on controlling groundwater flow and solute transport in the coastal subsurface environments and would have significant implications for studying physical, chemical, and biological processes in coastal subsurface environments, as aquifer stratification is prevalent in coastal regions.

1. Introduction

The mixing zone between freshwater and intruding seawater, which controls regional groundwater flow dynamics and reactive transport processes, is the most important component in coastal aquifers [e.g., *Cooper*, 1959; *Henry*, 1964; *Moore*, 1999; *Charette and Sholkovitz*, 2002; *Michael et al*., 2005; *Rezaei* et al., 2005; *Spiteri et al*., 2008]. It delineates the subsurface into regions with distinct fluid density and biogeochemical properties and controls the subsurface flow field and water exchange between groundwater and ocean environments with associated important transport processes (see Figure 1) such as seawater intrusion [2,3], submarine groundwater discharge (SGD) [4-6], and reactive transport processes [5, 7-9]. In addition, studies have shown that the mixing zone is a chemically-active environment and serves as a potential reaction site for extensive dissolution, aragonite neomorphism, and dolomitization of carbonate rocks [e.g., *Back et al*., 1979; *Randazzo and Bloom*, 1985; *Back et al*., 1986; *Randazzo et al*., 1987; *Budd et al*., 1988; *Smart et al*., 1988].

Under steady-state conditions, the thickness of a mixing zone depends basically on local dispersion. Specifically, local longitudinal dispersion on macroscopic transport in heterogeneous domains is of minor importance, while local transverse dispersion, by contrast, significantly contributes to solute mixing between freshwater and seawater bodies and has been widely recognized as a leading factor responsible for the thickness of a steady-state mixing zone [*Dagan*, 2006]. An increasing transverse dispersivity would have a shear effect, bringing the steady mixing zone seaward at the bottom and landward at the top and finally creating a broader mixing zone [*Abarca et al*., 2007]. However, pore-scale transverse dispersion only cause the presence of a thin mixing zone, as already visualized by many laboratory experiments [*Zhang et al*., 2002; *Goswami and Clement*, 2007; *Abarca and Clement*, 2009]. Thick mixing zones, ranging from hundreds of feet to miles, have been detected in many coastal aquifers all over the world [*Kohout*, 1964; *Wu et al*., 1993; *Xue et al*., 1993; *Price et al*., 2003; *Barlow*, 2003; *Dausman and Langevin*, 2005; *Cherry*, 2006]. For example, the width of the mixing zone in the surficial Biscayne aquifer of the Miami area, Florida, US, reaches several hundreds of miles, and is still increasing [*Kohout*, 1964; *Dausman and Langevin*, 2005]. Transverse dispersion coefficients derived in many field experiments are often small, with which only a thin mixing zone can be created [e.g., *Fiori and Dagan*, 1999; *Lebbe*, 1999]. In practice, thick mixing zones are usually created by assuming a large, perhaps unwarranted, value of transverse dispersivity. In other words, a large transverse dispersivity only provides a convenient way to reproduce the thick mixing zones found in reality, but sometimes seems to be unreasonable and holds a poor physical meaning [*Dagan*, 2006]. The theoretical analyses by *Held et al*. [2005] indicated that use of macroscopic dispersion coefficient is inappropriate and the effective dispersion coefficients are more close to the local-scale coefficients. Therefore, there should be some undetected mechanisms which could lead to thick mixing zones in coastal regions.

In past decades, a number of numerical studies targeted at simulating the mixing zone have been conducted in an attempt to gain better understanding of the mechanisms response for the mixing-zone development [e.g., *Volker and Rushton*, 1982; *Ataie-Ashtiani et al*., 1999, *Cartwright et al*., 2003; *Chen and Hsu*, 2004; *Abarca et al*., 2006; *Karasaki et al*., 2006; *Lu et al*., 2009; *Lu and Luo*, 2010]. In addition to

dispersion/diffusion, factors affecting flow and mixing in mixing zone mainly include: (1) transient tidal activities; (2) inland water table fluctuations; (3) kinetic mass transfer; and (4) hydraulic heterogeneity. *Ataie-Ashtiani et al*. [1999] and *Chen et al*. [2004] showed that tidal activities force the seawater to intrude further inland and also creates a thicker interface in comparison to a steady-state mixing zone. Field observations on an unconfined coastal aquifer in Australia suggested that the wave-induced groundwater pulse can cause significant oscillations in the mixing zone of the order of several meters in the horizontal direction [*Cartwright et al*., 2004]. By contrast, tidal fluctuations are unlikely to cause large interface fluctuations because damping of the tidal signal is much higher than that of the pulse signal [*Cartwright et al*., 2003; *Li et al*., 2004]. On the other hand, it is now becoming increasingly evident that inland water table fluctuations in response to pumpage, rainfall, and upstream canal stage would lead to monthly, yearly or decadal oscillations of the mixing zone. This long-term movement of the mixing zone, coupled with kinetic mass transfer effects, can significantly enhance the thickness of the mixing zone [*Lu et al*., 2009, *Lu and Luo*, 2010].

Heterogeneity in hydraulic conductivity of the formation perturbs flow over various length scales and is expected to play a very important role in the behavior of density-dependent systems [*Schincariol and Schwartz*, 1990; *Simmons et al*., 2001]. Most of previous studies regarding the effect of heterogeneity on density dependent flow focused on unstable configurations, i.e., the presence of higher density fluid over lower density fluid [e.g., *Schincariol and Schwartz*, 1990; *Schincariol et al*., 1997, *Schincariol*, 1998; *Prasad and Simmons*, 2003; *Post and Simmons*, 2010]. However, the effect of heterogeneity on stable configurations, namely, seawater intrusion problems, has little been studied [*Held et al*., 2005; *Abarca et al*., 2006; *Kerrou and Renard*, 2010]. *Abarca et al*. [2006] showed that the effects of moderate heterogeneity with random distribution on increasing the steady state mixing-zone thickness are small. In particular, there is very limited research regarding the effects of stratified heterogeneity on the mixing-zone development [e.g., *Oki et al*., 1998; *Nakagawa et al*., 2000], although several analytical solutions based on the sharp-interface approximation have been derived for locating the interface position [*Rumer and Shiau*, 1968; *Mualem and Bear*, 1974; *Essaid*, 1990]. In fact, the role of aquifer stratification on flow and transport in coastal aquifers is expected to be especially important since slanting upward flow of diluted saltwater and circulated seawater always occurs at the interface, which can be refracted from one layer to the other due to permeability contrast and thus would have significant impacts on the development of a mixing zone.

In this work, we carry out both experimental and numerical investigation of aquifer stratification effects on the shape, location, and thickness of a steady-state mixing zone. The experiment is conducted at laboratory scale through a flow tank. Subsequently, numerical simulations are employed to reproduce corresponding experimental cases and to provide theoretical explanations on observed phenomena. Finally, a field-scale model is designed to further demonstrate the effects of aquifer stratification on the mixing-zone development. The main objective of this study is to compare and contrast the mixing-zone profile in homogeneous and stratified formations and therefore to assess its importance with varying stratified heterogeneity on the pattern of the mixing-zone development. Most importantly, the mechanisms response for mixing enhancement in stratified aquifers are expected to be explained in this study, which would have great

implications for investigating flow and transport processes in coastal subsurface environments.

2. Experimental setup

Laboratory experiments on flow and transport in coastal aquifers were previously conducted by several researchers [e.g., *Zhang et al*., 2002; *Goswami and Clement*, 2007]. Our experiments were performed in a flow tank 1800 mm long, 600 mm high, and 100 mm wide, which is similar to that used in the work of *Zhang et al*. [2002]. The experimental setup is shown in Figure 1. Real coastal sands with two specifications were parked in the flow tank as porous media to form simple aquifer stratification with three horizontal layers. The porosity and the hydraulic conductivity measured for one specification (S1) of sands were 0.357 and 1.52 mm s^{-1}, and the other (S2) 0.368 and 0.297 mm s^{-1}, respectively. Salt (NaCl) solution was used as the seawater source. Dye with bright red color was added into salt solution to visualize the developed steady-state mixing zone. The concentration of salt-dye solution was prepared as 35 kg m^{-3}. The longitudinal dispersivities measured by column tests for salt solution transporting in two kinds of sands were 1.82 mm (S1) and 1.25 mm (S2), respectively. The value of transverse dispersivity was assumed to be one order of magnitude less than that of corresponding longitudinal dispersivity. The freshwater and saltwater heads were 440 mm and 428 mm, respectively, and maintained constant through two constant-head cells.

3. Numerical Simulations

The density-dependent groundwater flow code, SEAWAT-2000, is employed to simulate various cases in this study [*Langevin et al.*, 2003]. SEAWAT-2000 is based on groundwater flow code, MODFLOW-2000 and the solute transport code, MT3DMS, which has been extensively used in simulating coastal groundwater flow and transport problems [e.g., *Robinson et al*., 2006; *Lu et al*., 2009; *Lu and Luo*, 2010].

3.1. Governing Equations

The governing equation for saturated variable-density groundwater flow used by SEAWAT-2000 in terms of freshwater head is described by:

$$\nabla \cdot \left[\rho K \left(\nabla \cdot h_f + \frac{\rho - \rho_f}{\rho_f} \cdot \nabla z \right) \right] = \rho S_f \frac{\partial h_f}{\partial t} + \theta_e \frac{\partial \rho}{\partial t} - \rho_s q_s$$

(1)

Where z [L] is the vertical coordinate directing upward; K [LT^{-1}] is the equivalent freshwater hydraulic conductivity; h_f [L] is the equivalent freshwater head; ρ [ML^{-3}] is the fluid density; ρ_f [ML^{-3}] is the freshwater density; S_f [L^{-1}] is the equivalent freshwater storage coefficient; t [T] is the time; θ_e [-] is the effective porosity; and ρ_s [ML^{-3}] and q_s [T^{-1}] are the density and flow rate per unit volume of aquifer of the source/sink, respectively.

The governing equation for transport is given by:

$$\frac{\partial C}{\partial t} + \nabla \cdot (\vec{v}C) - \nabla \cdot (\mathbf{D}\nabla C) + q_s C_s = 0$$
(2)

Where C [ML^{-3}] is dissolved concentration; C_s [ML^{-3}] is dissolved concentration in the source zone; **D** [L^2T^{-1}] is the hydrodynamic dispersion coefficient tensor; $\vec{v}$ [LT^{-1}] is the pore water velocity. The relationship between the fluid density and salt concentration is represented by a simple linear function of state:

$$\rho = \rho_f + \varepsilon C$$
(3)

where ε [-] is a dimensionless constant having a value of 0.7143 for salt concentrations ranging from zero to that of seawater [*Langevin et al*., 2003].

3.2. A Field Scale Model

In addition to a tank scale model, a field scale model shown in Figure 2 was designed to further study effects of aquifer stratification on the mixing-zone development. The simulation domain extended 330 m landward and 70 m seaward from the shoreline. The height of the model domain was 42 m. The entire domain was divided into two zones: an ocean zone and an aquifer zone, which are separated by a slanted beach. The beach slope was 0.1 in the nearshore region. A high hydraulic conductivity (>10 m s^{-1}), an effective porosity of 1, and a constant saltwater concentration of 35 kg m^{-3} were assigned to the ocean zone to approximate free saltwater zone. In addition, a horizontal strip of cells (in red) were added on the top of the ocean surface to avoid a sloping ocean surface [*Brovelli et al*., 2007]. The aquifer has three horizontal layers with the heights from bottom to top being 10 m, 10 m, and 20.2 m, representing simple coastal aquifer stratification. The constant freshwater (blue color) and seawater (red color) heads were 40.2 m and 39 m, respectively. The aquifer was assumed isotropic with porosity being 0.4, longitudinal dispersivity and transverse dispersivity being 0.5 m and 0.05 m, respectively. The upper boundary is a phreatic surface with negligible groundwater recharge. The bottom of the domain is a no-flow boundary, which represents an impermeable aquifer base. 14 cases with different hydraulic conductivity combinations in three layers are chosen to conduct steady-state simulations (see Table 2).

3.3. Grid Spacing

Numerical simulations were conducted for both experimental cases and field-scale cases. Previous studies on variable density flow have indicated that the grid size is a critical factor that controls the accuracy of simulation results [e.g., *Voss and Souza*, 1987; *Schincariol et al*., 1994; *Mazzia et al*., 2001; *Diersch and Kolditz*, 2002]. A common criterion used to ensure that the grid spacing is acceptable is the Péclet number *Pe* [*Voss and Souza*, 1987]:

$$Pe = \frac{v\Delta L}{D_m + \alpha_L v} \approx \frac{\Delta L}{\alpha_L} \leq 4$$
(4)

where v [LT^{-1}] is the local seepage velocity, D_m [L^2T^{-1}] is the molecular diffusion coefficient, and ΔL [L] the grid spacing. The entire domain was discretized into a uniform grid with a cell size of 5 mm × 5 mm for the tank scale case and 0.5 m × 1 m for the filed scale case, respectively, yielding corresponding *Pe* of 4 and 2. The results of additional simulations with double mesh resolution show that the selected schemes of grid spacing are acceptable.

4. Results and Discussion

4.1. Experimental Observation and Simulation Results

Figure 3 shows the photographs of laboratory experiment results of quasi-steady-state mixing zone in the flow tank. Our laboratory experiments demonstrate that aquifer stratification can significantly impact the steady-state mixing-zone profile. As shown, a relatively uniform and narrow mixing zone forms due to density gradients between freshwater and saltwater and local dispersion in the roughly homogeneous sands, which is similar to those found in previous laboratory experiments [*Zhang et al*., 2002; *Goswami and Clement*, 2007]. However, a much broader mixing zone is observed in a lower-*K* layer overlying a higher-*K* layer in the case B. By contrast, the mixing zone in a higher-*K* layer overlying a lower-*K* layer is slightly narrowed in the case C. Moreover, the toe of the interface in this case significantly retreats seaward in comparison to other two cases.

Numerical simulations of density-coupled groundwater flow and solute transport reproduce the mixing zones observed in the experiments (Figure 4). Across the mixing zone, the salt concentration and fluid density gradually increase from freshwater to saltwater. The density gradient within the mixing zone causes the rise of diluted saltwater flow and flow circulation as the seawater moves towards the mixing zone to replace the diluted saltwater. In the presence of aquifer stratification, when slanting upward flow of diluted saltwater and circulated saltwater flow penetrates from a lower layer to an upper layer, flow refraction occurs. According to refraction law ($\tan \beta'/\tan \beta'' = K''/K'$), when streamlines slantingly penetrate from a higher-*K* layer into a lower-*K* layer, the refraction angle will less than the injection angle, resulting in the rise of the refracted streamlines (Figure 5A); by contrast, when streamlines slantingly penetrate from a lower-*K* layer into a higher-*K* layer, the refraction angle will larger than the injection angle, resulting in the decline of the refracted streamlines (Figure 5B) [*Bear*, 1972]. By using the potential theory and neglecting mixing between freshwater and saltwater, *Rumer and Shiau* [1968] showed that the refraction law is applicable to the interface between two layers. As a result, as streamlines penetrate from a higher-*K* layer to a lower-*K* layer, the risen streamlines enhance the separation of streamlines of the freshwater-saltwater mixture and resulting in a thicker mixing zone in which the streamline and concentration contour line are parallel, as shown in Figure 4B. By contrast, when the streamlines pass from a lower-*K* layer to a higher-*K* layer, refraction squeezes the streamlines and narrows the mixing zone in the higher-*K* layer, as shown in Figure 4C. It should be noted that our experimental findings are consistent with the field observation results of a layered costal aquifer system, Oahu, Hawaii, USA, where a thicker mixing zone was found in a low-permeability caprock layer overlying a highly permeable volcanic aquifer [*Oki et al*., 1998].

Figure 6 shows the velocity vector filed in the experimental case B. Due to a lower value of *K*, the flow velocities in the middle layer are significantly smaller than those in other two layers. At distances very far from the saltwater boundary, the flow directions in three layers are all horizontal, indicating that flow is not affected by saltwater. Theoretically, this inland specific flow rate in a specific layer can be calculated by:

$$q_i = \frac{K_i Q}{\sum_i^3 b_i K_i}$$

(5)

where b_i is height of layer *i*; K_i and q_i are hydraulic conductivity and specific flow rate in the layer *i*, respectively; and *Q* is the total flow rate, which is dependent on head gradient. As it approaches the interface, however, the flow direction in the middle layer, i.e., the lower-*K* layer, is first altered and tends to penetrate the interface between the top and middle layers. It is interesting that the loss of initial freshwater does not result in decreasing flow velocity. Instead, the flow velocity in this layer becomes larger and larger when it is close to the interface because of the recharged flow from the bottom layer. However, within the mixing zone, the flow velocity decreases as concentration increases. The similar behavior is also found in other layers (or elevations) as demonstrated in Figure 7, where variations of velocity at five different elevations are shown. It can be seen that within the mixing zone, velocities at all elevations significantly decrease as concentration increases. Therefore, it is possible to obtain an approximate mixing-zone profile according to a known velocity field.

4.2. Simulation Results of Filed Scale Cases

4.2.1. Effects on Mixing Zone and Flow Field

Figure 8 shows the developed mixing zones and streamlines in one homogenous case and two stratified cases. For the stratified cases, the value of *K* in the middle layer is assumed to be one order of magnitude lower (Model 2) and higher (Model 3) than that of the remaining part of the aquifer, respectively. The simulation results for the field-scale models are similar to our experimental results: mixing can be enhanced or weakened by flow refractions. It is clearly shown that in the simulation result of Model 3, the mixing zone in the middle layer is narrowed since the value of *K* in this layer is higher than that of the bottom layer, while the mixing zone in the top layer is widened because of the reversed condition.

In addition, one can observe that in homogeneous case all recirculated water all comes from the top ocean zone. This simulation result was also previously shown by other researchers [e.g., *Robinson et al*., 2007]. However, in the presence of aquifer stratification, recirculated water partially comes from right seaward boundary. Furthermore, simulation results indicate that aquifer stratification significantly alters the flow paths of freshwater, seawater, and the mixture of both. Therefore, one can conclude that aquifer stratification can have important impacts on altering various components of SGD.

4.2.2. Sensitivity Analysis

Figure 9 shows the simulation results of two homogeneous (Models 1 and 4) and four stratified cases (Models 2, 3, 5, and 6). For Models 2 and 5, and Models 3 and 6, the ratio of K between corresponding two layers is exactly the same, i.e., the inland specific flow rates (q_i) in corresponding layers are constant since the thicknesses of three layers keep constant. The results infer that the mixing-zone development under the steady-state condition in homogeneous aquifer is independent of K, which also can be deduced from Eq. (1). It is interesting that the mixing-zone profiles in Models 2 and 5, and Models 3 and 6 are almost the same, indicating that the ratio of $K_1/K_2/K_3$ (or $q_1/q_2/q_3$) controls the steady-state mixing-zone profile in stratified aquifer cases, although the timescales to reach the steady state may be different.

Figure 10 shows the sensitivity analysis results for the effects of magnitude of stratified heterogeneity on the mixing-zone development. It is shown that increasing heterogeneity, for both cases, causes the mixing zones become more vertical in the lower-K layer overlying a higher-K layer due to flow refraction. Apparently, the vertical mixing zone is created by vertical flow in the lower-K layer refracted from a lower higher-K layer due to an extremely high contrast of K between these two layers. *Oki et al.* [1998] found that groundwater flow is predominantly upward in the low-permeability sedimentary units in a layered coastal aquifer system, where the ratio of K between a higher-K and a lower-K layer in their case is larger than 100. Based on the assumption that the flow in the low-K layer is vertically upward, *Mualem and Bear* [1974] derived an analytical solution for the shape of the steady-state interface in a coastal aquifer where a thin horizontal semipervious layer is present. Our simulation results suggest that when q (or bK) of a layer is two orders of magnitude smaller than that of a lower layer, the flow and the mixing zone are almost vertically distributed in this lower-K layer. As the contrast between K_1 and K_2 is further increased, the mixing zone in the lower-K layer above a higher-K layer would gradually move seaward. As a result, the position of the toe retreats seaward accordingly. This indicates that the neglect of aquifer stratification may lead to overestimation of seawater intrusion. For the case where in the middle layer has a lower K, an extremely high heterogeneity could lead to the discontinuity of the mixing zone. Under such conditions, the sharp-interface solution derived by *Rumer and Shiau* [1968] is not correct because their solution is based on the continuity of the interface.

Figure 11 shows the quantitative effects of magnitude of stratified heterogeneity on the toe position, normalized total mass in the lower-K layer, and the position of the mixing zone (2.5% to 97.5% of saltwater concentration) in the lower-K layer. For all cases, $K_1 = K_3 \geq K_2$. The toe position is assumed at 50% of saltwater concentration. The normalized total mass is defined as the total mass in the lower-K layer normalized by the total mass in the corresponding part in the homogeneous case. It can be seen that with the increased ratio of K_1/K_2, the toe position gradually moves seaward, which indicates that the presence of a strong stratified heterogeneity in coastal aquifers would lead to the alleviation of seawater intrusion. On the other hand, the mixing zone in the middle layer first moves landward and then seaward after K_1/K_2 is larger than one order of magnitude, resulting that normalized total mass in the middle layer has same behavior. Similarly, the mixing-zone width in the middle layer is first increased and then decreased due to retreat of the mixing zone. For a limiting case where K_2 is infinitely small, which represents an

impermeable layer in coastal aquifers, the toe of the interface is found closest to the seaward boundary.

Figure 12 further demonstrates the importance of layer placement on the mixing-zone profiles. Simulation results are for two cases with same magnitude of stratified heterogeneity but with different layer placements, where $K_1/K_2/K_3$ = 1/10/100 in Model 13 and $K_1/K_2/K_3$ = 100/10/1 in Model 14. The significant differences in the location, shape, and thickness of the mixing zone are observed for these two cases. In Model 13, as expected, the thickness of the mixing zone becomes thicker and thicker from bottom to top, since flow refraction leads to the continuously increased mixing enhancement. Also, the pattern of flow refraction from a higher-*K* layer into a lower-*K* layer results in the retreat of the mixing zone and the toe. By contrast, in Model 14, the position and the thickness of the mixing zone is similar to that in the homogeneous case. Therefore, such aquifers can be approximately regarded as homogeneous ones when determining the shape of the interface.

4.3. Effects of Transient flow conditions

Previous studies have demonstrated that transient flow conditions in coastal aquifers may have significant effects on the mixing zone development [e.g., *Ataie-Ashtiani et al*., 1999; *Dausman and Langevin*, 2005; *Lu et al*., 2009; *Lu and Luo*, 2010]. According to the Ghyben-Herzberg equation the effect of freshwater level fluctuations on the interface position is much more significant than that created by saltwater level fluctuations. Here, we simply study a scenario that boundary freshwater level experiences an instantaneous decrease from 40.2 m to 39.2 m to show the importance of transient flow condition on mixing-zone profile in a stratified aquifer.

Figure 13 shows the simulation results of transient mixing-zone development based on the Model 3. After an instantaneous decrease of the freshwater level, seawater in each layer intrudes landward but with different speeds. The different intrusion speeds of mixing zones in different layers result in detaching the toe in the higher-*K* layer from the top of the mixing zone in the bottom layer, which subsequently leads to the density gradient between these two layers and the transport of salts into the lower layer, i.e., mixed convection. As a result, the mixing zones in both middle and bottom layers are significantly widened. On the other hand, after freshwater level experiences 1 m decrease, the system would need extremely long time to reproduce the steady state condition, indicating that the transient flow conditions cannot be easily neglected in studying the mixing-zone profile in stratified aquifers.

5. Conclusions

Stratification in hydraulic conductivity is prevalent in coastal aquifers, yet its impact on the mixing-zone development is often neglected. This study employs both numerical and experimental methods to investigate effects of aquifer stratification on the mixing-zone development under both steady-state and transient flow conditions. The specific findings include:

(1) When a lower-*K* layer overlies a layer with a higher *K*, the mixing zone in the lower-*K* layer would be widened due to enhanced separation of streamlines of the freshwater-saltwater mixture by flow refraction. On the contrary, when a higher-*K* layer

overlies a layer with a lower *K*, the mixing zone in the higher-*K* layer is slightly narrowed because flow refraction squeezes the streamlines penetrated from the lower layer;

(3) Assuming that the aquifer configuration keeps constant, the steady-state mixing-zone profile in stratified aquifers is only determined by the relative magnitude of *K* in different layers, i.e., the inflow rate in different layers;

(3) Increasing the magnitude of stratified heterogeneity would lead to the retreat of the toe, first increase and then decrease of the mixing-zone thickness;

(4) When a higher-*K* layer overlies a lower-*K* layer, a sharp decrease of the freshwater level could yield the unsynchronized movement of the mixing zone in different layers, resulting in enhanced density gradients and salt transport from one layer to a lower layer.

As previously shown by *Lu et al.* [2009], kinetic mass transfer effects may significantly widen a moving mixing zone. However, the results of this study suggest that aquifer stratification with appropriate configuration can lead to a thicker mixing zone under both steady state and transient flow conditions. Therefore, the mechanism response for a thick mixing zone in reality may be complex, which highly depends on the site-specific hydrogeologic conditions.

Acknowledgements:

This research was sponsored by the National Institutes of Water Resources (NIWR) and U.S. Geological Survey (USGS) under project ID 2007GA165G. This article has not been reviewed by the agency, and no official endorsement should be inferred. Any opinions, findings, and conclusions or recommendations expressed in this material are those of the authors and do not necessarily reflect the views of NIWR and USGS.

References:

Abarca, E. Seawater intrusion in complex geological environments. Ph.D. Thesis. Technical University of Catalonia, UPC; 2006.

Abarca E., J. Carrera, X. Sanchez-Vila, and M. Dentz (2007), Anisotropic dispersive Henry problem, *Adv. Water Resour*., 30(4), 913-926.

Abarca, E., and T. P. Clement (2009), A novel approach for characterizing the mixing zone of a saltwater wedge, *Geophys. Res. Lett.*, *36*, L06402, doi:10.1029/2008GL036995.

Ataie-Ashtiani, B., R. E. Volker, and D. A. Lockington (1999), Tidal effects on sea water intrusion in unconfined aquifers, *J. Hydrol*., *216*, 17-31.

Bear J. (1972), *Dynamics of Fluid in Porous Media*, Elsevier, New York.

Barlow, P.M. (2003), Ground water in freshwater-saltwater environments of the Atlantic coast: U.S. Geological Survey Circular 1262.

Back, W., B.B. Hanshaw, T.E. Pyler, L.N. Plummer, and A.E. Weide (1979), Geochemical significance of ground water discharge in Caleta Xel Ha, Quintana Roo, Mexico. *Water Resour. Res*., *15*, 1521-1535.

Back, W., B.B. Hanshaw, J.S. Herman, and J.N. Van Driel (1986), Differential dissolution of a Pleistocene reef in the ground-water mixing zone of coastal Yucatan, Mexico, *Geology*, *4*, 137-140.

Budd, D.A. (1988), Aragonite-to-calcite transformation during fresh-water diagenesis of carbonates: Insights from pore-water chemistry, *Geol. Soc. Am. Bull*., *100*, 1260-1270.

Brovelli A., X. Mao, and D. A. Barry (2007), Numerical modeling of tidal influence on density-dependent contaminant transport, *Water Resour. Res*., *43*, W10426, doi:10.1029/2006WR005173.

Cherry, G.S. (2006), U.S. Geological Survey Georgia Water Science Center and City of Brunswick-Glynn County Cooperative Water Program - Summary of Activities, July 2005 through June 2006, U.S.G.S. Open-File Report 2006-1368.

Charette, M.A. and E.R. Sholkovitz (2002). Oxidative precipitation of groundwater-drived ferrous iron in the subterranean estuary of a coastal bay. *Geophys. Res. Lett*., *29* doi:10.1029/2001GL014512 (2002).

Cooper, H. H. (1959), A hypothesis concerning the dynamic balance of fresh water and salt water in a coastal aquifer. *J. Geophys. Res. 64*, 461-467.

Cartwright, N., and P. Nielsen, (2003) Dynamics of the salt-freshwater mixing zone in ocean beaches. 2nd Intl. *Conf. on Salt Water Intrusion and Coastal Aquifers-Monitoring, Modeling and Management*, Merida, Mexico, March 30- April 2.

Chen B.F., and S.M. Hsu (2004), Numerical study of tidal effects on seawater intrusion in confined and unconfined aquifers by time-independent finite-difference method. *J. Water Port. C-ASCE*, 130(4), 191-206.

Cartwright, N., L. Li, and P. Nielsen (2004), Response of the salt-freshwater interface in a coastal aquifer to a wave-induced groundwater pulse: field observations and modelling, *Adv. Water Res*., *27*, 297-303.

Dagan, G. (2006), Transverse Mixing At Fresh-Water Salt-Water Interfaces: An Unresolved Issue. First International Joint Salt Water Intrusion Conference. Tutirials.

Dausman, A.M. and C.D. Langevin (2005), Movement of the saltwater interface in the surficial aquifer system in response to hydrologic stresses and water-managementpractices, Broward County, Florida. USGS Scientific Investigations Report 2004–5256.

Diersch, H.-J.G., and O. Kolditz (2002), Variable density flow and transport in porous media: Approach and challenges, *Adv. Water Res*., 25(8-12), 439-459.

Essaid, H. (1990), A multilayered sharp interface model of coupled freshwater and saltwater flow in coastal systems: Model development and application, *Water Resour. Res*., 16(7), 1431-1454.

Fiori, A., and G., Dagan (1999), Concentration fluctuations in transport by groundwater: comparison between theory and field experiments, *Water Resour. Res*., 35, 102-112.

Goswami, R.R., and T.P. Clement (2007), Laboratory-scale investigation of saltwater intrusion dynamics, Water Resour. Res., *43*, W04418.

Held, R., S. Attinger, and W. Kinzelbach (2005), Homogenization and effective parameters for the Henry problem in heterogeneous formations. *Water Resour. Res*., 41, W11420. doi:10.1029/2004WR003674.

Henry, H. R. (1964), Effects of dispersion on salt encroachment in coastal aquifers. *Water-Supply Paper 1613-C*, U.S. Geological Survey.

Kerrou, J., and P. Renard (2010), A numerical analysis of dimensionality and heterogeneity effects on advective dispersive seawater intrusion processes. *Hydrogeol. J*., 18(1), 55-72.

Kohout, F.A. (1964), The flow of fresh water and salt water in the Biscayne aquifer of the Miami area, Florida: U.S. *Geological Survey Water-Supply Paper 1613-C*, p. 12-32.

Karasaki, K., I. Kazumasa, and K. Maekawa (2006), Simulation of salt water intrusion, Proceedings, TOUGH Symposium, Lawrence Berkeley National Laboratory, Berkeley, California, May 15-17.

Kim, K.Y., H. Seong, T. Kim, P.H. Park, N.C. Woo, Y.S. Park, G.W. Koh, and W.B. Park (2006), tidal effects on variations of fresh-saltwater interface and groundwater flow in a multilayered coastal aquifer on a volcanic island (Jeju Island, Korea), *J. Hydrol*., 330(3-4), 525-542.

Nakagawa, K., K. Jinno, T. Hosokawa, and K. Iwamitsu (2000), Numerical study on saltwater intrusion in a heterogeneous stratified aquifer, *J. Fac. Agr., Kyushu Univ*., 45(1), 317-323.

Lu, C., P.K. Kitanidis, and J. Luo (2009), Effects of kinetic mass transfer and flow conditions on widening mixing zones in coastal aquifers, *Water Resour. Res*., 45, W12402, doi: 10.1029/2008WR007643.

Lu, C. and J. Luo (2010), Dynamics of freshwater-seawater mixing zone development in dual-domain formations, *Water Resour. Res*., 46, W11601, doi: 10.1029/2010WR009344.

Langevin, C. D., W. B. Shoemaker, and W. Guo (2003), Modflow-2000, The U.S. Geological Survey modular ground-water flow model Documentation of the Seawat-2000 version with the variable density flow process (VDF) and the integrated MT3DMS transport process (IMT), U.S. Geol. Surv. Open File Rep., 03-426, 43 p.

Lebbe, L. (1999), Parameter identification in fresh-saltwater flow based on borehole resistivities and freshwater head data, *Adv. Water Resour*. 22, 791-806.

Michael, H. A., A. E. Mulligan, and C. F. Harvey (2005), Seasonal oscillations in water exchange between aquifers and the coastal ocean. *Nature*, *436*, 1145-1148.

Mazzia, A., L. Bergamaschi, and M. Putti (2001), On the reliability of numerical solutions of brine transport in groundwater: Analysis of infiltration from a salt lake, *Transp. Porous Media*, 43(1), 65-86.

Moore, W.S. (1999), The subterranean estuary: a reaction zone of ground water and sea water. *Mar. Chem. 65*, 111-125.

Mualem, Y., and J. Bear (1974), Shape of interface in steady flow in a stratified aquifer. *Water Resour. Res*., 10(6), 1207-1215.

Oki, D.S., W.R. Souza, E.L. Bolke, and G.R. Bauer (1998), Numerical analysis of the hydrogeologic controls in a layered coastal aquifer system, Oahu, Hawaii, USA, *Hydrogeol. J*., 6, 243-263.

Prasad, A., and C.T. Simmons (2003), Unstable density-driven flow in heterogeneous porous media: A stochastic study of the Elder [1967b] “short heater” problem, *Water Resour. Res*., 39(1), 1007, doi:10.1029/2002WR001290.

Price, R. M., Z. Top, J. D. Happell, and P. K. Swart (2003), Use of tritium and helium to define groundwater flow conditions in Everglades National Park, *Water. Resour. Res.*, *39*(9), 1267. doi:10.1029/2002WR001929.

Rezaei, M., E. Sanz, E. Raeisi, C. Ayora, E. Vazquez-Sune and J. Carrera (2005), Reactive transport modeling of calcite dissolution in the fresh salt water mixing zone. *J. Hydrol*., 311, 282-298.

Robinson, C., L. Li, and D.A. Barry (2006), Effect of tidal forcing on a subterranean estuary, *Adv. Water Res*., *30*, 851-865.

Robinson, C., L. Li, and H. Prommer (2007), Tide-induced recirculation across the aquifer-ocean interface, *Water Resour. Res*., *43*, W07428, doi:10.1029/2006WR005679.

Randazzo, A. F. and J.I. Bloom (1985), Mineralogical changes along the freshwater/saltwater interface of a modern aquifer, *Sediment. Geol*., *43*, 219-239.

Randazzo, A.F. and D.J. Cook (1987), Characterization of dolomitic rocks from the coastal mixing zone of the Floridan aquifer, USA, *Sediment. Geol*., *54*, 169-192.

Rumer, R.R. Jr., and J.C. Shiau (1968), Salt Water Interface in a layered coastal aquifer, *Water Resour. Res*., 4(6), 1235-1247.

Spiteri, C., C.P. Slomp, K. Tuncay, and C. Meile (2008), Modeling biogeochemical processes in subterranean estuaries: Effect of flow dynamics and redox conditions on submarine groundwater discharge of nutrients. *Water Resour. Res*., ***44***, W02430, doi:10.1029/2007WR006071.

Smart, P.L., J.M. Dawans, and F. Whitaker (1988), Carbonate dissolution in a modern mixing zone. *Nature*, 335, 811-813.

Schincariol, R.A., and F.W. Schwartz (1990), An experimental investigation of variable density flow and mixing in homogenous and heterogeneous media, *Water Resour. Res*., 26(10), 2317-2329.

Schincariol, R.A., F.W. Schwartz, C.A. Mendoza (1994), Instabilities in variable density flows: Stability and sensitivity analyses for homogeneous and heterogonous media, *Water Resour. Res*., 30(4), 913-927.

Schincariol, R.A. (1998), Dispersive mixing dynamics of dense miscible plumes: nature perturbation initiation by local-scale heterogeneities, *J. Contam. Hydrol*., 34(3), 247-271.

Simmons, C.T., T.R. Fenstemaker, and J.M. Sharp Jr. (2001), Variable-density groundwater flow and solute transport in heterogeneous porous media: Approaches, resolutions and future challenges, *J. Contam. Hydrol*., 52, 245-275.

Volker, R. E., and K. R. Rushton (1982), An assessment of the importance of some parameters for seawater intrusion in aquifers and a comparison of dispersive and sharp-interface modelling approaches. *J. Hydrol*., *56*, 239-250.

Voss, C. I., and W. R. Souza (1987), Variable density flow and solute transport simulation of regional aquifers containing a narrow freshwater-seawater mixing zone, *Water Resour. Res*., 23, 1851-1866.

Wu, J. C., Y. Q. Xue, P. M. Liu, J. J. Wang, Q. B., Jiang, and H. W. Shi (1993), Sea-water intrusion in the coastal area of LaiZhou Bay, China. 2. Sea-water intrusion monitoring. *Ground Water*, *31*, 740-745.

Xue, Y.Q., J. C. Wu, P. M. Liu, J. J. Wang, Q. B. Jiang, and H. W. Shi (1993), Sea-water intrusion in the coastal area of LaiZhou Bay, China.1. Distribution of Sea-water Intrusion and its hydrochemical characteristics. *Ground Water*, *31*, 532-537.

Zhang Q., R. E. Volker, and D. A. Lockington (2002), Experimental investigation of contaminant transport in coastal groundwater. *Adv. Environ. Res*., 6(3), 229-237.

Table 1. Field-scale model input parameters.

Parameter	Unit	Value
Domain length	m	400
Domain height	m	42
Beach slope	-	0.1
Longitudinal dispersivity	m	0.5
Transverse dispersivity	m	0.05
Effective porosity	-	0.4
Constant seawater level	m	39
Constant freshwater level	m	40.2
Seawater density	kg/m^3	1025
Freshwater density	kg/m^3	1000
Salt concentration	kg/m^3	35

Table 2. *K* values of the field-scale model.

Model	K_1 [ms^{-1}]	K_2 [ms^{-1}]	K_3 [ms^{-1}]
1	1×10^{-4}	$K_2/K_1=1$	K_1
2	1×10^{-4}	$K_2/K_1=0.1$	K_1
3	1×10^{-5}	$K_2/K_1=10$	K_1
4	1×10^{-3}	$K_2/K_1=1$	K_1
5	1×10^{-3}	$K_2/K_1=0.1$	K_1
6	1×10^{-4}	$K_2/K_1=10$	K_1
7	K1/K2=50	1×10^{-5}	K_1
8	K1/K2=100	1×10^{-5}	K_1
9	K1/K2=200	1×10^{-5}	K_1
10	1×10^{-5}	K2/K1=50	K_1
11	1×10^{-5}	K2/K1=100	K_1
12	1×10^{-5}	K2/K1=200	K_1
13	1×10^{-5}	1×10^{-4}	1×10^{-3}
14	1×10^{-3}	1×10^{-4}	1×10^{-5}

Figure Captions

Figure 1. Experimental setup.

Figure 2. Schematic of a field scale model: boundary conditions and dimensions. The red color represents constant head boundary condition: blue is fresh (40.2 m) and red is saline (39 m).

Figure 3. Photographs of laboratory experiment results of quasi-steady-state mixing zone in the flow tank. Real coastal sands with two specifications were used. A: homogeneous case; B: stratified case (high *K*-low *K*-high *K*); and C: (low *K*-high *K*-low *K*).

Figure 4. Numerical simulation results for the corresponding experimental cases in the Figure 2. The dashed black lines in the B and C are the interfaces between two layers. White lines are the stramlines, where arrows indicte the directions.

Figure 5. Refraction of the streamlines at the interface between two layers with different hydraulic conductivities [*Bear*, 1972].

Figure 6. Velocity vector field associated with three normalized concentration contour lines 0.1, 0.5, and 0.9 in the experimental case where a lower-*K* layer between two higher-*K* layers.

Figure 7. Velocity variation with the distance at z = 50, 100, 150, 200, and 250 mm. The green lines indicate the stage that velocity decreases from maximum to minimum value. Corresponding spatial locations to this decreasing stage are shown by solid gray lines.

Figure 8. Simulation results for Models 1, 2, and 3. White lines indicate the streamlines.

Figure 9. Simulation results of Models 1-6. Models 1and 4 are homogeneous aquifer cases. $K_1/K_2/K_3$ is constant for the Models 2 and 5, and Models 3 and 6.

Figure 10. Sensitivity of magnitude of stratified heterogeneity on the mixing-zone profile.

Figure 11. The effects of the magnitude of aquifer heterogeneity on the toe position, normalized total mass in the lower-*K* layer, and the position of the mixing zone (2.5% to 97.5% of saltwater concentration) in the lower-*K* layer. The toe position is assumed at 50% of saltwater concentration. ( ): normalized total mass in the low *K* layer; (O): toe position; (—): the position of the mixing zone in the low-*K* layer. For all cases, $K_1 = K_3$.

Figure 12. Simulation results of Models 13 and 14.

Figure 13. Simulation results of Model 3 under the transient flow condition. The left boundary is assumed to undergo an instantaneous decrease of 1 m.

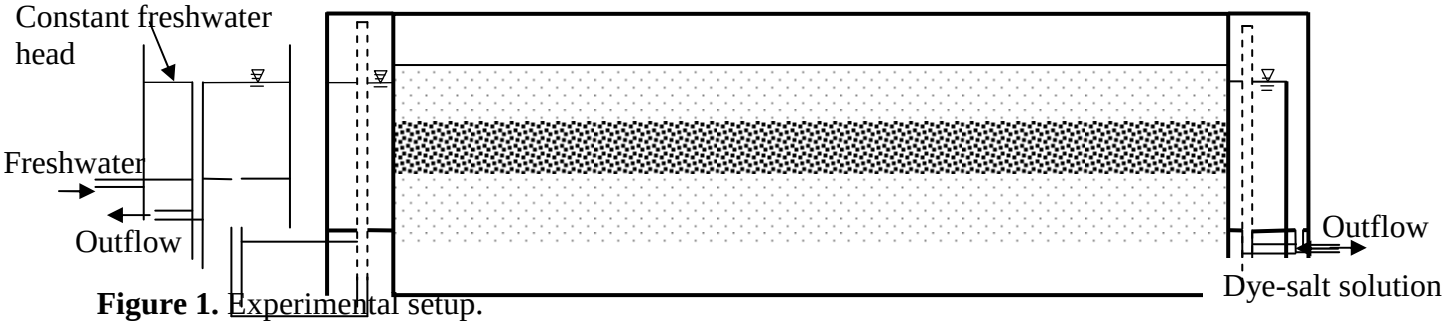

Figure 1. Experimental setup.

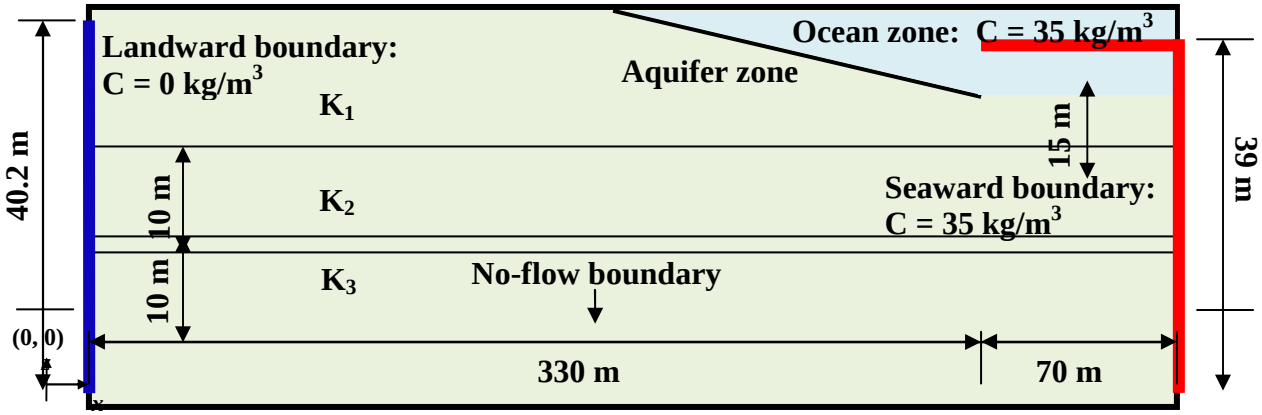

Figure 2. Schematic of a field scale model: boundary conditions and dimensions. The red color represents constant head boundary condition: blue is fresh (40.2 m) and red is saline (39 m).

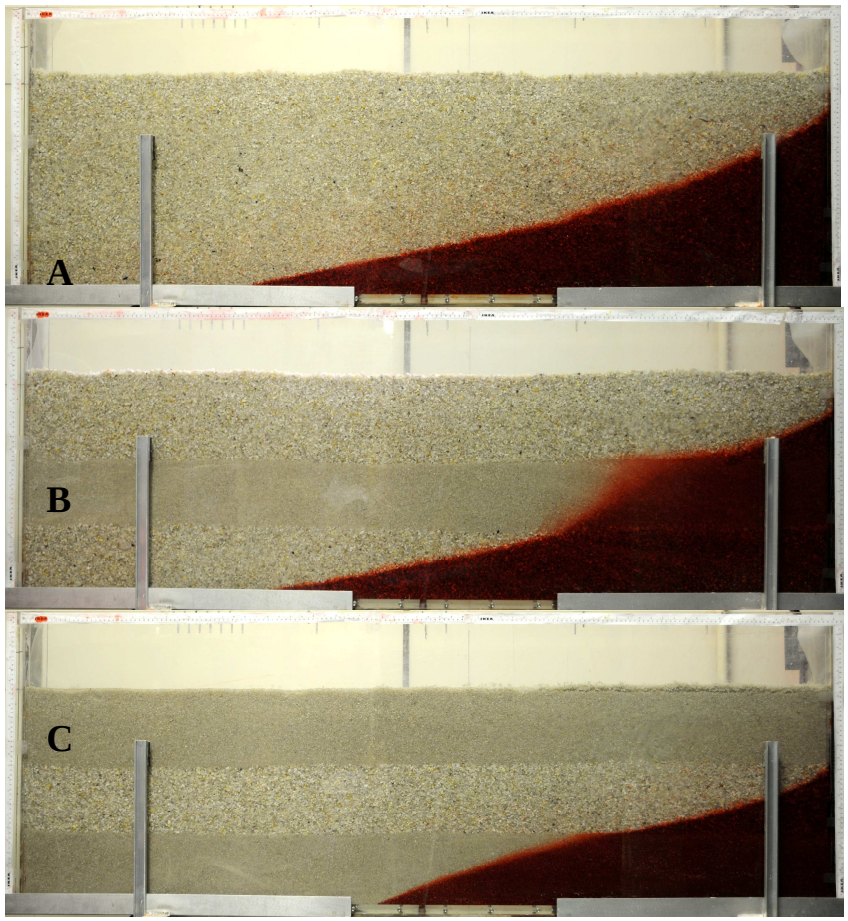

Figure 3. Photographs of laboratory experiment results of quasi-steady-state mixing zone in the flow tank. Real coastal sands with two specifications were used. A: homogeneous case; B: stratified case (high *K*-low *K*-high *K*); and C: (low *K*-high *K*-low *K*).

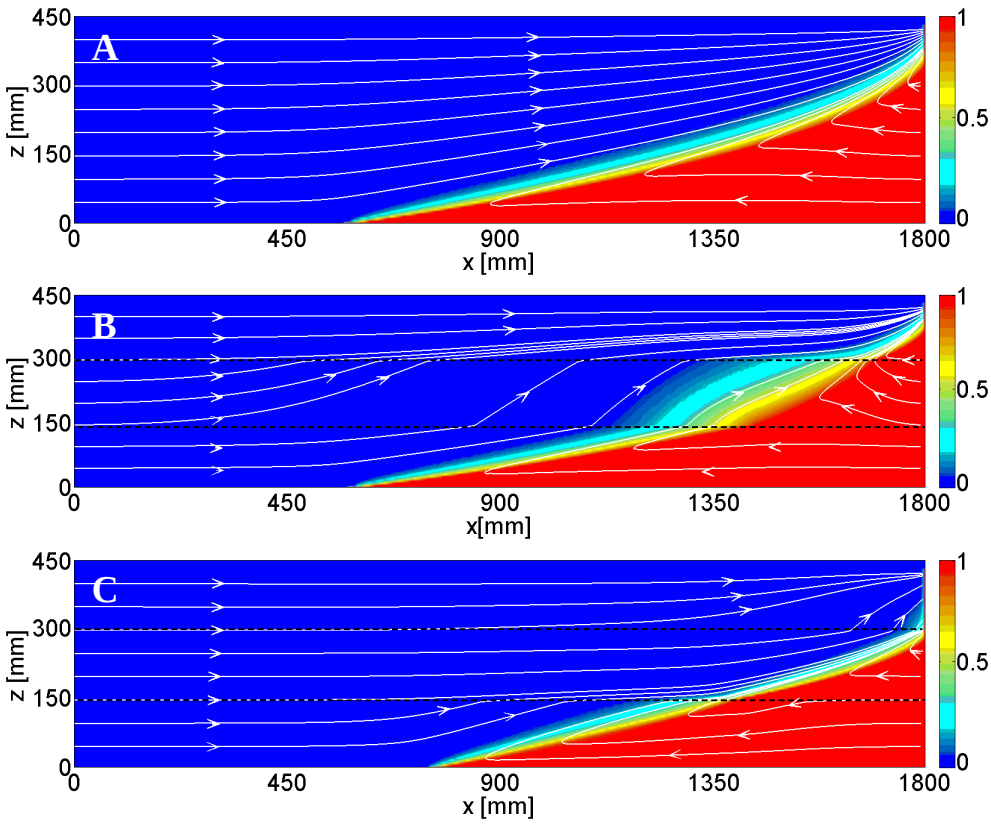

Figure 4. Numerical simulation results for the corresponding experimental cases in the Fig. 2. The dashed black lines in the B and C are the interfaces between two layers. White lines are the stramlines, where arrows indicte the directions.

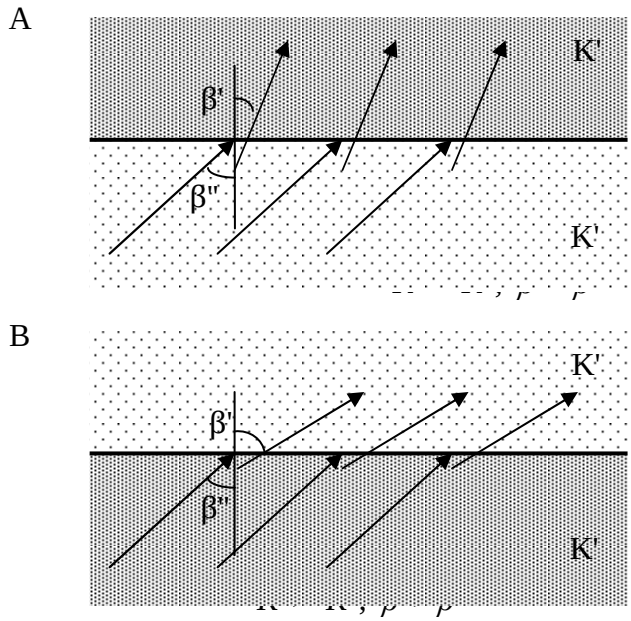

Figure 5. Refraction of the streamlines at the interface between two layers with different hydraulic conductivities [*Bear*, 1972].

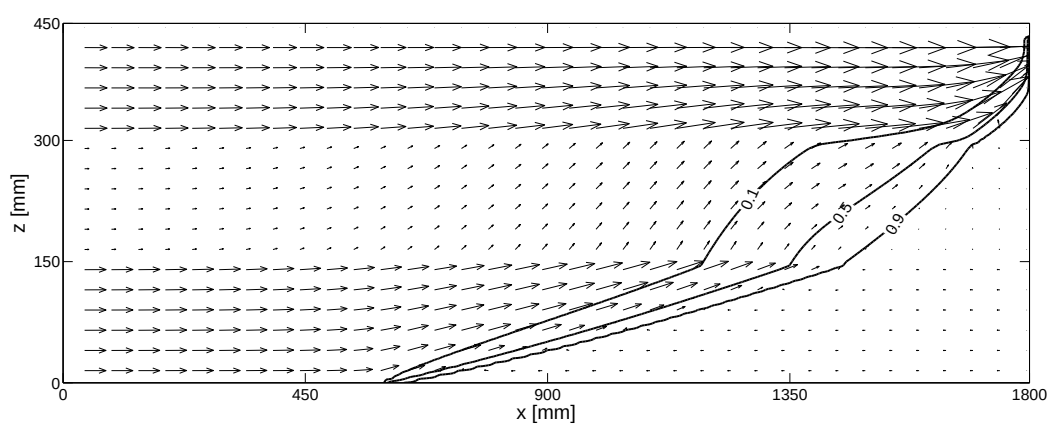

Figure 6. Velocity vector field associated with three normalized concentration contour lines 0.1, 0.5, and 0.9 in the experimental case where a lower-*K* layer between two higher-*K* layers.

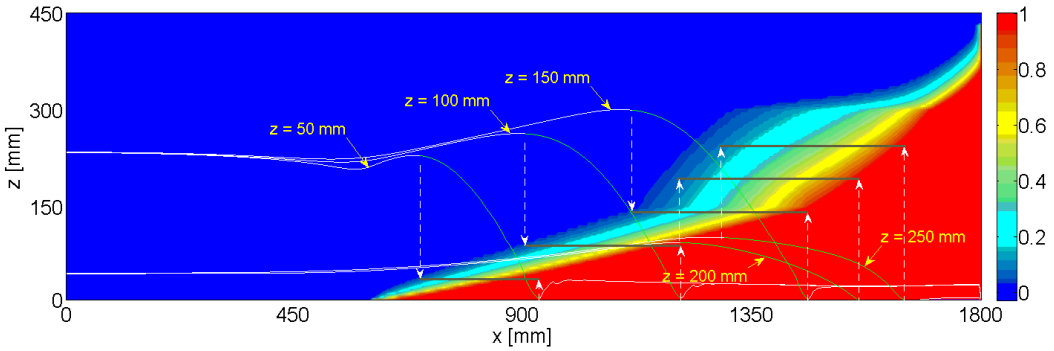

Figure 7. Velocity variation with the distance at z = 50, 100, 150, 200, and 250 mm. The green lines indicate the stage that velocity decreases from maximum to minimum value. Corresponding spatial locations to this decreasing stage are shown by solid gray lines.

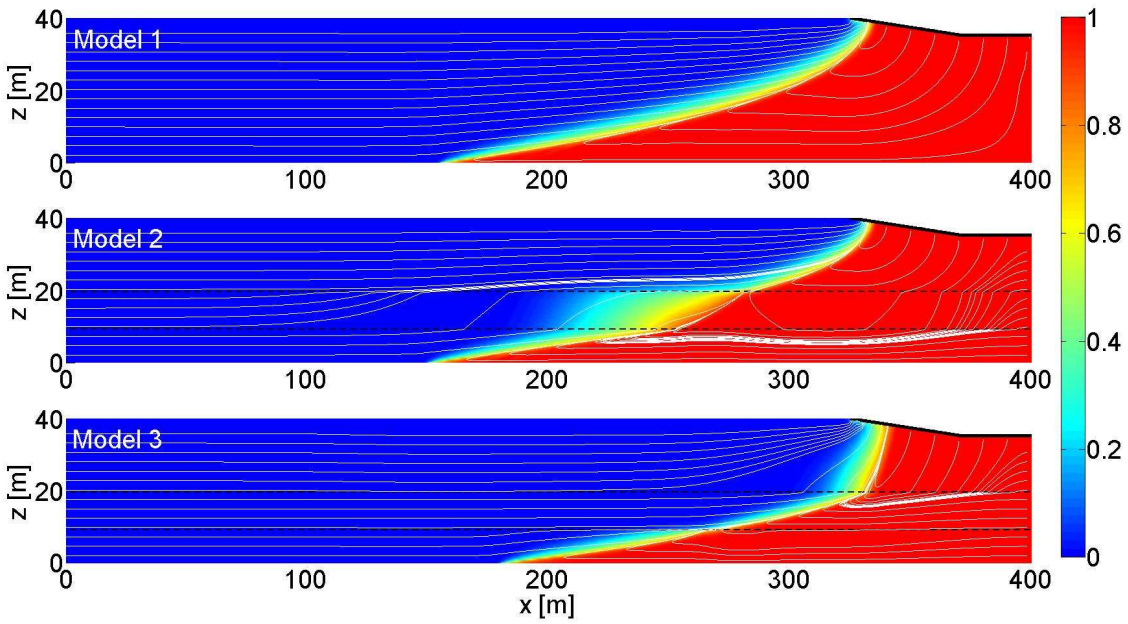

Figure 8. Simulation results for Models 1, 2, and 3. White lines indicate the streamlines.

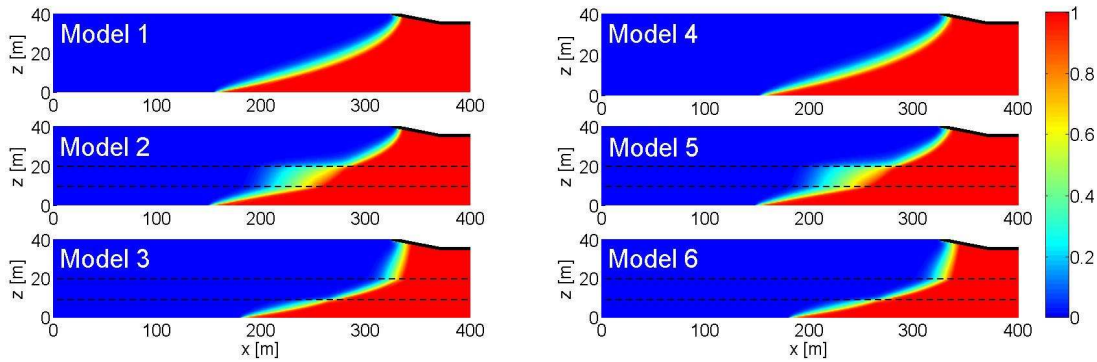

Figure 9. Simulation results of Models 1-6. Models 1and 4 are homogeneous aquifer cases. $K_1/K_2/K_3$ is constant for the Models 2 and 5, and Models 3 and 6.

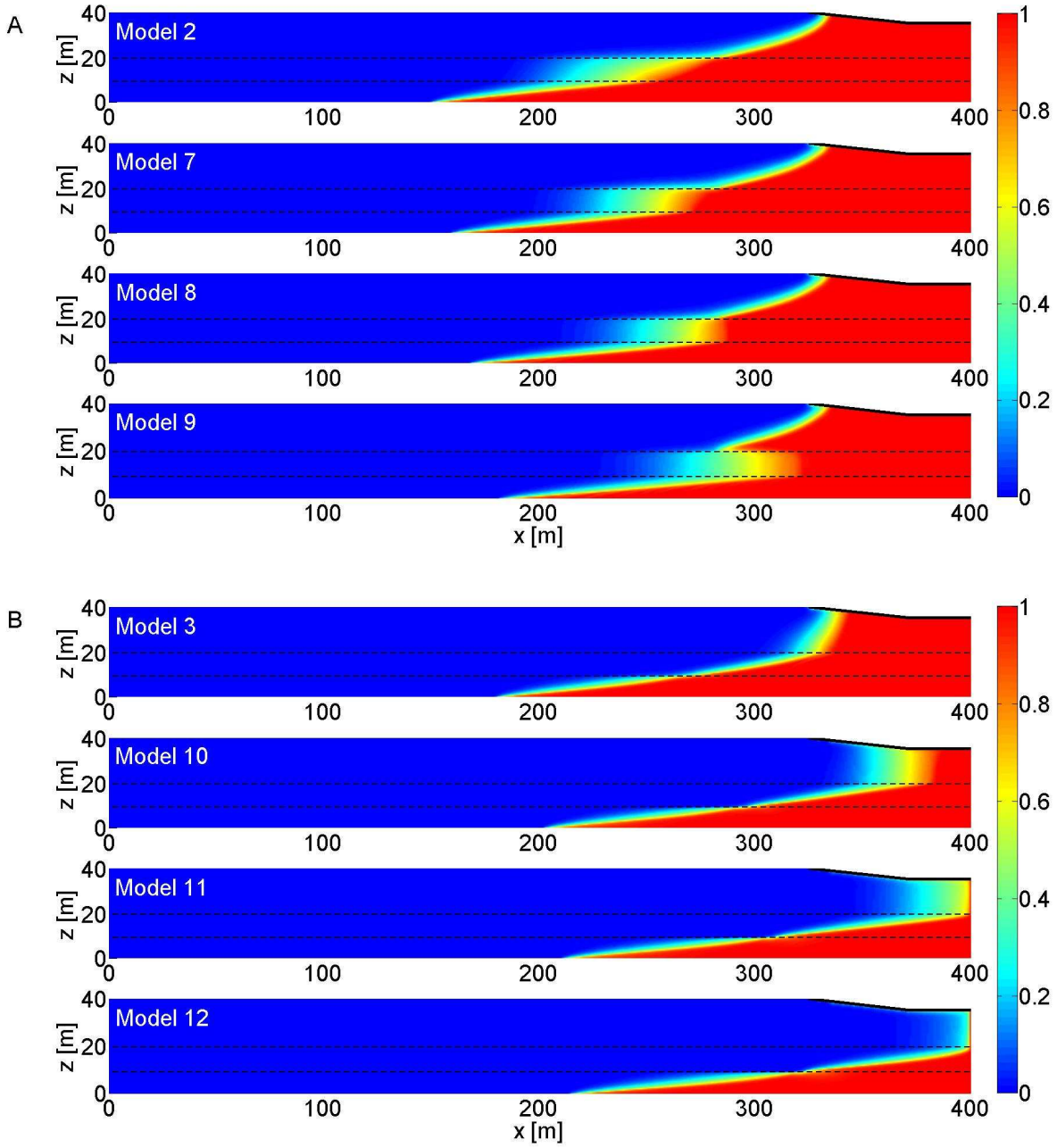

Figure 10. Sensitivity of magnitude of stratified heterogeneity on the mixing-zone profile.

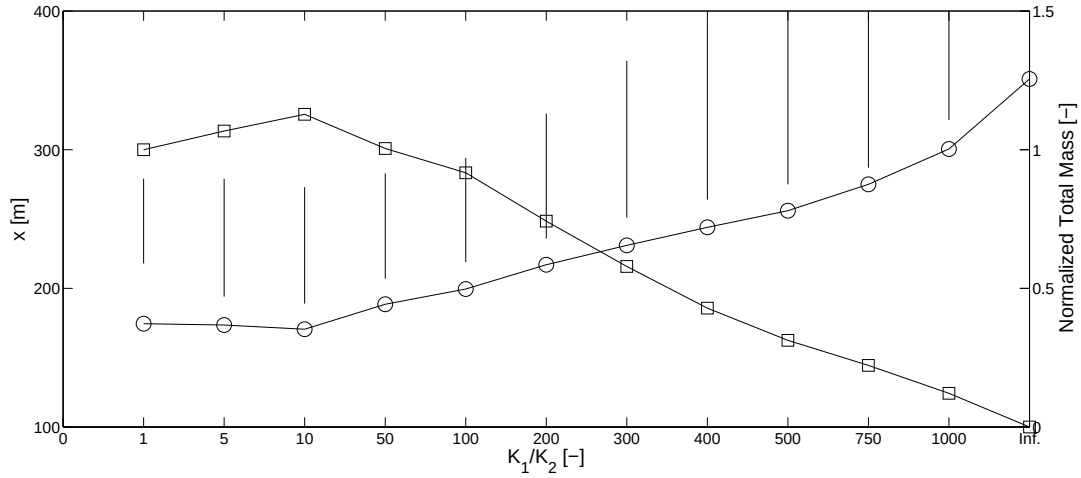

Figure 11. The effects of the magnitude of aquifer heterogeneity on the toe position, normalized total mass in the lower-*K* layer, and the position of the mixing zone (2.5% to 97.5% of saltwater concentration) in the lower-*K* layer. The toe position is assumed at 50% of saltwater concentration. ( ): normalized total mass in the low *K* layer; (O): toe position; (—): the position of the mixing zone in the low-*K* layer. For all cases, $K_1 = K_3$.

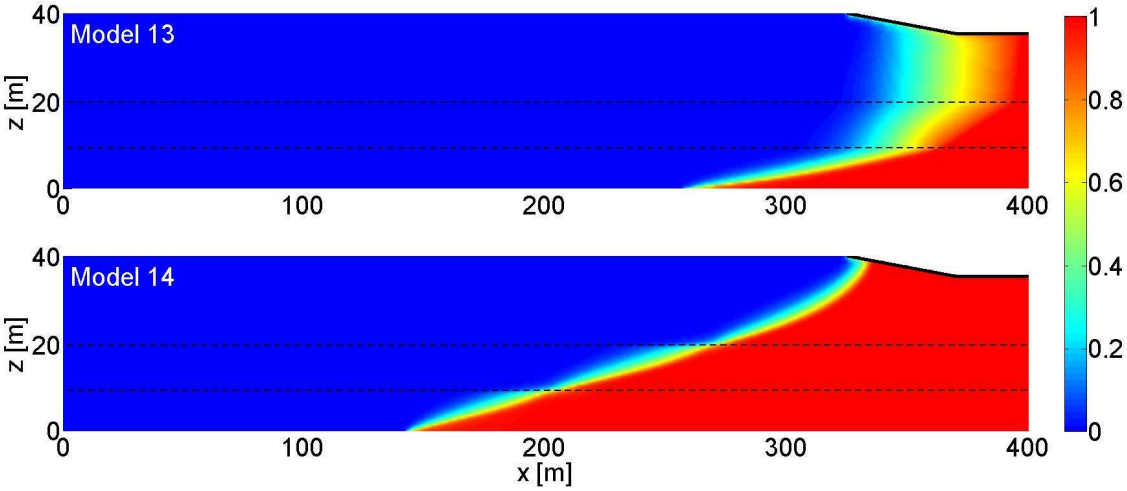

Figure 12. Simulation results of Models 13 and 14.

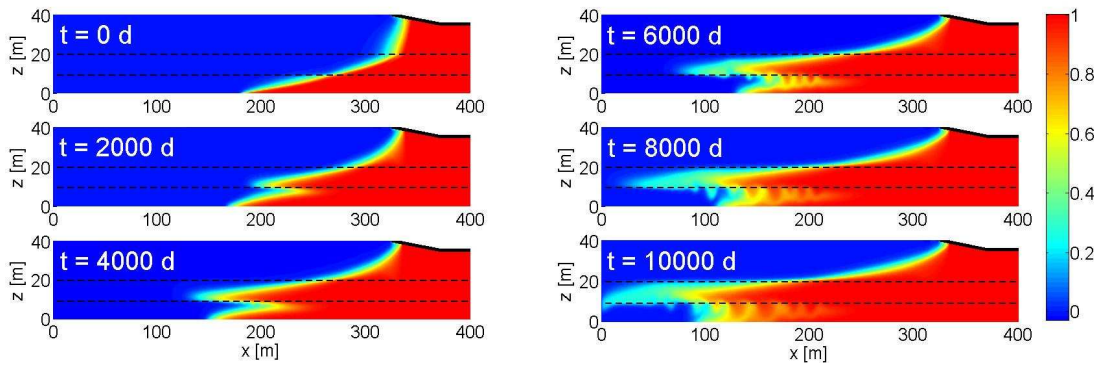

Figure 13. Simulation results of Model 3 under the transient flow condition. The left boundary is assumed to undergo an instantaneous decrease of 1 m.

Flood Risk and Homeowners' Flood Risk Perceptions: Evidence from Property Prices in Georgia

Basic Information

Title:	Flood Risk and Homeowners' Flood Risk Perceptions: Evidence from Property Prices in Georgia
Project Number:	2011GA275B
Start Date:	3/1/2011
End Date:	2/29/2012
Funding Source:	104B
Congressional District:	GA-010
Research Category:	Social Sciences
Focus Category:	Floods, Economics, Education
Descriptors:	
Principal Investigators:	Susana Ferreira, Susana Ferreira

Publications

1. Atreya, A., S. Ferreira and W. Kriesel (2012) “Forgetting the Flood? Changes in Flood risk Perceptions over Time”,University of Georgia, Athens, GA. Presented at UGA Department of Agricultural and Applied Economics Seminar Series, Athens, August 17, 2011
2. Atreya, A., S. Ferreira and W. Kriesel (2012) “Forgetting the Flood? Changes in Flood risk Perceptions over Time”,University of Georgia, Athens, GA. Presented at UNICT- EAERE- FEEM Belpasso International Summer School on Environmental and Resource Economics, Belpasso, Sicily, Italy, Sept 4-10, 2011.
3. Atreya, A. and S. Ferreira (2012) “Analysis of Spatial Variation in Flood Risk Perception” Presented at UGA Department of Agricultural and Applied Economics Seminar Series, Athens, January 18, 2012.
4. Atreya, A. and S. Ferreira (2012) “Analysis of Spatial Variation in Flood Risk Perception” Presented at Southern Agricultural Economics Association 2012 Annual Meeting, Birmingham, Alabama, February 4-7, 2012.
5. Atreya, A. and S. Ferreira (2011) “Flood Risk and Risk Perception: Evidence from Property Prices in Fulton County, Georgia” Presented at CIMR- Climate Information for Managing Risk, Local to Regional Adaptation and Mitigation Strategies, An International Symposium, Orlando Florida, May 24-27, 2011.
6. Atreya, A. and S. Ferreira (2012) “Variation in Flood Risk Perception: Does Scale Matter?” Presented at ICARUS- Initiative on Climate Adaptation Research and Understanding through the Social Sciences, Columbia University, New York, May 18-20, 2012.
7. Atreya, A. and S. Ferreira (2012) “Spatial Variation in Flood Risk Perception: A Spatial Econometric Approach” To be presented Agricultural and Applied Economics Association 2012 Annual Meeting, Seattle, Washington, August 12-14, 2012.
8. Atreya, A., S. Ferreira and W. Kriesel (2012) “Forgetting the Flood? Changes in Flood risk Perceptions over Time” Submitted to Land Economics

Final Report

"Flood Risk and Homeowners' Flood Risk Perceptions: Evidence from Property Prices in Georgia"

USGS 104B/GWRI Project # 2011GA275B

May 15, 2012

Susana Ferreira
Department of Agricultural & Applied Economics
University of Georgia
313 Conner Hall
Athens GA 30602-7509, USA
+1 706-542-0086
sferreir@uga.edu

TABLE OF CONTENTS

SUMMARY OF ACTIVITIES AND ACCOMPLISHMENTS.....3

PAPER

1. FORGETTING THE FLOOD? CHANGES IN FLOOD RISK PERCEPTIONS OVER TIME 5

Abstract 5

Introduction 6

Study Area 9

Methods 11

Data 17

Results 18

Ordinary Least Squares Estimates 18

Estimates of the SARAR Model 21

Conclusion 23

Figures 26

Tables 30

References 34

2. ANALYSIS OF SPATIAL VARIATION IN FLOOD RISK PERCEPTION 37

Abstract 37

Introduction 38

Study Area 39

Methods 41

Data 44

Results 45

Flood Risk Perception: City of Albany 45

Flood Risk Perception: Inundation Study Area, Albany.....46

Conclusion 48

Tables 49

Figures 54
References 56
3. FLOOD RISK AND HOMEOWNER'S FLOOD RISK PERCEPTIONS: EVIDENCE FROM PROPERTY PRICES IN FULTON COUNTY, GEORGIA 57
Abstract 57
Introduction 58
Previous Research 60
Study Area 62
Model 63
Data 65
Empirical Results 66
Flood Risk Discount: No Flood Event Included.....66
Flood Risk Discount: 1994 Flood Event Included.....67
Conclusion 68
Figures 69
Tables 73
References 75

Summary of Activities and Accomplishments

The aim of this project is to improve our understanding of the perception of flood risks among homeowners in Georgia. The concentration of both capital and people into flood plains and other high-risk areas in Georgia and worldwide, driving up the costs, economic and otherwise when a flood occurs, raises important questions: Do homeowners have accurate information about flood risks? Do they understand this information? How does this information translate into their perceived flood risk as reflected into property prices?

Our research addresses these and other specific research questions: (i) Do homeowners in Georgia perceive the flood risk as designated by the Federal Emergency Management Agency's (FEMA's) flood hazard maps (known as Flood Insurance Rate Maps, or FIRMs)? (ii) What are the price differentials between properties inside and outside the floodplain as defined by the FIRMs? (iii) How do these compare with flood insurance premiums? (iv) Do property prices change after new information is provided (e.g. after a large flood event)? (v) How do homeowners adapt their risk perceptions after a flood shock? (vi) Are the effects of this new information temporary or permanent? (vii) How do these effects vary spatially depending on the location and characteristics of properties?

As planned, during Spring 2011 we constructed a unique dataset matching property prices with key property characteristics including location characteristics relevant to assess flood risks for Fulton County in Georgia. In the course of our research, we learnt that the United States Geological Survey (USGS) along with partners in the National Weather Service (NWS), U.S. Army Corps of Engineers (USACE), FEMA, state agencies, local agencies, and universities had developed a web-based tool, for flood response and mitigation. The USGS had modeled potential flow characteristics of flooding along a 4.8-mile reach of the Flint River in Albany, Dougherty county, Georgia. Simulated inundated areas, in 1-foot (ft) increments, were created for water-surface altitudes at the Flint River at Albany stream gage from 179.5-ft to 192.5-ft. 192.5-ft corresponds to the 1994 "flood-of-the-century" stage at Flint River caused by tropical storm Alberto. We thus decided to focus on this county and on this particular flood event to answer our research questions since, in addition to the FEMA hazard maps, we could use the USGS simulated map of the actual inundation in 1994.

Deliverables

The research arising from this project has crystallized into three manuscripts. They are included into this report to show the details of the research activities. As indicated below, they have been broadly disseminated in seminars, regional, national and international meetings and conferences, and are in different stages in the process of publication in peer-reviewed journals.

Atreya, A., S. Ferreira and W. Kriesel (2012) "Forgetting the Flood? Changes in Flood risk Perceptions over Time"

- Presented at UGA Department of Agricultural and Applied Economics Seminar Series, Athens, August 17, 2011.
- Presented at UNICT- EAERE- FEEM Belpasso International Summer School on Environmental and Resource Economics, Belpasso, Sicily, Italy, Sept 4-10, 2011.
- Selected to represent UGA Department of Agricultural and Applied Economics for E. Broadus Browne Research Awards for Outstanding Graduate Research, College of Agriculture and Environmental Sciences, University of Georgia, March 27, 2012.
- Submitted to *Land Economics*

Atreya, A. and S. Ferreira (2012) "Analysis of Spatial Variation in Flood Risk Perception"

- Presented at UGA Department of Agricultural and Applied Economics Seminar Series, Athens, January 18, 2012.
- Presented at Southern Agricultural Economics Association 2012 Annual Meeting, Birmingham, Alabama, February 4-7, 2012.
- Currently being polished for subsequent journal submission

Atreya, A. and S. Ferreira (2011) "Flood Risk and Risk Perception: Evidence from Property Prices in Fulton County, Georgia"

- Presented at CIMR- Climate Information for Managing Risk, Local to Regional Adaptation and Mitigation Strategies, An International Symposium, Orlando Florida, May 24-27, 2011.
- Currently being polished for subsequent journal submission

In addition of these three papers included in the report, we are currently finalizing two additional manuscripts that have been accepted for presentation at two national conferences and that we intend to submit to peer-reviewed journals following revision to incorporate the feedback received at these conferences.

Atreya, A. and S. Ferreira (2012) "Variation in Flood Risk Perception: Does Scale Matter?"

- To be presented at ICARUS- Initiative on Climate Adaptation Research and Understanding through the Social Sciences, Columbia University, New York, May 18-20, 2012.

Atreya, A. and S. Ferreira (2012) "Spatial Variation in Flood Risk Perception: A Spatial Econometric Approach"

- To be presented Agricultural and Applied Economics Association 2012 Annual Meeting, Seattle, Washington, August 12-14, 2012.

Regarding training, Ajita Atreya (PhD student) was supported by the project. Research outputs from this project will be an integral part of her PhD thesis. Research from this project has been used to inform lectures in the PI's undergraduate course Environmental Economics (ENVM 4650) offered in Spring 2012.

Forgetting the Flood? Changes in Flood Risk Perceptions over Time

Ajita Atreya, Susana Ferreira and Warren Kriesel
Department of Ag. & Applied Economics
University of Georgia
Athens, GA 30602

Abstract

We examine whether homebuyers update their flood risk assessment following a large flood event, and whether changes in risk perceptions induced by large flood events are temporary or permanent. We use single family residential property sales in Dougherty County, Georgia, between 1985 and 2010 in a Difference-in-Difference spatial hedonic model framework. After the "flood of the century" in 1994, prices of properties in the 100-year and 500-year floodplain fell significantly indicating that homebuyers in Dougherty County capitalized the flood risk in the property prices. This effect was, however, short-lived. It decayed at a rate of 1.4 to 2.7 percent annually.

JEL codes: Q51, Q54

1. Introduction

Floods are the most common natural disaster. Between 1985 and 2009, floods represented 40 percent of natural disasters worldwide and accounted for 13 percent of the deaths and 53 percent of the number of people affected by natural disasters (EMDAT, 2010).[1] In the United States, floods kill about 140 people and cause $6 billion in property damage in the average year (USGS, 2006). Between 1955 and 2009 economic damages from flooding in the United States amounted to over $260 billion in constant 2009 dollars.

Flood damage has increased in the United States, despite local efforts and federal encouragement to mitigate flood hazards and regulate development in flood-prone areas (Pielke, et al., 2002). IPCC (2001) and SwissRe (2006) have reported dramatic increases in related damages over time. The increased damages are believed to have two causes. The first is an increase in the frequency and intensity of extreme weather events associated with climate change. A warmer climate, with its increased weather variability, is expected to increase the risk of both floods and droughts (Wetherald and Manabe, 2002). The second cause, and of particular interest to this paper, is the increased value of property at risk in hazardous areas (Kunreuther and Michel-Kerjan, 2007). Both capital and people have been moving into flood plains and other high-risk areas (Freeman, 2003; IPCC, 2007) driving up the costs, economic and otherwise when a flood occurs. In the United States, as of year 2000, there were over six million buildings located in 100-year floodplains, that is, with a 1% chance of flooding in any given year (Burby, 2001). This raises important questions about the individual perceptions of floods: Do homebuyers have accurate information about flood risks? Do they understand this information? Do homebuyers update their

[1] To be considered a disaster and included in the widely used EM-DAT global disaster database, an event needs to fulfill at least one of the following criteria: (i) 10 or more people killed, (ii) 100 or more people reported affected (typically displaced), (iii) a declaration of a state of emergency, or (iv) a call for international assistance (OFDA/CRED 2010).

flood risk perception following a large flood event? If so, is the perceived risk persistent over time?

Several previous studies have addressed the first two questions, and have shown that a house located within a floodplain sells for a lower market value than an equivalent house located outside the floodplain (Shilling et al., 1985; MacDonald et al., 1987; Speyrer and Ragas, 1991; Harrison et al., 2001; Beatley et al., 2002; Bin and Polasky, 2004; Bin and Kruse, 2006; Bin et al., 2008; Kousky, 2010). However, they also find that if property buyers underestimate the cost of flooding, or if they are relatively unaware of flood hazards, there might be little reduction in the value of properties within a floodplain.

Fewer studies have investigated the third question, or how actual flood events alter homebuyers' risk perceptions (Skantz and Strickland, 1996; Bin and Polasky, 2004; Carbone et al., 2006; Kousky, 2010; Bin and Landry, 2011). These studies find that a significant flood event acts as a source of updated risk information and that after the event properties within the floodplain experience a drop in market value compared to equivalent houses located outside the floodplain. However, the results are mixed. For example, Kousky shows that, after the 1993 flood on the Missouri and Mississippi rivers, property prices in the 100-year floodplain did not change significantly but prices of properties in the 500-year floodplain declined by 2%. On the contrary, Bin and Landry find that it is properties within the 100-year flood plain that were discounted after a large flood event. To the best of our knowledge, these are the only studies that, in addition, have looked at the fourth question, or at the persistence of changes in perceived flood risk induced by a large flood event. The results in both papers suggest that consumer willingness to pay for a decrease in flood risk after the flood event decays with time. However, in Kousky's analysis the results are statistically insignificant, In Bin and Landry's analysis the significance of

the results depend on how the floodplains are specified, and their analysis is restricted to post-flood property transactions, starting 3 years after the flood event.

We intend to add to this limited literature by examining whether changes in risk perceptions induced by a large flood event are temporary or permanent by accounting explicitly for the number of years since the flood has taken place in a difference-in-difference (DD) framework. In addition, our hedonic model accounts for spatial dependence among neighboring properties via a combination of spatial lagging of the dependent variable and correcting for autocorrelation in the error term.

We use a hedonic property model (Rosen, 1974; Freeman, 2003) to determine the price differential between residential properties within and outside the floodplain over the years 1985-2010 in Dougherty County, Georgia. Within the hedonic model we analyze the impact of the 1994 "flood of the century" on that differential. Results of the hedonic regression on pre-flood data show that there was a significant discount of almost 16% associated with properties in the 100-year floodplain. This suggests that the homebuyers in the 100-year floodplain capitalized the flood risk into property prices. We did not find any significant discount associated with properties in the 500-year floodplain before the flood.

In order to explore the change in risk perception after the 1994 flood event we use a difference-in-difference (DD) model as in Bin and Polasky, and Kousky. We find that right after the 1994 flood there was a significant discount for properties in the 100-year floodplain, with the discount varying between 17% to 22% and an even larger discount of 22% to 27% for properties in the 500-year floodplain depending on the specification. This result is consistent with Kousky's. She also finds that after a large flood event, properties in the 500-year floodplain were discounted.

By comparison our estimates of the discount are larger in magnitude. Unlike Kousky but like Bin and Landry we also find a discount for properties in the 100-year floodplain immediately after the flood.

Community participation in the National Flood Insurance Program (NFIP) enables property owners to purchase insurance protection against losses from flooding. Most homeowners with mortgages in the 100-year floodplain are mandated to buy flood insurance, so they should be more aware of the associated flood hazard than homeowners of properties in the 500-year floodplain, who are not required to buy flood insurance. The information update effect provided by the flood should thus be larger for properties in the 500-year floodplain, and, accordingly, we find higher discounts after the flood for properties in the 500-year floodplain.

The large discount is, however, short lived. We find that it decays rapidly; at the rate of 2.4 to 2.7 percent annually for 100-year and 1.4 to 2.2 percent annually for 500-year floodplain properties, depending on the specification. Overall our results suggest the existence of the "availability heuristic" (Tversky and Kahneman, 1973) which is defined as a cognitive heuristic in which a decision maker relies upon knowledge that is readily available (e.g. what is recent or dramatic) rather than searching alternative information sources.

2. Study Area

In 1994, the Flint River overran its banks from the effects of Tropical Storm Alberto, causing a major flood in Southwest Georgia. Dougherty County, where 15 people were killed and almost 78,000 people were displaced by the flood, suffered the greatest damage. Divided by the Flint River into two halves, Dougherty County was founded in the early 1800s and today it is the core of a metropolitan area. Illustrated in Figure 1, it has a total area of 334.64 square miles, of which

329.60 square miles are land and 5.04 square miles are water (US Census Bureau, 2010). The city of Albany was hit worst by the flood. The flood submerged most of South Albany, inundating 4,200 residences with $99.4 million in damages to residential, commercial and other structures, 62,502 tons of flood debris dumped in landfills, 4,907 workers temporarily unemployed, and $80 million in home and small business loans issued by the Small Business Administration (Formwalt, 1996). Peak discharges greater than the 100-year flood discharge were recorded at all U.S. Geological Survey gauging stations on the Flint River (Stamey, 1996). According to the USGS, the Flint River peaked at a stage about five feet higher than that of a flood in 1925, which was the previous maximum flood ever recorded at Albany.

According to the Federal Emergency Management Agency (FEMA), nearly 20,000 communities across the United States and its territories participate in the National Flood Insurance Program (NFIP). When a community joins the NFIP it agrees to adopt and enforce floodplain management ordinances to reduce future flood damage. In exchange, the NFIP makes federally backed flood insurance available to homeowners, renters, and business owners in these communities. Community participation in the NFIP is voluntary. In order to actuarially rate new construction for flood insurance and create broad-based awareness of the flood hazards, FEMA maps 100-year and 500-year floodplains in participating communities. The City of Albany has been a participating community in the NFIP since 1974. All the other parts of Dougherty County joined the NFIP in 1978 (FEMA, Community Status Book Report).

Figure 2 is a map of the Flint River, housing units and the associated floodplains for southwestern parts of Dougherty County. Almost 11 percent of the properties sold between the years of 1985 to 2010 fall in the floodplain. Many properties in the designated flood hazard zones had not experienced a flood in decades. At the same time there have been cases of

properties outside the 100-year flood zone that have unexpectedly experienced floods. In some cases, individuals in the 100-year flood plain may erroneously think that since they have experienced a flood, there will not be more flooding in 100 years. In these cases the risks and costs associated with living in a flood prone area may not be fully understood by homebuyers.

3. Methods

Hedonic models (Rosen, 1974; Freeman, 2003) have been used extensively to estimate the contribution to the total value of a property of each characteristic possessed by the property. Hedonic property models have also been proven to be an effective tool for estimating the marginal willingness to pay (MWTP) for changes in environmental quality since their early applications in the late 1960s (Halstead, et al., 1997). Consistent with earlier studies we use a hedonic model to determine the shadow value of a non-market environmental attribute: flood risk. In hedonic property models, the price of a property, *P*, is modeled as a function of structural characteristics, **S** (e.g. number of rooms, size of the house), neighborhood and location characteristics, **L** (e.g. distance to rivers, distance to parks, median household income, percent of non-whites), and an environmental variable of interest, in this case flood risk, *R*.

$$P_{it} = \beta_0 + \beta_1^{'} L_i + \beta_2^{'} S_{it} + \beta_3 R_i + \varepsilon_{it} \qquad (1)$$

In equation (1) subscripts *i* and *t* represent property and time respectively. $\beta_3 = \partial P_{it} / \partial R_i$, the coefficient on the risk variable, captures homebuyers' perception of flood risk, and it can be interpreted as the MWTP for a reduction in flood risk. Regarding the functional form, we performed a Box-Cox transformation of the dependent variable and after comparing the residual sum of squares we concluded that the natural log of price as the dependent variable was the best specification for our model. After testing several transformations of the independent variables,

the location variables were best fitted in their log form while the other attributes were fitted best in their quadratic specification, which is consistent with the functional form used by Bin and Polasky.

To measure flood risk we use two dummy variables, one for the 100-year floodplain and one for the 500-year floodplain. There were around 800 properties in zone D which FEMA defines as "An area of undetermined but possible flood hazard." These properties were dropped from the analysis, but including them in the 100-year floodplain, or, alternatively in the 500-year floodplain, did not affect the results.[2] Thus, the hedonic model would be:

$$\ln(P_{it}) = \beta_0 + \beta_1^{'} \ln L_i + \beta_2^{'} S_{it} + \beta_3^{'} S_{it}^2 + \beta_4 100yrFP_i + \beta_5 500yrFP_i + \delta_t + \varepsilon_{it} \qquad (2)$$

The variable 100*yrFP* (100-year floodplain) in this model is a dummy equal to 1 if the property falls within the 100-year floodplain and 0 otherwise. Similarly, the variable 500*yrFP* (500-year floodplain) is a dummy equal to 1 if the property falls within the 500-year floodplain and 0 otherwise. Year fixed effects (δ_t) were included to capture annual shocks that may affect all of the properties. Throughout, we use White's heteroskedasticity- consistent standard errors.

In order to determine the effect of the 1994 flood on property prices the DD model traditionally used is:

$$\ln(P_{it}) = \beta_0 + \beta_1^{'} \ln L_i + \beta_2^{'} S_{it} + \beta_3^{'} S_{it}^2 + \beta_4 100yrFP_i + \beta_5 500yrFP_i + \beta_6 Flood_i + \beta_7 100yrFP_i * Flood_i + \beta_8 500yrFP_i * Flood_i + \delta_t + \varepsilon_{it}$$

This DD model has been used in previous studies (Bin and Polasky; Kousky) to examine the information effects of a natural disaster. In this model, properties that fall within a floodplain are

[2] These results are available upon request.

the treatment group and properties outside the floodplain are the control group. The variable *Flood* is a dummy variable equal to one if the sale happened after the flood (July 1994 in our case). The interaction term between the 100-year floodplain variable (100*yrFP*) and *Flood* tells us how the 1994 flood might have affected the prices of properties that are in the 100-year floodplain and that are sold after the 1994 flood. A similar interpretation applies to the 500-year floodplain and the flood dummy interaction.

We expanded the traditional DD model to incorporate a potential information decay effect in the model:

$$\ln(P_{it}) = \beta_0 + \beta_1^{'} \ln L_i + \beta_2^{'} S_{it} + \beta_3^{'} S_{it}^2 + \beta_4 100yrFP_i + \beta_5 500yrFP_i + \beta_6 Flood_i + \beta_7 100yrFP_i * Flood_i$$
$$+ \beta_8 500yrFP_i * Flood_i + \beta_9 years + \beta_{10} years * 100yrFP_i + \beta_{11} years * 500yrFP_i + \delta_t + \varepsilon_{it}$$

To examine the persistence of a risk premium over the years after the 1994 flood event we used the interaction between *years* and the floodplain variables, where the variable "*years*" is a time trend that represents the number of years after the 1994 flood. The interaction term estimates how the risk premium changed over time after the 1994 flood.

It is hypothesized that if homebuyers are aware of flood hazards, prices for houses lying within the floodplain will be lower than those of comparable properties lying outside the floodplain. We also hypothesize that the perceived risk will be heightened after the 1994 flood event and the risk premium will decline as time passes. Rejecting the first hypothesis could indicate a need to improve the system of communication of flood risk to homeowners through effective education and outreach and efforts. If we find temporal decay in the flood risk discount, this could indicate the need for implementing information programs that act as a reminder to the homeowners.

Another econometric issue concerns the potential spatial dependence of the observations. Neighboring properties are likely to share common unobserved location features, similar structural characteristics due to contemporaneous construction, neighborhood effects and other causes of spatial dependence. Ignoring the problem could result in inefficient or inconsistent parameter estimates (Anselin and Bera, 1998). Testing for the presence of spatial dependence can proceed via maximum likelihood estimation of alternative models and applying appropriate Lagrange multiplier tests. Another approach tests the significance of Moran's I spatial autocorrelation coefficient estimated from the OLS residuals. However, both approaches require the specification of a spatial weights matrix.

As noted by Donovan et al. (2007), the specification of the matrix can be arbitrary and it can influence the outcome of the tests. To minimize the guess work, our analysis follows their lead and employs a semivariance analysis of the properties. This is a geostatistical technique that was first employed in mining exploration but has since been used in varied fields including environmental health and hydrology (Cressie, 1992). The semivariance is a measure of association between pairs of properties that are within the distance intervals specified by the researcher. Spatial dependence is indicated by increasing semivariance as the distance between pairs is increased, i.e. as properties lose their grouping into neighborhoods they become less alike. If the semivariance is plotted over distance, insight into the weights matrix specification can be obtained.

Figure 3 displays plots of two semivariances for pairs of properties within 20 meter intervals, going out to 1,000 meters. In the lowest plotted line the regression's residual semivariance increases dramatically in the first intervals up to about 50 meters, then it increases slightly to 200 meters after which it levels off. Within the GIS overlay of Doughtery County, these distances

are measured from the parcels' centroids rather than the actual houses. Given the size of the parcels, pairs within 50 meters of each other tend to represent contiguous properties. Pairs within 200 meters of each other are separated by four to six neighboring houses. The second plot of the regression's dependent variable semivariance, the logarithm of property price, also increases dramatically from the origin but it continues to increase over the full range of distance intervals. While the prices display the classic symptoms of spatial dependence, the residuals only display a neighbor effect. This comparison of the two plots suggests that the regression model is accounting for the majority of spatial dependence with its set of spatial and neighborhood-level variables.

Concerning the spatial weights matrix, *W*, this analysis suggests that two different specifications may be appropriate. In our estimation, we use two common parameterizations for *W*: a contiguity matrix, where adjacent properties get a weight of one and zero otherwise, and an inverse distance matrix, $w_{ij} = \frac{1}{D_{(i,j)}}$, where $D_{(i,j)}$ is the distance between parcels i & j, for distances less than 200 meters, and $w_{ij} = 0$ otherwise[3]. The second specification could be the most appropriate if the additional increase in semivariance between 50 and 200 meters, from 0.13 to 0.15, is large enough to indicate spatial dependence when the first specification does not.

We incorporate the spatial weights matrix, *W*, into a spatially lagged and autoregressive disturbance model which is frequently referred to as a SARAR model (Anselin and Florax, 1995). The model allows for spatial interactions in the dependent variable, the exogenous variables, and the disturbances. Spatial interactions in the dependent variable are modeled through a spatial lag structure that assumes an indirect effect based on proximity; the weighted

[3] We use a min-max normalized inverse distance matrix since normalizing matrix by a scalar preserves symmetry and the basic model specification (Drukker et. al, 2011).

average of other housing prices affects the price of each house. The error term incorporates spatial considerations through a spatially weighted error structure which assumes at least one omitted variable that varies spatially leading to measurement error. The general form of our SARAR model is as follows:

$$\begin{aligned}\ln(P_{it}) = {} & \beta_0 + \lambda W_i \ln(P_{it}) + \beta_1^{'} \ln L_i + \beta_2^{'} S_{it} + \beta_3^{'} S_{it}^2 + \beta_4 100\, yrFP_i + \beta_5 500\, yrFP_i \\ & + \beta_6 Flood_i + \beta_7 100\, yrFP_i * Flood_i + \beta_8 500\, yrFP_i * Flood_i \\ & + \beta_9 years + \beta_{10} years * 100\, yrFP_i + \beta_{11} years * 500\, yrFP_i + \delta_t + \varepsilon_{it}\end{aligned}$$

Where $\varepsilon_{it} = \rho M_i \varepsilon_{it} + u_{it}$

The above model is similar to equation (4) except that we introduce λ and ρ; a spatial lag parameter and a spatial autocorrelation coefficient, respectively. W and M are n x n spatial weights matrices that are taken to be known and non-stochastic. As in Fingleton (2008), Fingleton and Le Gallo (2008), Kissling and Carl (2008), and Kelejian and Prucha (2010) we assume W=M.[4] The existence of spatial autocorrelation increases the possibility that the errors will not be distributed normally.[5] Maximum likelihood estimation procedures, as those used by Bin and Landry, depend on the assumption of normality of the regression error term, while the generalized moments approach does not. Thus, a generalized two stage least squares estimator that produces consistent estimates is employed (Arraiz, et al., 2010). The disturbances u_{it} are assumed to be independent and identically distributed (IID).

[4] According to Anselin and Bera, the SARAR model requires that either $W \neq M$ or the existence of one or more explanatory variables. The latter is true for our model.
[5] The Jarque-Bera test for normality of the residuals suggested that the residuals are not normally distributed.

4. Data

A unique dataset was constructed by merging individual property sales data for residential homes in Dougherty County from the Dougherty County's Tax Assessor's office for all available years, 1985 to 2010, with a parcel-level Geographic Information System (GIS) database. In order to use the spatial weight matrices to control for the lag and error dependence in our model, we limit our sample to the most recent sale, i.e. there are no repeated sales.[6] The property records contain information on housing characteristics (number of bedrooms, number of bathrooms, total square footage, total acres, size of the house, etc.), vector **S** in equations (1)-(5), as well as sale date and sale price. All the property sales prices were adjusted to 2010 constant dollars, using the housing price index for the Albany metropolitan area from the Office of Federal Housing Enterprise Oversight.

GIS was utilized to measure the distance from each property to important features that could influence property values such as nearby major highways, railroads, and amenities such as parks and rivers. The neighborhood characteristics (median household income and percent of non-white residents) were determined at the block group level using 2000 census data.[7] These proximity and neighborhood variables are denoted by vector **L** in equations (1)-(5). To measure flood risk, we used a GIS layer of FEMA Q3 flood data to identify parcels in 100-year and 500-year floodplains as represented on Flood Insurance Rate maps (FIRMs) published in 1996.[8]

Studies have shown that there are price premiums associated with elevated properties (McKenzie and Levendis, 2010). To see if that is true for Dougherty County, elevation of each property was

[6] To create an inverse distance matrix the observations must have unique coordinates. For a contiguity matrix the only requirement is that the shape file of the dataset be a polygon.
[7] Block Groups generally contain between 600 and 3,000 people, with a typical size of 1,500 people.
[8] The newest floodplain map available was published in 2009 but we choose the 1996 map as the large flood event in our study occurred in 1994 and most of our sales transaction occurred before 2009.

determined using the GIS file of contour lines. We also determined if the house was built after the National flood Insurance Program (NFIP) in Dougherty County i.e. after 1978. We included NFIP as a dummy equal to 1 if the property was built after 1978 (0 otherwise) to capture the effect of the NFIP in Dougherty County.[9]

After dropping properties for which (a) data were missing, (b) sale price was less than $5,000 or more than $500,000, or (c) they were not single family residential properties, 12,151 property transactions were included in the dataset.[10] Table 1 presents their descriptive statistics. The average house was 43 years old with the oldest home built in 1841 and the newest built in 2010. The mean property value in 2010 constant dollars was $99,713. The mean distance to the Flint River was about 4.8 kilometers. The average of median household incomes in the census block groups was $39,483. 81 percent of the properties were sold after the 1994 flood. 26 percent of the houses were built after the NFIP with a mean elevation of 206 meters. Most importantly, of all sales between 1985 and 2010, almost 8.6% of the properties were in high risk zones such as the 100-year floodplain and almost 2.0% of the properties were in the 500-year floodplain.

5. Results

5.1 Ordinary Least Squares Estimates:

Using the OLS regression on pooled data for all sale dates prior to the July 1994 flood, we find that there was a significant discount associated with properties in the 100-year floodplain, but 500-year floodplain properties were not discounted significantly (Table 2, Column 1). This suggests that before the 1994 flood, homebuyers in the 500-year floodplain in Dougherty County

[9] Communities participating in the NFIP must fully comply with its building code that requires the lowest floor of any new residential building to be elevated above the base flood elevation.

[10] Properties sold for less than $5,000 were probably family transfers and not real sales. Since the maximum NFIP coverage is $250,000, flood insurance is less important for very expensive houses

were probably unaware of the flood risk and, therefore, the flood risk was not capitalized into property prices. The coefficient for NFIP is positive and significant, implying that homes constructed under the more stringent building codes are worth more. The neighborhood variables, median household income and percent of non-white residents by block group, have an expected significant positive and negative sign respectively. All coefficients for structural housing characteristics have the expected sign and most of the parameters are statistically significant. The quadratic specification seems to capture diminishing marginal effects for age, bedrooms and full baths. The results indicate that proximity to the Flint River, lakes and ponds, utility lines and parks increases the property prices significantly. There was a small price premium associated with elevated properties; when evaluated for an average priced home the premium equals almost $184.

Table 2, column 2 shows the effect of the 1994 flood on the estimated discount for property prices within the floodplain in a DD framework. Assuming that properties outside the floodplain represent a valid control group, the causal effect of the change in information, attributable to the 1994 major flood event on flood prone property values, is reflected in the coefficients of the interaction terms between the flood and floodplain dummies. The result indicates that immediately after the 1994 flood, there was a significant discount of 22% for 100-year floodplain properties. This discount is equivalent to $21,936 when evaluated at an average priced home in Dougherty County. The 500-year floodplain properties were also significantly discounted after the flood by 27%. These discounts are much larger than the present value of the insurance premium under discount rates of 3, 5 and 7 percent for an average home. The present value of the flood insurance rate at a 3% discount for an average house is equal to $8,967 (Table 3). This difference could be due to the concealed costs associated with a flood event, such as the

hassle and the uninsurable costs (e.g. sentimental attachment to the house and its contents) being perceived by the homebuyers.

The discount, however, is not persistent over time. The information decay effect is prominent and statistically significant for both the 100-year and 500-year flood zones as indicated by positive and significant floodplain and year interaction terms across all specifications in Table 2. This suggests that the information effect associated with the 1994 flood receded over time. For properties in the 100-year floodplain the information effect decreased by approximately 2.8% annually. Properties in the 500-year floodplain were discounted dramatically but this information effect decayed by 2.2% annually. This decay effect is consistent with the theory of the availability heuristic, a cognitive illusion that is influenced by what is recent or dramatic. As the recollection of a flood experience fades over time, the construction of the availability heuristic based on that event becomes more difficult (Pryce, et al., 2011). The property discount vanishes after seven years and eleven years for properties in the 100-year and 500-yearfloodplains, respectively (Figure 4). Figure 4 shows the average flood risk discount, calculated by multiplying the mean property price times the risk coefficient accounting for the temporal decay (e.g. a 100-year floodplain property is discounted by $19,161 the first year after the flood, by $16,385 the second year after the flood, and so on). The displayed error bands account for the standard errors that ranged from $1,685 to $2,328 depending upon the specifications.

As a robustness test we estimated a model in which, as in Kousky, we interacted the year dummy variables with the floodplain variables. The interaction between the year dummy variables and

the floodplain variables showed a similar decay effect, and the price discount for properties in the 100- year flood plain vanished five years after the flood event.[11]

Consistent with the pre-flood regression, we find a price premium associated with properties built after the NFIP regulations in Dougherty County; here it was almost 20% larger for properties in the 100-year floodplain. Unlike the results from the pre-flood regression, we find that the proximity to school adds value to the property prices but the proximity to utility lines does not.

5.2 Estimates of the SARAR Model:

The estimation results of the SARAR model with two different spatial weights matrices are presented in columns 3 and 4 of Table 2. Column 3 presents the results from the use of the contiguity matrix, and column 4 the results from the use of the inverse distance matrix. As with the OLS regressions, there is a significant discount for properties in the 100-year and 500-year floodplains after the flood. This is consistent with the results of Mueller and Loomis (2008) that spatially corrected estimates of implicit prices are often found to be similar to those obtained using pooled regression. However, the magnitudes of the discount slightly vary across specifications.

With the contiguity specification for the *W* matrix, we find that after the 1994 flood the discount for properties in the 100-year floodplain was almost 20% whereas the discount for properties in the 500-year floodplain was almost 25% which is equivalent to $19,942 and $23,931 price discounts for 100-year and 500-year properties, respectively, when evaluated at the average priced home. Most importantly, we find evidence of the information decay effect (i.e., the

[11] These results are available upon request.

coefficients for $100yrFP * Years$ and $500yrFP * Years$ are positive and statistically significant). This implies that the flood risk discount vanishes after seven years for properties within the 100-year floodplain and after twelve years for those in the 500-year floodplain (Figure 5).[12] The significant spatial autocorrelation parameter (ρ) and spatial autoregressive coefficient (λ), towards the bottom of the third column in Table 2, suggest that there is, in fact, spatial dependence among the properties in our dataset in the expected direction: a positive adjacency effect. For example, we would expect a positive λ since a higher sale price of neighboring properties would result in a higher average sale price, *ceteris paribus*. Conforming to intuition, λ is estimated at 0.00121 and is significant at a 5 percent level, indicating that if the weighted average of neighboring houses' sale price increase by 1 percent, the sale price of an individual house increases by approximately 0.0012 percent.

Using the inverse distance matrix as the weights matrix, we find that properties in the 100-year floodplain were discounted by almost 18% after the 1994 flood. A 4% additional discount was found for properties in the 500-year floodplain (Figure 6). The flood risk information decayed at the rates of 2.4 % and 1.5%, implying that the discounts vanished seven years and fifteen years after the flood for properties in the 100-year and 500-year floodplains, respectively. We also find evidence of spatial dependence indicated by a positive and significant λ parameter. Dependence in the error is also confirmed by a significant ρ parameter.

In comparing results across the three models in Table 2, a key element is the difference in the marginal effects. According to Kim, Phipps, and Anselin (2003), the marginal effect of a variable from the traditional OLS model or the spatial error model is just the first derivative with

[12] We account for the spatial multiplier (1/1-λ) when calculating the price discounts using contiguity and inverse distance matrices.

respect to the characteristic of interest. In the spatial lag model, however, marginal effects are calculated by multiplying the first derivative times a spatial multiplier, $1/(1-\lambda)$, where λ is the spatial lag parameter from equation 5 with the property. A larger λ means a larger spatial dependence and thus, a larger spatial multiplier. We find that λ is an order of magnitude larger for the inverse distance matrix which means the inverse distance matrix is accounting for much more of spatial dependence than the contiguity matrix. However, this increase in the spatial multiplier can be offset by changes in the magnitude of the model beta coefficients. This is the case with our results, since the discount decreased from 19.9% to 17.6% for properties in the 100-year floodplain.

Using either of the two weights matrices, we find that the NFIP variable has a marked impact in raising the price of the properties in 100-year floodplain. Proximity to river, lake and pond, and park increased the property prices significantly. Increased median income increased the property prices whereas the increase in the percent of non-white residents in the block group decreased the property prices.

6. Conclusion

This study offers evidence of the effect of a large 1994 flood event on the price of flood-prone properties in Dougherty County, Georgia, while also exploring whether or not the information effect of the flood recedes over time. Consistent with previous studies (Bin and Polasky, 2004; Kousky, 2010) we find that, right after the flood, the prices of properties located within the floodplain were significantly discounted compared to properties located outside the floodplain. Before the 1994 flood, the residents in Dougherty County seemed to be aware of the flood risk in 100-year floodplain properties as suggested by significant price discount estimates. However, the

1994 flood seems to have provided more information about the existing flood risk. After the 1994 flood, homebuyers in the 100-year floodplain discounted the property prices significantly (i.e. capitalized the flood risk into property prices after the flood) with the discount varying between 18% to 22%. An even larger discount of 22% to 27% was found for properties in the 500-year floodplain. This result agrees with Kousky's, who also finds that after a significant flood event, properties in the 500-year floodplain were discounted significantly. Unlike her results, our estimates of the discount are larger in magnitude. Unlike Kousky but like Bin and Landry we also find a discount for properties in the 100-year floodplain immediately after the flood.

The estimated discount for floodplain properties is larger than the present value of the insurance premium under discount rates of 3, 5 and 7 percent indicating that property buyers may be considering uninsurable losses in their decisions. Recovering from a flood involves a substantial hassle and emotional attachment to the property that is probably considered by homebuyers. The information updating impact of the flood is more marked on prices of properties in the 500-year flood plain. This would be the case if flood risk awareness was even more limited among these residents. This is to be expected as only homebuyers of properties in the 100-year floodplain are required to acquire flood insurance.

While homebuyers are quick to adjust their risk perception right after the flooding event, the effect of this new information is transitory. We find that the risk perception decays rapidly; at the rate of 2.4 to 2.7 percent annually for 100-year and 1.4 to 2.2 percent annually for 500-year floodplain properties, depending on the model specification. Furthermore, we found it to be nonexistent twelve years after the flood event for properties in the 100-year floodplain. Overall our results highlight the continuing relevance of Tversky’s and Kahneman’s "availability

heuristic," i.e. the cognitive state in which a decision maker relies upon knowledge that is readily available (e.g. what is recent or dramatic) rather than searching alternative information sources.

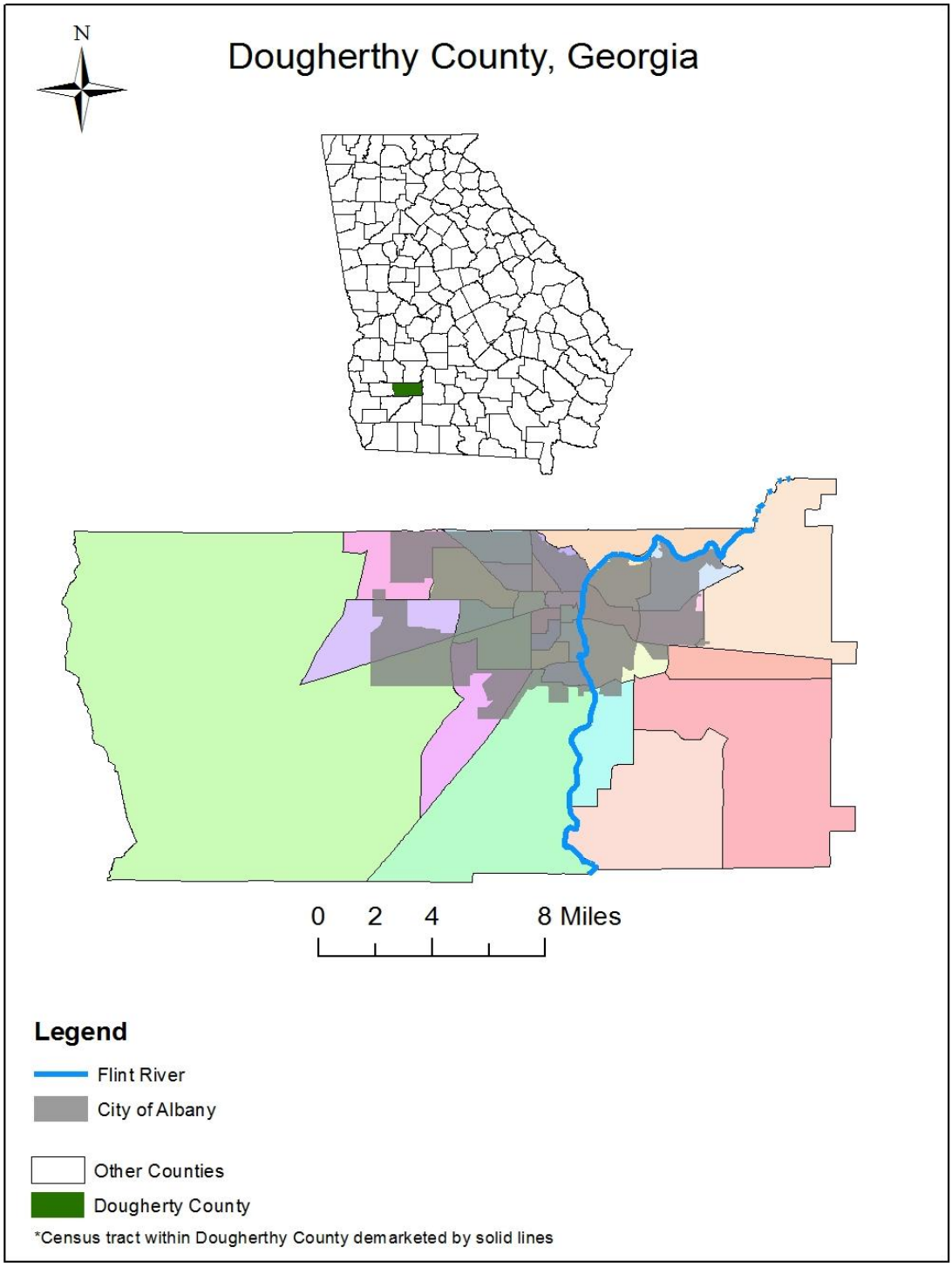

Prepared by : Ajita Atreya

Figure 1: Study area -Dougherty County, GA, showing City of Albany and Flint River

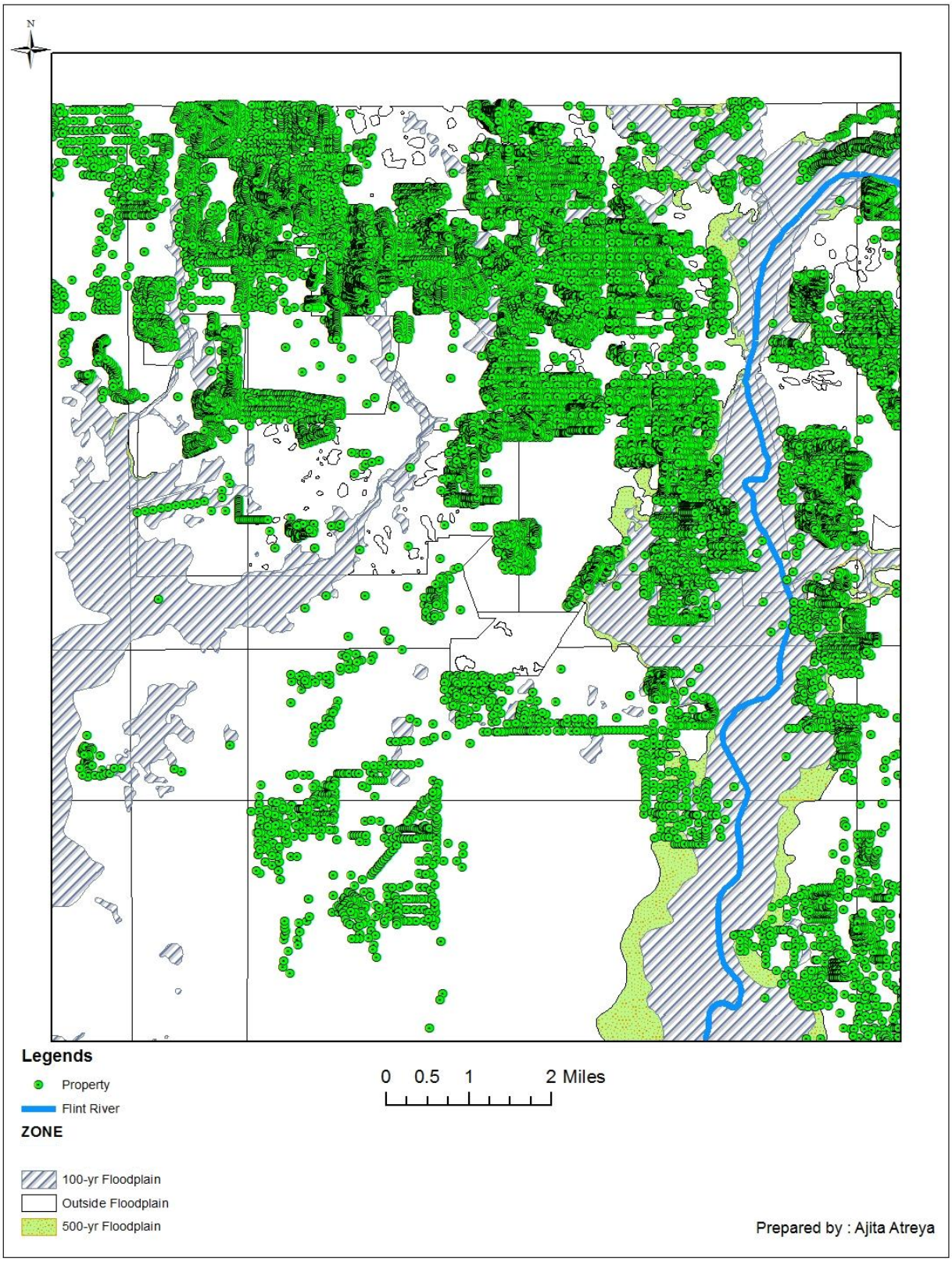

Figure 2: Flint River, Housing Units and Associated Floodplains in Dougherty County

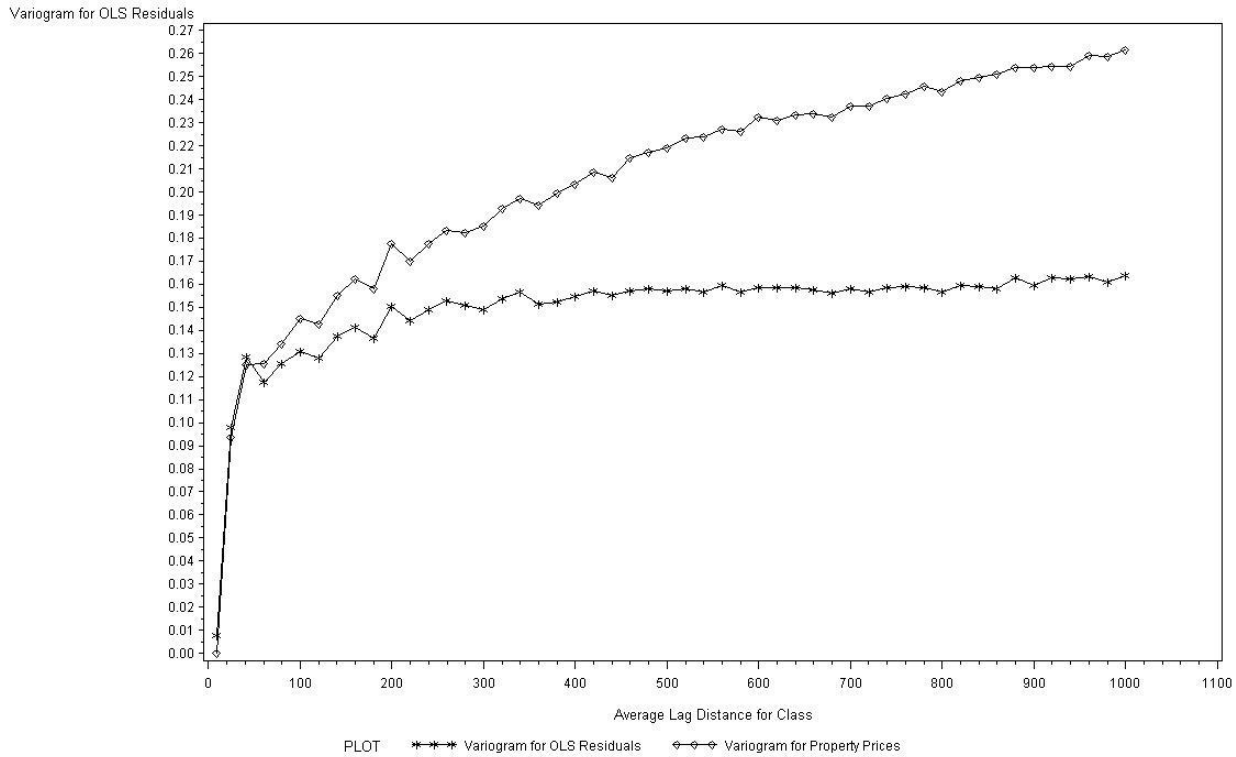

Figure 3: Semivariance Graph of Observed Prices (logged) and OLS Residuals.

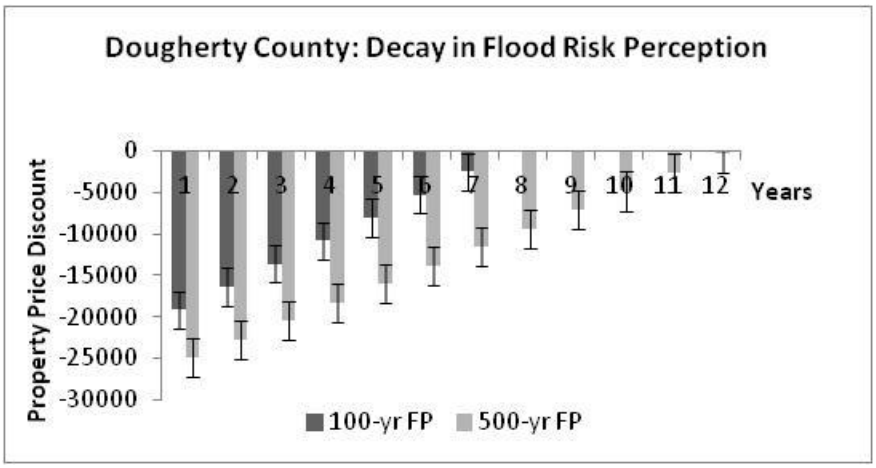

Figure 4: Flood Risk Persistence in Dougherty County: Estimates based on OLS Regression

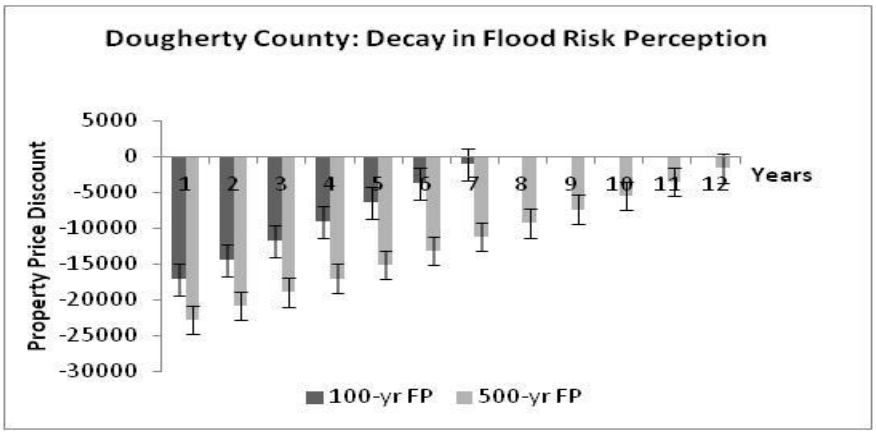

Figure 5: Flood Risk Persistence in Dougherty County: Estimates based on the use of a contiguity matrix

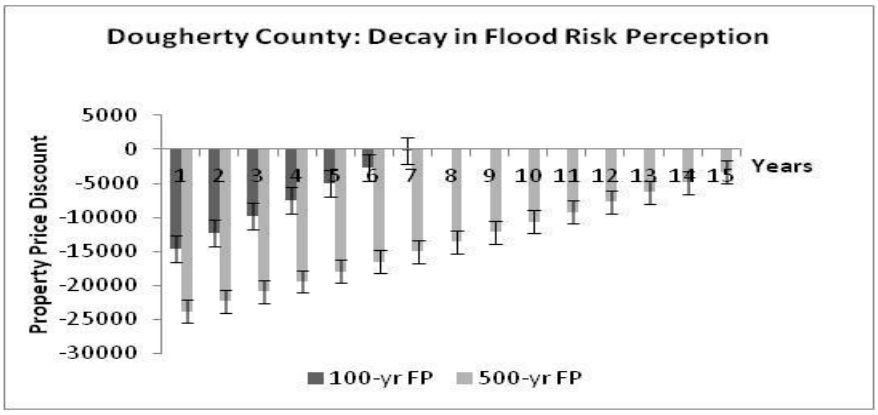

Figure 6: Flood Risk Persistence in Dougherty County: Estimates based on the use of an inverse distance matrix

Table 1: Variable and Descriptive Statistics

Variables	Description	Mean	Std. Dev.	Min	Max
Price	Sale price of property adjusted to 2010 constant dollars	99,713	74441.53	5024.6	489649.5
Flood Variables					
100yr FP	1 if 100-year flood zone, 0 otherwise	8.6%	28%	0	1
500yr FP	1 if 500-year flood zone, 0 otherwise	2.0%	14%	0	1
Years	Number of years after 1994 flood	7.14	5.40	0	16
Location Attributes in Meter (m)					
Elevation	Elevation of property	205.84	16.96	153	309
River	Distance to nearest river	802.66	655.82	3.25	5699.27
Lake	Distance to nearest lake	529.11	366.75	0	2439.82
Railroad	Distance to nearest railroad	1937.72	1850.27	15.81	11489.95
Highway	Distance to nearest highway	45.15	50.31	0.01	818.73
Utilities	Distance to nearest utility lines	2931.61	1839.10	5.75	13212.04
Park	Distance to nearest park	3409.28	2676.60	45.24	18510.93
School	Distance to nearest school	1808.71	2033.20	25.45	15183.09
Flint	Distance to Flint River	4822.23	3487.51	62.66	21387.79
Structural Attributes					
Yearbuilt	Year the property was built	1967	18.58	1841	2010
Acres	Total acreage of the property	0.91	4.39	0.01	265.54
Bedrooms	Number of bedrooms	3.04	.66	1	30
Fullbths	Number of full baths	1.69	0.68	0	7
Halfbths	Number of half baths	0.17	0.38	0	2
Htdsqft	Heated square feet	1668.23	735.88	0	18783
Fireplace	Number of fireplaces	0.48	0.57	0	6
Dummy variables					
AC	1 if central AC present, 0 otherwise	0.88	0.32	0	1
Garage	1 if garage present, 0 otherwise	0.18	0.38	0	1
Brick	1 if brick exterior, 0 otherwise	0.01	0.12	0	1
Flood	1 if sold after July 1994,0 otherwise	81%	38%	0	1
NFIP	1 if the property was built after the National Flood Insurance Program, 0 otherwise	0.26	0.44	0	1
Neighborhood Variables (2000 Census By Block Group)					
Income	Median household income	39482.55	18870.27	6907	80000
PcNW	Percent of non-white residents	51.87%	31.74%	0	100%
Fixed Effects					
Year Fixed Effect	Property sold1985-2010				

Table 2: OLS and SARAR Model Results for Dougherty County

	Ordinary Least Squares (OLS)		SARAR Model	
	Pre 1994	1985-2010	Contiguity Matrix	Inverse Distance Matrix
VARIABLES		lnprice	lnprice	Lnprice
100yr FP	-0.156**	-0.162***	-0.180***	-0.170***
	(0.0609)	(0.0517)	(0.0467)	(0.0505)
500yr FP	-0.107	0.0604	0.0426	0.0367
	(0.108)	(0.0874)	(0.0874)	(0.0884)
Flood		0.0667	0.0659	0.0732
		(0.0502)	(0.0526)	(0.0511)
100yr FP*Flood		-0.220***	-0.199***	-0.176***
		(0.0715)	(0.0596)	(0.0588)
500yr FP*Flood		-0.273**	-0.248**	-0.223**
		(0.131)	(0.115)	(0.112)
Years		-0.07224***	-0.07044***	-0.06422***
		(0.00183)	(0.00178)	(0.00173)
100yr FP*Years		0.02784***	0.02688***	0.024***
		(0.000427)	(0.000356)	(0.000349)
500yr FP*Years		0.0224**	0.0193**	0.0146*
		(0.000838)	(0.000726)	(0.000727)
NFIP	0.157***	0.123***	0.122***	0.130***
	(0.0509)	(0.0309)	(0.0253)	(0.0279)
100yr FP*NFIP	0.104	0.199***	0.224***	0.268***
	(0.122)	(0.0547)	(0.0447)	(0.0493)
500yr FP*NFIP	0.207	0.0193	0.0471	0.0605
	(0.158)	(0.0901)	(0.0836)	(0.0904)
Elevation	0.00185*	0.00139***	0.00135***	0.00101*
	(0.00107)	(0.000410)	(0.000427)	(0.000524)
Ln (River)	-0.0244	-0.0300***	-0.0320***	-0.0230**
	(0.0171)	(0.00728)	(0.00766)	(0.0108)
Ln (Flint)	-0.0443*	0.0467***	0.0446***	0.0316**
	(0.0236)	(0.0109)	(0.0104)	(0.0147)
Ln (lakepond)	-0.0560***	-0.0170**	-0.0192**	-0.0258***
	(0.0184)	(0.00767)	(0.00770)	(0.00994)
Ln (Railroad)	-0.0114	-0.0101	-0.00792	0.0103
	(0.0146)	(0.00678)	(0.00710)	(0.0104)
Ln (Highway)	-0.0110	-0.00540	-0.00620	-0.00296
	(0.0117)	(0.00507)	(0.00546)	(0.00557)
Ln (Utilities)	-0.0468**	-0.00241	-0.000726	0.0109
	(0.0227)	(0.0102)	(0.00951)	(0.0113)
Ln (Park)	-0.0452***	-0.0471***	-0.0471***	-0.0395**
	(0.0172)	(0.00772)	(0.00865)	(0.0157)
Ln (school)	0.00460	-0.0277***	-0.0265***	-0.0164
	(0.0165)	(0.00769)	(0.00829)	(0.0128)
Acres	0.000296	0.00815**	0.0106***	0.0117***
	(0.00413)	(0.00338)	(0.00235)	(0.00232)
Acresq	9.88e-06	-1.49e-05	-3.05e-05**	-3.34e-05**
	(1.60e-05)	(1.25e-05)	(1.34e-05)	(1.33e-05)

Age	0.0376***	0.0180***	0.0186***	0.0220***
	(0.00441)	(0.00290)	(0.00123)	(0.00129)
Agesq	-0.000501***	-0.000233***	-0.000233***	-0.000256***
	(6.95e-05)	(3.87e-05)	(1.24e-05)	(1.27e-05)
Bedrooms	0.366**	0.0344*	0.0343**	0.0363**
	(0.153)	(0.0195)	(0.0158)	(0.0156)
Bedsq	-0.0462*	-0.000423	-0.000435	-0.000507
	(0.0240)	(0.000567)	(0.000729)	(0.000708)
Fullbths	0.378***	0.425***	0.388***	0.300***
	(0.0961)	(0.0413)	(0.0336)	(0.0345)
Fullbathsq	-0.0547**	-0.0768***	-0.0694***	-0.0542***
	(0.0247)	(0.0104)	(0.00747)	(0.00752)
Halfbths	0.275	0.396***	0.366***	0.353***
	(0.271)	(0.0919)	(0.0712)	(0.0697)
Halfbathsq	-0.211	-0.337***	-0.307***	-0.307***
	(0.264)	(0.0885)	(0.0668)	(0.0653)
Htdsqft	0.000303***	0.000308***	0.000300***	0.000303***
	(9.86e-05)	(3.11e-05)	(2.04e-05)	(2.06e-05)
Htsqftsq	-2.92e-08	-1.77e-08***	-1.66e-08***	-1.71e-08***
	(1.93e-08)	(5.17e-09)	(2.30e-09)	(2.26e-09)
Fireplace	0.0671**	0.0598***	0.0553***	0.0547***
	(0.0279)	(0.0117)	(0.0113)	(0.0114)
Garage	0.0268	0.110***	0.110***	0.0955***
	(0.0394)	(0.0167)	(0.0163)	(0.0165)
AC	0.206***	0.169***	0.175***	0.154***
	(0.0429)	(0.0234)	(0.0185)	(0.0189)
Brick Exterior	0.143*	-0.00823	-0.00187	-0.0167
	(0.0749)	(0.0447)	(0.0411)	(0.0405)
Ln (Income)	0.489***	0.359***	0.378***	0.461***
	(0.0546)	(0.0259)	(0.0247)	(0.0365)
Non-White (%)	-0.00134**	-0.00233***	-0.00234***	-0.00168***
	(0.000633)	(0.000301)	(0.000322)	(0.000524)
Constant	5.641***	5.196***	5.034***	3.935***
	(0.745)	(0.470)	(0.477)	(0.577)
Year Fixed Effect	Y	Y	Y	Y
Lambda	-	-	0.00121**	0.0304***
			(0.000519)	(0.00564)
Rho	-	-	0.0882***	2.551***
			(0.00520)	(0.0921)
Observations	2,234	12,151	12,151	12,151
R-squared	0.439	0.459		

Robust standard errors in parentheses
*** p<0.01, ** p<0.05, * p<0.1

Table 3: Present Value of Flood Insurance Premium at Various Discount Rates

		Present Value of Insurance Premium Under Discount Rates of		
Value of Houses	Annual Flood Insurance Premium	3%	5%	7%
$75,000	$203	$ 6,742	$4,055	$2,896
$99,713	$270	$ 8,967	$ 5,393	$ 3,851
$200,000	$540	$ 17,999	$ 10,800	$7,714

Note: Flood insurance premium for an average valued single-family house in the 100-year floodplain, without a basement and with estimated base flood elevation of 3 feet or more, is equal to $270. This is calculated using 0.27 as the annual post firm construction rate per $100 of coverage as designated in the NFIP flood insurance manual, effective January 1, 2011.

References:

Anselin, L., and A.K. Bera. 1998. "Spatial dependence in linear regression models with an introduction to spatial econometrics." *in A. Ullah and D. Giles, eds., Handbook of Applied Economic Statistics* 155:237-290.

Anselin, L., and R. Florax. "Small Sample Properties of Tests for Spatial Dependence in Regression Models: Some Further Results." In L. Anselin and R.Florax (eds.), *New Directions in Spatial Econometrics*, Berlin: Springer-Verlag, 1995: 21–74

Arraiz, I., D.M. Drukker, H.H. Kelejian, and I.R. Prucha. 2010. "A spatial Cliff-Ord type model with heteroskedastic innovations: small and large sample results." *Journal of Regional Science* 50(2):592-614.

Beatley, T., D. Brower, and A. Schwab. 2002. *An Introduction to Coastal Zone Management*, 2nd ed. Island Press

Bin, O., and J. Kruse. 2006. "Real estate market response to coastal flood hazards." *Natural Hazards Review* 7:137.

Bin, O., J. Kruse, and C. Landry. 2008. "Flood hazards, insurance rates, and amenities: Evidence from the coastal housing market." *Journal of Risk and Insurance* 75(1):63-82.

Bin, O., and C. Landry. 2011. "Changes in Implicit Flood Risk Premiums: Empirical Evidence from the Housing Market. ." *Available at SSRN: http://ssrn.com/abstract=1850671.*

Bin, O., and S. Polasky. 2004. "Effects of flood hazards on property values: evidence before and after Hurricane Floyd." *Land Economics* 80(4):490.

Burby, R.J. 2001. "Flood insurance and floodplain management: the US experience." *Global Environmental Change Part B: Environmental Hazards* 3(3-4):111-122.

Carbone, J., D. Hallstrom, and V. Smith. 2006. "Can natural experiments measure behavioral responses to environmental risks?" *Environmental and Resource Economics* 33(3):273-297.

Cressie, N. 1993. *Statistics for Spatial Data*. Wiley and Sons, New York.

Donovan, G.H., P.A. Champ, and D.T. Butry. 2007. "Wildfire risk and housing prices: a case study from Colorado Springs." *Land Economics* 83(2):217-233.

Drukker, D.M., H. Peng, I.R. Prucha, and R. Raciborski. 2011 "Creating and managing spatial weighting matrices using the spmat command." Retrived March 1,2012 from http://econweb.umd.edu/~prucha/Papers/WP_spmat_2011.pdf

EMDAT. 2010. "OFDA/CRED (Office of Foreign Disaster Assistance, USAID / Center for Research of the Epidemiology of Disasters) 2010." *International Disaster Database -www.emdat.be-Universite Catholique de Louvain, Brussels, Belgium*.

Federal Emergency Management Agency, Community Status Book Report, Georgia, *Comminities Participating in the National Flood Program* Retrieved February 20, 2012 from http://www.fema.gov/cis/GA.html

Fingleton, B. 2008. "A generalized method of moments estimator for a spatial model with moving average errors, with application to real estate prices." *Empirical Economics* 34(1):35-57.

Fingleton, B., and J. Le Gallo. 2008. "Estimating spatial models with endogenous variables, a spatial lag and spatially dependent disturbances: Finite sample properties." *Papers in Regional Science* 87(3):319-339.

Freeman, A. 2003. *The measurement of environmental and resource values: theory and methods*: RFF press.

Formwalt, L.W. 1996. "A Garden of Irony and Diversity."In *The New Georgia Guide*: University of Georgia Press, Athens, Georgia , pp. 535.

Halstead, J.M., R.A. Bouvier, and B.E. Hansen. 1997. "On the issue of functional form choice in hedonic price functions: further evidence." *Environmental Management* 21(5):759-765.

Harrison, D.M., G. T. Smersh, and A.L. Schwartz. 2001. "Environmental determinants of housing prices: the impact of flood zone status." *Journal of Real Estate Research* 21(1):3-20.

IPCC. 2001. "Intergovernmental Panel on Climate Change. Climate Change 2001: Impacts, Adaptation and Vulnerability, Cambridge University Press, Cambridge UK.".

IPCC. 2007. "Intergovernmental Panel on Climate Change. Impacts, Adaptation and Vulnerability, Cambridge University Press, Cambridge UK."

Kelejian, H.H., and I.R. Prucha. 2010. "Specification and estimation of spatial autoregressive models with autoregressive and heteroskedastic disturbances." *Journal of Econometrics* 157(1):53-67.

Kim, C.W., T. T. Phipps, and L.Anselin. 2003. "Measuring the Benefits of air quality improvement: A spatial hedonic approach."*Journal of Environmental Economics and Management* 45 (1):24-39

Kissling, W.D., and G. Carl. 2008. "Spatial autocorrelation and the selection of simultaneous autoregressive models." *Global Ecology and Biogeography* 17(1):59-71.

Kousky, C. 2010. "Learning from Extreme Events: Risk Perceptions after the Flood." *Land Economics* 86(3):395.

Kunreuther, H., and E. Michel-Kerjan (2007) Climate change, insurability of large-scale disasters and the emerging liability challenge, National Bureau of Economic Research Cambridge, Mass., USA.

MacDonald, D., J. Murdoch, and H. White. 1987. "Uncertain hazards, insurance, and consumer choice: Evidence from housing markets." *Land Economics* 63(4):361-371.

McKenzie, R., and J. Levendis. 2010. "Flood hazards and urban housing markets: The effects of Katrina on New Orleans." *The Journal of Real Estate Finance and Economics* 40(1):62-76.

Mueller, J.M., and J.B. Loomis. 2008. "Spatial dependence in hedonic property models: Do different corrections for spatial dependence result in economically significant differences in estimated implicit prices?" *Journal of Agricultural and Resource Economics* 33(2).

Pielke, R.A., M.W. Downton, and J.Z.B. Miller. 2002. *Flood damage in the United States, 1926-2000: a reanalysis of National Weather Service estimates*: University Corp. for Atmospheric Research.

Pryce, G., Y. Chen, and G. Galster. 2011. "The impact of floods on house prices: An imperfect information approach with myopia and amnesia." *Housing Studies* 26(02):259-279.

Rosen, S. 1974. "Hedonic prices and implicit markets: product differentiation in pure competition." *The Journal of Political Economy* 82(1):34-55.

Shilling, J., J. Benjamin, and C. Sirmans. 1985. "Adjusting comparable sales for floodplain location." *The Appraisal Journal* 53(3):429-436.

Skantz, T., and T. Strickland. 1996. "House prices and a flood event: an empirical investigation of market efficiency." *Journal of Real Estate Research* 2(2):75-83.

Speyrer, J.F., and W.R. Ragas. 1991. "Housing prices and flood risk: an examination using spline regression." *The Journal of Real Estate Finance and Economics* 4(4):395-407.

Stamey, T.C. 1996. "Summary of data-collection activities and effects of flooding from Tropical Storm Alberto in parts of Georgia, Alabama, and Florida, July 1994."

SwissRe. 2006. "The effect of climate change: storm damage in Europe on the rise, Focus report."

Tversky, A., and D. Kahneman. 1973. "Availability: A heuristic for judging frequency and probability." *Cognitive psychology* 5(2):207-232.

U.S. Census Bureau.2010. *State and County Quick Facts*:Dougherty County, Georgia, Retrieved February 20, 2012 from http://quickfacts.census.gov/qfd/states/13/13095.html

USGS. 2006. "Flood hazards—A national threat: U.S. Geological Survey Fact Sheet 2006–3026, 2 p.".

Wetherald, R.T., and S. Manabe. 2002. "Simulation of hydrologic changes associated with global warming." *J. Geophys. Res* 107(D19):4379-4702.

Analysis of Spatial Variation in Flood Risk Perception

Ajita Atreya and Susana Ferreira
Department of Ag. & Applied Economics
University of Georgia
Athens, GA 30602

Abstract

We use hedonic property models to estimate the spatial variation in flood risk in the city of Albany, GA. In addition to knowing whether a property is in the floodplain, we have a unique dataset with actual inundation maps from tropical storm Alberto that hit Albany in 1994. In the absence of information on the structural damages caused by a flood, having information on the actual inundated area can be useful to tease out the information effect of a flood shock from potential reconstruction or other costs. We find that the discount in inundated properties is substantially larger than in comparable properties in the floodplain that did not get inundated. Our results thus suggest that not accounting for whether properties in the floodplains are inundated may overestimate the informational effect of large flood events. In addition of capturing an information effect, the larger discount in inundated properties captures potential reconstruction costs, and supports a hypothesis that homeowners respond better to what they have visualized ("seeing is believing").

1. Introduction

A key element in hazard and disaster management is the understanding of how stakeholders perceive risk. Risk perception is the subjective assessment of the probability of a specific hazard happening and of the consequences of the negative outcome (Sjöberg, 2000). All the individuals of a community may assess the risk of being flooded differently, because there are discrepancies in the probability of the flood hazard (e.g. as homes differ in terms of their location with respect to the floodplain), and in the flow of information about the probability of the flood hazard; and also because each individual is exposed to different scenarios of flooding e.g. from being actually inundated to merely hearing about a flood event in the media. The actual amount of flood damage caused by a specific flood event is higher in an area that is more exposed to the hazard and intuitively, the flood risk perception of an individual should be pronounced in those areas directly hit by a flood.

This paper considers the 1994 flood in Albany as a source of flood risk information to homeowners in Albany and examines the spatial variation in perceived flood risk. Previous studies have used FEMA designated flood hazard maps as a proxy for flood risk zones, and specific flood events as a dummy to capture the informational effect on perceived flood risk. In addition to FEMA hazard maps, we use a map of the area that was inundated by the flood of 1994 in Albany to tease out the information effect from other potential effects of flooding (most notably cleaning and reconstruction costs) on property prices. To the extent of our knowledge, this is the first paper that uses actual inundation map to determine the effects of flood events on property prices. We hypothesize that the discount in these properties will be large for 2 reasons: First, because homeowners are more likely to have experienced physical damages after the flood, and second because people respond better to what they have experienced directly ("seeing is

believing"). More generally, this paper analyzes whether there is spatial variation in the flood risk perception, i.e. whether the flood risk discount is limited to the area directly affected by the flood or whether it extends beyond and how far beyond the heavily affected area.

Two different areas are selected for the study. One is the City of Albany and the other is the area within Albany near Flint River where the majority of the damage occurred. We used a hedonic property model in a difference-in-difference framework to determine the risk perception in the city of Albany and also in the actually inundated study area near Flint River in Albany. We find that for the city of Albany, there was significant discount of 15% in 100-year floodplain and a discount of 33% in 500-year floodplain immediately after the 1994 flood as seen in table 3. In the inundation study area (table 4) the discount was 35% for properties in floodplains[13] and even higher discount of 46% was found for actually inundated area. These results were robust to incorporating the spatial lag and spatial error term corrections in the model.

2. Study Area

Albany was founded in the early 1800s along the Flint River in southwest Georgia. The city of Albany has a total area of 55.9 square miles, of which 55.5 square miles is land and 0.3 square miles is water (US Census Bureau, 2010). In 1994, a severe flood caused by tropical storm Alberto hit Albany, and destroyed parts of downtown and south Albany, causing 15 deaths and displacing almost 22,000 people. Peak discharges greater than the 100-year flood discharge were recorded at all USGS Flint River gauging stations (Stamey, 1996). According to USGS, at Albany, the Flint River peaked at a stage about 5 ft higher than the 1925 flood, which was the previous maximum flood at that gauging station. Figure 1 maps the Flint River, housing units

[13] We included only the 100-year floodplain properties in the floodplain (FP) variable in table 4.

and the associated floodplains for the Albany region. In figure 1, it is evident that there are many properties that fall in the floodplain. Almost 10 percent of the properties sold between the years of 1985 to 2010 fall in 100-year and 500-year floodplain.

According to FEMA, nearly 20,000 communities across the United States and its territories participate in the National Flood Insurance Program (NFIP) enacted in 1968, by adopting and enforcing floodplain management ordinances to reduce future flood damage. In exchange, the NFIP makes federally backed flood insurance available to homeowners, renters, and business owners in these communities. Community participation in the NFIP is voluntary. In order to actuarially rate new construction for flood insurance and create broad-based awareness of the flood hazards, FEMA maps 100-year and 500 year flood-plains in participating communities. Albany, Georgia is one of the participating communities in NFIP since 1974. Homes and buildings in high risk flood areas, those with 1% or greater chance of flooding in any given year and with mortgages from federally regulated or insured lenders are required to have flood insurance.

With a major goal of reducing vulnerability of people and areas most at risk from natural hazard; United States Geological survey (USGS) along with partners the National Weather Service (NWS), U.S. Army Corps of Engineers (USACE), the Federal Emergency Management Agency (FEMA), state agencies, local agencies, and universities have developed a web-based tool for flood response and mitigation. It provides digital geospatial flood-inundation maps that show flood water extent and depth on the land surface. USGS have modeled potential flow characteristics of flooding along a 4.8-mile reach of the Flint River in Albany, Georgia, simulated using recent digital-elevation-model data and the U.S. Geological Survey finite-element surface-water modeling system for two-dimensional flow in the horizontal plane.

Simulated inundated areas, in 1-foot (ft) increments, were created by USGS for water-surface altitudes at the Flint River at Albany stream gage from 179.5-ft altitude to 192.5-ft altitude. Figure 2 shows the study area and the inundated area when the water surface altitude is 192.5 feet at Flint River, which corresponds to the 1994 flood caused by tropical storm Alberto. In addition to the FEMA hazard maps, we use this map of the area that was actually inundated by the 1994 flood in Albany to capture flood risk.

3. Methods

We use a quasi-experimental approach known as Difference-In-Difference (DD) method to measure the effect of a flood event on flood prone property prices in Albany, Georgia. The DD method allows us to isolate the effect attributable to the flood event from the effect of other contemporaneous variables that might influence property prices. The control group in DD approach is composed of properties outside of floodplains. In order to determine the effect of the 1994 flood on property prices the Difference-in-Difference (DD) hedonic model traditionally used is:

$$\begin{aligned}\ln(P_{it}) = \beta_0 + \beta_1^{'} \ln L_i + \beta_2^{'} S_{it} + \beta_3^{'} S_{it}^2 + \beta_4 100yrFP_i + \beta_5 500yrFP_i \\ + \beta_6 Flood + \beta_7 100yrFP_i * Flood + \beta_8 500yrFP_i * Flood + \gamma_i + \delta_t + \varepsilon_{it}\end{aligned} \quad (1)$$

Hedonic models (Rosen, 1974; Freeman, 2003) have been extensively used to estimate the contribution to the total value of a property of each characteristic possessed by the property. In our model, the price of a property, *P*, is modeled as a function of structural characteristics, *S*, (e.g. number of rooms, size of the house), neighborhood and location characteristics, *L*, (e.g. distance to river, distance to parks), and an environmental variable of interest, in this case the flood risk zones: 100*yrFP* and 500*yrFP*. The variable 100*yrFP* (100-year floodplain) in this

model is a dummy equal to 1 if the property falls within the 100-year floodplain and 0 otherwise. Similarly, the variable 500*yrFP* (500-year floodplain) is a dummy equal to 1 if the property falls within 500-year floodplain and 0 otherwise. The variable *Flood* in the DD model is a dummy variable equal to one if the sale happened after the flood (July 1994 in our case). The interaction term between the 100-year floodplain variable (100*yrFP*) and *Flood* tells us how the 1994 flood might have affected the prices of properties that are in the 100-year floodplain and that are sold after the 1994 flood. A similar interpretation is true for the 500-year floodplain and flood dummy interaction. Census tract fixed effects (γ_i) were included to control for possible omitted variables such as crime rate or other unobserved characteristics in the community that are constant over time.[14] Year fixed effects (δ_t) were included to capture yearly shocks that affect all the properties. Subscripts *i* and *t* represent property and time respectively.

We expanded the traditional DD model to incorporate an information decay effect following (Atreya, et al., 2011). Thus, the new hedonic model in DD framework model is as follows:

$$\begin{aligned}\ln(P_{it}) = {} & \beta_0 + \beta_1^{'} \ln L_i + \beta_2^{'} S_{it} + \beta_3^{'} S_{it}^2 + \beta_4 100yrFP_i + \beta_5 500yrFP_i \\ & + \beta_6 Flood + \beta_7 100yrFP_i * Flood + \beta_8 500yrFP_i * Flood \\ & + \beta_9 years + \beta_{10} years * 100yrFP_i + \beta_{11} years * 500yrFP_i + \gamma_i + \delta_t + \varepsilon_{it}\end{aligned} \quad (2)$$

To examine the persistence of risk premium over time after the 1994 flood event we used interaction terms between *years* and the floodplain variables. The variable "*years*" is a time trend that represents the number of years after the 1994 flood. The interaction term estimates how the risk premium changed over time after 1994 flood.

[14] In future, I plan to use average median income and race at census block group level instead of census tract fixed effect.

In order to determine the changes in property prices in the actually inundated area after the 1994 flood, we used the actual inundation map as a proxy for flood risk instead of the floodplain maps. Therefore, the specification used for the analysis is:

$$\begin{aligned}\ln(P_{it}) = {} & \beta_0 + \beta_1^{'} \ln L_i + \beta_2^{'} S_{it} + \beta_3^{'} S_{it}^2 + \beta_4 IND_i + \beta_5 Flood + \beta_6 IND_i * Flood \\ & \beta_7 years + \beta_8 years * IND + \gamma_i + \delta_t + \varepsilon_{it}\end{aligned} \tag{3}$$

The term IND (inundation) is a dummy equal to 1 if the property was inundated by 1994 flood and 0 otherwise.

To tease out a potential information effect of the flood shock from potential reconstruction and other inundation-related costs (inundation effect); we used an interaction term between the floodplain dummy variables and the inundation dummy variable in a specification as follows:

$$\begin{aligned}\ln(P_{it}) = {} & \beta_0 + \beta_1^{'} \ln L_i + \beta_2^{'} S_{it} + \beta_3^{'} S_{it}^2 + \beta_4 IND_i + \beta_5 FP_i \\ & + \beta_6 Flood + \beta_7 IND_i * Flood + \beta_8 FP_i * Flood + \beta_9 IND_i * FP_i + \beta_{10} FP_i * IND_i * Flood_i \\ & + \beta_{11} years + \beta_{12} years * FP_i + \beta_{13} years * IND_i + \gamma_i + \delta_t + \varepsilon_{it}\end{aligned} \tag{4}$$

We also divided the zones within study area into four mutually exclusive groups: inundated and in floodplain (IN_FP), inundated outside floodplain (IN_OFP), non-inundated and in floodplain (NIN_FP) and non-inundated outside floodplain (NIN_OFP). A DD model was employed to see the effect of the 1994 flood in these mutually exclusive groups. The specification employed is as follows:

$$\begin{aligned}\ln(P_{it}) = {} & \beta_0 + \beta_1^{'} \ln L_i + \beta_2^{'} S_{it} + \beta_3^{'} S_{it}^2 + \beta_4 IN_FP_i + \beta_5 IN_OFP_i + \beta_6 NIN_FP_i \\ & + \beta_7 Flood + \beta_8 IN_FP_i * Flood + \beta_9 IN_OFP_i * Flood + \beta_{10} NIN_FP_i \\ & + \beta_{11} years + \beta_{12} years * IN_FP_i + \beta_{13} years * IN_OFP_i + \beta_{14} years * NIN_FP_i \\ & + \gamma_i + \delta_t + \varepsilon_{it}\end{aligned} \tag{5}$$

4. Data

Three data sources are used to construct our data: individual property sales data for residential homes in city of Albany from the Dougherty County's Tax Assessor's Office; parcel level Geographic information System (GIS) database from Georgia's GIS clearinghouse; and simulated flood inundation maps of Flint River at Albany, Georgia prepared by USGS. Each property is a single-family residence sold at least once between 1985 and 2010.

Individual property sales data contain information on housing characteristics such as number of bedrooms, number of bathrooms, heated square feet, presence of garage etc. in addition to sale date and sale price. Property sale prices were adjusted to 2010 constant dollars, using the housing price index for Albany metropolitan area from the Office of federal Housing Enterprise Oversight. The GIS database was utilized to determine the location attributes of the properties such as proximity to river, railroad, major roads, parks etc. The floodplain map published as Q3 data by FEMA was used to determine if the parcel was in 100-year, 500-year or outside floodplain. Simulated flood inundation for a water surface altitude of 192.5 feet at Albany stream gauge that corresponds to 1994 flood was used to determine the inundated area.

After dropping properties for which (a) data were missing, (b) sale price was less than $2,000 or more than $500,000, or (c) they were not single family residential properties, 18,000 property transactions were included in the dataset.

To better capture the effect of flood in inundated area vs. non-inundated area, we confined our study area to flood inundation study area at Flint River, Albany, prepared by USGS (Figure 2). A little over 3000 single family residences were used to study the variation in risk perception within the city of Albany.

Table 1 reports the summary statistics for the variables included in the final empirical model for the City of Albany. The mean property price was 106,951 in 2010 constant dollars. The oldest property was built in 1841 with 0.41 average acres. The maximum elevation of the property was 290 meters and the minimum was 150 meters. Mean distance to Flint River was 15,524 feet. Twenty-one census tracts were included in the model as fixed effects. Of all the sales between 1985 and 2010, 8.7% of the properties were in high risk zone that has 1% annual chance of getting flooded or 26% chance of getting flooding at least once in 30 year mortgage. 1.3% of the properties were in low risk zone that has 0.2% probability of getting flooded each year. The summary statistics of the variables for the flood inundation study area are presented in table 2. The average property price in the study area was $ 77,614. Mean elevation of the property in study area was 191 meters which is 16 meters less than an average elevation of a property elevation in Albany. Average distance of a property in the study area to Flint River was 4,526 feet. During the 1994 flood, 30.6% of the properties in the study area were inundated.

5. Results

Flood Risk Perception: City of Albany

Table 3 reports our estimates of the effect of 1994 flood as risk information in the City of Albany using standard DD and SARAR models. The DD estimates show that there was a significant discount of almost 9% before 1994 flood, indicating that Albany residents capitalized the flood risk in property prices even prior to the flood event. OLS regression on pooled data for all sale

dates prior to 1994 flood also showed us the same results.[15] Immediately after the flood there was a significant discount of 15% and 34% in 100-year and 500-year floodplain respectively. However, the perception of flood risk was decreasing over time by 2.5% and 4.5% annually for 100-year and 500-year floodplain respectively. Consistent with results of Atreya et al. (2012), the value of the properties in 100-year and 500-year floodplain increased by $2654 and $4776 annually, respectively, indicating the temporary nature of homeowner's heightened flood risk perception. Spatial lag and spatial error was incorporated in the model since the Wald statistics suggested the presence of error dependence and lag dependence in the data set. Incorporating the spatial effect in the model however did not change the results as seen in column 2, Table 3.

People's perception of flood risk is also expected to rely on the information about the location of properties at risk, their elevation, their proximity to rivers, their closeness to inundation areas etc. The results indicate that proximity to river, lakes and ponds and other amenities such as schools, roads, and parks increased the property prices in Albany, but only proximity to rivers and parks are statistically significant. There was no significant premium associated with elevated properties. The results show that increasing the acres, number of bathrooms; having a fireplace and a central A/C would increase the property prices. It seems that Albany residents would pay more for historic homes because there is a price premium of 1.2% for the older homes.

Flood Risk Perception: Inundation Study Area, Albany

Using the inundated area as a proxy to flood risk zones, we estimated the effect of the 1994 flood in the area around Flint River where the majority of damage due to inundation took place. Table 4 reports the estimates of a DD model.

[15] Results are available upon request

In column (1), we estimate the effect of the 1994 flood in flood prone properties in the study area as measured by whether they fall in the floodplain. We find that floodplain properties in the study area sell for 36% less than the properties outside the floodplain immediately following the flood. We included properties in 500-year floodplain in the "outside floodplain" sample since there were only 183 properties in 500-year floodplain. In addition, homeowners are not required to buy flood insurance if they are located in 500-year floodplain and therefore might be unaware of the flood hazard associated with being in 500-year floodplain.

In column (2), we determine the effect of the flood, but for properties in theinundated area. We find that immediately after the 1994 flood the property price discount for those properties is as high as 46%.

To tease out the effect of being inundated from the informational effect of being in the floodplain, we estimated equation (4) and present the results in column (3). We find that the inundated properties were discounted by 46% immediately after the flood but there was no significant additional discount associated with being in the floodplain.

Finally, we divided the study area into four mutually exclusive groups[16] to see the effect of the 1994 flood in each of these groups. In column (4) we find that there was a significant discount of 47% and 43% for properties that lie on the inundated and in floodplain and inundated and outside floodplain, respectively. This result is consistent with that in column (3) and suggests that the discount is mainly driven from an inundation effect rather than an informational effect.

[16] Definitions of each mutually exclusive group are given in descriptive statistics.

6. Conclusion

Natural hazards provide exogenous risk information to the households. Studies have found that this information is capitalized into property prices. Previous studies use floodplain maps to measure flood risk, but our study of Albany suggests that most of the discount in property prices in the area affected by the flood comes from having been inundated. Our results thus suggest that not accounting for whether properties in the floodplains are inundated may overestimate the informational effect of large flood events. In addition of an information effect, the discount in inundated properties captures potential reconstruction costs, and supports a hypothesis that homeowners respond better to what they have visualized ("seeing is believing"). Unfortunately, without data on actual damages on the inundated properties we are not able to estimate the relative magnitude of these effects.

Table 1: Variables and Descriptive Statistics for City of Albany

Variable	Description	Mean	Std. Dev.	Min	Max
Price	Sale price of Property adjusted to 2010 constant dollars	106,951	116117.6	1854	3254400
Flood Variables					
100yr FP	An Area Inundated by 100-year Flooding	8.7%	28.30%	0	1
500yr FP	An Area Inundated by 500-year Flooding	1.3%	11.40%	0	1
Years	Number of Years after 1994 Flood	5.49	5.19	0	16
Location Attributes					
Elevation	Elevation of Property in Meter	207.84	15.57	150	290
River	Distance to Nearest River in Feet	2233.99	1560.09	10.67	7695.5
Lake	Distance to Nearest Lake in Feet	1802.67	1240.54	0	6410.27
Railroad	Distance to Nearest Railroad in Feet	5786.86	4787.93	51.87	21872.46
Roads	Distance to Nearest Road in Feet	118.40	99.14	0.02	1383.66
Utilities	Distance to Nearest Utility Lines in Feet	9790.06	4792.89	313.09	21944.55
Park	Distance to Nearest Park in Feet	8068.55	5526.33	148.41	24556.23
School	Distance to Nearest School in Feet	3586.35	2413.21	83.51	13591.46
Flint	Distance to Flint River in Feet	15524.12	9777.15	274.36	38899.21
Structural Attributes					
Year built	Year the Property was built	1966	18	1841	2010
Acres	Total Acreage of the Property	0.41	0.64	0.01	32.41
Bedrooms	Number of Bedrooms	3.03	0.72	0	30
Fullbths	Number of Full baths	1.66	0.66	0	7
Halfbths	Number of Half Baths	0.16	0.37	0	2
Htdsqft	Heated Square Feet	1615.2	663.1	0	7576
Fireplace	Number of Fireplaces	0.49	0.57	0	8
Dummy Variables					
AC	1 if central AC present, 0 otherwise	0.87	0.32	0	1
Garage	1 if garage present, 0 otherwise	0.17	0.38	0	1
Brick	1 if Brick exterior, 0 otherwise	0.01	0.12	0	1
Flood	1 if sold after July 1994,0 otherwise	0.69	0.45	0	1
Fixed Effects					
Census Tract Fixed effect (21)					
Year Fixed Effect (1985-2010)					

Table 2: Variables and Descriptive Statistics of "Flood Inundation Study Area", Albany

Variable	Description	Mean	Std. Dev.	Min	Max
price	Sale price of Property adjusted to 2010 constant dollars	77,614	146250.6	1854	1400000
Flood Variables					
IN	An inundated area during 1994 Flood	30.6%	46.1%	0	1
Years	Number of years after 1994 Flood	5.96	5.33	0	16
Location Attributes					
Elevation	Elevation of Property in Meter	191.60	9.34	175	216
River	Distance to Nearest River in Feet	2186.48	1525.62	19.24	7695.5
Lake	Distance to Nearest Lake in Feet	2389.39	1141.53	33.42	5514.74
Railroad	Distance to Nearest Railroad in Feet	3469.32	2112.04	69.09	9020.49
Roads	Distance to Nearest Road in Feet	97.93	74.76	0.05	505.53
Utilities	Distance to Nearest Utility Lines in Feet	11407.27	4748.22	2409.79	20563.9
Park	Distance to Nearest Park in Feet	5765.67	2424.77	152.65	10291.2
School	Distance to Nearest School in Feet	2820.652	1422.16	145.9	6681.04
Flint	Distance to Flint River in Feet	4526.79	1996.96	1007	11726.2
Structural Attributes					
Year built	Year the Property was built	1961.715	22.34672	1883	2009
Acres	Total Acreage of the Property	0.25	0.20	0	3.73
Bedrooms	Number of Bedrooms	2.81	0.58	0	8
Fullbths	Number of Full baths	1.30	0.51	0	7
Halfbths	Number of Half Baths	0.10	0.30	0	2
Htdsqft	Heated Square Feet	1195.77	425.04	480	4714
Fireplace	Number of Fireplaces	0.14	0.35	0	1
Dummy Variables					
AC	1 if central AC present, 0 otherwise	0.67	0.47	0	1
Garage	1 if garage present, 0 otherwise	0.03	0.16	0	1
Brick	1 if Brick exterior, 0 otherwise	0.03	0.16	0	1
Flood	1 if sold after July 1994,0 otherwise	0.73	0.44	0	1
FP	1 if 100yr Floodplain, 0 otherwise	23%	42%	0	1
Mutually Exclusive Groups					
IN_FP	1 if inundated in FP, 0 otherwise	21.5%	41%	0	1
IN_OFP	1 if inundated outside FP, 0 otherwise	9.1%	21%	0	1
NIN_FP	1 if non inundated in FP, 0 otherwise	2.5%	15%	0	1
NIN_OFP	1 if non inundated outside FP, 0 otherwise	66.9%	47%	0	1
Fixed Effects					
Census Tract Fixed effect (14)					
Year Fixed Effect (1985-2010)					

Table 3: A Difference-In-Difference (DD) Model and Spatial Hedonic Model Results for City of Albany

VARIABLES	(DD Model) Ln (Price)	(Spatial Hedonic Model) Ln (Price)
100yr FP	-0.0866*	-0.0770*
	(0.0448)	(0.0399)
500yr FP	-0.000865	0.0106
	(0.101)	(0.0895)
Flood	0.00780	0.0112
	(0.0408)	(0.0429)
100yr FP*Flood	-0.153***	-0.160***
	(0.0585)	(0.0511)
500yr FP*Flood	-0.337**	-0.341***
	(0.170)	(0.130)
Years	-0.0670	-0.0679*
	(0.0438)	(0.0412)
100yr FP*Years	0.0255***	0.0250***
	(0.00542)	(0.00421)
500yr FP*Years	0.0459***	0.0462***
	(0.0141)	(0.0103)
Elevation	7.40e-05	-6.60e-05
	(0.000524)	(0.000561)
Ln (River)	-0.0286***	-0.0281***
	(0.00918)	(0.00915)
Ln (Flint)	-0.0202	-0.0202
	(0.0372)	(0.0259)
Ln (lakepond)	-0.0155	-0.0171*
	(0.0102)	(0.00998)
Ln (railroad)	-0.0147	-0.0160
	(0.0124)	(0.0112)
Ln (road)	-0.00605	-0.00535
	(0.00560)	(0.00539)
Ln (utilities)	-0.0286	-0.0262
	(0.0198)	(0.0207)
Ln (park)	-0.0263*	-0.0253
	(0.0151)	(0.0163)
Ln (school)	-0.00536	-0.00612
	(0.0114)	(0.0117)
Acres	0.0707**	0.0781***
	(0.0333)	(0.0189)
Acresq	-0.00283**	-0.00300***
	(0.00130)	(0.000806)
Age	0.0127***	0.0129***
	(0.00229)	(0.000885)
Agesq	-0.000228***	-0.000230***
	(4.29e-05)	(1.12e-05)
Bedrooms	0.00228	0.000269
	(0.0215)	(0.0168)

Bedsq	0.000266	0.000320
	(0.000916)	(0.000685)
Fullbths	0.246***	0.259***
	(0.0446)	(0.0402)
Fullbathsq	-0.0418***	-0.0446***
	(0.0109)	(0.00931)
Halfbths	0.0290	0.0232
	(0.0439)	(0.100)
Halfbathsq	0.0273	0.0370
	(0.0362)	(0.0967)
Htdsqft	0.000335***	0.000337***
	(3.96e-05)	(3.92e-05)
Htsqftsq	-1.15e-08	-1.14e-08
	(7.39e-09)	(7.50e-09)
Fireplace	0.0636***	0.0572***
	(0.0120)	(0.0122)
AC	0.120***	0.122***
	(0.0272)	(0.0196)
Brick	0.0335	0.0352
	(0.0478)	(0.0437)
Census Tract Fixed Effect	Y	Y
Year fixed Effect	Y	Y
Constant	12.25***	12.40***
	(0.830)	(0.779)
Lambda		0.0135***
		(0.00306)
Rho		0.562***
		(0.0285)
Observations	18,647	18,647
Number of id	9,332	

Robust standard errors in parentheses
*** p<0.01, ** p<0.05, * p<0.1

Table 4: A Difference-In-Difference (DD) Model for Flood Inundation Study Area, Albany[17]

VARIABLES	(1) lnprice	(2) lnprice	(3) lnprice	(4) lnprice
FP	-0.155		-0.124	
	(0.101)		(0.199)	
IN		-0.148	-0.0747	
		(0.0906)	(0.140)	
FP*IN			-0.00553	
			(0.252)	
FP*Flood	-0.357***		0.0893	
	(0.122)		(0.270)	
Flood*IN		-0.461***	-0.466**	
		(0.115)	(0.189)	
FP* IN *Flood			-0.0867	
			(0.291)	
IN* Years		0.0630***	0.0552***	
		(0.00920)	(0.0132)	
FP* Years	0.0543***		0.0120	
	(0.00990)		(0.0141)	
IN_FP				-0.206*
				(0.117)
IN_OFP				-0.0761
				(0.140)
NIN_FP				-0.125
				(0.199)
Flood	0.216	0.308*	0.306*	0.302*
	(0.178)	(0.179)	(0.179)	(0.179)
IN_FP*Flood				-0.471***
				(0.129)
IN_OFP*Flood				-0.431**
				(0.197)
NIN_FP*Flood				0.227
				(0.352)
Years	-0.0220**	-0.0309***	-0.0314***	-0.0308***
	(0.00882)	(0.00907)	(0.00910)	(0.00916)
IN_FP*Years				0.0681***
				(0.0105)
IN_OFP*Years				0.0511***
				(0.0148)
NIN_FP*Years				-0.00301
				(0.0284)
Constant	13.33***	13.40***	13.53***	13.55***
	(1.737)	(1.724)	(1.757)	(1.757)
Observations	3,007	3,007	3,007	3,007
R-squared	0.191	0.196	0.196	0.196

Robust standard errors in parentheses
*** p<0.01, ** p<0.05, * p<0.1

[17] The location attributes, structural attributes, census tract fixed effects and year fixed effect are included in the model

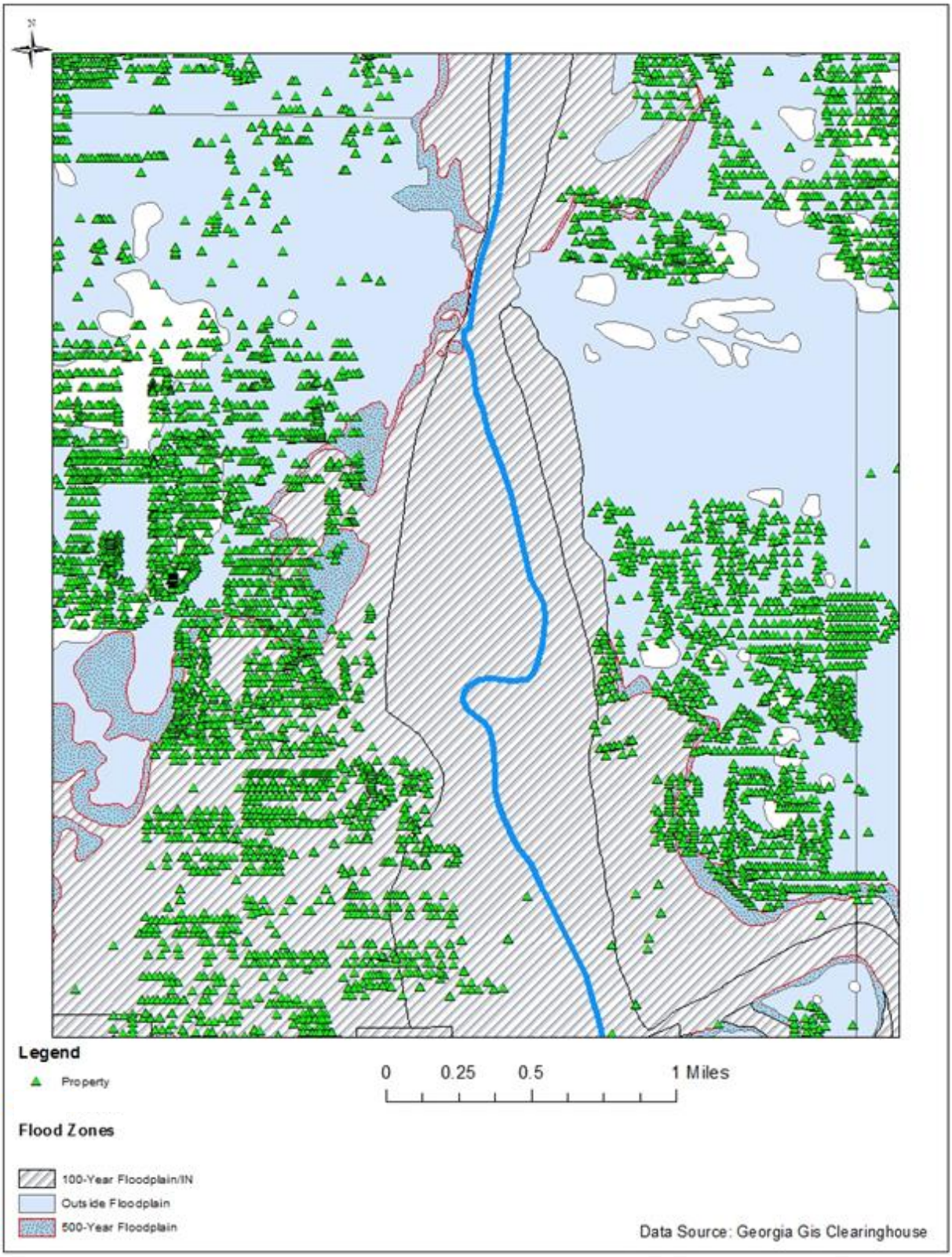

Figure 1: Flint River and FEMA Designated Flood Plains in Albany, Georgia

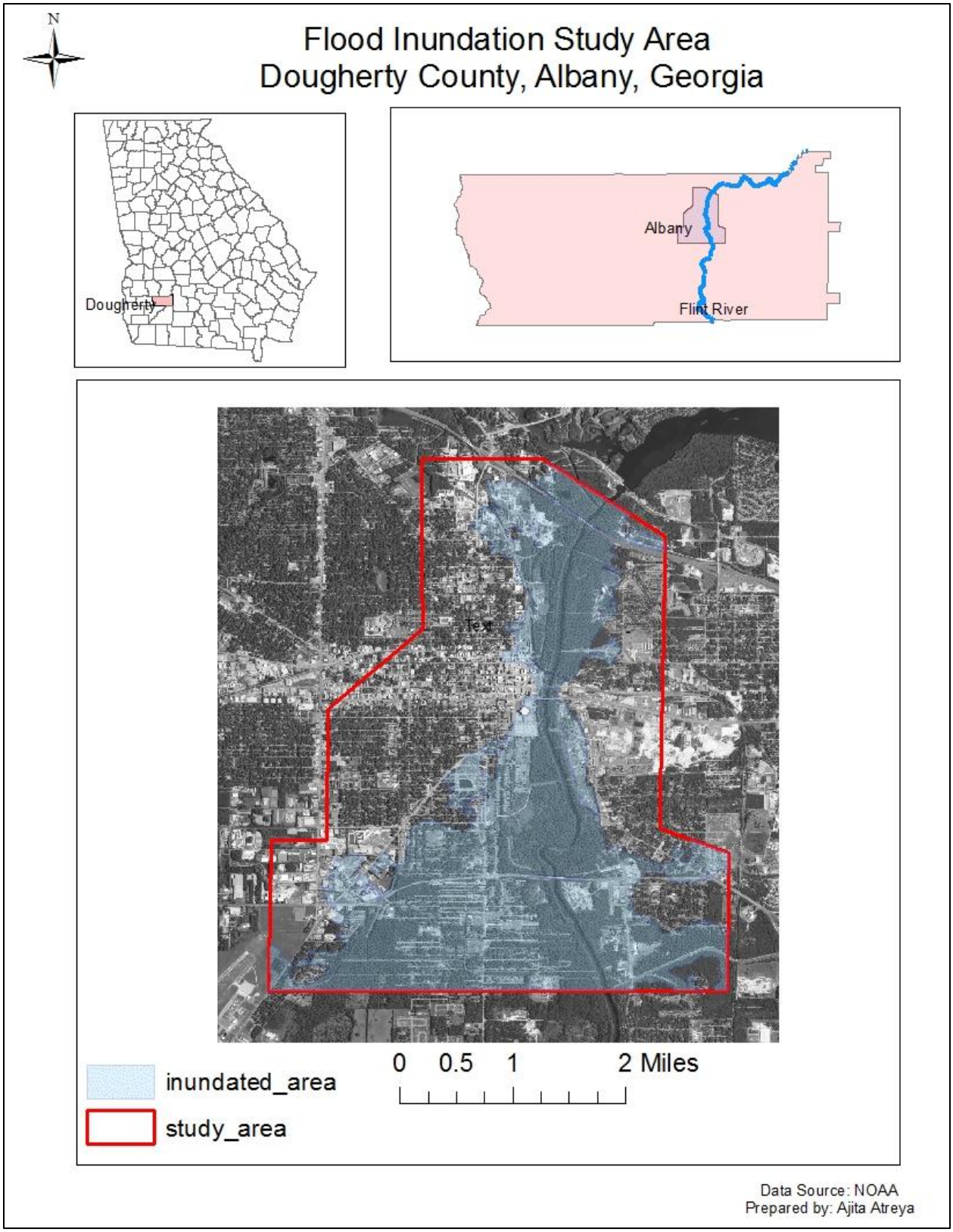

Figure 2: Flood Inundation Study Area, Albany, Georgia

References:

Anselin, L., and R. Florax. 1995. "Small sample properties of tests for spatial dependence in regression models: Some further results." *New directions in spatial econometrics*:21-74.

Arraiz, I., D.M. Drukker, H.H. Kelejian, and I.R. Prucha. 2010. "A Spatial Cliff-Ord Type Model with Heteroskedastic Innovations: Small and Large Sample Results." *Journal of Regional Science* 50(2):592-614.

Atreya, A., S. Ferreira, and W. Kriesel. 2011. "Forgetting the flood: Changes in Flood Risk Perception Over Time " *Selected Paper, UNICT- EAERE- FEEM Belpasso International Summer School on Environmental and Resource Economics, Belpasso, Sicily, Italy, Sept 4-10 September, 2011*.

Bin, O., and C. Landry. 2011. "Changes in Implicit Flood Risk Premiums: Empirical Evidence from the Housing Market. ." *Available at SSRN: http://ssrn.com/abstract=1850671*.

Freeman, A. 2003. *The measurement of environmental and resource values: theory and methods*: RFF press.

Rosen, S. 1974. "Hedonic prices and implicit markets: product differentiation in pure competition." *The Journal of Political Economy* 82(1):34-55.

Sjöberg, L. 2000. "Factors in risk perception." *Risk analysis* 20(1):1-12.

Stamey, T.C. 1996. "Summary of data-collection activities and effects of flooding from Tropical Storm Alberto in parts of Georgia, Alabama, and Florida, July 1994."

Flood Risk and Homeowners' Flood Risk Perceptions: Evidence from Property Prices in Fulton County, Georgia

Ajita Atreya and Susana Ferreira
Department of Ag. & Applied Economics
University of Georgia
Athens, GA 30602

Abstract

Many towns have been historically built in the floodplain, which is a flat or nearly flat surface adjacent to rivers or streams that is subject to periodic flooding. Four percent of residential properties sold between the years of 1977 and 2007 fall within the floodplain in Fulton County, GA. Movement of people to floodplain areas poses an important question as to whether homeowners in Fulton County, and generally, perceive flood risk or not. This paper studies homeowners perceptions of flood risk as seen in a change in price of floodplain property after an extreme flood event. Residential home sales data over 30 years are used in a hedonic model to estimate the changes in flood risk perception. It is found that after a major flood event in 1994, property prices in the floodplain declined by almost 2 percent when evaluated at the average property value.

1. Introduction

Almost two thirds of the direct damages from natural disaster can be attributed to floods and hurricanes (Van der Vink, et al., 1998). A warmer climate, with its increased climate variability, is expected to increase the risk of both floods and droughts (Wetherald and Manabe, 2002). The rise in sea level, global climate change, and weather pattern associated with such phenomena as the El Niño Southern Oscillation are processes that influence the impact and occurrences of floods, hurricanes and tornadoes (Van der Vink, et al., 1998). Flooding can be caused by heavy rains, melting snow, inadequate drainage systems, failed protective devices such as levees and dams, as well as by tropical storms and hurricanes. In addition, many towns have been built on a floodplain historically. Floodplains are the flat or nearly flat surfaces adjacent to a river or stream that are subject to periodic flooding. The United States is no exception when it comes to property damage due to flood events. In the United States, during the 20th century, floods accounted for more lives lost and more property damage than any other disaster (Perry, 2000). Each year, on average, floods kill about 140 people and cause $6 billion in property damage (USGS, 2006).

In recent years, the Southeastern region of the US has been hit by numerous hurricanes (including Hurricane Isabel in 2003, Hurricanes Gaston, Alex, Frances, Jeanne, Ivan and Charley in 2004, and Hurricanes Dennis, Katrina, Rita, Wilma and Ophelia in 2005) causing substantial monetary and non-monetary damages. For example, Hurricane Frances's total economic damage was estimated to be about US$9 billion. In the State of Georgia, it resulted in a loss of 30 percent of the crops, and a death toll of 8. Specifically, people and capital moving into coastal areas, and thus to floodplains, raises the disaster-related costs when a storm or flood takes place (Montz and Gruntfest, 1986). The concentration of people and capital into floodplains poses important questions: Do homeowners have accurate information about flood risks? Do they understand this

information? How does this information translate into their perceived flood risk as reflected into property prices?

A precondition to prepare for and adapt to natural disasters is to understand the potential risks. The Federal Emergency Management Agency's (FEMA's) flood hazard maps (known as Flood Insurance Rate Maps, or FIRMs) are one of the essential tools for identifying flood risks and implementing flood mitigation in the United States. However, it is not clear how much homeowner rely on or trusts the FEMA designations. This study will shed light into the general question of whether homeowners in Fulton County discount the property prices based on the flood maps published by FEMA especially after hit by a significant flood event.

Fulton County was among one of the presidential disaster declared counties in Georgia during a large flood in 1994. Thus, I use the 1994 flood as an extreme event and use the capitalization of flood risk into property prices to determine the homeowners updated their perceived risk after that particular extreme event. I hypothesize that if homeowners were perfectly aware of the flood risks of different properties, the flood risks would be capitalized into property prices (i.e. houses perceived to be at a higher risk of flooding sell at a discount). Thus, we can look at property prices to analyze whether and how homeowners perceive flood risk. The results should help design effective education, outreach and extension programs on this issue. If our research identifies that homeowners are misinformed about flood risks, so that, for example, after a major flood event (1994 flood in our case) they mistakenly assume that they are safer, a primary focus could be education. Flood events are referred to by experts and press as X-year events (e.g. as 100-year flood). This might be misinterpreted by the homeowners, not as a 1 percent probability of flooding each year, but as the start of the safe period after a major flood.

The hedonic property model (Freeman, 2003, Rosen, 1974) is used to determine the price differential between residential properties within and outside the floodplain over the years 1977-2007. Without considering the effect of the 1994 flood we find that there is a price discount of almost 1.6% for a property in a floodplain. (This price discount is estimated as a percentage of the value of an average house). When the flood event is included in the model we find a statistically significant decline in prices for properties in the floodplain after the 1994 flood.

2. Previous research

The hedonic model (Freeman, 2003, Rosen, 1974) has been extensively used to estimate the contribution to the total value of a property attributable to each characteristic possessed by the property. In general, structural characteristics of the houses have been shown to have significant impact on the price of house. Hedonic model have also been proven to be an effective tool for estimating the effects of changes in environmental quality on housing price since its earliest uses in property value studies in the late 1960s (Halstead et al., 1997). Previous studies have used hedonic pricing models to examine the effect of flood risk on property values (Beatley et al., 2002, Bin and Kruse, 2006, Bin et al., 2008, Harrison et al., 2001, MacDonald et al., 1987, Shilling et al., 1985, Speyrer and Ragas, 1991). Most of these studies attempt to determine the discount associated with location within floodplain.

Previous studies have shown that a house located within a floodplain has a lower market value than an equivalent house located outside the floodplain (Bin and Polasky, 2004, Kousky, 2010). Kousky found that after the 1993 flood on the Missouri and Mississippi rivers, property prices in the 500-year floodplain (those with 26% chance of flooding at least once during 30 year mortgage) did not change significantly but prices in the 100-year floodplain declined by 2% to

5%. However, they also found that if property owners underestimate the cost of flooding, or homeowners are relatively unaware of flood hazards, there might be little reduction in the value of properties within a floodplain (Bin and Polasky, 2004). McKenzie and Levendis (2010) studied the impact of elevation, which buyers did not know for certain prior to the storm, and may now infer from water level marks, and found it to have a positive relationship with selling prices. In their study, they found that the premium associated with elevation was only 1.4% per foot in flood prone area before Hurricane Katrina but this increased to 4.6% for flooded areas after Katrina. None of these studies, however, focuses on Georgia. Moreover, most previous studies use cross-sectional data. That is, they do not consider the same properties over time and how their value may change due to, for example new information as a recent flood event. We aim to estimate whether or not homeowners' flood risk perceptions change with the new information provided by a significant flood event.

Only four studies (Bin and Polasky, 2004, Carbone, et al., 2006, Kousky, 2010, Skantz and Strickland, 1996) investigate how actual flood events alter homeowners risk perceptions. They find that after a significant flood event, properties within a floodplain have a lower market value than equivalent houses located outside the floodplain. They also find that the discount was higher if the flooding was recent which means that consumer's willingness to pay for an increase in flood risk decay with time. A difference in difference (DD) approach was used by Kousky and Bin and Polasky to determine the effect of an extreme event on the property prices. Kousky, also used repeat sales model (Palmquist, 1982) to remove unobserved, time invariant characteristics of a property which would hinder DD approach.

We aim to add to this scarce literature by looking at the case of Georgia. The perceived risk in Fulton County might be different from what we have seen so far in the literature.

3. Study Area

The study area is Fulton County, one of the most populated counties in the state of Georgia According to census information in 2010, the population in Fulton County has increased by 12.1 percent and the number of housing units has increased by 25.4 percent since 2000 which makes this county an interesting case study because increases in impervious surface is one of the major reasons of increased flooding. Impervious surfaces tend to increase with population since a growing population is accommodated by expanding urban areas particularly for residential use (Kriesel and Mullen, 2009). Most of the earlier studies have looked into the flood risk in coastal counties since coastal counties are particularly susceptible to hydrological disasters. Fulton County, an inland county will provide an interesting comparison with the coastal counties, as flood-risk perceptions of homeowners in inland regions might be different from those of residents of coastal regions, despite some of the inland regions being significantly affected by flood hazards.

According to the U.S. Census Bureau, Fulton County has a total area of 535 square miles, of which 529 square miles is land and 6 square miles is water. In 1994, Fulton County was hit by storm Alberto which caused significant damages. Storm Alberto began its journey to Georgia as a tropical wave. Towns in West Georgia in the path of Alberto, including the Atlanta region in Fulton County, received record amounts of rainfall. Floodplains in Fulton County are located mostly adjacent to rivers, streams and creeks. Figure 1 maps the rivers and streams, lakes and ponds, housing units and the associated floodplains.

A FEMA managed program, the National Flood Insurance Program (NFIP) enacted in 1968 provides flood insurance to homeowners. Flood insurance is mandatory if properties lie in 100

year floodplain (1% chance of flooding in any given year or a 26% chance of flooding at least once during a 30-year mortgage). If mandatory purchase is effective, then home buyers should be aware of the flood risk if their property lies in 100 year floodplain. Figure 2 shows the Chattahoochee River, elevation in meters and the associated floodplain. In figure 2, we can see that floodplains mostly lie in the lower elevation. We also consider the relationship between elevation and property prices in our research.

4. Model

A hedonic model is employed to determine the shadow value of non market environmental commodities such as flood risk. In hedonic property models (Freeman, 2003, Rosen, 1974), the price of a property, P, is modeled as a function of structural characteristics, S, (e.g. number of rooms, size of the house), neighborhood and location characteristics, L, (e.g. distance to river, distance to parks), and an environmental variable of interest, in this case flood risk, R.

$$P_{it} = \beta_0 + \beta_1 L_{it} + \beta_2 S_{it} + \beta_3 R_i + \varepsilon_{it} \qquad (1)$$

In equation (1) subscripts i and t represent property and time respectively. β_3 , the coefficient on the risk variable, captures homeowners' perception to flood risk. For choosing functional form in hedonic model, the only guidance provided is that the first derivative with respect to environmental characteristics be negative if the characteristic is a “bad” and vice versa (Halstead, et al., 1997). Most of the researchers have used natural log of price as the dependent variable in their hedonic regression as it is usually normally distributed (Bin and Polasky, 2004, Kousky, 2010). We also used natural log of price as the dependent variable for a similar reason. After testing several transformations of the independent variables the location variables were best fitted in their log form while the other attributes were fitted best in their linear form. To

approximate the flood risk we used dummy variables to indicate whether the property is within the floodplain. Although the flood plain was divided into four different zones: A, AE, X500 and X, we merged zone A, AE and X500 into a floodplain variable (FP) and gave the value of 1 if the property fell under these categories and 0 otherwise. Thus, the hedonic model used is:

$$ln\ (P_{it)} = \beta_0 + \beta_1 ln L_{it} + \beta_2 S_{it} + \beta_3 FP_i + \varepsilon_{it} \qquad (2)$$

We used community fixed effect to control for possible omitted variables such as crimes and any other community-specific characteristics that remain stable during the time period considered. Year fixed effects were also included to capture yearly shocks and trends that may affect all properties. White's method was used to get estimates of standard error that are corrected for potential heteroskedasticity.

In order to determine the effect of 1994 flood on the property prices we used the following model:

$$ln\ (P_{it)} = \beta_0 + \beta_1 ln L_{it} + \beta_2 S_{it} + \beta_3 FP_i + \beta_4 Flood_{it} + \beta_5 FP_i * Flood_{it} + \varepsilon_{it} \qquad (3)$$

This is the Difference in Difference (DD) model that has been used by previous researchers (Bin and Polasky, 2004, Kousky, 2010) to examine the information effects of a disaster. In this model we assumed that properties that fall in a floodplain are the treatment group and properties that don't fall in a floodplain are the control group. The variable *Flood* in the DD model is a dummy variable equal to one if the sale happened after 1994 flood. The interaction of floodplain (FP) and *Flood* tells us how the 1994 flood might have affected the prices of properties that are in the floodplains and are sold after 1994 flood. We hypothesize that if homeowners are aware of flood hazards, property prices for houses lying within the floodplain will be lower than those of comparable properties lying outside the floodplain. We also hypothesize that the perceived risk

will be heightened after a major flood event. Rejecting these hypotheses could indicate a need to improve the system of communication of flood risk to homeowners through effective education, outreach and extension systems.

5. Data

We constructed a unique dataset by merging individual property sales data for residential homes from the Fulton County's Tax Assessor's office for years 1977 to 2007, with a parcel-level Geographic Information System (GIS) database from Georgia's GIS clearinghouse. The property records contain information on housing characteristics (number of rooms, size of the house, etc.), S in equation (1), as well as sale date and price. All the property sales prices were adjusted to 2007 constant dollars, using the housing price index for Atlanta-Sandy Springs-Marietta metropolitan area from the Office of Federal Housing Enterprise Oversight.

We utilized GIS to measure the distance from each property to important features that could influence property values such as proximity to major roads and highways; distance of properties to nearest railroads, airports and also to other amenities such as parks and rivers. These variables are denoted by L in equation (1). To measure flood risk, R in equation (1), we used a GIS layer of Federal Emergency Management Agency's (FEMA) data to identify parcels in 100-year and 500-year floodplains. For this analysis, I used FEMA Q3 flood data published in 1996[18] which depicts 100 year and 500 year floodplains as represented on Flood Insurance Rate maps (FIRMs), i.e. properties in the A, AE, and X500 zones. After dropping properties for which the

[18] The State of Georgia is updating the flood hazard map as a part of FEMA's nationwide effort to update map called Flood Map Modernization. The updated flood map should provide more relevant results

data were missing, properties that sold for less than $2,000or more than $10 million, more than 100,000 sales were included in the data.[19]

Table 1 provides definitions and summary statistics for each variable. The mean property value in 2007 constant dollar was found to be $45,196. The mean age of the property was 33 years with the oldest home built in 1800 and the newest built in 2006. The mean area of the property is half of an acre. The total room in the house ranged from 1 to 14 with an average of 3 bedrooms, and the number of stories in the house ranged from one to three. The mean distance to river Chattahoochee was 7,745 meters. The basement, building type and building mater fixed effect capture the different styles, type and the materials used to build the house. Ten communities and unincorporated area was included as community fixed effect. Of all sales, most houses lie in the City of Atlanta, and almost 4 percent of the houses lie in flood risk zones (zone A, AE and X500).

6. Empirical Results

6.1 Flood Risk Discount: No Flood Event Included

The estimation results for the risk discount without accounting for the effect of the 1994 flood are presented in Table 2. As shown in Table 2, most of the variables are statistically significant and have the expected sign. The flood plain variable (FP) in Table 2 column 1 has a negative sign and is statistically significant at a 5% level of significance indicating that the location within the floodplain lowers the property value by approximately $723, which is approximately equivalent to 1.6% reduction in sales price for an average valued house.

[19] Sales less than $2000 were probably transfers and not true sales. There were just two properties that were over $10, 000000.

The elevation variable also has a significant effect on the sales price of the property. Interestingly, there is a discount associated with elevated homes, but the flood plain and elevation interaction term suggest that properties in floodplain are discounted less if they are elevated which accords with intutition. The variable *near_chatriver* is a dummy variable which equals to one if the property is within 400 meters of Chattahoochee River and the results suggest that after controlling for location within the floodplain, living closer to the river increases home prices.

Other estimated coefficients are also as expected. Property prices increase with the proximity to amenities such as parks and airports. The nearer the house is to major roads and highways, runways, utility lines and schools the lower the property prices. The results are intuitive as people prefer being near the public transport facilities and people try to avoid being near noisy places such as highways, runways and school areas. The lower property prices for being near utility lines may probably be because of safety reasons. Property prices increase with increase in acres, number of stories, bedrooms, full baths, half baths, plumbing fixtures, fireplaces and the area of heated floor.

6.2 Flood Risk Discount: 1994 Flood Event Included

Table 3 shows the effect of the 1994 flood on the estimated discount for property prices within the floodplain. There seems to be no discount for the property within floodplain before the 1994 flood. But, post 1994 flood the estimated discount is approximately $1,325. This is equivalent to almost 2% reduction in sales price for an averaged valued house. This result indicates that the damages caused by flood changed the perception of homeowners in Fulton County and also the discount in the property within the floodplain.

The coefficients of structural variables have expected signs and are statistically significant. The results indicate that having a full bath has the highest increment in the property prices which is approximately by $4881 compared to other structural characteristics. The results also indicate that, as before, proximity to Chattahoochee River, to the nearest park, airport and the Marta rail station increased the property prices, while proximity to nearest roads and highways, utility lines, runway and school decreased the property prices. For instance, moving 1000 meter closer to utility lines decreases estimated sales value by approximately $400, evaluated at an average valued house. The marginal effect of distance related variables which is naturally logged is calculated by multiplying the coefficients of the distance with the average price of the property and dividing them by the average distance.

7. Conclusion

The estimates of the effect of property location within a floodplain in property prices is found to be consistent with the results from previous studies (Bin and Polasky, 2004, Kousky, 2010) that the price of properties located within the floodplain is lower than for properties located outside a floodplain. But, the price discount is found to be lower in Fulton County, Georgia. Location within floodplain lowers the property prices by approximately 1.6%, evaluated at an average priced house. It is also found that there was no price discount for a property located within a floodplain before 1994 flood. In fact, before 1994 floods, homes in floodplain commanded a price premium most probably because people enjoyed living near rivers and streams because of its aesthetic values ignoring the fact that they were living on a floodplain. But, post 1994 floods, the scenario changed and there was a price discount for houses in the floodplain. The estimated discount is found to be approximately $1325 post-1994 flood. This is equivalent to almost 2% reduction in sales price for an averaged valued house.

Table 1: Variables used in the analysis and summary statistics

Variables	Description	Mean	Std. Dev.	Min	Max
sale_07	Sale Price of property adjusted to 2007 constant dollars	45196.97	64946.66	2002.326	6479345
Structural Variables					
saleyear	Sale Year of the house	1998.78	7.92	1977	2007
age	Age of the house	33.47	25.49	1	207
acres	Total acreage of the Property	0.50	1.30	0.001	124.812
heated_flo	Total heated floor in square feet	2366.95	1307.71	200	28347
bedrooms	Number of bedrooms in the house	3.34	0.91	1	14
full_baths	Number of full bath in the house	2.18	0.94	0	9
half_baths	Number of Half Bath in the house	0.53	0.56	0	9
total_fixt	Total number of fixtures	10.89	4.41	2	48
fireplace_	Total number of fireplaces	0.38	0.61	0	9
Location Variables					
chat_dist	Distance to Chattahoochee river in meter	7745.61	5015.38	46.87	21818.7
airport_dist	Distance to nearest airport in meter	22785.74	13292.72	319.03	50828.43
lake_dist	Distance to Nearest lake in meter	793.31	759.370	0	4515.245
marta_dist	Distance to MARTA railroad in meter	8141.75	6691.93	2.97	35658.46
park_dist	Distance to Nearest Park in meter	6126.76	3897.20	37.35	17123.28
road_dist	Distance to Nearest Road or Highway in meter	49.01	55.84	0.008	840.4005
runway_dist	Distance to nearest Runway in meter	20359.61	14430.5	149.39	49908.25
utility_dist	Distance to nearest utility lines in meter	6326.18	4196.46	0.108	16563.93
school_dist	Distance to Nearest school in meter	3762.90	3281.36	27.26	13889.93
Flood Variables					
Zone_A	An area inundated by 100 year flooding, for which no BFEs have been established	0.002	0.048	0	1

Zone_AE	An area inundated by 100-year flooding, for which BFEs (base Flood Elevation) have been determined.	0.009	0.097	0	1
Zone_X500	An area inundated by 500-year flooding; an area inundated by 100-year flooding with average depths of less than 1 foot or with drainage areas less than 1 square mile; or an area protected by levees from 100-year flooding.	0.014	0.121	0	1
Zone_X	An area that is determined to be outside the 100- and 500-year floodplains	0.773	0.418	0	1
Dummy variables					
FP	1 if property is within A, AE and X500 floodplain				
Near_chatriver	1 if property is within 400 meters of Chattahoochee River				
Flood	1 if property is sold after 1994 Flood				
Fixed Effects	Basement, Build Type, Build Matter, Community, Year				

Table 2: Estimated Results of the Hedonic Model (No Post Flood Interaction)

VARIABLES	(1) sale_07	(2) sale_07	(3) sale_07	(4) sale_07
FP	-0.0160**	-0.0392***	-0.0318**	-0.0255*
	(0.00740)	(0.0132)	(0.0137)	(0.0138)
elevation	-9.21e-05***	-9.98e-05***	-0.000103***	-0.000103***
	(2.55e-05)	(2.88e-05)	(2.86e-05)	(2.86e-05)
FP_elevation		7.80e-05**	7.60e-05**	7.56e-05*
		(3.61e-05)	(3.83e-05)	(3.88e-05)
near_chatriver			0.0152	0.0315**
			(0.0149)	(0.0152)
FP_nearchatriver				-0.146***
				(0.0562)
Ln (chat_dist)	-0.0485***	-0.0485***		
	(0.00218)	(0.00218)		
Ln (park_dist)	-0.0204***	-0.0204***	-0.0371***	-0.0370***
	(0.00262)	(0.00262)	(0.00243)	(0.00243)
Ln (airport_dist)	-0.163***	-0.163***	-0.216***	-0.216***
	(0.00689)	(0.00689)	(0.00656)	(0.00656)
Ln (marta_dist)	-0.0426***	-0.0426***	-0.0413***	-0.0412***
	(0.00212)	(0.00212)	(0.00212)	(0.00212)
Ln (utility_dist)	0.0864***	0.0864***	0.0930***	0.0930***
	(0.00194)	(0.00194)	(0.00193)	(0.00193)
Ln (road_dist)	0.0390***	0.0390***	0.0336***	0.0334***
	(0.00235)	(0.00235)	(0.00233)	(0.00234)
Ln (runway_dist)	0.393***	0.393***	0.439***	0.439***
	(0.00591)	(0.00591)	(0.00568)	(0.00568)
Ln (school_dist)	0.0568***	0.0568***	0.0516***	0.0518***
	(0.00199)	(0.00199)	(0.00198)	(0.00198)
acres	0.0332***	0.0332***	0.0315***	0.0315***
	(0.00398)	(0.00398)	(0.00393)	(0.00393)
year_built	0.000895***	0.000896***	0.000734***	0.000735***
	(0.000125)	(0.000125)	(0.000125)	(0.000125)
num_storie	0.0518***	0.0517***	0.0552***	0.0550***
	(0.00507)	(0.00507)	(0.00510)	(0.00510)
bedrooms	0.000388	0.000405	0.000316	0.000328
	(0.00278)	(0.00278)	(0.00279)	(0.00279)
full_baths	0.108***	0.108***	0.112***	0.112***
	(0.00504)	(0.00504)	(0.00508)	(0.00508)
half_baths	0.0475***	0.0476***	0.0514***	0.0513***
	(0.00418)	(0.00418)	(0.00419)	(0.00418)
total_fixt	0.00882***	0.00881***	0.00815***	0.00821***
	(0.00121)	(0.00121)	(0.00122)	(0.00122)
fireplace_	0.106***	0.106***	0.107***	0.107***
	(0.00351)	(0.00351)	(0.00352)	(0.00351)
ground_flo	8.28e-05***	8.27e-05***	7.97e-05***	7.99e-05***
	(5.48e-06)	(5.48e-06)	(5.51e-06)	(5.51e-06)
heated_flo	0.000161***	0.000161***	0.000167***	0.000167***
	(4.29e-06)	(4.29e-06)	(4.32e-06)	(4.32e-06)
Constant	4.094***	4.095***	4.300***	4.295***
	(0.252)	(0.252)	(0.253)	(0.253)
Community, Year , Style, Type and Basement Fixed Effects	Y	Y	Y	Y
Observations	106,505	106,505	106,505	106,505
R-squared	0.738	0.738	0.737	0.737

Robust standard errors in parentheses
*** p<0.01, ** p<0.05, * p<0.1

Table 3: Estimated Results of the Hedonic Model (Post Flood Interaction)

VARIABLES	(1) sale_07	(2) sale_07
FP	-0.0159**	0.0396**
	(0.00740)	(0.0195)
Flood	0.804***	0.806***
	(0.0160)	(0.0160)
FP*Flood		-0.0689***
		(0.0210)
Ln (chat_dist)	-0.0491***	-0.0491***
	(0.00218)	(0.00218)
Ln (lake_dist)	-0.0552***	-0.0553***
	(0.00187)	(0.00187)
Ln (park_dist)	-0.0204***	-0.0204***
	(0.00262)	(0.00262)
Ln (airport_dist)	-0.163***	-0.163***
	(0.00688)	(0.00689)
Ln (arta_dist)	-0.0428***	-0.0428***
	(0.00212)	(0.00212)
Ln (utility_dist)	0.0858***	0.0858***
	(0.00194)	(0.00194)
Ln (road_dist)	0.0392***	0.0393***
	(0.00235)	(0.00235)
Ln (runway_dist)	0.391***	0.391***
	(0.00590)	(0.00590)
Ln (school_dist)	0.0577***	0.0577***
	(0.00198)	(0.00198)
acres	0.0332***	0.0332***
	(0.00398)	(0.00398)
year_built	0.000899***	0.000897***
	(0.000125)	(0.000125)
num_storie	0.0517***	0.0516***
	(0.00507)	(0.00507)
bedrooms	0.000386	0.000401
	(0.00278)	(0.00278)
full_baths	0.108***	0.108***
	(0.00504)	(0.00504)
half_baths	0.0477***	0.0477***
	(0.00418)	(0.00418)
total_fixt	0.00881***	0.00882***
	(0.00121)	(0.00121)
fireplace_	0.106***	0.106***
	(0.00351)	(0.00351)
ground_flo	8.29e-05***	8.29e-05***
	(5.48e-06)	(5.48e-06)
heated_flo	0.000161***	0.000161***
	(4.29e-06)	(4.29e-06)
Constant	4.076***	4.077***
	(0.252)	(0.253)
Community, Year , Style, Type and Basement Fixed Effects	Y	Y
Observations	106,505	106,505
R-squared	0.738	0.738

Robust standard errors in parentheses
*** p<0.01, ** p<0.05, * p<0.1

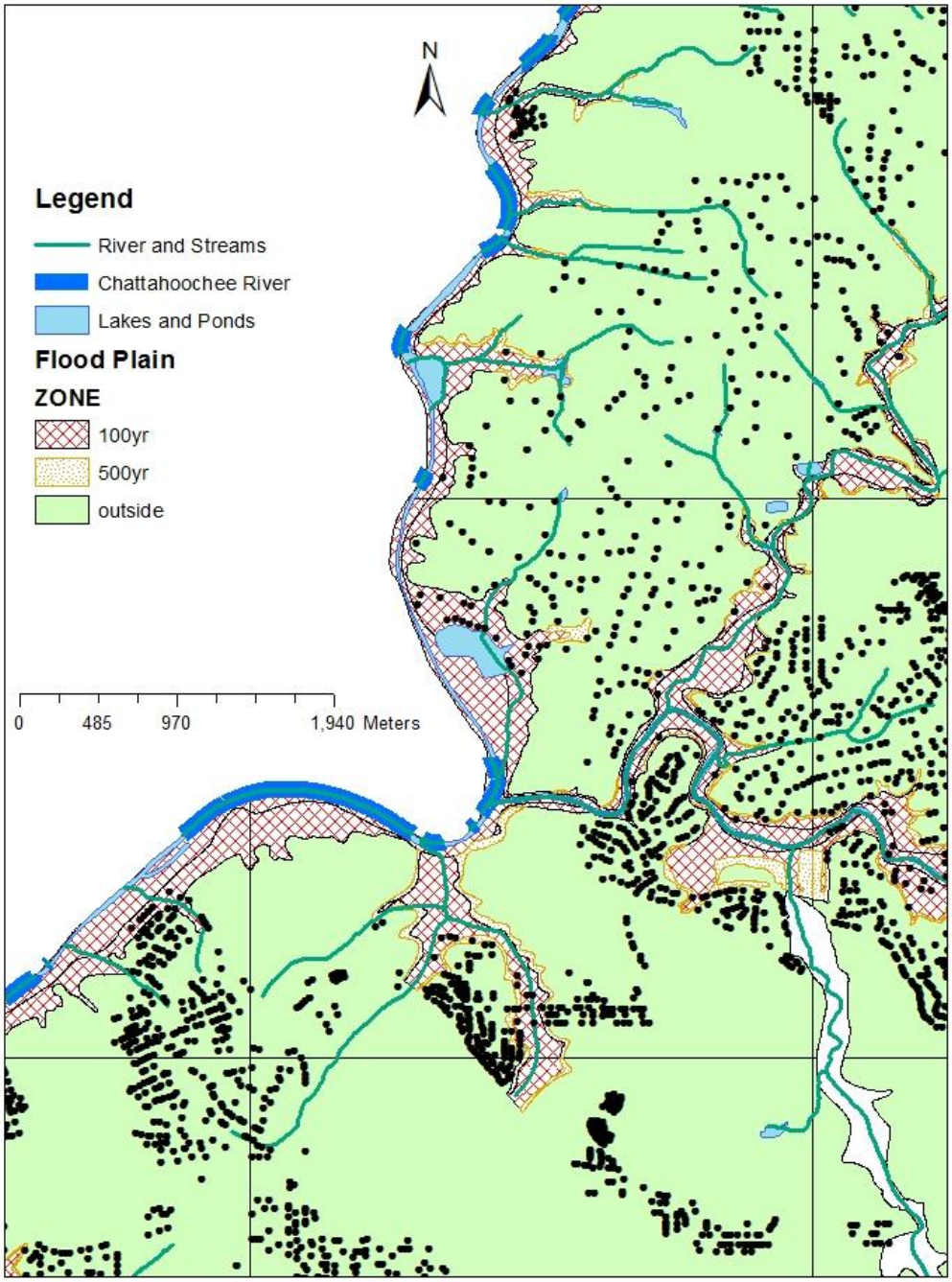

Figure 1: Water Bodies and Federal Emergency management Agency Designated Floodplains in Fulton County, GA. The dots represent the housing units that were sold in years 1977-2007.

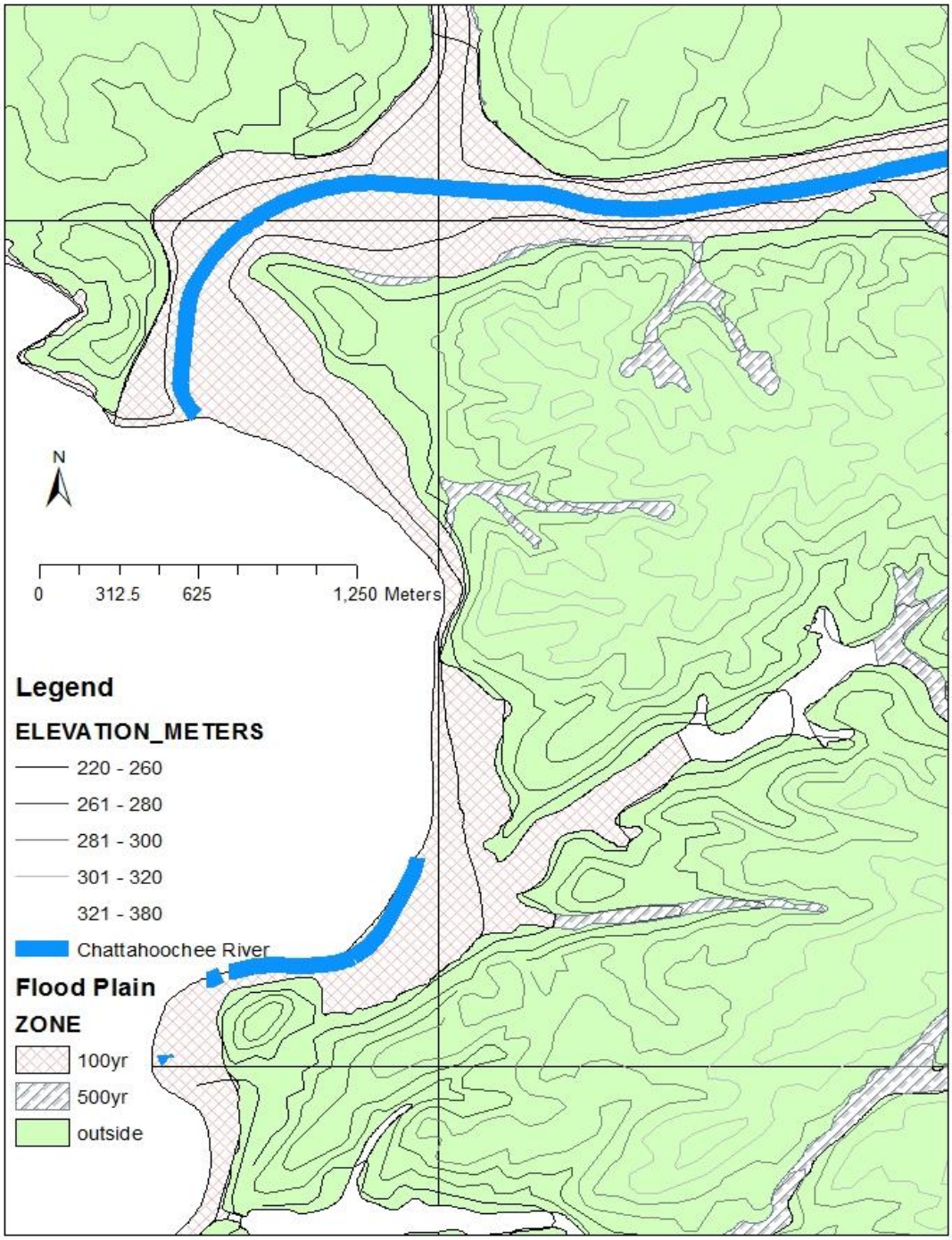

Figure 2: The Chattahoochee River with associated Floodplains and Elevation, Fulton County Georgia.

References:

Beatley, T., D. Brower, and A. Schwab. 2002. *An introduction to coastal zone management*: Island Pr.

Bergstedt, A., P. Deyo, and M. Youngwrith (1999) Conservation Subdivisions: Ecological, Landscape and Construction, and Legal Applications to Cherokee County, Georgia.

Bin, O., and J. Kruse. 2006. "Real estate market response to coastal flood hazards." *Natural Hazards Review* 7:137.

Bin, O., J. Kruse, and C. Landry. 2008. "Flood hazards, insurance rates, and amenities: Evidence from the coastal housing market." *Journal of Risk and Insurance* 75(1):63-82.

Bin, O., and S. Polasky. 2004. "Effects of flood hazards on property values: evidence before and after Hurricane Floyd." *Land Economics* 80(4):490.

Carbone, J., D. Hallstrom, and V. Smith. 2006. "Can natural experiments measure behavioral responses to environmental risks?" *Environmental and Resource Economics* 33(3):273-297.

Freeman, A. 2003. *The measurement of environmental and resource values: theory and methods*: RFF press.

Halstead, J.M., R.A. Bouvier, and B.E. Hansen. 1997. "On the issue of functional form choice in hedonic price functions: further evidence." *Environmental Management* 21(5):759-765.

Harrison, D., G. T. Smersh, and A. Schwartz. 2001. "Environmental determinants of housing prices: the impact of flood zone status." *Journal of Real Estate Research* 21(1):3-20.

Kousky, C. 2010. "Learning from Extreme Events: Risk Perceptions after the Flood." *Land Economics* 86(3):395.

Kriesel, W., and J. Mullen (2009) Alternative Housing Development Strategies in Georgia's Coastal Marshlands, Agricultural and Applied Economics Association.

Kriesel, W., and J.D. Mullen (2009) Alternative Housing Development Strategies in Georgia's Coastal Marshlands, Agricultural and Applied Economics Association.

MacDonald, D., J. Murdoch, and H. White. 1987. "Uncertain hazards, insurance, and consumer choice: Evidence from housing markets." *Land Economics* 63(4):361-371.

McKenzie, R., and J. Levendis. 2010. "Flood Hazards and Urban Housing Markets: The Effects of Katrina on New Orleans." *The Journal of Real Estate Finance and Economics* 40(1):62-76.

Montz, B., and E. Gruntfest. 1986. "Changes in American urban floodplain occupancy since 1958: the experiences of nine cities." *Applied Geography* 6(4):325-338.

Palmquist, R.B. 1982. "Measuring environmental effects on property values without hedonic regressions." *Journal of Urban Economics* 11(3):333-347.

Perry, C. 2000. *Significant Floods in the United States During the 20th Century: USGS Measures a Century of Floods*: US Dept. of the Interior, US Geological Survey.

Rosen, S. 1974. "Hedonic prices and implicit markets: product differentiation in pure competition." *The Journal of Political Economy* 82(1):34-55.

Shilling, J., J. Benjamin, and C. Sirmans. 1985. "Adjusting comparable sales for floodplain location." *The Appraisal Journal* 53(3):429-436.

Skantz, T., and T. Strickland. 1996. "House prices and a flood event: an empirical investigation of market efficiency." *Journal of Real Estate Research* 2(2):75-83.

Speyrer, J., and W. Ragas. 1991. "Housing prices and flood risk: an examination using spline regression." *The Journal of Real Estate Finance and Economics* 4(4):395-407.

USGS. 2006. "Flood Hazards—A National Threat."
Van der Vink, G., R. Allen, J. Chapin, M. Crooks, W. Fraley, J. Krantz, A. Lavigne, A. LeCuyer, E. MacColl, and W. Morgan. 1998. "Why the United States is becoming more vulnerable to natural disasters." *Eos*:533.
Wetherald, R., and S. Manabe. 2002. "Simulation of hydrologic changes associated with global warming." *J. Geophys. Res* 107(D19):4379-4702.

Assessment of endocrine disruption in fish and estrogenic potency of waters in Georgia

Basic Information

Title:	Assessment of endocrine disruption in fish and estrogenic potency of waters in Georgia
Project Number:	2011GA287B
Start Date:	3/1/2011
End Date:	2/29/2012
Funding Source:	104B
Congressional District:	GA-010
Research Category:	Water Quality
Focus Category:	Surface Water, Wastewater, Water Quality
Descriptors:	None
Principal Investigators:	Robert Bringolf, Cecil A. Jennings, Jeffrey A Zuiderveen

Publications

1. Kellock, K., B. Trushel, P. Ely, C. Jennings and R.B. Bringolf. High rate of intersex in bass from small impoundments. Journal of Aquatic Animal Health: to be submitted June 2012
2. Kellock, K. and R.B. Bringolf. 2011. Assessment of endocrine disruption in fish and estrogenic potency of waters in Georgia. Proceedings of the 2011 Georgia Water Resources Conference, Athens, GA, April 11–13, 2011.
3. Intersex fish in small impoundments: why won't the boys be boys? Iowa State University, Department of Natural Resource Ecology and Management. Ames, IA. May 4, 2012.
4. Intersex fish in Georgia. University of Georgia Fisheries Society. Athens, GA. February 16, 2012.
5. A survey of intersex bass in Georgia: Serendipity strikes again? University of Georgia, Warnell School of Forestry & Natural Resources. Athens, GA. September 22, 2011.
6. Intersex fish: not just in Wastewater anymore. Auburn University, Department of Fisheries and Allied Aquaculture. Auburn, AL. September 16, 2011.
7. K. Kellock, C. Jennings, P. Ely, B. Trushel, and R.B. Bringolf. Intersex fish: Not just in wastewater anymore. Presented at the 2012 Southeast Regional Chapter of the Society of Environmental Toxicology and Chemistry. Pensacoala, FL. Mar. 16-17, 2012.
8. Kellock, K.A., C.A. Jennings, P. Ely, B. Trushel, and R.B. Bringolf. Intersex fish influenced by factors other than municipal wastewater effluent. Presented at the 2012 annual meeting of the Georgia Chapter of the American Fisheries Society. Macon, GA. Feb. 7-9, 2012.
9. Bringolf, R.B., K. Kellock, B. Trushel, P. Ely, and C. Jennings. Intersex fish: Not just in wastewater anymore. Presented at the 2012 annual meeting of the Southern Division of American Fisheries Society. Biloxi, MS. Jan. 26-29, 2012.
10. Kellock, K. and R.B. Bringolf. Intersex fish influenced by factors other than municipal wastewater effluent. Presented at the 2011 Society of Environmental Toxicology and Chemistry North America Meeting. Boston, MA. Nov. 7-12, 2011.
11. Kellock, K. and R.B. Bringolf. Assessment of endocrine disruption in fish and estrogenic potency of waters in Georgia. Presented at the 2011 Georgia Water Resources Conference, Athens, GA, April 11–13, 2011. Awarded Best Student Presentation.
12. Bringolf, R.B., K. Kellock, B. Trushel, P. Ely and C. Jennings. Survey of intersex bass and estrogens in GA waters. Presented at the 2011 Meeting of the Georgia Chapter of the American Fisheries

Society. Perry, GA. Feb. 2-3, 2011.

Assessment of Endocrine Disruption in Fish and Estrogenic Potency of Waters in Georgia

Annual Report for the Period:
March 1, 2011 through May 15, 2012

Submitted to:

Georgia Water Resources Institute

By

Robert B. Bringolf, Ph.D.
University of Georgia
Warnell School of Forestry & Natural Resources
Athens, GA 30602-2152
Tel: 706-542-1477
Fax: 706-542-8356
E-mail: rbringolf@warnell.uga.edu

Cecil Jennings, Ph.D.
Unit Leader
USGS Georgia Cooperative Fish & Wildlife Research Unit
Warnell School of Forestry & Natural Resources
Athens, GA 30602-2152
Tel: 706-542-4837
Fax: 706-542-8356
E-mail: jennings@uga.edu

Jeffrey Zuiderveen, Ph.D.
Columbus State University
Department of Biology
Tel: 706-569-3019
E-mail: zuiderveen_jeffrey@colstate.edu

Submitted May 25, 2012

Executive summary

The overall goal of this project was to provide information on the incidence of intersex bass and estrogenic potency of waters across the state of Georgia. Specific objectives in 2011 were to 1) Determine incidence of intersex in fish and estrogenic activity in water collected in the Flint, Chattahoochee, and Conasauga Rivers in Georgia (other major GA rivers were sampled in 2010), 2) Determine incidence of intersex in bass collected from various lakes and ponds across Georgia to compare with the rate of intersex from fish collected in rivers, 3) Continue analysis of spatial and temporal trends of the total estrogenic activity of water samples collected when fish were collected, 4) For fish, determine how water temperature during early life stages affects their sensitivity to estrogen exposures later in life (as adults).

This project has supported one Ph.D. student, Kristen Kellock, in the UGA Interdisciplinary Toxicology Program. Kristen received the Best Student Presentation Award at the 2011 Georgia Water Resources Conference held in Athens, GA, April 11-13, 2011. Kristen published her findings in the Conference Proceedings (Kellock and Bringolf 2011) and has two additional manuscripts in preparation for submission to peer-reviewed journals (Journal of Aquatic Animal Health and Science of the Total Environment). Since 2011 this project has been the focus of 3 invited seminars and 6 contributed oral presentations at regional, national and international scientific meetings.

After the first year of sampling (2010) we confirmed that intersex is prevalent in some water bodies across the state and that intersex is not confined to rivers that receive wastewater effluent. In 2010, we collected 147 male bass from 11 impoundments and 4 rivers. In 2011 we expanded our sample sites and collected an additional 205 male bass from 8 additional impoundments and 5 sites on 3 rivers. In 2011, 36.0% of all male fish were intersex (contained eggs in testes). Of the male fish collected from impoundments, 37% were intersex and 35% of males from rivers were intersex. Similar to 2010, intersex rates were highest (62.7%) in male bass collected from impoundments with a surface area of 20 acres or less (N=3). Intersex rates were <30% in all rivers except the North Oconee, which had a 70% intersex rate.

The yeast-based estrogen assay (YES assay) successfully measured activity of estrogen-like compounds in water samples where fish were collected in 2010 and 2011. Intersex was not highly correlated with estrogen activity as measured by YES, but the site with the highest intersex also had the highest response in the YES assay. We also analyzed selected estrogen hormones by gas chromatography and found that the activity in YES assay did not always correlate with high levels of hormones, suggesting that other estrogen-like compounds may be biologically active in some bodies of water. A preliminary test indicated that nitrate, a ubiquitous contaminant in surface and ground waters, demonstrated estrogenic activity in the YES assay and also stimulated vitellogenin production by male fish, a process that is estrogen

dependent. Additional tests are needed to fully understand the role of nitrate in the development of intersex in fish.

To determine if water temperature influences the effects of early-life estrogen exposure, we performed a preliminary lab study with newly-hatched fathead minnows that were exposed to an estrogen at various temperatures. Interestingly, no intersex was evident by 75 days post hatch (dph) which suggests that the E2 exposure did not induce intersex, or the fish 'recovered' from the intersex condition by 75 dph. There was high mortality in the 35°C treatment but all fish at 30°C appeared healthy and grew better than those exposed to 25°C for 15 d early in life. Although all fish were cultured at the different temperatures for just 15 days prior to transfer to 25°C for grow out, all fish (regardless of E2 exposure) raised at 30°C for 15 days were significantly less responsive to the second estrogen exposure than those raised at 25°C early in life. This suggests that a permanent effect occurred in the fish exposed to 30°C that resulted in estrogen insensitivity later in life. This study must be repeated and requires further investigation before the full implication of temperature effects on estrogen sensitivity can be understood.

Overall, this research has greatly advanced the understanding of the distribution and severity of the intersex condition in bass in Georgia and has discovered substantial, unexpected and novel trends in the waters where intersex occurs most frequently. Additional investigation is warranted to more completely understand the primary factors involved in development of intersex gonads, to elucidate the relative sensitivity of bass compared to other fishes, and to determine potential population-level effects of the condition.

Introduction

Reports of intersex fish in water bodies around the world (including Georgia) have stimulated widespread concern about the effects that chemicals are having in the environment. Intersex is a term used to describe the presence of both male and female characteristics in individual fish, most commonly presence of oocytes (eggs) in testicular tissue, a pathological condition that is not routinely observed in most fish species (Hecker et al. 2006). The intersex condition has often been associated with a hormonally active component of municipal wastewater effluent discharge and has been induced in laboratory studies where fish were exposed to natural and synthetic hormones (Jobling et al. 2002), which are routinely measured in treated municipal wastewater effluent. The intersex condition has individual- as well as population-level implications; intersex male fish have been shown to have altered sperm production and reproductive success compared to non-intersex male fish (Jobling et al. 2002). These findings generate numerous questions about the ecological implications of intersex fish and fuel widespread concerns about the role of chemicals in well-documented trends in reproductive abnormalities in human health as well (Colborn et al. 1994). Understanding the extent and distribution of intersex fish in the environment and the chemicals that are known to induce this condition is a critical first step toward developing a management strategy.

In a widely-publicized recent scientific article, Hinck et al. 2009 reported that intersex largemouth bass (*Micropterus salmoides*) were found in rivers across the US. Intersex bass were more common (up to 91%) in Southeastern US rivers than in other sampled areas of the country. The Chattahoochee, Flint and Savannah Rivers in Georgia were included in the sampling, and of the five sites sampled in these rivers, the incidence of intersex in bass ranged from 30–50%. The fish all appeared to be male but had oocytes in their testes. Causes for the intersex condition are currently unknown and in this study the authors did not analyze water samples for the presence of estrogens or other hormones that have previously been associated with this condition. Sample sites were not associated with wastewater effluent or particular contaminants but were stratified by land use (urban, agricultural, etc.). Other indicators of reproductive system abnormalities were not assessed.

In 2010 we were funded by GWRI to begin the first systematic sampling of rivers and impoundments across Georgia for intersex bass and estrogenic activity in the water. After our first year of sampling (2010), we confirmed that intersex is prevalent in some water bodies across Georgia and that intersex is not confined to rivers that receive wastewater effluent. In 2010, we collected 147 male bass from 11 impoundments and 4 rivers and reported that 52% of male fish from impoundments were intersex and 12.1% of male fish from rivers were intersex. In 2011 our objectives were to: 1) Determine incidence of intersex in fish and estrogenic activity in water collected in the Flint, Chattahoochee, and Conasauga Rivers in Georgia (other major

GA rivers were sampled in 2010), 2) Determine incidence of intersex in bass collected from various lakes and ponds across Georgia to compare with the rate of intersex from fish collected in rivers, 3) Continue analysis of spatial and temporal trends of the total estrogenic activity of water samples collected when fish were collected, 4) For fish, determine how water temperature during early life stages affects their sensitivity to estrogen exposures later in life (as adults).

Methods

RIVER SAMPLING. Black bass sampling was conducted from April – June 2011. Fish were collected by boat electroshocking and/or hook and line from the North Oconee River, Conasauga River, Chattahoochee River (at Columbus, GA and below Morgan Falls Dam) in Georgia. The target was to collect 15 adult (age 1+) male fish at each site but this was not reached in any of the river samples (Table 1). Fish from all rivers were collected within 1 km of a municipal wastewater effluent outfall. The fish were kept alive in an aerated live well until sufficient numbers were obtained. Fish were anesthetized by buffered MS-222 overdose, weighed and measured. Gonads from each fish were examined macroscopically for confirmation of gender. Gonads were dissected from each fish, weighed and preserved in 10% buffered formalin for histological preparation by the Fish Pathology Laboratory at the University of Georgia, College of Veterinary Medicine Diagnostic Lab. We determined the incidence and severity of intersex based on presence of oocytes in the testes of apparent (macroscopic) male fish. Severity of intersex was rated with criteria described previously (Blazer et al. 2007) for smallmouth bass by scoring each fish on a scale of 0 (no intersex) to 4 (multiple clusters of more than 5 closely associated oocytes in the testes). A mean index of severity was calculated for fish from each river.

IMPOUNDMENT SAMPLING. Black bass were collected (also in April – June 2011) by boat electroshocking from eight impoundments across Georgia. Nine to 15 adult male bass (age 1+) were obtained from each lake. The fish were kept alive in an aerated live well until sufficient numbers were obtained. Fish were anesthetized by buffered MS-222 overdose, weighed and measured. Gonads were dissected from the fish, weighed and preserved in 10% buffered formalin for histological analysis.

ANALYSIS. Rates of intersex male bass from the lakes were compared to the intersex rate in males from rivers. Severity of intersex was rated with criteria described previously for river fish. A mean index of severity was calculated for fish from each impoundment. We calculated gonadosomatic index (GSI) as the percentage of total body weight comprised by the gonads. We calculated body condition factor (K) for all male fish as: (total weight (g) x 10,000) / (total length (mm)) x 100.

ESTROGENIC POTENCY. River water samples (2 L) were collected from sites where fish were collected. The water samples were filtered to remove suspended solids and extracted on a C-18 solid phase extraction column. The column was eluted with 3 x 1 ml methanol and the extracts were stored at 4°C until analysis. Total estrogenic activity was determined by the yeast estrogen screen (YES) assay, an in vitro assay with yeast (*Saccharomyces cerevisiae*) cells transfected with the human estrogen receptor and an enzyme reporter gene. Estrogenic activity was normalized to equivalents of 17β-estradiol. In addition, water samples were analyzed by gas chromatograph coupled with mass spectroscopy (GC-MS) for three natural estrogens (17β-estradiol, estriol, estrone) and a synthetic estrogen (17α-ethinylestradiol). All estrogen activity was reported in pg/ml concentrations.

TEMPERATURE EFFECTS ON INTERSEX. We performed a preliminary lab study with newly-hatched fathead minnows that were exposed to an estrogen early in life at various temperatures. Larval fathead minnows were exposed to 10 or 100 ng/L of 17-β estradiol (E2) at different temperatures (25, 30, 35 ^{o}C) from day 0 to 15 days post-hatch (dph). Three replicates of 600-ml glass beakers with 500 ml of dechlorinated tap water and 20 larval fish were used for each treatment. Water was renewed (90%) daily. Prior to renewal, water samples (n=3) were collected for confirmation of estradiol exposure concentrations. Following estradiol exposure, all fish were transferred to 19 L aquaria with clean, dechlorinated tap water at 25°C and cultured to 75 dph. Fish were fed flake food and live A*rtemia* nauplii daily to satiation. At 75 dph, all fish were challenged with an exposure of 100 ng/L of E2. At 82 dph, fish were euthanized, weighed, measured, gonads were dissected out and the carcass was homogenized and frozen at -80°C. The gonads were fixed in 10% buffered formalin and processed for sectioning and H&E stain. Gonads were staged (development) and evaluated for incidence and severity of intersex. Fish homogenates were assayed for vitellogenin, the egg yolk protein precursor, which is induced by exposure to estrogens.

CYANOBACTERIA EFFECTS ON INTERSEX. At the time of fish sampling we observed that many of the small impoundments had blooms of cyanobacteria. Recently, Rogers et al. (2011) reported that cyanobacteria produced a compound that induced synthesis of vitellogenin mRNA in male fish, a standard biomarker of estrogen exposure. We performed a preliminary test with two species of cyanobacteria (*Microcystis aeruginosa* and *Anabaena* spp.) and a green algae (*Selenastrum* spp.) to determine if they induce vitellogenin protein in fish. Briefly, we exposed juvenile (<60 days old) fathead minnows to one of the three algae species (all at an optical density of 2.0) for 14 days. There were five replicates of each algal species and each replicate consisted of a 4-L glass jar with 3 L of aerated test water and five juvenile fathead minnows. Upon termination of exposure, fish were anesthetized, weighed, homogenized and analyzed for vitellogenin with a commercially available ELISA kit (Cayman Chemical).

Table 1. Intersex black bass collected in 2011 from Georgia rivers and impoundments.

Water Body Type	Site	GA County	Surface Area (ac)	Total Males	Intersex Males	% Intersex Males
Impoundment	Private pond 1	Clarke	5	16	6	37.5
Impoundment	Private pond 3	Wilkes	7	17	14	82.4
Impoundment	Private pond 2	Wilkes	20	18	12	66.7
Impoundment	Dodge PFA	Dodge	104	22	9	40.9
Impoundment	Lake Heath	Floyd	202	14	3	21.4
Impoundment	Lake Antioch	Floyd	357	15	3	20.0
Impoundment	Par Pond SREL	Barnwell Co., SC	2767	16	0	0
Impoundment	Lake Allatoona	Cherokee	12,010	9	0	0
River	Chattahoochee	Fulton	n/a	24	7	29.2
River	Chattahoochee	Muscogee	n/a	22	4	18.2
River	Conasauga	Whitfield	n/a	6	1	16.7
River	Middle Oconee	Clarke	n/a	6	1	16.7
River	North Oconee	Clarke	n/a	20	14	70

Results and Discussion

Our results suggest that intersex is prevalent in some water bodies across Georgia and that intersex is not confined to rivers that receive wastewater effluent (Table 1). Of the 205 male bass collected in 2011, 36% were intersex. Of the male fish collected from impoundments, 37% were intersex and 35% of males from rivers were intersex. Among fish from rivers, bass from the North Oconee River (downstream of wastewater effluent) had the highest incidence of intersex rate at 70%. All other rivers had <30% intersex.

Consistent with our findings from 2010 (Kellock and Bringolf 2011), the highest rate of intersex was found in small impoundments, particularly those less than 200 surface acres (Table 1). With 2010 and 2011 data combined, we collected a grand total of 558 bass, of which 352 were males and 128 (36.4%) of the males were intersex. Largemouth bass comprised 84% of the bass collected, 13% were spotted bass, and the remaining 3% were other bass species (e.g., redeye, shoal). Surface area was a strong predictor of intersex rate, accounting for 77% of the variability in incidence of intersex among fish from impoundments (Figure 1). Severity of intersex did not differ (nested ANOVA, $F_{2,127} = 0.219$, $P > 0.899$) between rivers (2.42 ± 0.48), large impoundments (2.53 ± 0.50), and small impoundments (2.66 ± 0.21). Severity of intersex was not correlated with surface area of the impoundment (Figure 2). Gonadosomatic index was significantly lower (nested ANOVA, $F_{2,351} = 44.3$, $p < 0.01$) in intersex bass than normal bass collected in rivers and large impoundments (Fig. 3). Intersex males and normal males collected

from small impoundments had similar GSIs. Intersex bass from large impoundments had lower GSI than normal males from large impoundments but intersex bass from small impoundments and from rivers did not exhibit a smaller condition compared to their normal counterparts (Fig. 4). Fish with a smaller GSI and lower body condition are less fit than those with higher GSI and body condition. Reasons for the site-specific (small impoundment vs. large impoundment vs. river) differences in GSI and condition factor are not fully understood and require further investigation.

Prior to beginning the study we expected to see the highest rates of intersex in fish collected from rivers; however, our results suggest that black bass from small ponds (<200 acres) are highly susceptible to the intersex condition. Factors affecting intersex in small ponds are not known at this time but are likely different from those in river that receive wastewater effluent containing estrogens and other hormone-mimicing compounds. Some of the factors that differ among the various impoundments include: 1) small ponds sampled in this study generally had dense, overcrowded, bass populations as opposed to the larger impoundments which had much lower bass densities; 2) small ponds were generally more eutrophic than larger bodies of water; and 3) water temperature was greater in ponds than in other waters. These factors have led us to a number of hypotheses regarding factors that may be involved in intersex. Clearly, additional studies will be necessary to determine the factors that lead to development of intersex in bass and other fishes. We have not collected species other than bass from the locations where intersex was reported and we are thus uncertain if this condition is specific to bass or if all species demonstrate intersex. Additional research is needed to understand the prevalence of this condition among different species of fish.

Analysis of estrogenic potency of water samples collected from rivers and lakes revealed that estrogens or estrogen-like chemicals were detected in many of the waters with intersex fish (Fig. 5). We hypothesized that the highest estrogen concentrations would be found in water samples from areas with greater incidence of intersex fish and this was sometimes the case (e.g. DNR hatchery); however, high incidence of intersex was not always correlated with high estrogenic potential (e.g private ponds). The water samples reveal only a single measure in time of estrogenic potency which may change over time. Because intersex may result from an exposure to estrogens during a sensitive period of development, water samples collected at the time of fish collection may not be indicative of conditions during the most sensitive period of development. Sources of estrogens in the small impoundments are not fully understood but may be related to septic seepage, livestock, or other sources. Small impoundments were not surrounded by intensive agriculture (e.g. row crops) but some had pastures in the watershed. Generally the small impoundments were managed for recreation (fishing and hunting) and did not have frequent or regular pesticide application in the watershed. Additional land use

analyses are currently under investigation. Spatial and temporal trends of estrogenic potency in river water are currently under investigation.

In the lab study, all of the fish exposed to 35°C died by the end of the 15-day exposure. All fish cultured at 25 and 30°C survived. Sex ratio ranged from 50% males to 72% males and did not differ among any of the temperatures or estradiol treatments (ANOVA, Tukey's Test, N=3, df=5, p=0.899). Measured concentrations of estradiol were 84-210% of target concentrations and no estradiol was detected in the controls. Males and females cultured at 30°C early in life, regardless of estrogen exposure, were generally in later stages of gonadal development by 82 dph. Early life estradiol exposure stimulated gonad development in both males and females. Early life exposure to estradiol did not significantly alter sensitivity to estrogen exposure (i.e. vitellogenin induction) later in life, at 75 dph (Figure 3); however, fish cultured at 30°C early in life were much less sensitive to estradiol (less vitellogenin induction) at 75 dph than those that were cultured at 25°C throughout life (Figure 3). The same trends existed for males (Figure 4).

We expected skewed sex ratios in favor of females but this did not occur. Because exposure concentrations were verified, we conclude that the exposure concentrations or duration were insufficient to induce alteration of sex ratio. Based on published literature, we expected to se intersex and this did not occur either. We conclude that one of two things occurred, either 1) fish developed intersex then 'recovered' once placed in clean water for 60 days, or 2) intersex did not develop during the test period. Previous studies have used a similar exposure period and estradiol concentrations to induce intersex, but those investigators cultured the fish in clean water for at least 150 days. The possibility exists that intersex does not manifest until the fish become reproductively mature. Further study is warranted to fully understand the effects of temperature and early life estrogen exposure on reproductive health.

Conclusions. This study will provide the first systematic investigation of estrogens in Georgia's surface waters and intersex fish in many of Georgia's rivers and lakes. The results are critical for understanding the spatial distribution of intersex in the state and types of habitat where intersex fish occur. Intersex is currently thought to be an abnormal condition for bass, but little research on the background incidence of intersex has been reported. We had hoped that comparison of intersex in fish from rivers and lakes would allow insight into the 'normal' background incidence of intersex in basses but additional research is needed before we will understand the background rate of intersex. We have some evidence that the condition is indeed linked to estrogens in the water but our results also suggest that factors other than estrogens may be involved in development of the condition. Our preliminary results suggest that intersex rates are high in some bass populations, including those in small impoundments, but the factors influencing intersex are currently poorly understood. Results of our sampling

suggest that intersex is not confined to fish in Georgia rivers but occurs in lake populations as well. Additional sampling is required to elucidate the incidence and severity of intersex in other species of fish, to determine if the phenomenon of intersex in small impoundments occurs beyond Georgia, and to determine potential causes of the condition, particularly in small impoundments.

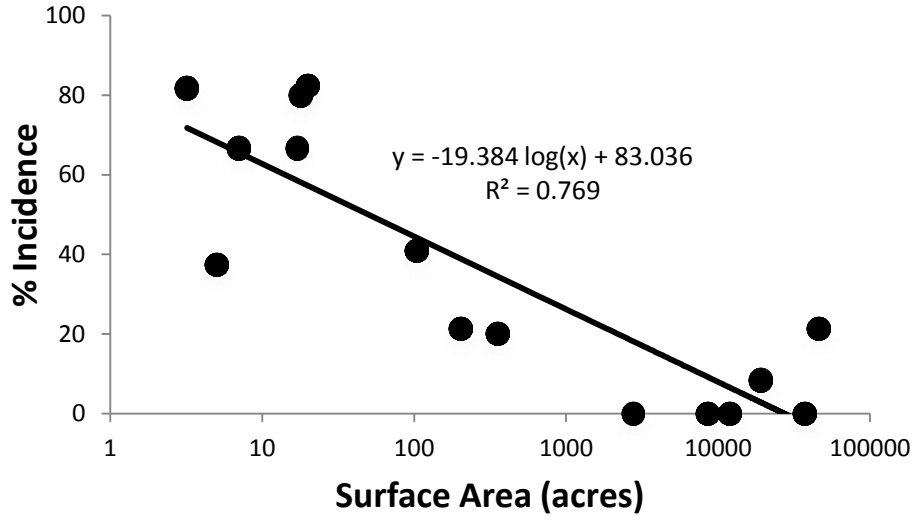

Fig. 1. Relationship between incidence of intersex in bass and surface area of Georgia impoundments Fish were collected in 2010 and 2011.

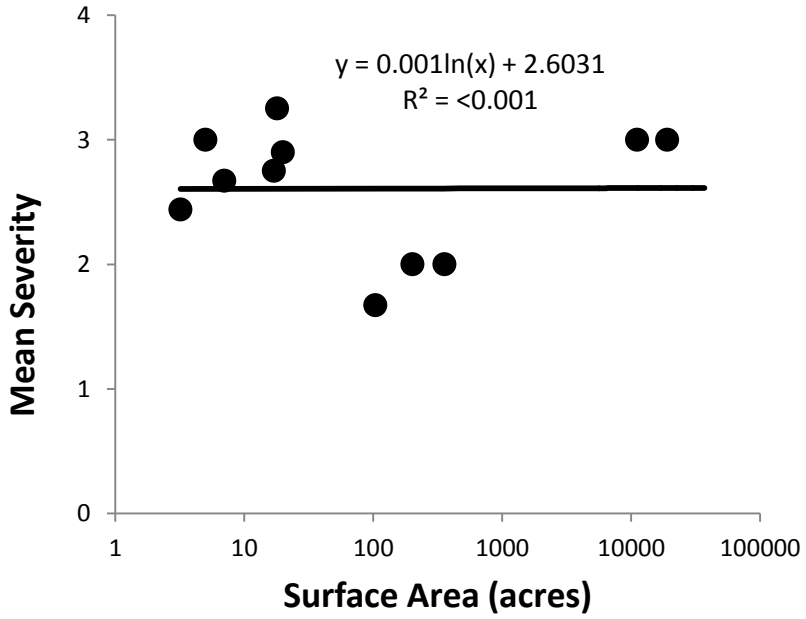

Fig. 2. Relationship between severity of intersex in male bass and surface area of Georgia impoundments. Fish were collected in 2010 and 2011.

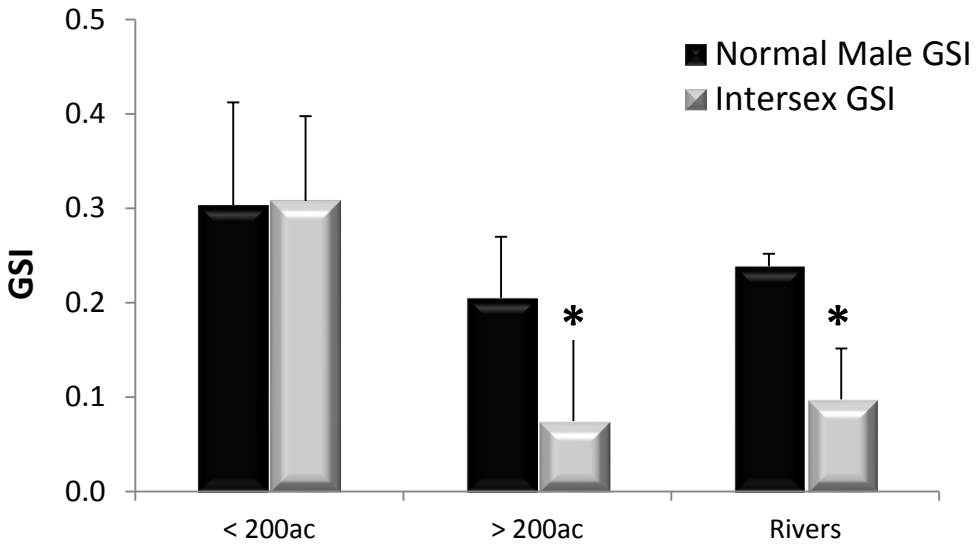

Fig. 3. Gonadosomatic index (GSI) of normal male and intersex male bass collected from small impoundments (< 200 ac), large impoundments (>200 ac), and rivers across Georgia. Fish were collected in 2010 (n = 205) and 2011 (n = 147). Asterisks indicate a significant difference (ANOVA, Tukey's, $p < 0.05$) in GSI between normal males and intersex males within a group (e.g., large impoundments, rivers).

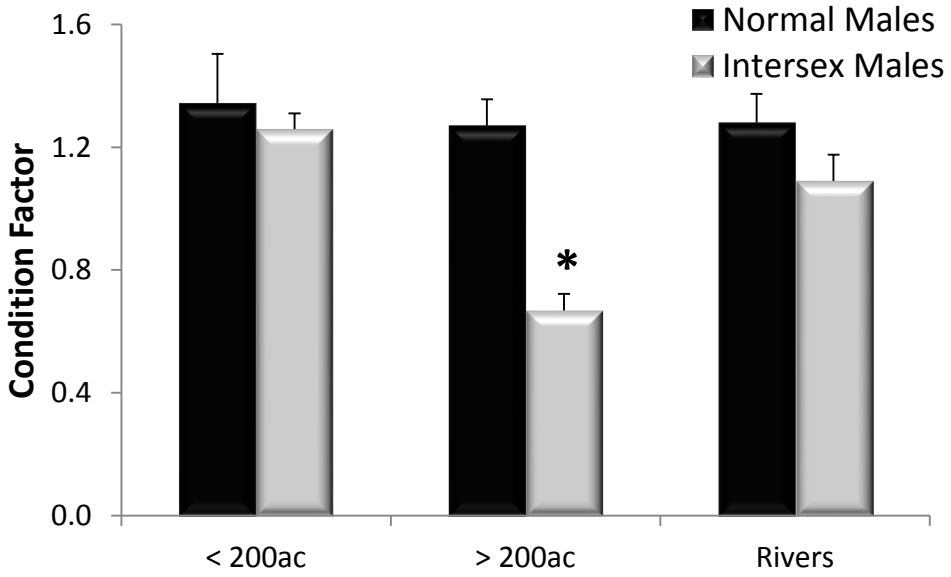

Fig. 4. Condition factor of normal male and intersex male bass collected from small impoundments (< 200 ac), large impoundments (>200 ac), and rivers across Georgia. Fish were collected in 2010 (n = 205) and 2011 (n = 147). Asterisk indicates a significant difference (ANOVA, Tukey's, $p < 0.05$) in condition factor between normal males and intersex males from large impoundments. Differences in condition factor were not significant for small impoundments and rivers.

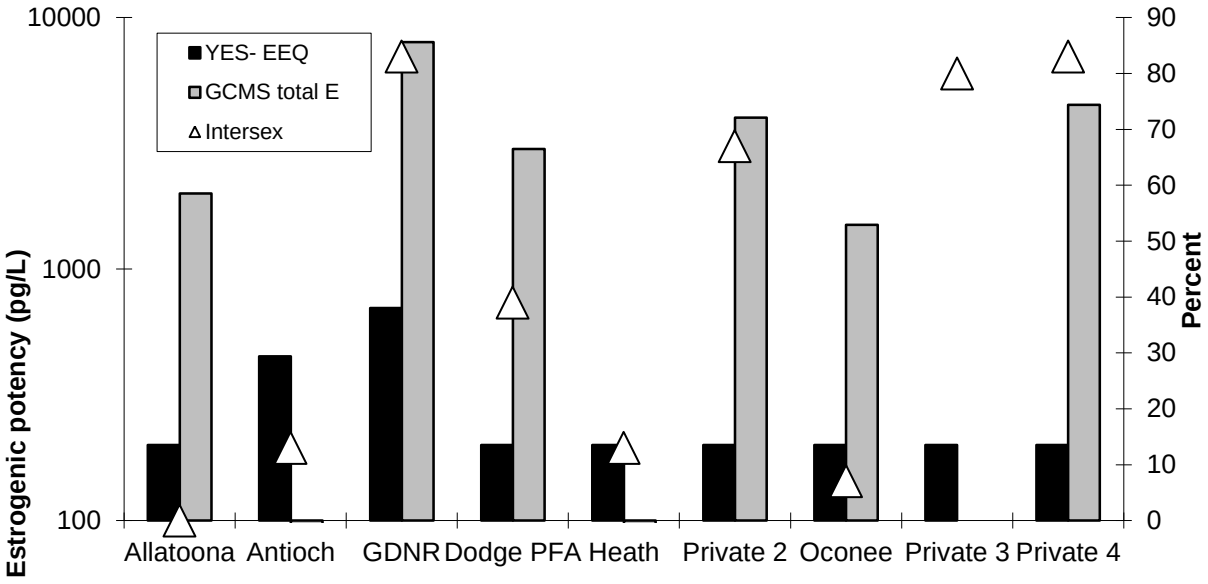

Fig. 5. Estrogenic potency (pg/ml) of water samples where fish were collected for intersex analysis, analyzed by yeast estrogen screen (YES) and GC-MS (primary y-axis). Percent intersex is on the secondary y-axis.

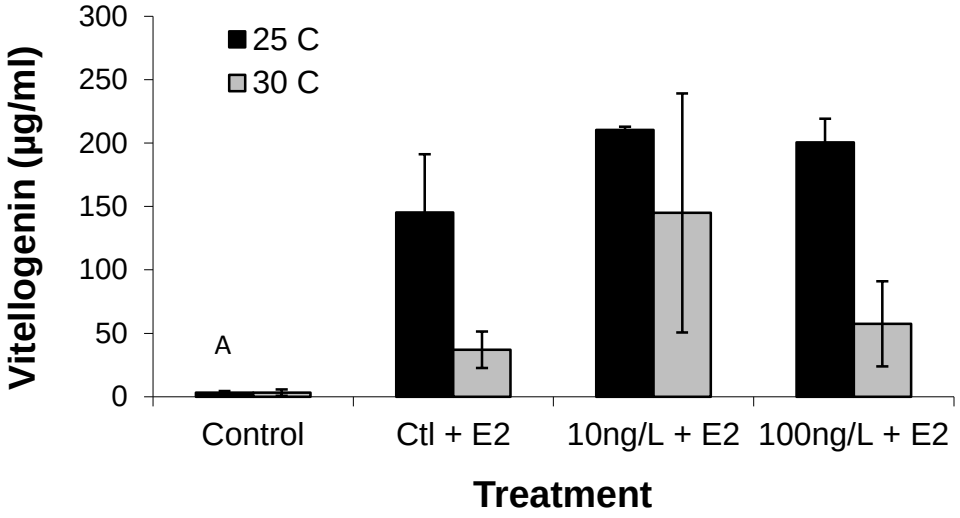

Fig. 6. Effects of early life exposure to estradiol at two temperatures (25 or 30°C) during days 0 to 15 dph. Fish were cultured in clean water at 25°C from 15 dph to 75 dph then exposed to estradiol until 82 dph. Different letters indicate significant differences ($p<0.05$) among treatments within a temperature (ANOVA, Tukey's, N=3).

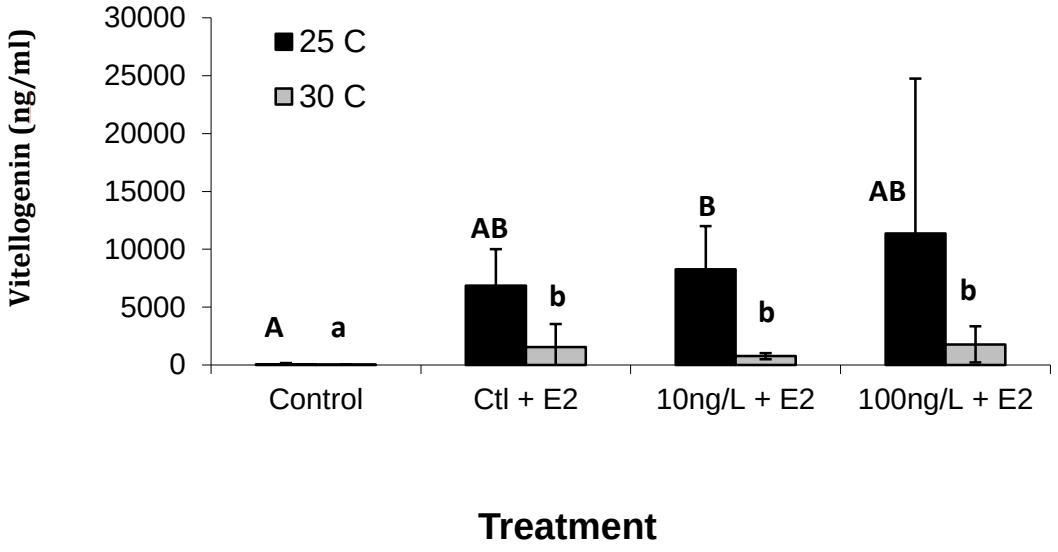

Fig. 7. Effects of early life exposure to estradiol at two temperatures (25 or 30°C) during days 0 to 15 dph. Fish were cultured in clean water at 25°C from 15 dph to 75 dph then exposed to estradiol until 82 dph. Different letters indicate significant differences ($p<0.05$) among treatments within a temperature (ANOVA, Tukey's, N=3).

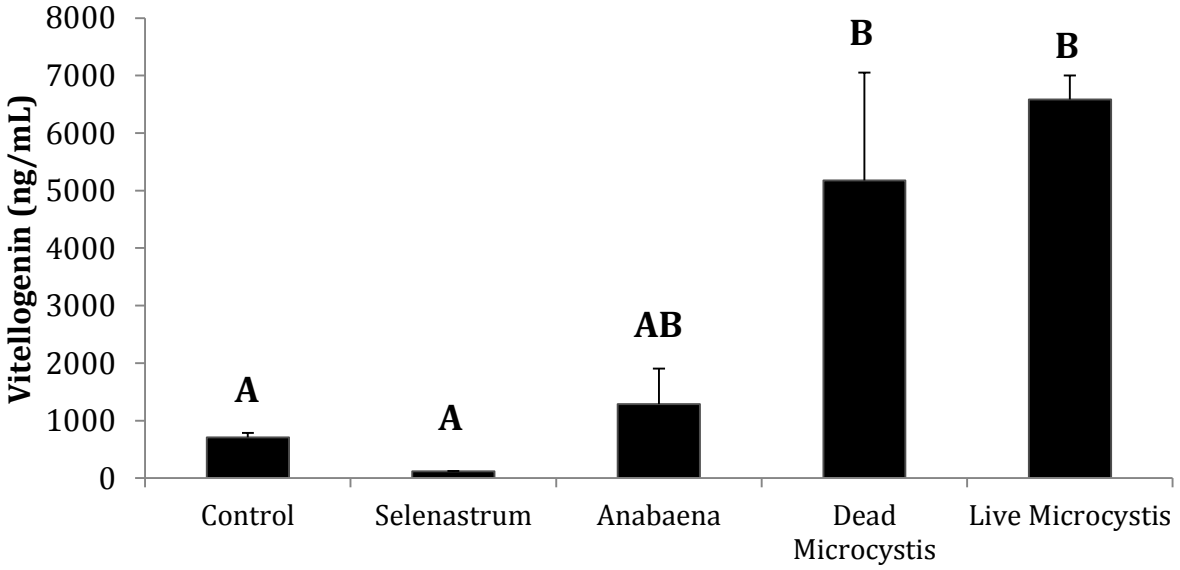

Fig. 8. Vitellogenin induction in juvenile fathead minnows exposed to green algae (*Selenastrum*), or cyanobacteria (*Anabaena* spp., *Microcystis aeruginosa*).

REFERENCES

Blazer, V. 2007. Intersex (testicular oocytes) in smallmouth bass from the Potomac River and selected nearby drainages. Journal of Aquatic Animal Health 19:242-253.

Colborn, T., F. vom Saal, and A. Soto. 1994. Developmental effects of endocrine-disrupting chemicals in wildlife and humans. Environmental Impact Assessment Review 14:469-489.

Hecker, M., M. Murphy, K. Coady, D. Villeneuve, P. Jones, J. Carr, K. Solomon, E. Smith, G. Van Der Kraak, and T. Gross. 2006. Terminology of gonadal anomalies in fish and amphibians resulting from chemical exposures. Reviews of Environmental Contamination and Toxicology 187:103-131.

Hinck, J.E., V.S. Blazer, C. Schmitt, D. Papoulias, and D. Tillitt. 2009. Widespread occurrence of intersex in black basses (Micropterus spp.) from US rivers, 1995–2004. Aquatic Toxicology 95: 60-70.

Jobling, S., S. Coey, J. Whitmore, D. Kime, K. Van Look, B. McAllister, N. Beresford, A. Henshaw, G. Brighty, and C. Tyler. 2002. Wild intersex roach (Rutilus rutilus) have reduced fertility. Biology of Reproduction 67:515-524.

Rogers, E.D., T.B. Henry, M.J. Twiner, J.S. Gouffon, J.T. McPherson, G.L. Boyer, G.S. Sayler, and S.W. Wilhelm. 2011. Global gene expression profiling in larval zebrafish exposed to microcystin-LR and microcystis reveals endocrine disrupting effects of Cyanobacteria. Environmental Science and Technology 45:1962-1969.

Routledge, E.J. and J.P. Sumpter. 1996. Estrogenic activity of surfactants and some of their degradation products assessed using a recombinant yeast screen. Environmental Toxicology and Chemistry 15:241-248.

Project Related Peer-Reviewed Publications (as of May 15, 2012)

Kellock, K., B. Trushel, P. Ely, C. Jennings and R.B. Bringolf. High rate of intersex in bass from small impoundments. Journal of Aquatic Animal Health: *to be submitted June 2012*

Kellock, K. and R.B. Bringolf. 2011. Assessment of endocrine disruption in fish and estrogenic potency of waters in Georgia. Proceedings of the 2011 Georgia Water Resources Conference, Athens, GA, April 11–13, 2011.

Project Related Presentations (as of May 15, 2012)

Invited Seminars

1. Intersex fish in small impoundments: why won't the boys be boys? Iowa State University, Department of Natural Resource Ecology and Management. Ames, IA. May 4, 2012.
2. Intersex fish in Georgia. University of Georgia Fisheries Society. Athens, GA. February 16, 2012.
3. A survey of intersex bass in Georgia: Serendipity strikes again? University of Georgia, Warnell School of Forestry & Natural Resources. Athens, GA. September 22, 2011.
4. Intersex fish: not just in wastewater anymore. Auburn University, Department of Fisheries and Allied Aquaculture. Auburn, AL. September 16, 2011.

Contributed Presentations

6. K. Kellock, C. Jennings, P. Ely, B. Trushel, and R.B. Bringolf. Intersex fish: Not just in wastewater anymore. Presented at the 2012 Southeast Regional Chapter of the Society of Environmental Toxicology and Chemistry. Pensacoala, FL. Mar. 16-17, 2012.

5. Kellock, K.A., C.A. Jennings, P. Ely, B. Trushel, and R.B. Bringolf. Intersex fish influenced by factors other than municipal wastewater effluent. Presented at the 2012 annual meeting of the Georgia Chapter of the American Fisheries Society. Macon, GA. Feb. 7-9, 2012.

4. Bringolf, R.B., K. Kellock, B. Trushel, P. Ely, and C. Jennings. Intersex fish: Not just in wastewater anymore. Presented at the 2012 annual meeting of the Southern Division of American Fisheries Society. Biloxi, MS. Jan. 26-29, 2012.

3. Kellock, K. and R.B. Bringolf. Intersex fish influenced by factors other than municipal wastewater effluent. Presented at the 2011 Society of Environmental Toxicology and Chemistry North America Meeting. Boston, MA. Nov. 7-12, 2011.

2. Kellock, K. and R.B. Bringolf. Assessment of endocrine disruption in fish and estrogenic potency of waters in Georgia. Presented at the 2011 Georgia Water Resources Conference, Athens, GA, April 11–13, 2011. **Awarded Best Student Presentation.**

1. Bringolf, R.B., K. Kellock, B. Trushel, P. Ely and C. Jennings. Survey of intersex bass and estrogens in GA waters. Presented at the 2011 Meeting of the Georgia Chapter of the American Fisheries Society. Perry, GA. Feb. 2-3, 2011.

Impact of Upstream Water Use on Salinity and Ecology of Apalachicola Bay

Basic Information

Title:	Impact of Upstream Water Use on Salinity and Ecology of Apalachicola Bay
Project Number:	2011GA289B
Start Date:	3/1/2011
End Date:	2/29/2012
Funding Source:	104B
Congressional District:	5th
Research Category:	Water Quality
Focus Category:	Surface Water, Water Quality, Hydrology
Descriptors:	None
Principal Investigators:	Philip Roberts, Philip Roberts

Publications

There are no publications.

Impact of Upstream Water Use on Salinity and Ecology of Apalachicola Bay

Final Report

Beatriz Villegas and Philip J. W. Roberts

School of Civil and Environmental Engineering

Georgia Institute of Technology

Atlanta, GA 30332

May 15, 2012

CONTENTS

Contents i

Executive Summary ii

List of Figures iii

1. Introduction 1
2. Study Area 2
3. Previous Studies and Field Measurements 4
4. The Model 5
5. Project Data 6
6. Model Setup 8
7. Model Calibration 10
8. Model Validation 12
9. Salinity Statistics 16
10. Conclusions 18
11. References 19

Appendix: Salinity Statistics 21

EXECUTIVE SUMMARY

The salinity in Apalachicola Bay, Florida, is heavily influenced by flows in the Apalachicola River, a part of the Apalachicola-Chattahoochee-Flint (ACF) river basin. The ACF is shared by Alabama, Florida, and Georgia, and is subject to conflicting water demands that may result in significant changes in the operation of the system and its flow rates. Apalachicola Bay is the termination of the ACF basin and its most important ecosystem. Biological productivity is strongly influenced by freshwater inflows that provide nutrients and determine salinity variations; in particular, oyster growth and mortality are directly related to salinity.

The bay is hydrodynamically complex. The main river flow enters perpendicular to the main estuary axis as a surface buoyant jet. Its subsequent mixing in the bay is influenced by periodic tidal currents that are primarily diurnal and semidiurnal. Winds, particularly those blowing along the long estuary axis, can significantly affect circulation and volume fluxes and therefore salinity and water quality. Although the bay is very shallow it can have strong vertical density stratification. The relative magnitudes of the various driving forces, wind, tide, and freshwater inflow, vary, resulting in significant temporal and horizontal and vertical variations of salinity.

In this phase of the project a three-dimensional hydrodynamic model of the bay was developed. The purpose of the model is to be a tool to assess the effects of varying freshwater inflow on salinity. The model is based on Delft3D, which is widely used around the world to investigate hydrodynamics, sediment transport, morphology, and water quality in lakes, rivers, coastal waters, and estuaries. Data were obtained from various sources on bathymetry, river inflows, water surface elevations, and wind speed and direction. The model was calibrated by running it for the year 2008 and comparing the predicted results with observations of water surface elevations and salinity at three locations in the bay. Following calibration, the model was further run using historical data for the years 2009 and 2010 and validated versus this data.

The water surface elevations were closely predicted in phase and magnitude. Daily average salinities were also closely simulated, but higher frequency fluctuations were not. No current data were available for comparisons.

In order to understand the effects of hydrological variables on salinity and their possible ecological impacts, various statistical parameters were computed. For the year 2008, values of monthly median, quartiles, and maxima and minima of salinity were computed at two measuring stations in the bay. Then time series of salinities at 452 observation points were obtained for three years, 2008 to 2010. From these time series averages, standard deviations, maxima, and minima were computed. The results are presented as contour plots for the surface and bottom layers by month for the three years. In addition, animations of the salinity variations and currents were made. In the second phase of the project, further statistical parameters of the salinity relevant to the ecosystem, especially oyster growth and mortality, and possible effects of global warming will be evaluated.

LIST OF FIGURES

Figure 1. ACF River Basin, sub-basins, nodes, storage and hydropower projects..... 1
Figure 2. Apalachicola Bay..... 3
Figure 3. Seasonal Apalachicola satellite images from NASA Rapid Response System..... 4
Figure 4. Bathymetry (NOAA National Geophysical Data Center U.S. Coastal Relief Model)..... 7
Figure 5. Recording stations..... 7
Figure 6. Model domain and grid..... 8
Figure 7. Apalachicola River daily average discharges at Sumatra..... 8
Figure 8. Wind speed and direction frequency distributions at APCF1..... 9
Figure 9. Daily average salinity and Apalachicola River discharge at DryBar, January to July 2009. 10
Figure 10. Simulated and observed water levels from April 1 to June 1, 2008..... 11
Figure 11. Simulated and observed salinity and water levels at Cat Point from April 1 to June 1, 2008..... 11
Figure 12. Simulated and observed salinity and water levels at Dry Bar from Apr. 1st to Jun. 1st 2008..... 12
Figure 13. Depth averaged velocity (m/s)..... 13
Figure 14. Water levels, North America Vertical Datum (NAVD)..... 13
Figure 15. Surface salinity..... 13
Figure 16. Simulated and observed salinity and water levels at Cat Point from Sep 1st to Nov 1st 2009..... 14
Figure 17. Simulated and observed salinity and water levels at Dry Bar from Sep 1st to Nov 1st 2009..... 15
Figure 18. Typical simulated salinity profiles for two monitoring points: CP and DB..... 15
Figure 19. Typical contours of simulated surface layer salinity..... 16
Figure 20. Observation points for extraction of time series..... 17
Figure 21. Simulated monthly median, quartiles and extreme values at CatPoint and DryBar.. 17
Figure 22. Daily average discharge at Apalachicola (Sumatra) during 2008..... 18
Figure 23. Salinity Monthly Averages - January..... 22
Figure 24. Salinity Monthly Standard Deviation - January..... 34
Figure 25. Salinity Monthly Maxima – January..... 46
Figure 26. Salinity Monthly Minima – January..... 58

1. Introduction

The southeastern US has had abundant water resources with most issues concerned with flooding due to hurricane-induced tropical storms. Although these issues still exist, recent decades have seen rapid population growth with accompanying increases in water demand, agricultural expansion, severe droughts, urbanization, river pollution, endangered ecosystems, and litigious transboundary water disputes. The latter are particularly intense in the Apalachicola-Chattahoochee-Flint (ACF) River Basin which is shared by Alabama, Florida, and Georgia. This basin (Figure 1) delineates the geographic context of the present project.

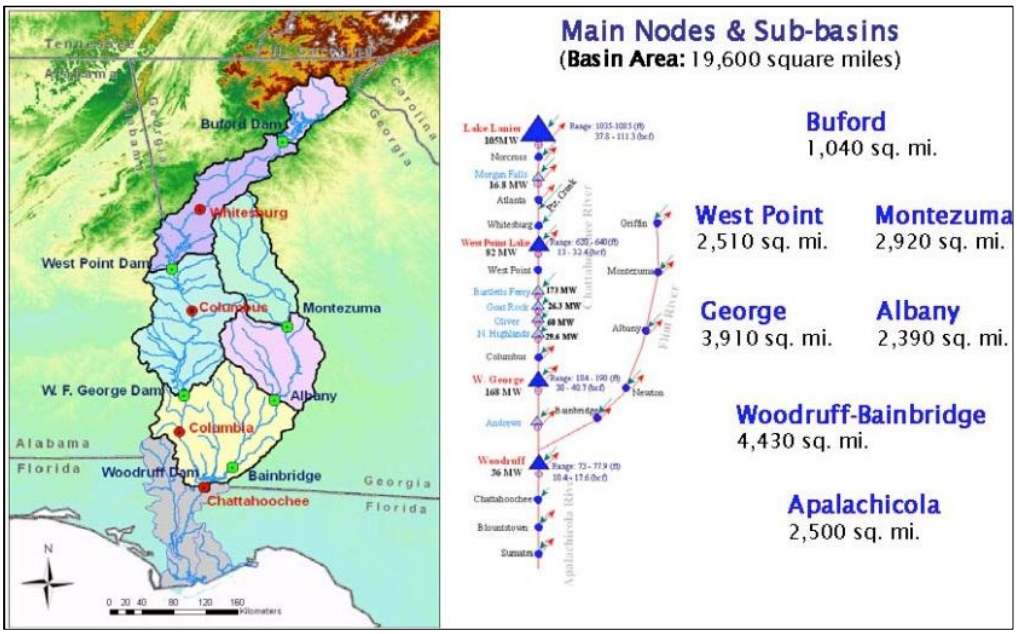

Figure 1. ACF River Basin, sub-basins, nodes, storage and hydropower projects

The ACF terminates in Apalachicola Bay, which is a very productive estuarine system that supports a diverse and abundant supply of fish with huge economic and ecological importance. The water management decisions in the ACF could have large impacts on the bay in terms of flushing, water quality, and particularly salinity. In this project, we develop a three-dimensional model of the bay as a tool to further understand the effects of varying river flows on the salinity and the impacts of various water supply strategies on this salinity.

Apalachicola Bay is the most important ecosystem in the ACF. It supports 131 freshwater and estuarine fish species and serves as a nursery for many significant Gulf of Mexico species (e.g., the Gulf sturgeon and oysters). It produces 90% of the state's oyster harvest, and the third largest shrimp catch. The river and estuary ecology depend on historical hydrological conditions under which they have evolved. These include magnitude, variability, frequency, and persistence of floods, droughts, and normal periods. Biological productivity of the bay is strongly influenced by the amount, timing, and duration of the freshwater inflow. It provides essential nutrients

that form the base for the food web in the bay and any alteration of flow in the watershed can disrupt the nutrient inputs to the ecosystem. The main factors affecting oyster population are salinity and temperature; Livingston et al. (2000) showed that oyster mortality is directly proportional to salinity in the bay. Developing a comprehensive understanding of the linkages between river hydrology, estuarine salinity, and fish ecology is critical for the development of a sound instream flow policy for ecosystem protection and sustainability. As an interim policy in Georgia, the monthly 7Q10 flow statistic (the minimum seven day average flow with a return period of 10 years) is used as a minimum instream flow requirement.

The hydrodynamics of the bay are complex. It is subject to periodic tides that are primarily diurnal and semidiurnal. Circulation and volume fluxes are significantly affected by winds blowing along the long estuary axis, which therefore significantly affect salinity and water quality in the bay. Although the bay is very shallow it can have strong vertical density stratification. The relative magnitudes of the various driving forces, wind, tide, and freshwater inflow, vary, resulting in significant spatial (in the horizontal and vertical) and temporal salinity variations. These factors make prediction of the effects of varying freshwater inflow on salinity challenging.

The ACF River Basin drains 19,600 square miles and has an average annual rainfall of 45 inches. The monthly average flows indicate a distinct seasonality of wet springs and dry summers and early falls. The percent return of the surface water withdrawals varies by water use, with thermoelectric withdrawals returning more than 90% and irrigation less than 10%.

In this report we describe the development of the three-dimensional hydrodynamic model of the bay, its calibration and comparisons with measured data, and computations of various statistical properties of salinity in the bay by month over a three year period, 2008 to 2010.

2. Study Area

Apalachicola Bay is a barrier island estuarine system located in the Florida Panhandle (Figure 2). It is approximately 65 km long and 5.5 to 12 km wide, except at its western end, where it narrows to less than 2 km. It is a shallow water system, with depth varying gently from approximately 6 m near the ocean openings to about 3 m near the river mouth. The long axis of the bay is approximately in the east - west direction. It is connected to the Gulf of Mexico through five inlets, Indian Pass, West Pass, East Pass, Sikes Cut, and Lanark Reef, and receives freshwater input from the Apalachicola River in the south end of the ACF Basin. The ACF Basin terminates in Apalachicola Bay.

Figure 2. Apalachicola Bay

Three river systems (the Apalachicola, the Whiskey George and Cash Creek, and the Carrabelle) contribute freshwater into Apalachicola Bay, with the major quantity (about 90%) flowing through the main stem of the Apalachicola River. The river flow is quite substantial, with monthly average flows ranging from 450 to 1350 m^3/s based on historic data from 1976 to 1996. The river inflow acts like a strong freshwater surface buoyant jet discharged into a saline receiving water. Seasonal variations of the Apalachicola River result in significant differences in estuary characteristics as can be observed from the NASA satellite images (Figure 3).

The hydrodynamics of the bay are complex. It is subject to periodic tides that are primarily diurnal and semidiurnal. Due to the East-West estuary axis and the long wind fetch along this axis with major inlets at each end, winds can play a significant role in volume exchanges between the Bay and the Gulf and can significantly affect salinity and water quality in the bay. The main river flow enters perpendicular to this axis as a surface buoyant jet. Even though the water is shallow, field observations show that the bay can be vertically strongly stratified. The relative magnitudes of the various driving functions, wind, tide, and freshwater inflow, vary, resulting in significant horizontal and vertical salinity variations in the bay. Flows and circulation result from baroclinic forcing (density currents) and barotropic forcing (due to tides and winds). Vertical mixing is significantly affected (reduced) by the vertical density stratification. These factors make prediction of salinity variations challenging; the vertical stratification dictates a three-dimensional (3D) model.

Terra/MODIS. January 7th 2011_ Winter **Terra/MODIS. October 4th 2008_Autum**

Aqua/MODIS. April 6th 2009_ Spring **Terra/MODIS. July 8th 2010_ Summer**

Figure 3. Seasonal Apalachicola satellite images from NASA Rapid Response System.

3. Previous Studies and Field Measurements

Huang and Jones (1997) set up, calibrated, and verified a hydrodynamic model of Apalachicola Bay using daily freshwater inflows from the Apalachicola River measured by the USGS and an extensive field data observation program conducted by NW Florida Water Management District (NWFWMD) during May to November 1993. Within the bay, hourly data were obtained from two tidal stations, six salinity stations, and several current stations. Hourly wind speed and direction were observed at mid-bay. Data were also collected at five boundary openings connected to the Gulf (Indian Pass, West Pass, Sikes Cut, East Pass, and Lanark Reef) that included hourly salinity and temperature (surface and bottom), and surface elevation.

Huang and Jones (2001) used their model to investigate the long-term transport of fresh water in the bay and Huang and Jones (2010) developed an integrated hydrodynamic modeling and probability analysis approach to assess the long-term effects of changing river inflows on the estuarine ecosystem. Their analysis of spatial distributions of seasonal average salinity and currents shows that the long-term freshwater transport was strongly affected by the forcing functions of wind and density gradient in the bay. The water column was strongly stratified near the river mouth, gradually changing to well mixed near the ocean boundaries. Vertical stratification in

the bay changed due to wind-induced mixing and mass transport. Due to the density gradients, surface residual currents carrying fresher water were directed away from the river toward the Gulf, while the bottom residual currents with more saline water entered the bay from the Gulf of Mexico. To assess the long-term effects of changing river inflows on the estuarine ecosystem, Huang and Jones predicted long-term salinity data with the calibrated 3D hydrodynamic model under two river inflow conditions over a 10-year period and used probability analysis to characterize and quantify the changes of river flow and salinity patterns over the 10-year period.

Sun and Koch (2001) used water elevations, wind speed, current velocity, and salinity collected at multiple stations by the MWFWMD at half hour intervals from April 1993 to August 1994. The authors employed cross-correlation techniques, autoregressive integrated moving average (ARIMA), and dynamic regression transfer models using the Box-Jenkins methodology to analyze the time series data. Among their main conclusions is that tidal water level fluctuations result only in short-term periodic variations in salinity, with a linear transfer function that has a lag-two as the highest coefficient. The cross-correlation analysis shows that the Apalachicola River, being the major freshwater source of the bay, strongly affects the currents and salinity in the bay area over the long term. Though regional precipitation controls the amount of fresh-water inflow, either through river discharge or groundwater seepage, its effect on the daily variations in salinity is statistically insignificant. In contrast, the effect of daily wind stress is significant. Salinity is positively correlated with western currents in the bay because most of the oceanic flow enters the bay from the east. A lag between the daily discharge and salinity indicates that up to a week is required for the peak of the inflow fresh water to flush through the exit of the bay.

A hydrographic survey was conducted on April 5-6, 2003 by Faure and Dottori (2003) in the western part of Apalachicola Bay. They measured temperature and salinity. The density profiles are dominated by salinity variations with temperature playing an insignificant role. Although the bay is very shallow, there can be very strong vertical density gradients.

4. The Model

The hydrodynamic model is Delft3D, a world-leading two and three-dimensional modeling system to investigate hydrodynamics, sediment transport, morphology, and water quality. While applicable to a wide variety of situations, the package is mostly used for the modeling of lakes, rivers, coastal waters, and estuaries. It has a user-friendly interface and extensive graphics capabilities for presentation and animation of the simulation results. Extensive technical data on the model is available from the technical manuals; a brief summary of its main capabilities is given below.

Delft3D simulates the temporal and spatial variations of six phenomena and their interconnections. The FLOW module of Delft3D is a multi-dimensional (2D or 3D) hydrodynamic (and sediment transport) simulation program which calculates unsteady flow and transport phenomena resulting from tidal and meteorological forcing on a curvilinear, boundary-fitted grid. Delft3D consists of an advanced

integrated and well-validated modeling environment for six linked modules: hydrodynamics [Delft3D-FLOW], waves [Delft3D-WAVE], water quality [Delft3D-WAQ], morphology [Delft3D-MOR], sediment transport [Delft3D-SED], and ecology [Delft3D-ECO]. In addition, a particle tracking model, Delft3D-PART, is available.

The hydrodynamic module Delft3D-FLOW solves the unsteady non-linear shallow water equations in three dimensions with a hydrostatic assumption. This module calculates unsteady flow and baroclinic circulation in three dimensions and transport phenomena resulting from various forcing mechanisms. The equations are formulated in orthogonal curvilinear coordinates or in spherical global coordinates. The utilization of sigma grids tolerates much smaller levels of horizontal viscosity and diffusivity. The model includes tidal forcing, Coriolis forces, baroclinic motions (density-driven flows as pressure gradient terms in the momentum equations), an advection-diffusion solver to compute density gradients with an optional facility to treat very sharp gradients in the vertical, space and time varying wind and atmospheric pressure, advanced turbulence models to account for the vertical turbulent viscosity, and diffusivity based on the eddy viscosity concept. The driving forces are open boundary conditions (water levels), inflows from adjacent rivers, and meteorology (winds). The standard drying and flooding algorithm in Delft3D-FLOW is efficient and accurate for coastal regions, tidal inlets, estuaries, and rivers.

Delft3D allows for terrain-following, the so called sigma coordinate system. The main advantage of sigma coordinates is that, when cast in a finite difference form, a smooth representation of the bottom topography is obtained.

5. Project Data

The entire data base available for the project is described here. Physical, hydrological, and meteorological data were obtained from the NOAA National Geophysical Data Center, U.S. Geological Survey (USGS), Apalachicola National Estuarine Research Reserve (ANERR), Northwest Florida Water Management District, and the National Data Buoy Center (NDBC_NOAA), and used to set up the grid, define boundary and initial conditions, and perform model calibration and validation. The initial model calibration simulations were done for the year 2008 and model validation includes two consecutive years, 2009 and 2010.

The bathymetric data was downloaded from the NOAA National Geophysical Data Center U.S. Coastal Relief Model (www.ngdc.noaa.gov/mgg/coastal/crm.html). The water depth gently varies from approximately six meters near the ocean openings to about three meters near the river mouth (Figure 4).

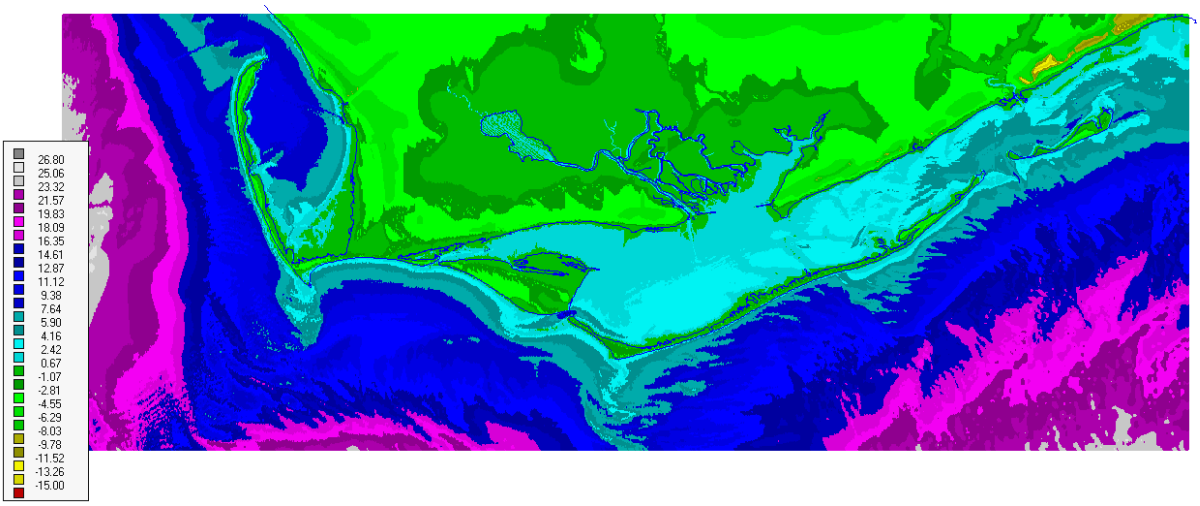

Figure 4. Bathymetry (NOAA National Geophysical Data Center U.S. Coastal Relief Model)

Water level data recorded every 6 minutes at the NOAA station named Apalachicola was used at the model open boundaries. Daily average river discharges measured by the USGS at the Sumatra hydrological stations were used to represent the Apalachicola river freshwater contribution to the estuary. Winds recorded every 6 minutes at the NOAA meteorological station APCF1 were used to represent the wind field over the bay. ANERR salinity and sensor depth data recorded at three points inside the bay: CatPoint (CP), DryBar (DB) and EastBay (EB), were used to perform model calibration and validation. The stations are shown in Figure 5.

Figure 5. Recording stations

6. Model Setup

A three-dimensional model for the Apalachicola Bay was set up, calibrated, and validated. The data base available is described in Chapter 5. The driving forces were divided into open boundary conditions (water levels), hydrology of the adjacent watershed (river tributaries), and meteorological conditions (winds). The simulations were made using time series data.

The horizontal grid was implemented using Delft3D_RFGGrid (Figure 6) and the vertical numerical grid (i.e. cell depths) was implemented using Deltft3D_QUICKIN. Model grid sizes were defined based on analyses of the local bathymetry and numerical stability issues. The grid sizes ranged from 200 m near the Apalachicola river mouth to 600 m near the barrier islands. The vertical grid consists of five uniform sigma layers.

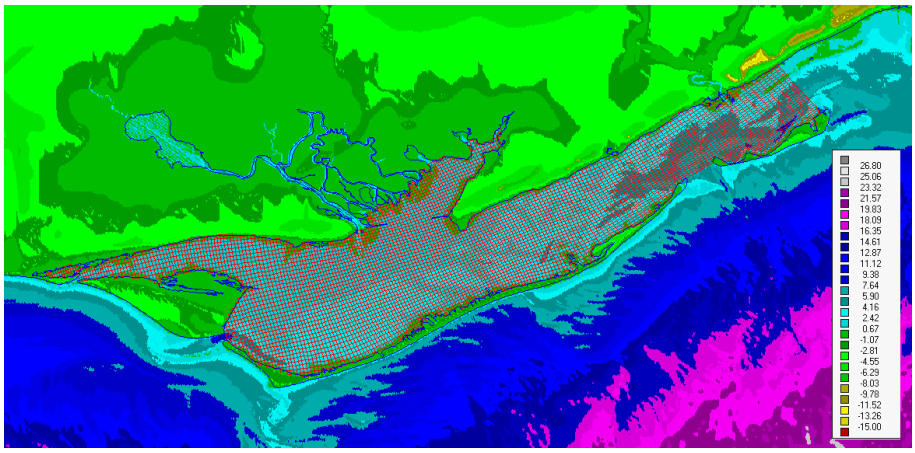

Figure 6. Model domain and grid

The model was run for three consecutive years: 2008, 2009, and 2010, which covered 3 different hydrologic periods: dry, wet, and normal. The Apalachicola River daily average discharges recorded at the Sumatra hydrological station are shown in Figure 7. The monthly average wind speeds at NOAA meteorological station APCF1 for the studied period are summarized in Table 1.

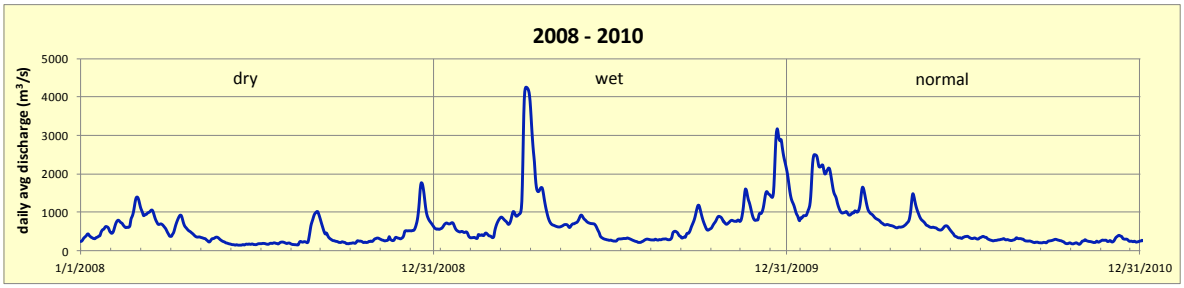

Figure 7. Apalachicola River daily average discharges at Sumatra

Table 1. Average monthly wind speeds (m/s) at APCF1

Month	2008	2009	2010
January	3.64	2.90	3.38
February	2.80	2.90	3.10
March	3.59	3.33	3.03
April	3.11	3.52	3.37
May	3.08	3.70	3.27
June	2.16	2.44	2.56
July	2.14	2.28	3.09
August	2.86	2.45	3.00
September	3.55	3.10	3.00
October	3.91	2.77	2.85
November	3.06	3.49	3.04
December	2.88	3.41	2.32

Frequency distribution of the wind speeds and directions from January 2008 to December 2010 are shown in Figure 8. For this data period the average wind speed is 3 m/s. The winds are predominantly from the northeast with speeds ranging mostly from 2 to 4 m/s. The highest speed recorded was 14.3 m/s on October 24, 2008 from 73°. The second and third strongest winds occurred on May 21 2009: 13.7 m/s at 55° from the north, and November 10 2009: 13.7 m/s at 82° from the north.

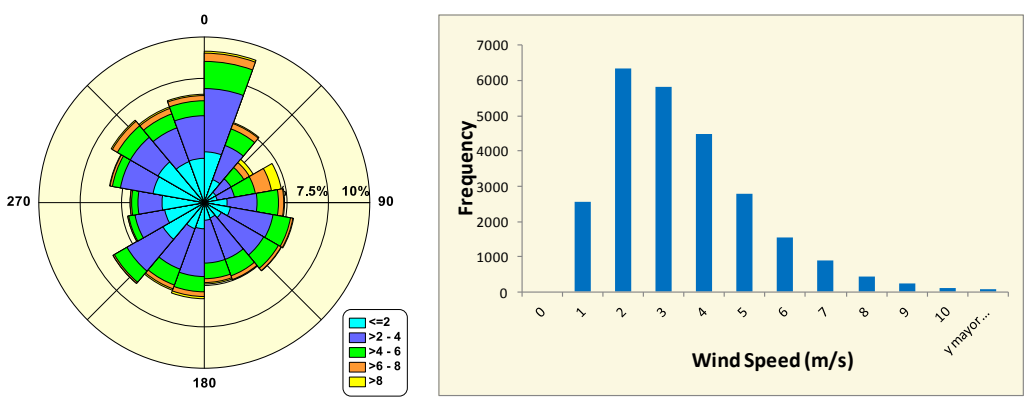

Figure 8. Wind speed and direction frequency distributions at APCF1

Time series data for measured daily average salinity at DryBar and daily average Apalachicola River discharges (from January to July 2009) are presented on Figure 9. During this time period a peak discharge of 4250 m^3/s was recorded for the Apalachicola River. During this event Apalachicola Bay salinities went to zero at Drybar.

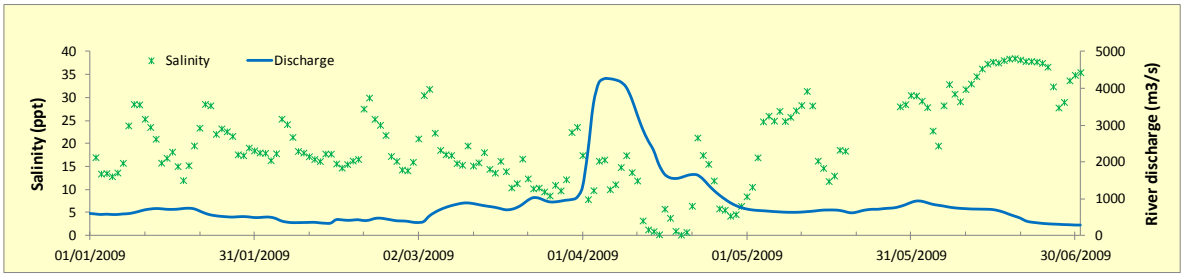

Figure 9. Daily average salinity and Apalachicola River discharge at DryBar, January to July 2009.

The initial hydrodynamic condition for the entire domain corresponds to a stationary condition (zero velocity, or cold start). Uniform values for all dependent variables were assumed at the start of the simulation. The initial water level and salinity conditions were set according to measured values and the time step was set according to accuracy arguments (Courant Number) and sensitivity analyses. Initial values for physical parameters like bottom roughness, wind drag coefficients and viscosities where estimated according to former studies and literature review.

7. Model Calibration

For calibration purposes the model was run from October 2007 until December 2008. The first three months corresponds to a warm up period. Time series of simulated and measured salinities and water levels were compared at three different locations inside the bay (CP, DB, and EB). The model parameters were adjusted to achieve acceptable agreement. For the statistical comparison of observed and simulated parameters we use the normalized Fourier norm (*Fn*) as defined by Schwab (1983) as,

$$Fn = \frac{\|V_0, V_c\|}{\|V_o, 0\|}$$

where,

$$\|Vo, Vc\| = \sqrt{\frac{1}{\mathrm{M}} \sum_{\mathrm{t}=\Delta}^{\mathrm{M}\Delta\mathrm{t}} |\mathrm{V}_0 - \mathrm{V}_\mathrm{c}|^2}$$

$$\|Vo, 0\| = \sqrt{\frac{1}{\mathrm{M}} \sum_{\mathrm{t}=\Delta}^{\mathrm{M}\Delta\mathrm{t}} |\mathrm{V}_0 - 0|^2}$$

The *Fn* can be thought of as the relative percentage of variance in the observed parameter (Vo) that is unexplained by the calculated parameter (Vc). In the case of perfect prediction $Fn = 0$. In the case $0 < Fn < 1$, model predictions are better than no prediction at all.

Figure 10 shows water level comparisons at EB for a 2 month period (from April 1 to June 1, 2008); for this period an *Fn* value of 0.06 was achieved, meaning 94% correct model predictions.

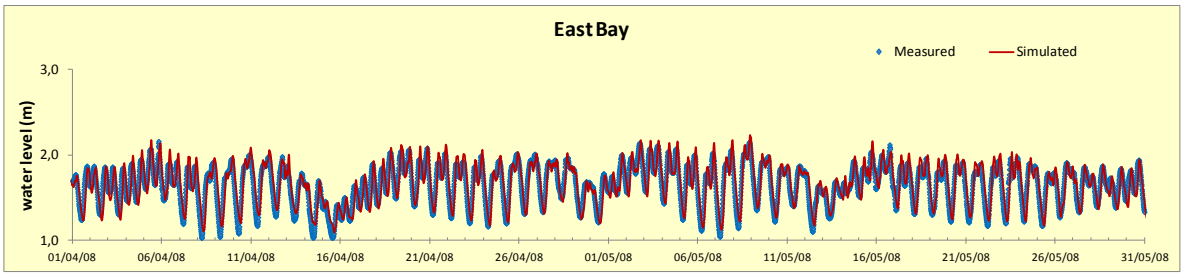

Figure 10. Simulated and observed water levels from April 1 to June 1, 2008.

Salinity and water level comparisons at DB and CP for a two month period (from April 1st to June 1st, 2008) are presented in Figures 11 and 12. The modeled water levels were in very good agreement in phase and magnitude with measured values. Daily average salinity results also reasonably followed the general trend of field observations, but high frequency fluctuations were not so well simulated.

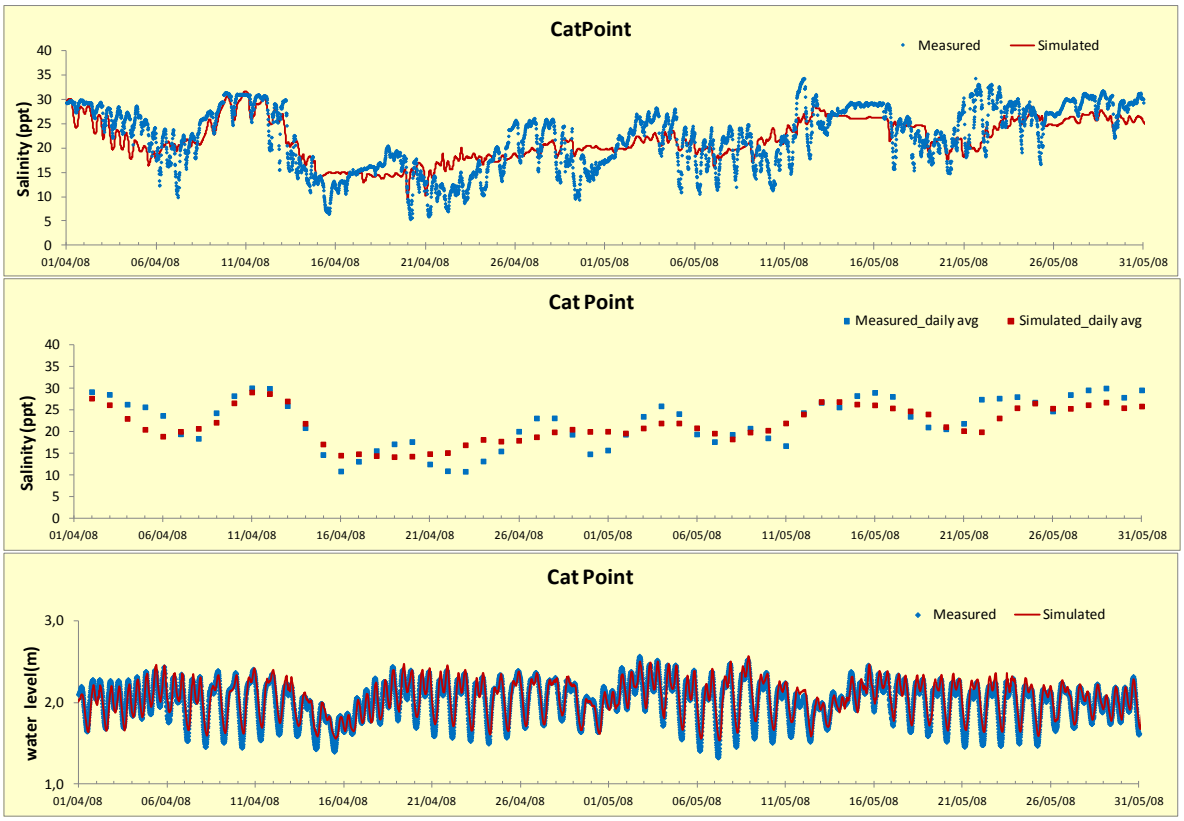

Figure 11. Simulated and observed salinity and water levels at Cat Point from April 1 to June 1, 2008

During this period there is an evident disagreement between depth sensor measurements and simulated values from May 8th to May 23rd at station DB. Given that the differences between the two values is constant and that this temporary behavior is seen several times during the simulated period it is clear that the difference is due to a temporary instrumental miscalibration. Notice also the evident discrepancy between the measured and simulated salinities for those same days; it is probable that the salinity sensor is miscalibrated too.

At the end of the calibration process the following values where adopted for the physical parameters: Manning roughness: 0.015, horizontal eddy viscosity and diffusivity: 10 m^2/s, and wind drag coefficient: 0.0012.

Figure 12. Simulated and observed salinity and water levels at Dry Bar from Apr. 1st to Jun. 1st 2008

8. Model Validation

After finishing the calibration stage the model was run for another two consecutive years: 2009 and 2010. Typical depth-averaged velocity vectors, water levels, and salinity over the model domain for an arbitrary simulation time are shown in Figures 13, 14, and 15.

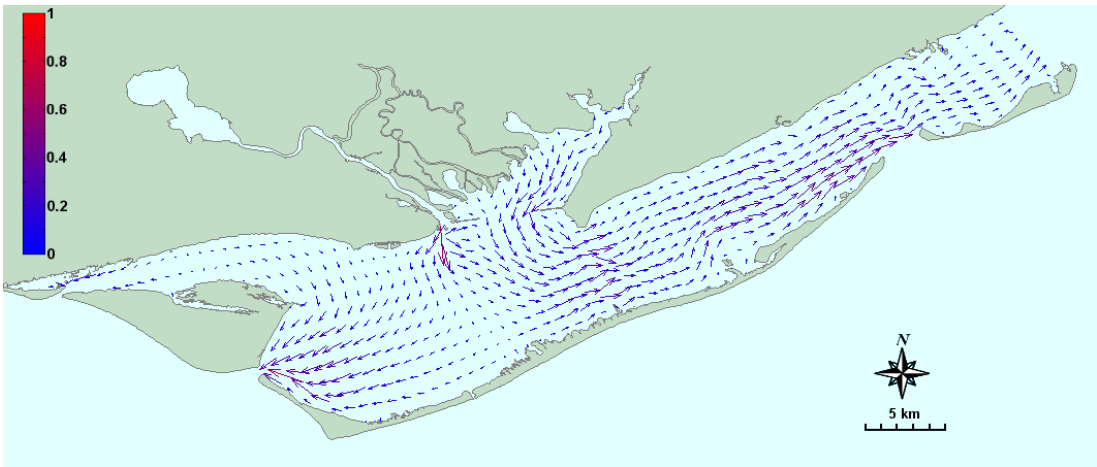

Figure 13. Depth averaged velocity (m/s).

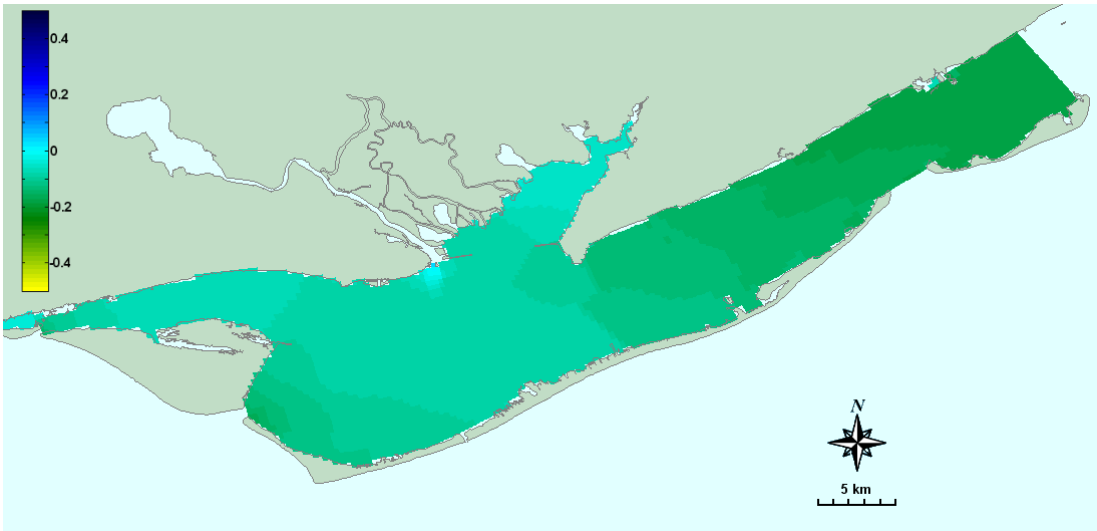

Figure 14. Water levels, North America Vertical Datum (NAVD).

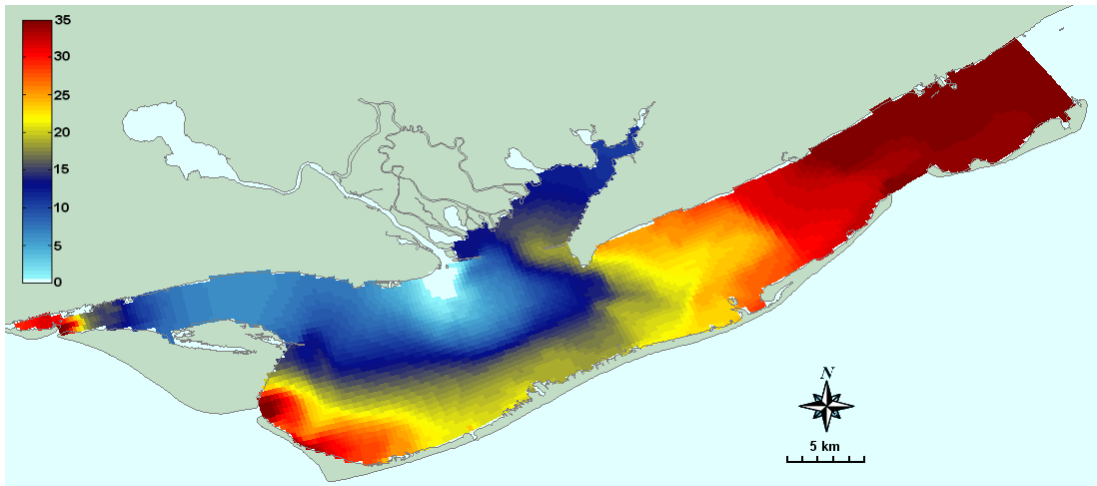

Figure 15. Surface salinity.

The velocities of the currents in the bay vary from 0 to more than 1 m/s, and the flow directions change from predominantly southwest at high tides to northeast at low tides. The central part of the bay has relatively weak currents. The currents are stronger at the river entrance and the eastward ocean entrance. Fluctuations of tidal water levels result only in short-term periodic variations in salinity.

Salinity and water level comparisons at DB and CP for a two month period (from September 1st to November 1st, 2009) are presented in Figures 16 and 17. The modeled water levels were again in very good agreement in phase and magnitude with measured values. Salinity results also reasonably followed the general trend of field observations. Depth miscalibration events can also be observed during this time period.

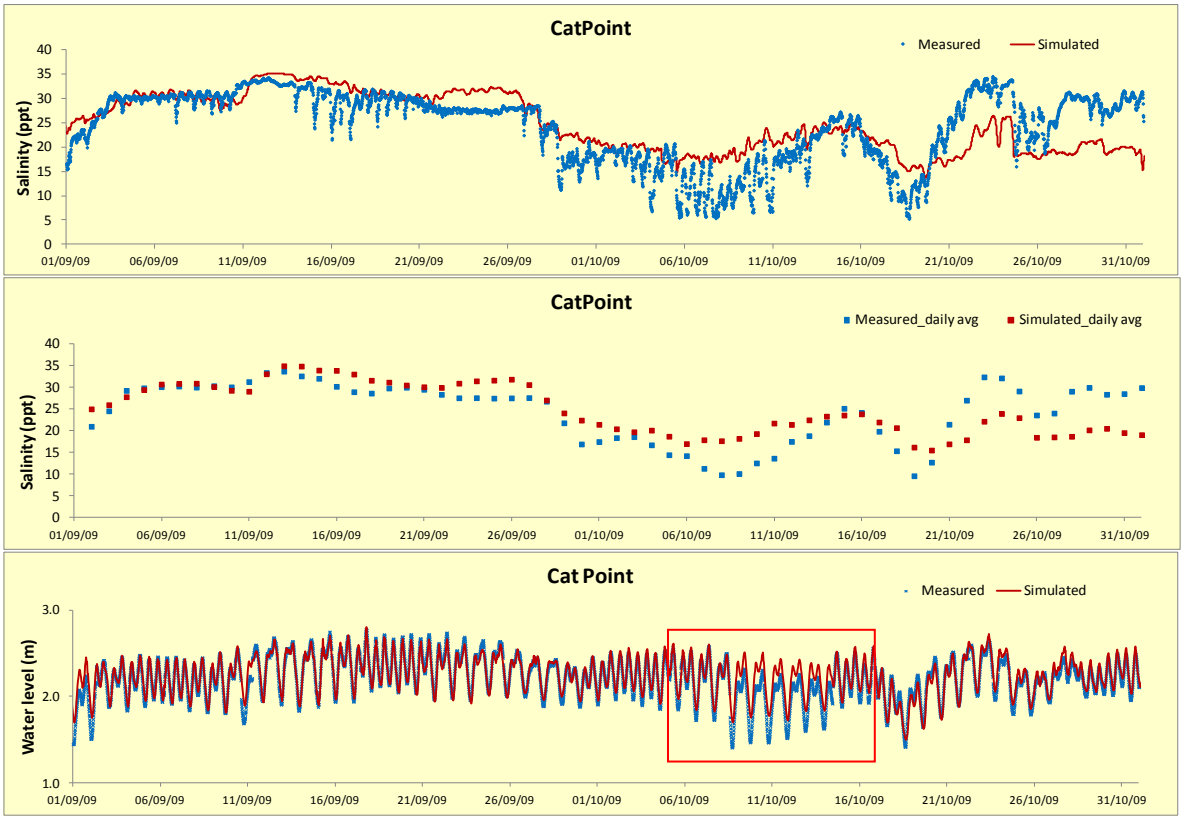

Figure 16. Simulated and observed salinity and water levels at Cat Point from Sep 1st to Nov 1st 2009

Although no direct validation can be done for the present results, mainly because there are no currents or vertical stratification measurements available for the simulated time frame, the present model setup resulted in plausible simulations of the estuary's major hydrodynamic characteristics. The modeled water levels were in very good agreement in phase and magnitude with measured values for all available recording stations for the entire simulation with *Fn* values bigger than 90%. Salinity results also reasonably followed the general trend of field observations; model to field data comparisons of the monthly average salinity were extremely close resulting in *Fn* values higher than 80%.

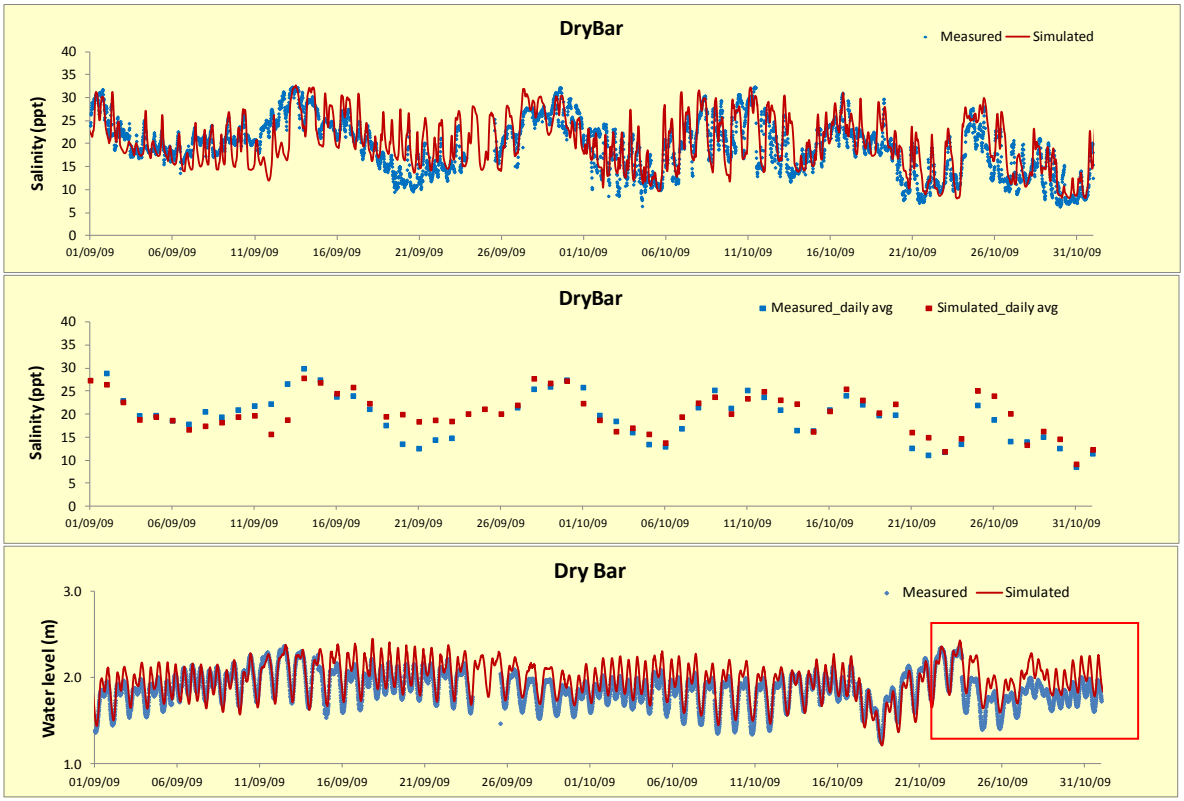

Figure 17. Simulated and observed salinity and water levels at Dry Bar from Sep 1st to Nov 1st 2009

Figure 18 shows two simulated salinity profiles for two different monitoring points: CP and DB, and Figure 19 shows surface layer simulated salinity contour lines at arbitrary times. The bottom water is more saline than the surface water because of the density difference between salty and fresh water.

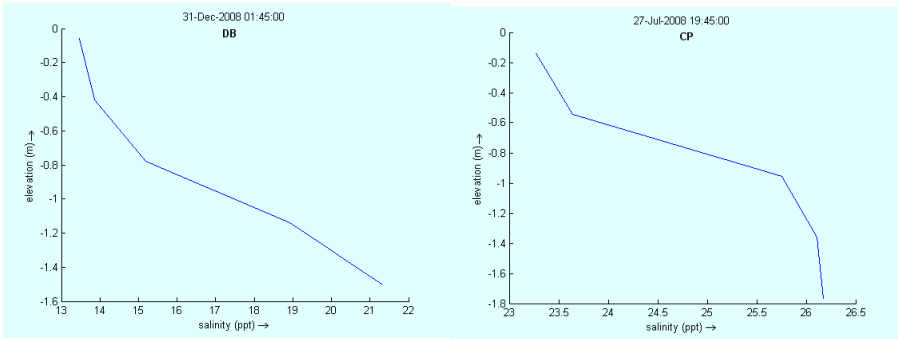

Figure 18. Typical simulated salinity profiles for two monitoring points: CP and DB.

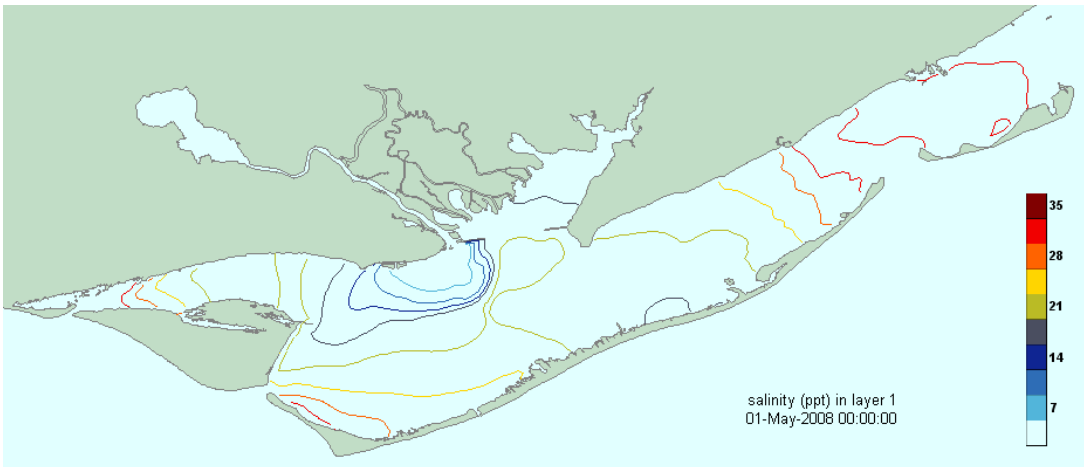

Figure 19. Typical contours of simulated surface layer salinity.

Because the entrance to the Apalachicola River is in the northwest segment of the bay, the west and north sides of the bay are less saline than the east and south sides. The west and north sides of the bay also have larger seasonal fluctuations due to seasonal changes in precipitation and therefore river discharge.

9. Salinity Statistics

Some statistical parameters of the salinity variations were computed from the simulated time series at 452 observation points defined inside the model domain (Figure 20). The parameters are: monthly averages, monthly standard deviation, monthly maxima, and monthly minima. The computed values at each observation point were used to generate the contour plots shown in the Appendix (Figures 23, 24, 25, and 26). These figures show the seasonal salinity variability and the effect of the variable river discharge through the year for three consecutive years: 2008, 2009, and 2010.

The effect of river discharge is evident on several occasions. For example, July summer months with similar river discharges have similar statistical parameters. On the other hand, for particularly wet months like April 2009, the statistical parameters differ drastically from previous (2008) and later (2010) years.

This effect is also evident in Figure 21 where the 2008 monthly median, quartiles, and extreme values at CatPoint and DryBar are plotted. The corresponding daily average river discharges are shown in Figure 22.

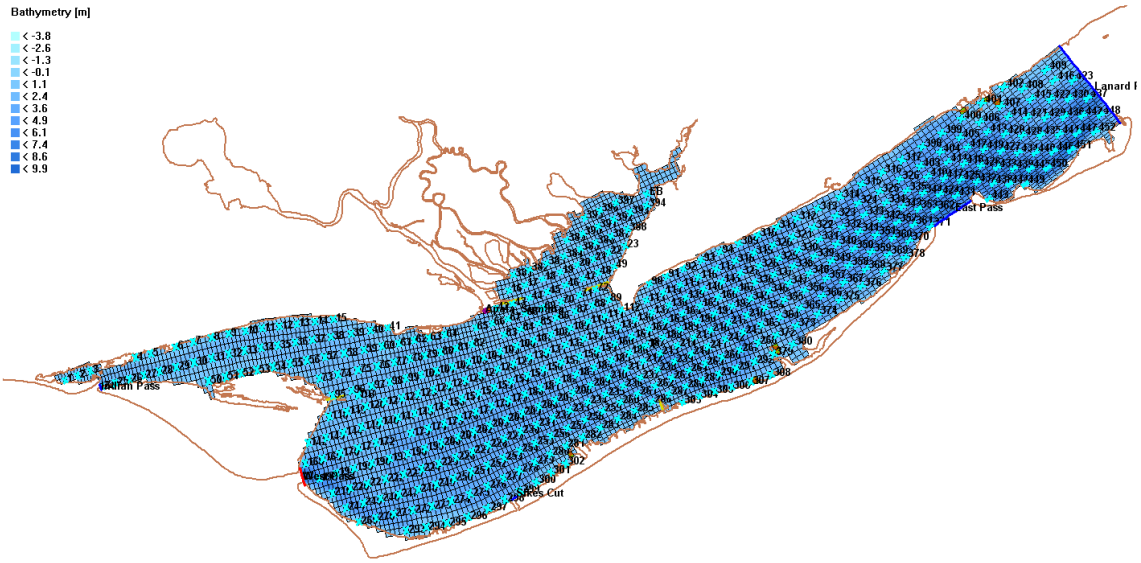

Figure 20. Observation points for extraction of time series.

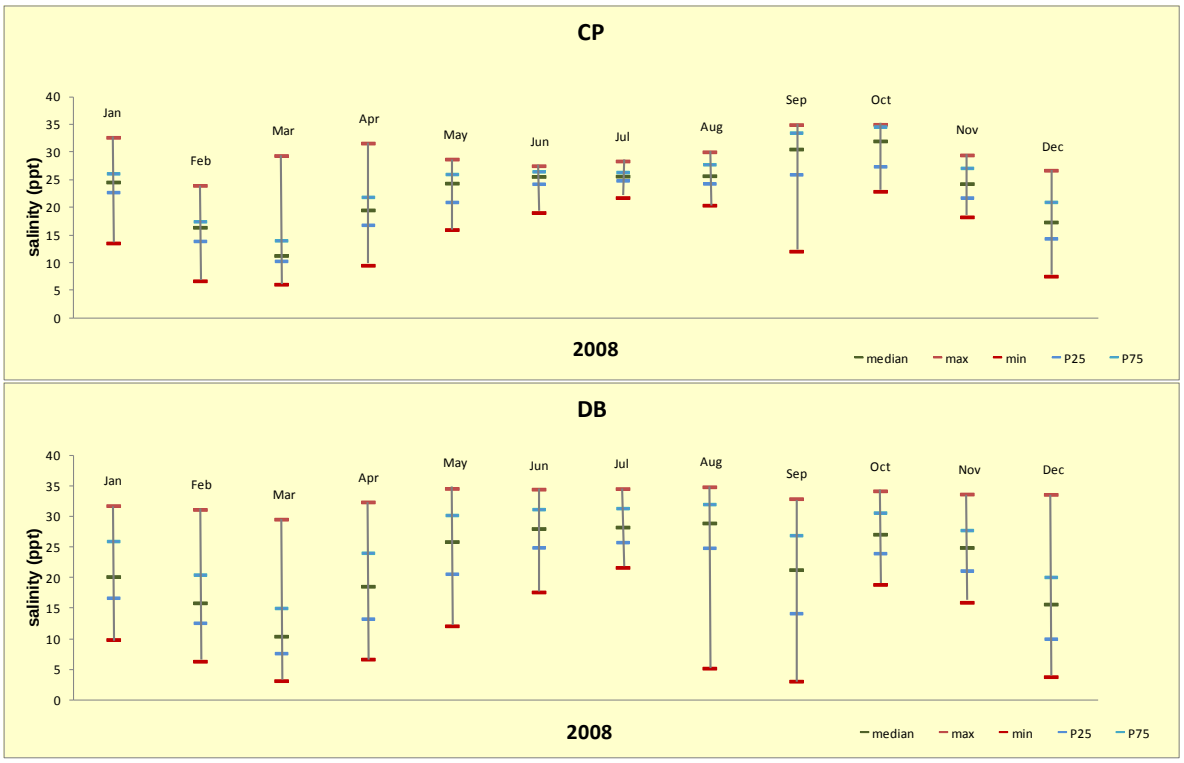

Figure 21. Simulated monthly median, quartiles and extreme values at CatPoint and DryBar.

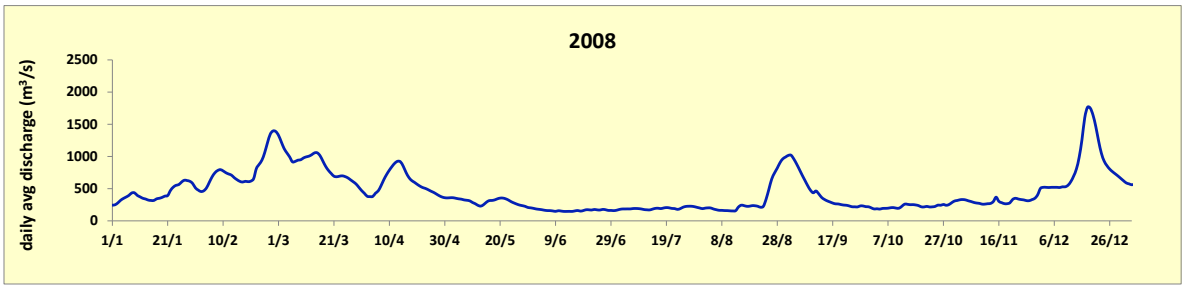

Figure 22. Daily average discharge at Apalachicola (Sumatra) during 2008.

10. Conclusions

A three-dimensional modeling framework using the hydrodynamic model Delft3D-Flow was set up for Apalachicola Bay. The model incorporates the estuary's bathymetry and external forcing (boundary conditions) to predict estuarine circulation and salinity changes caused by tides, major tributary flows, and wind stresses.

The study was based on existing data and did not include field work. Due to this limitation this modeling effort must be seen as only the first step. The bathymetric data were downloaded from the NOAA National Geophysical Data Center U.S. Coastal Relief Model. Water level data at the NOAA station named Apalachicola was used at the model open boundaries. Daily average river discharges measured by the USGS at the Sumatra hydrological stations were used to represent the Apalachicola river freshwater contribution to the estuary. Winds recorded at the NOAA meteorological station APCF1 were used to represent the wind field over the bay. ANERR salinity and sensor depth data recorded at three points inside the bay: CatPoint (CP), DryBar (DB) and EastBay (EB), were used to perform model calibration. Further model refinement will require interaction between model calibration and field measurements.

The model was calibrated by varying the coefficients for bottom roughness, wind stress, and horizontal viscosity. These coefficients were varied systematically, and the model water level and salinity predictions were compared with the salinity and sensor depths measured at the ANERR stations. The optimum calibration coefficients were chosen that minimized the errors between the measured and predicted values.

The present model setup resulted in reasonable simulations of the estuary's major hydrodynamic characteristics. The modeled water levels were in very good agreement in phase and magnitude with measured values for all available recording stations for the entire simulation. Salinity results also reasonably followed the general trend of field observations.

Monthly averages, monthly standard deviation, monthly maxima, and monthly minima of salinity were computed from the time series simulated at several observation points defined inside the model domain. A graphical representation of these parameters reflects the salinity seasonal variability and the evident effect of the river discharge throughout the year.

The calibrated hydrodynamic model will be used to simulate salinity responses to different river inflows scenarios. Effects of the flow scenario resulting from the

changing upstream water demands and reservoir operations can be examined by comparing salinity probability distributions and exceedance probability.

11. References

Chen, S., Huang, W., Wang, H., and Li, D. (2009). "Remote sensing assessment of sediment re-suspension during Hurricane Frances in Apalachicola Bay, USA." *Remote Sensing of Environment*, 113, 2670-2681.

Dulaiova, H., and Burnett, W.C. (2008). "Evaluation of the flushing rates of Apalachicola Bay, Florida via natural geochemical tracers." *Marine Chemistry*, 109, 395-408.

Faure, V., and Dottori, M. (2003). "Hydrographic Measurements in Apalachicola Bay." Florida State University, Department of Oceanography, Tallahasee, Florida.

Georgakakos A., Zhang, F., and Yao, H. (2010). *"Climate and Demand Change Impact Assessmentfor the Southeast US."* Final Technical Report, sponsored by NOAA, USGS, and the GeorgiaDepartment of Natural Resources. Georgia Water Resources Institute, Atlanta.

Georgakakos, A. (2006). "Decision Support Systems for Integrated Water Resources Managementwith an Application to the Nile Basin." Book chapter in "*Topics on System Analysis andIntegrated Water Resources Management,"* eds. A. Castelletti and R. Soncini-Sessa, Elsevier.

Georgakakos, K.P., Graham, N.H., Carpenter, T.M., Georgakakos, A.P., and Yao, H. (2005). "Integrating Climate-Hydrology Forecasts and Multi-Objective Reservoir Managementfor Northern California." *EOS Transactions, American Geophysical Union*, Vol. 86, No. 12, pages 122-127, March 2005.

Huang, W. and Jones, W.K. (1997). Hydrodynamic Modeling of Circulation and Salinity for the Low Flow Seasons in Apalachicola Bay. Water Resources Special Report 97-1, Northwest Florida Water Management District, Havana, Florida.

Huang, W and Jones, W.K. (2001). Characteristics of long term freshwater transport in Apalachicola Bay. Journal of the American Water Resources Association. Vol. 37, No. 3, June 2001.

Huang, W., Jones, W.K., and Wu, T.S. (2002). "Modelling Wind Effects on Subtidal Salinity in Apalachicola Bay, Florida." *Est., Coastal and Shelf Sc.*, 55, 33-46.

Huang, W and Jones, W.K. (2010). "Hydrodynamic modeling and ecohydrological analysis of river inflow effects on Apalachicola Bay, Florida, USA." *Est., Coastal and Shelf Sc.*, 86, 526-534.

Huang, W. (2010). Hydrodynamic modeling and ecohydrological analysis of river inflow effects on Apalachicola Bay, Florida, USA. Estuarine, Coastal and Shelf Science 86 (2010) 526–534.Liu, X., and Huang, W. (2009). "Modeling sediment resuspension and transport induced by storm wind in Apalachicola Bay, USA." *Environmental Modelling & Software*, 24, 1302-1313.

Livingston, R.J., Lewis, F.G., Woodsum, G.C., Niu, X.F., Galperin, B., and Huang, W. (2000). "Modeling oyster population response to variation in freshwater input." *Estuarine, Coastal and Shelf Science*, 50, 655–672.

Sun, H. and Koch, M.. (2001). Case study: Analysis and forecasting of salinity in Apalachicola Bay, Florida, using Box-Jenkins Arima Models. Journal of Hydraulic Engineering. September 2001.

Wang, H., Huang, W., Harwell, M.A., Edmiston, L., Johnson, E., Hsieh, P., (2008.)

"Modeling oyster growth rate by coupling oyster population and hydrodynamicmodels for Apalachicola Bay, Florida, USA."*Journal of Ecological Modeling*, 211(1–2), 77–89.

Wang, H., Hladik, C. M., Huang, W., Milla, K., Edmiston, L., Harwell, M. A., and Schalles, J. F. (2010). "Detecting the spatial and temporal variability of chlorophyll-a concentration and total suspended solids in Apalachicola Bay, Florida using MODIS imagery." *Int. J. Remote Sensing*, 31(2), 439-453.

APPENDIX: SALINITY STATISTICS

In this Appendix, contours of various statistical parameters of salinity computed at the 452 observation points shown in Figure 20 are presented. The data are shown for the surface layer (left column) and bottom layer (right column) by month for three years, 2008 to 2010. Plots are presented for monthly averages, standard deviations, maxima, and minima.

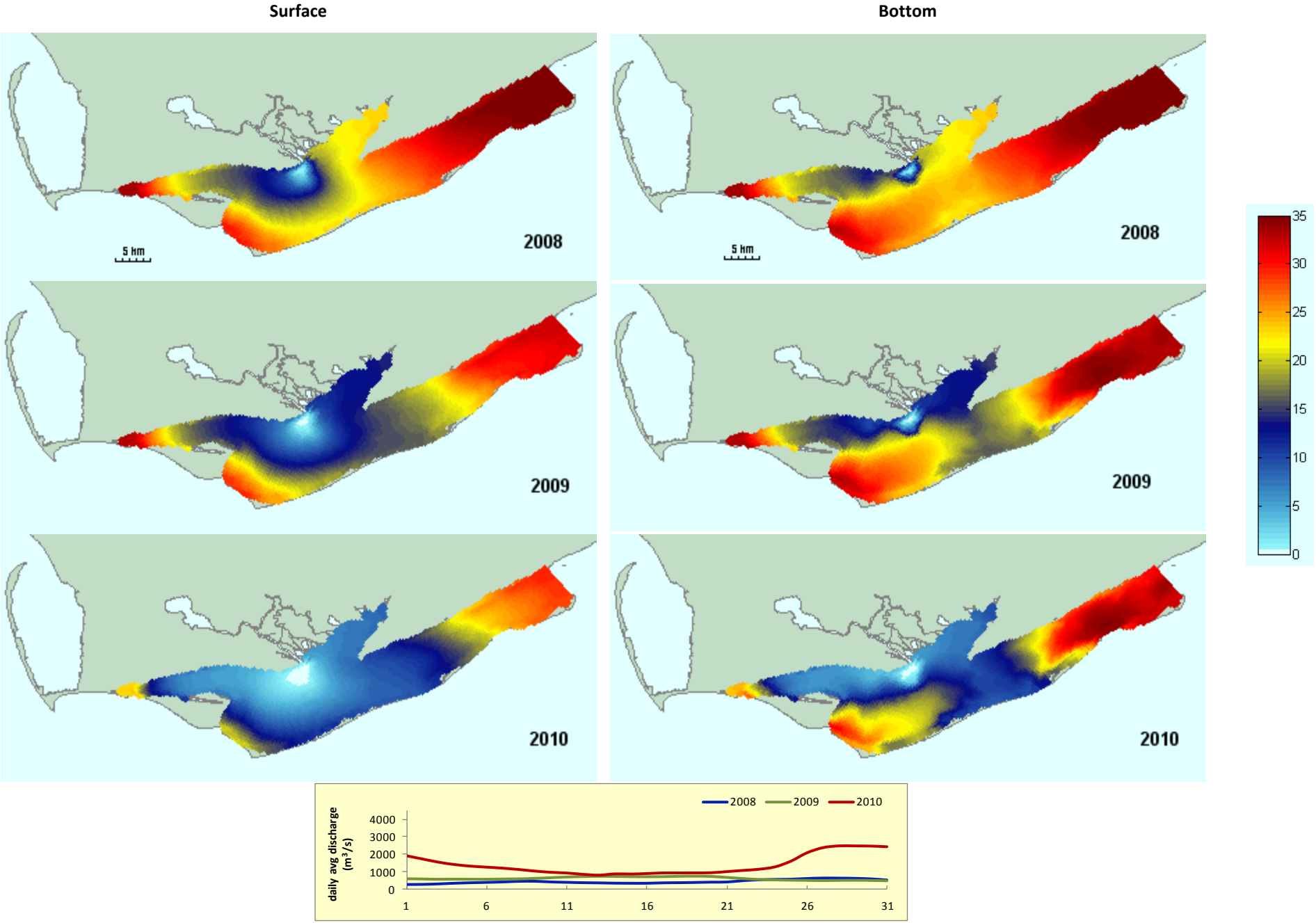

Figure 23. Salinity Monthly Averages - January

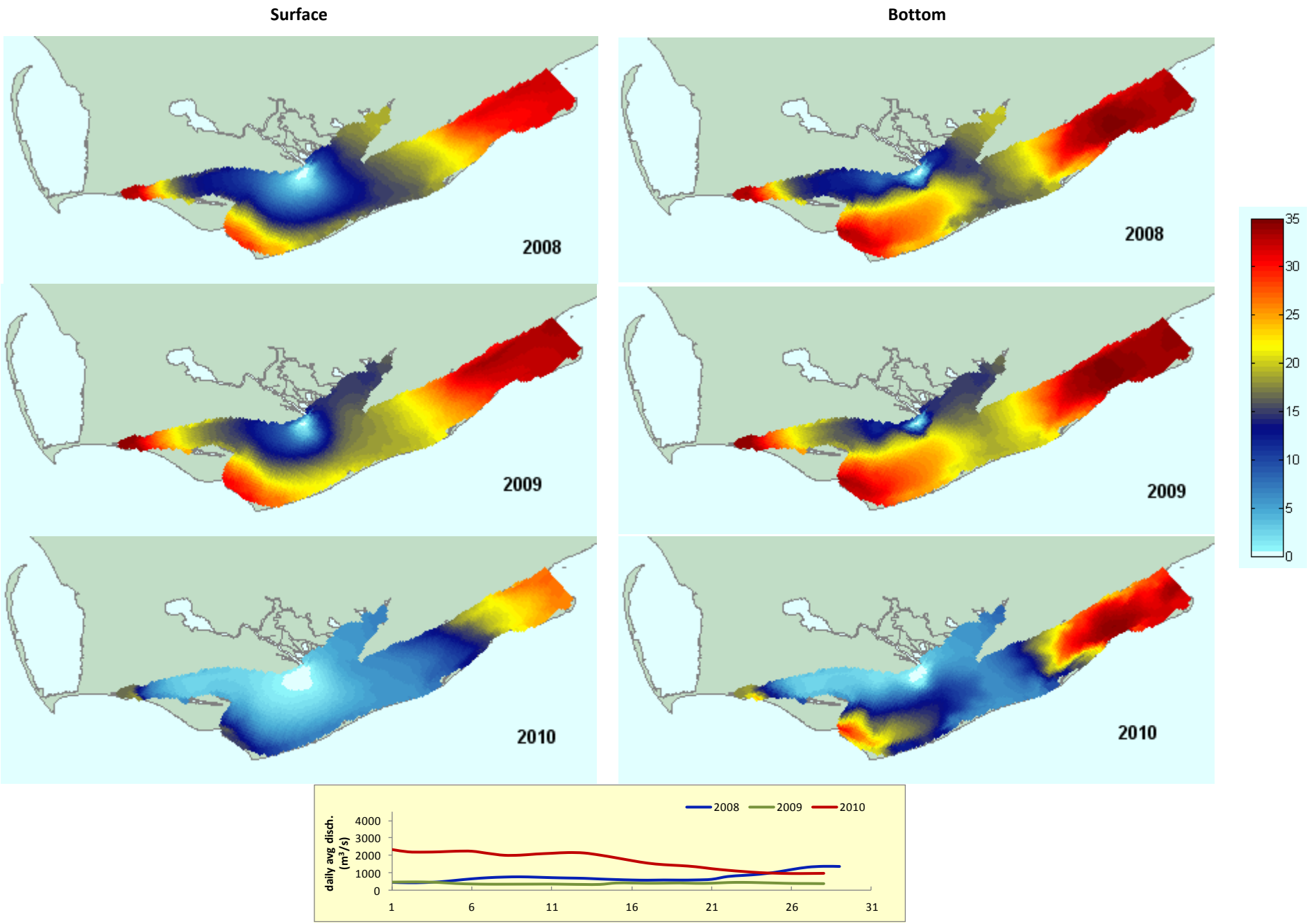

Figure 23 (contd). Salinity Monthly Averages - February

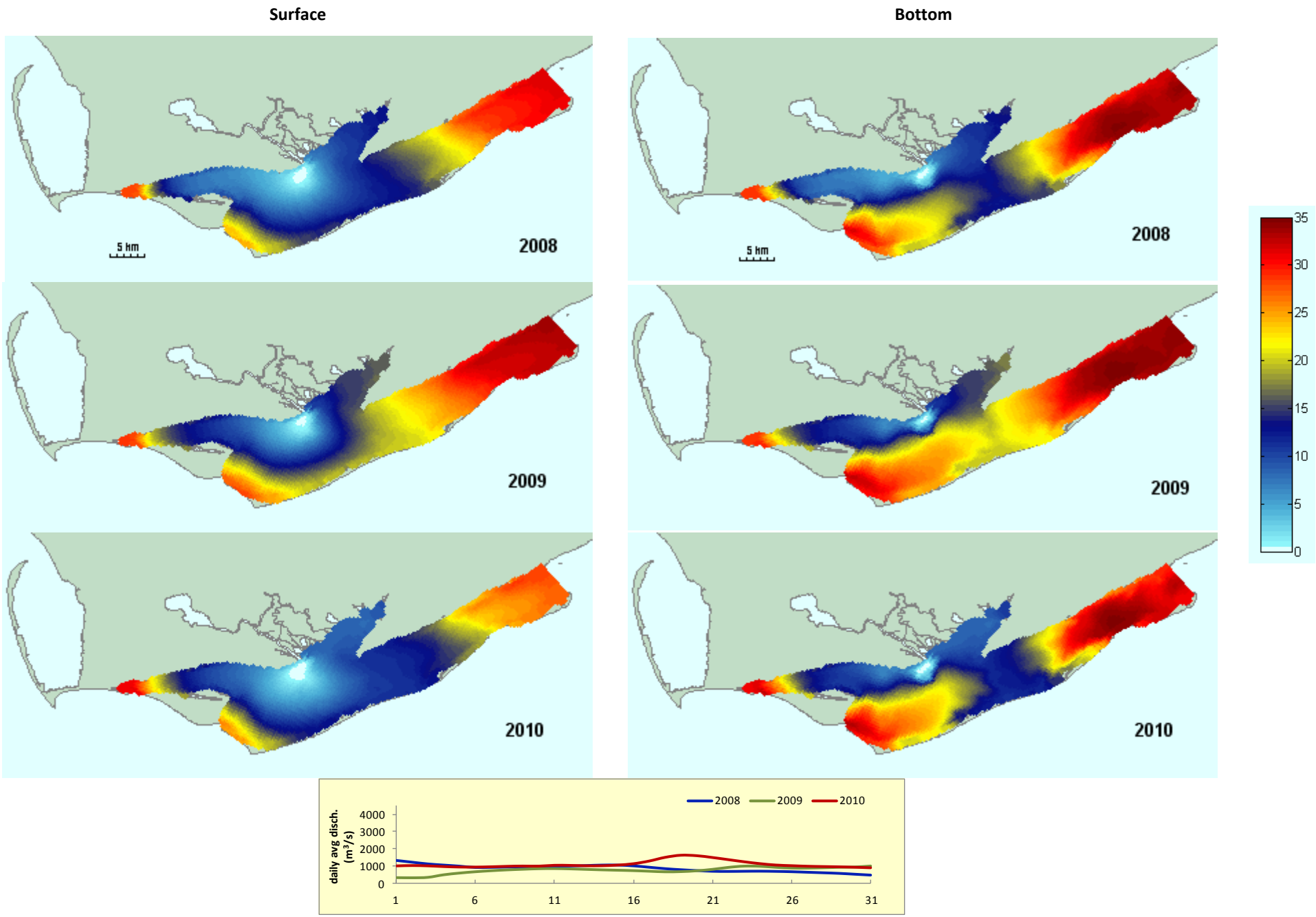

Figure 23 (contd). Salinity Monthly Averages - March

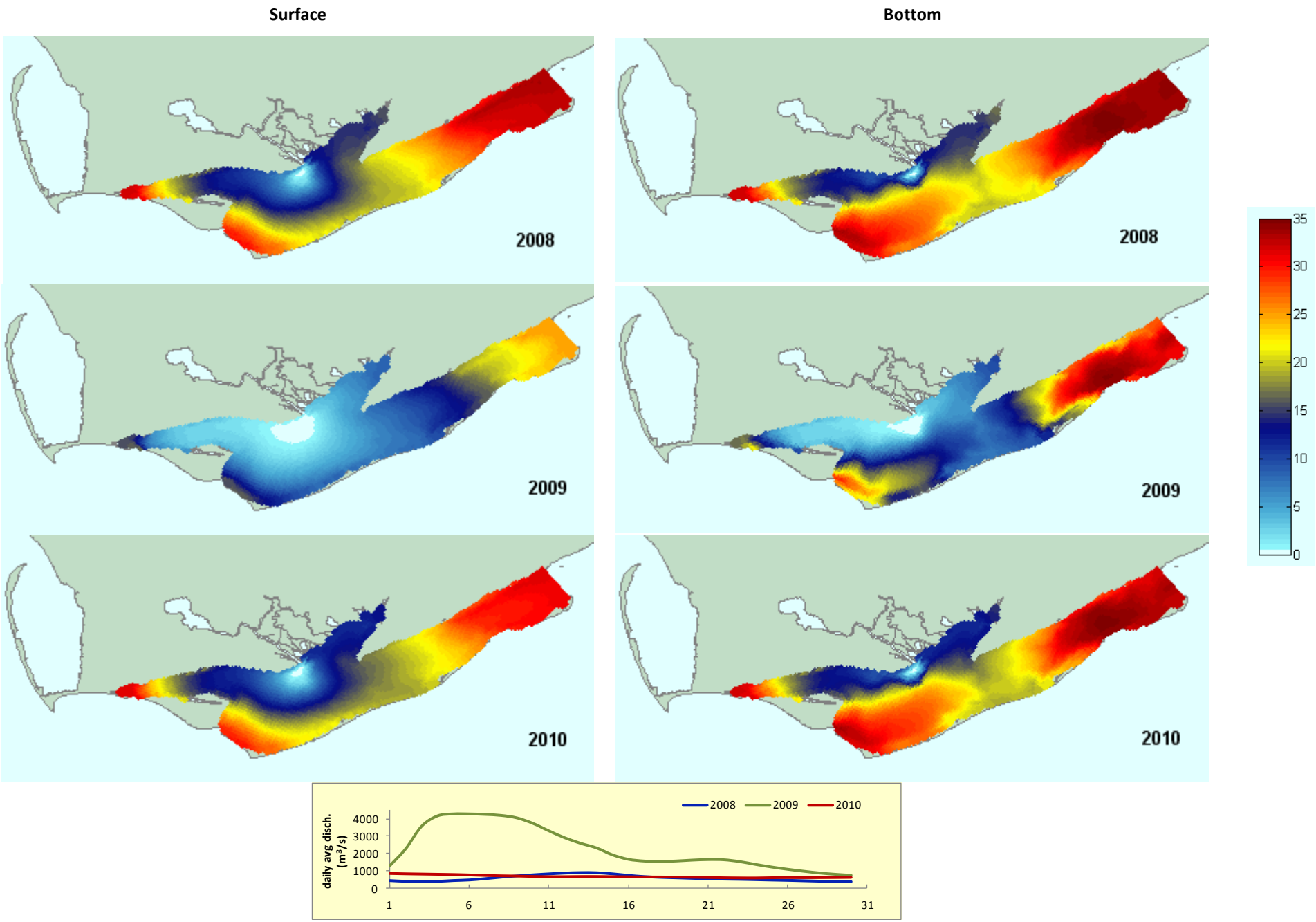

Figure 23 (contd). Salinity Monthly Averages - April

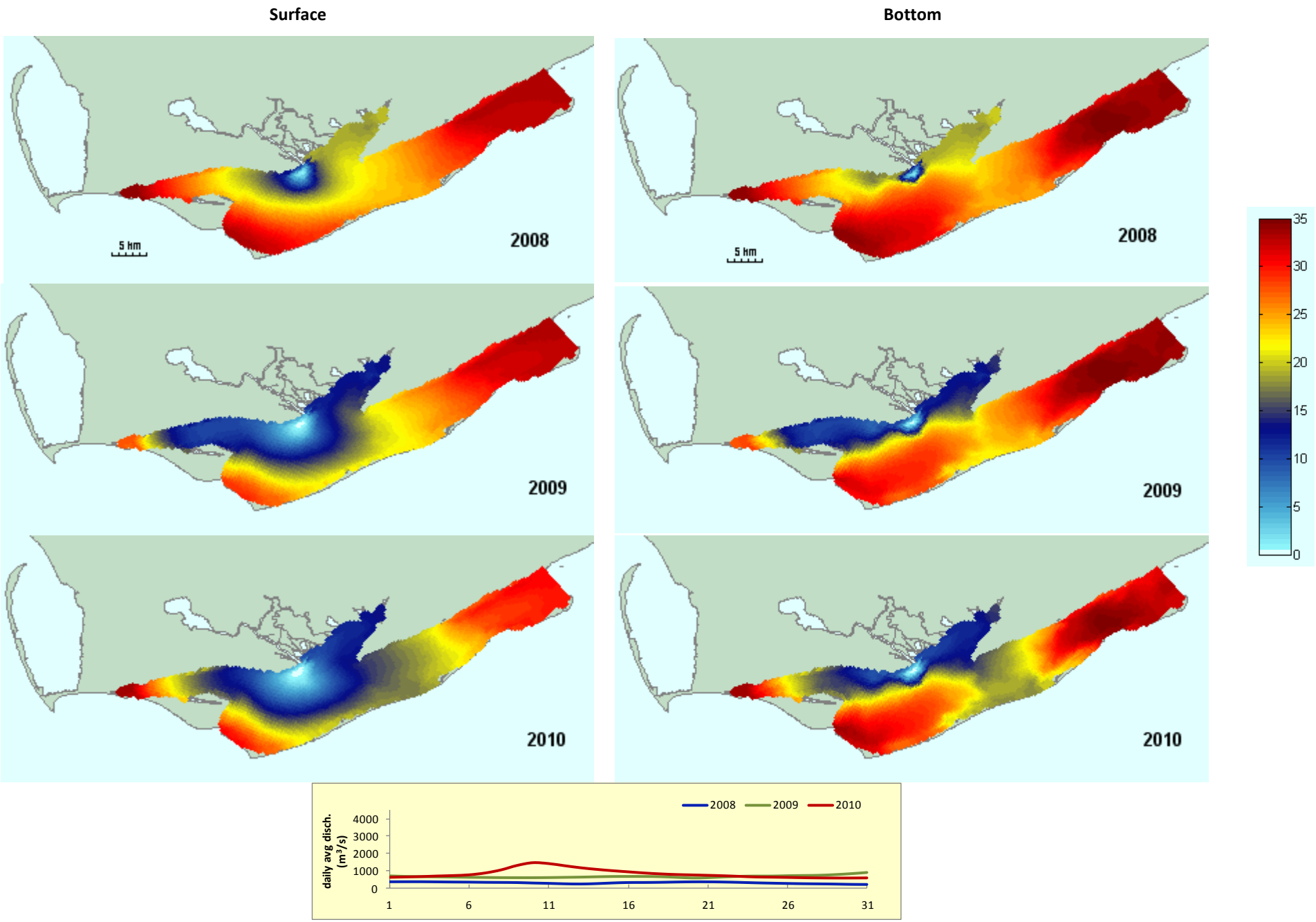

Figure 23 (contd). Salinity Monthly Averages - May

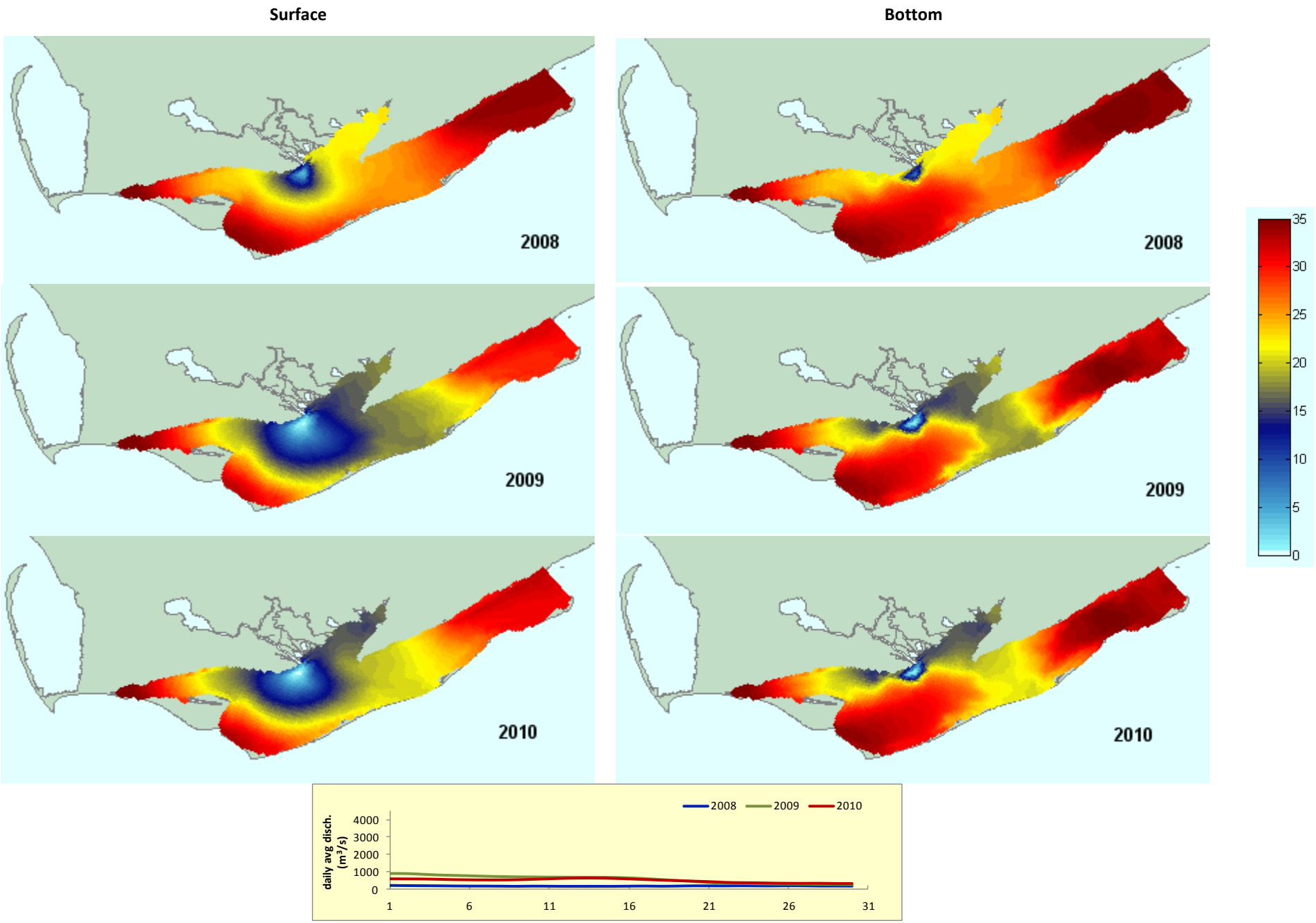

Figure 23 (contd). Salinity Monthly Averages - June

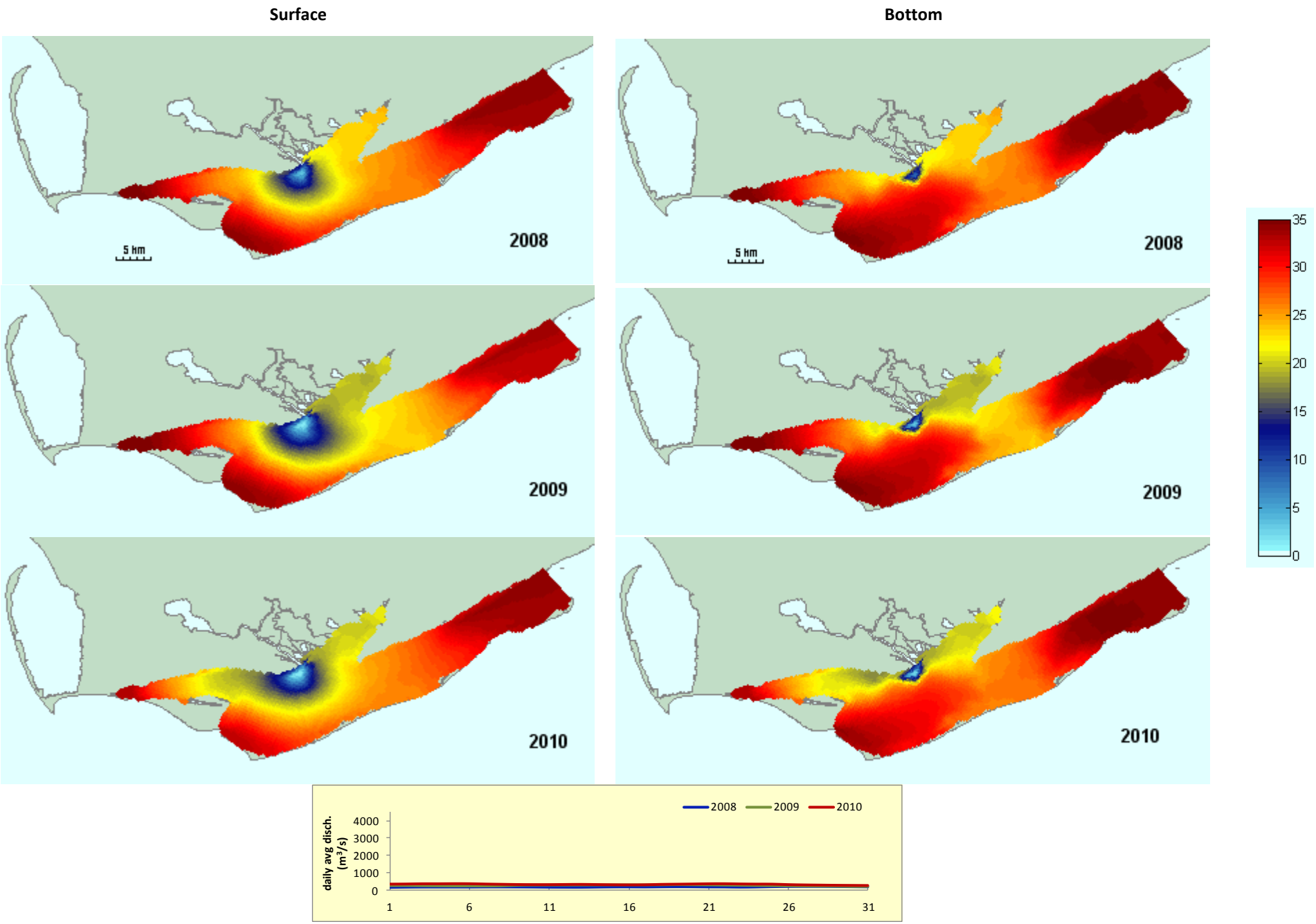

Figure 23 (contd). Salinity Monthly Averages - July

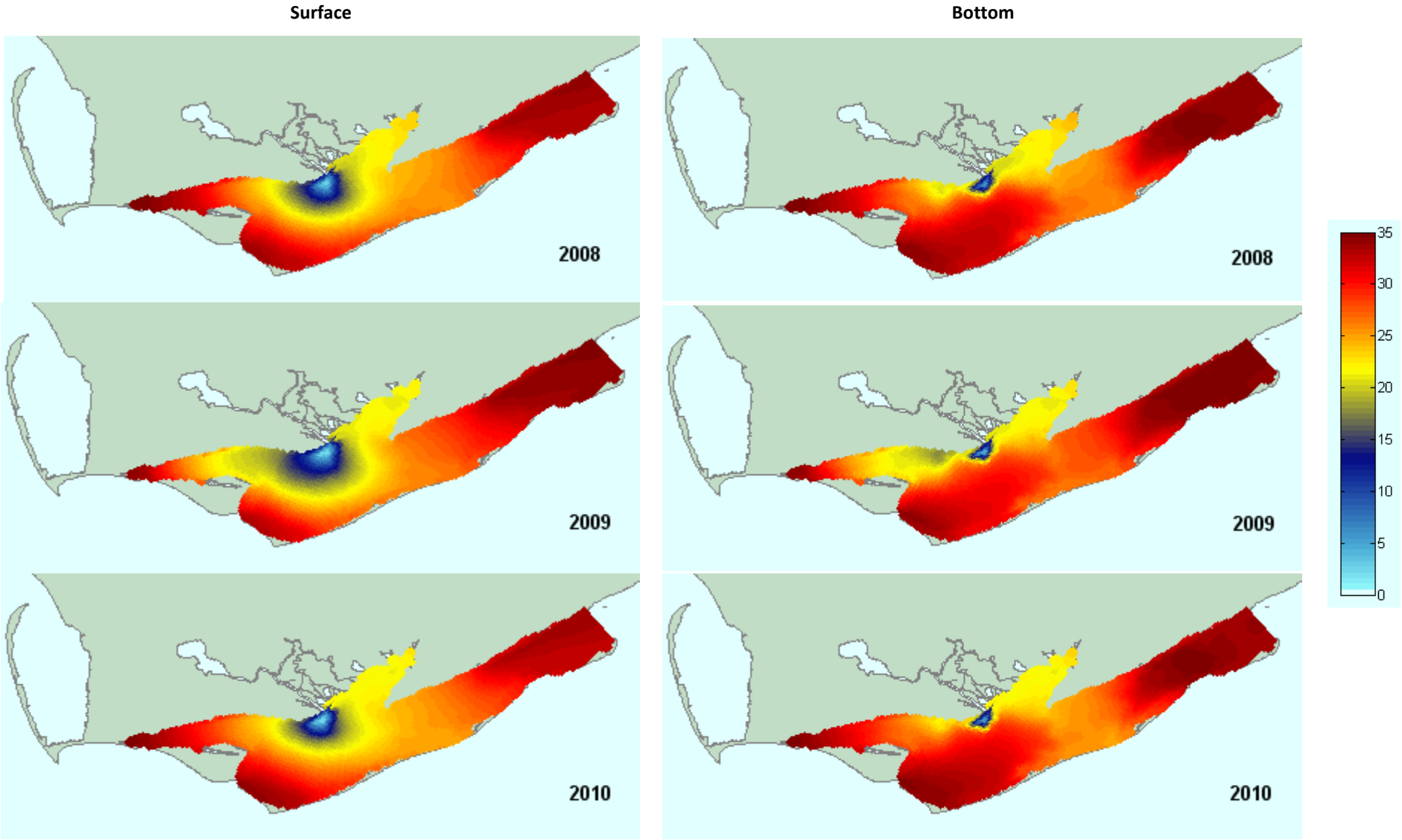

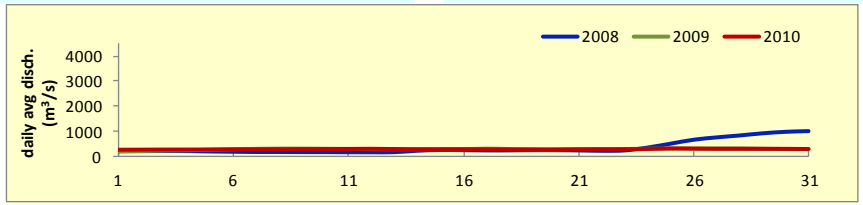

Figure 23 (contd). Salinity Monthly Averages - August

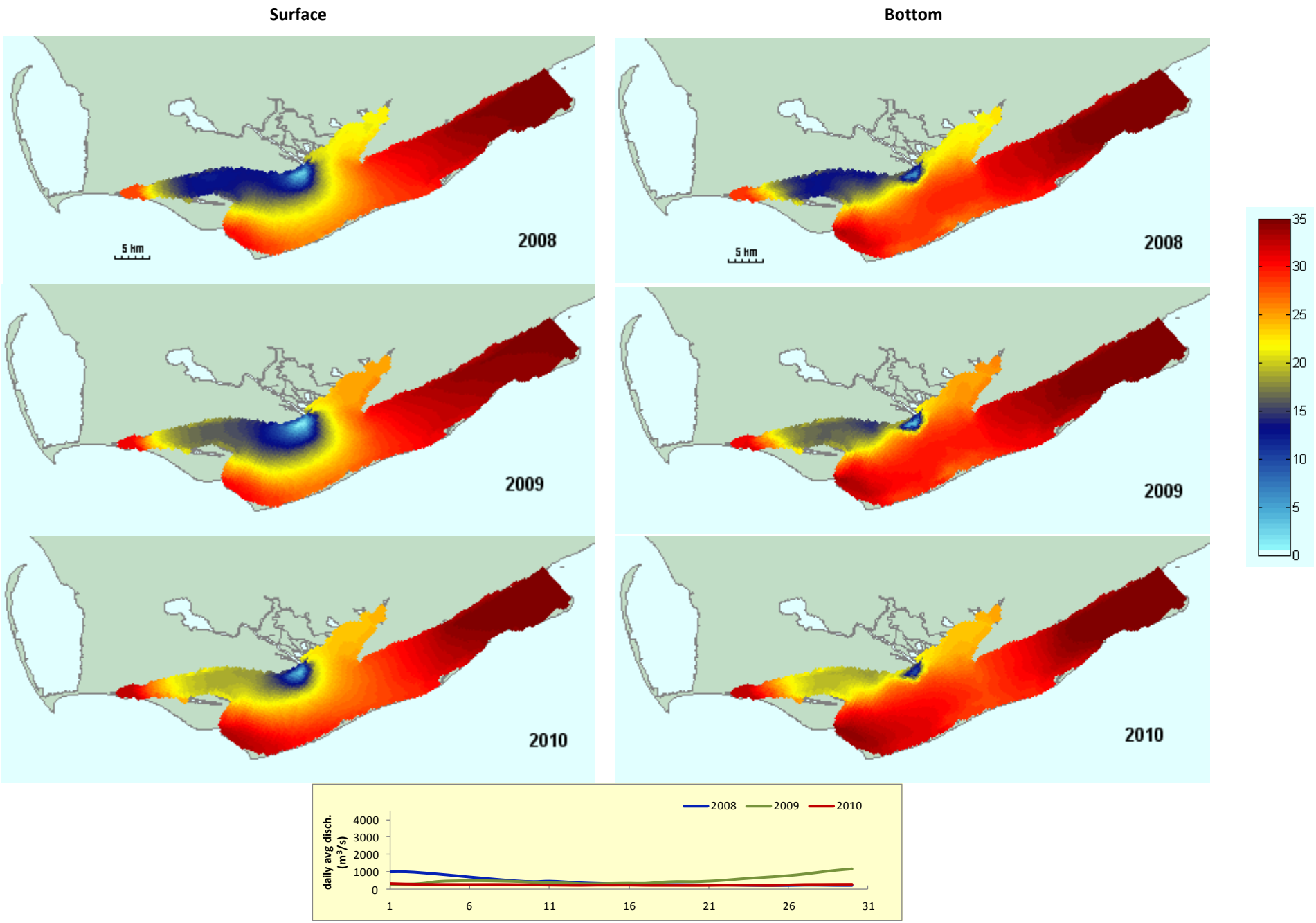

Figure 23 (contd). Salinity Monthly Averages - September

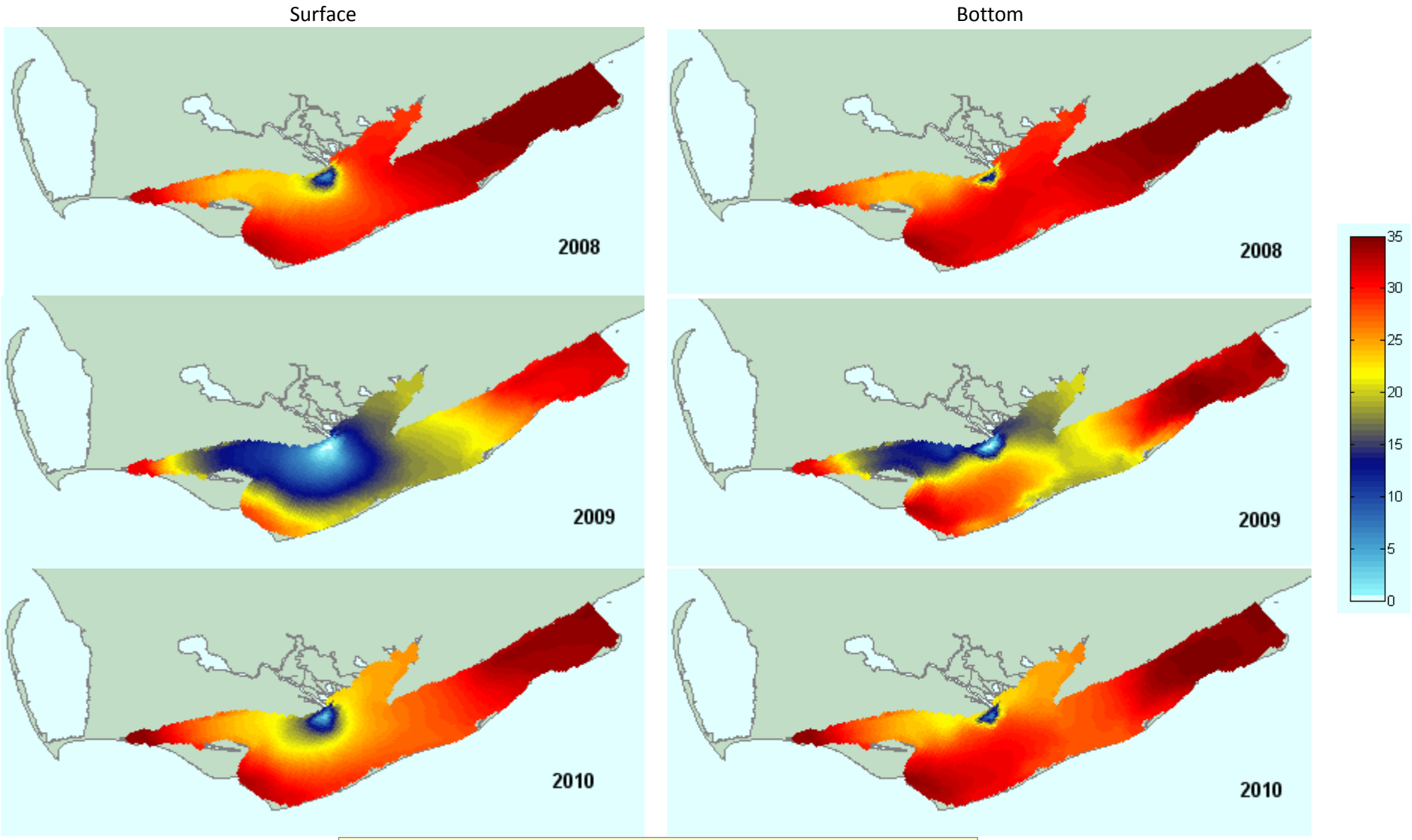

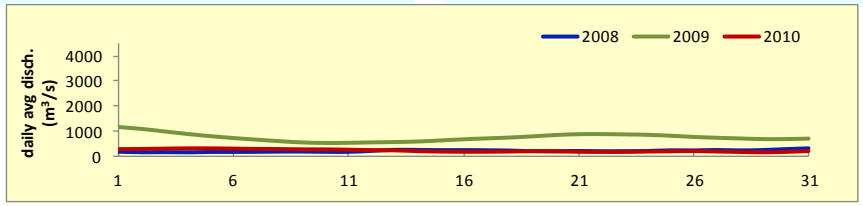

Figure 23 (contd). Salinity Monthly Averages - October

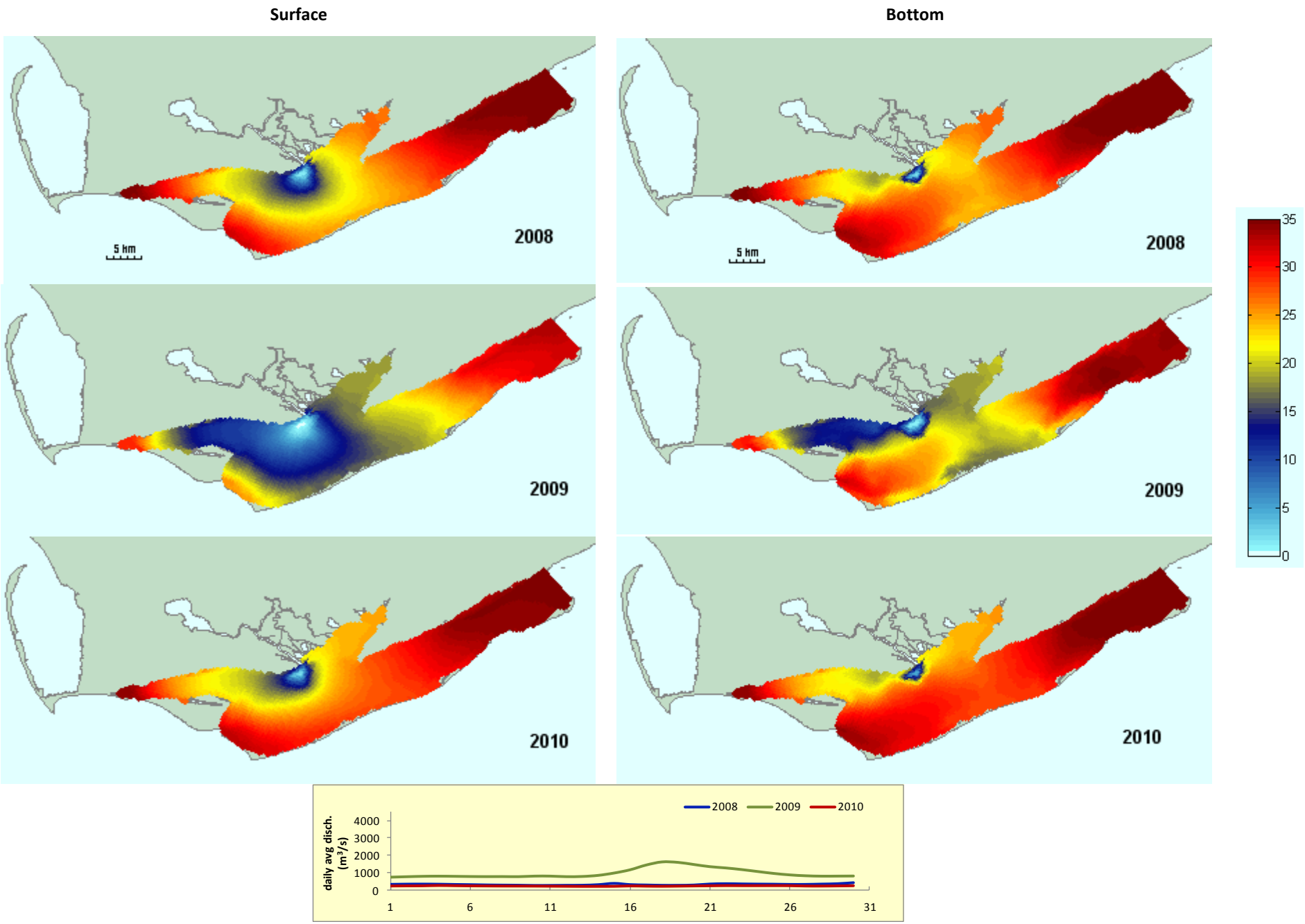

Figure 23 (contd). Salinity Monthly Averages - November

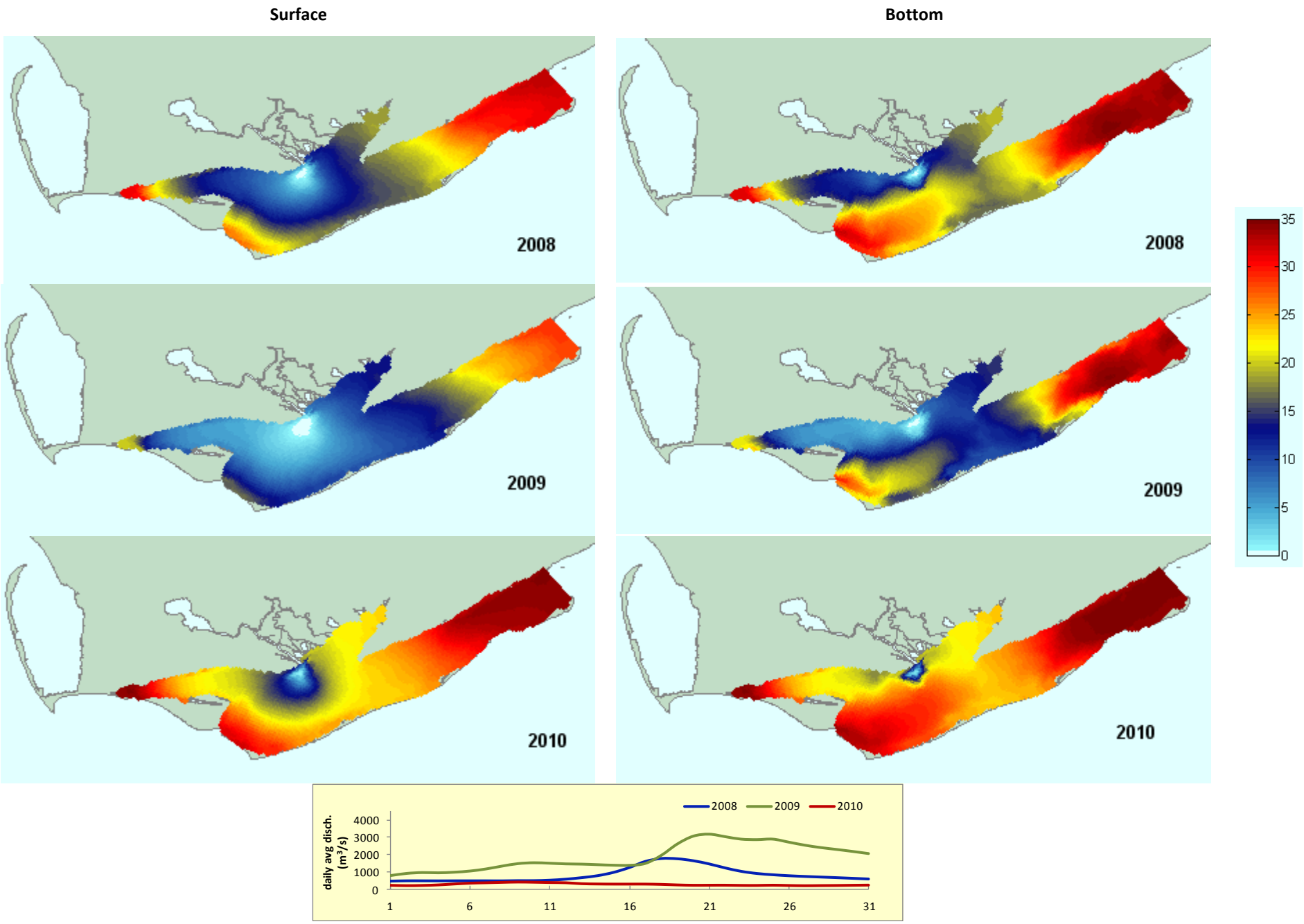

Figure 23 (contd). Salinity Monthly Averages - December

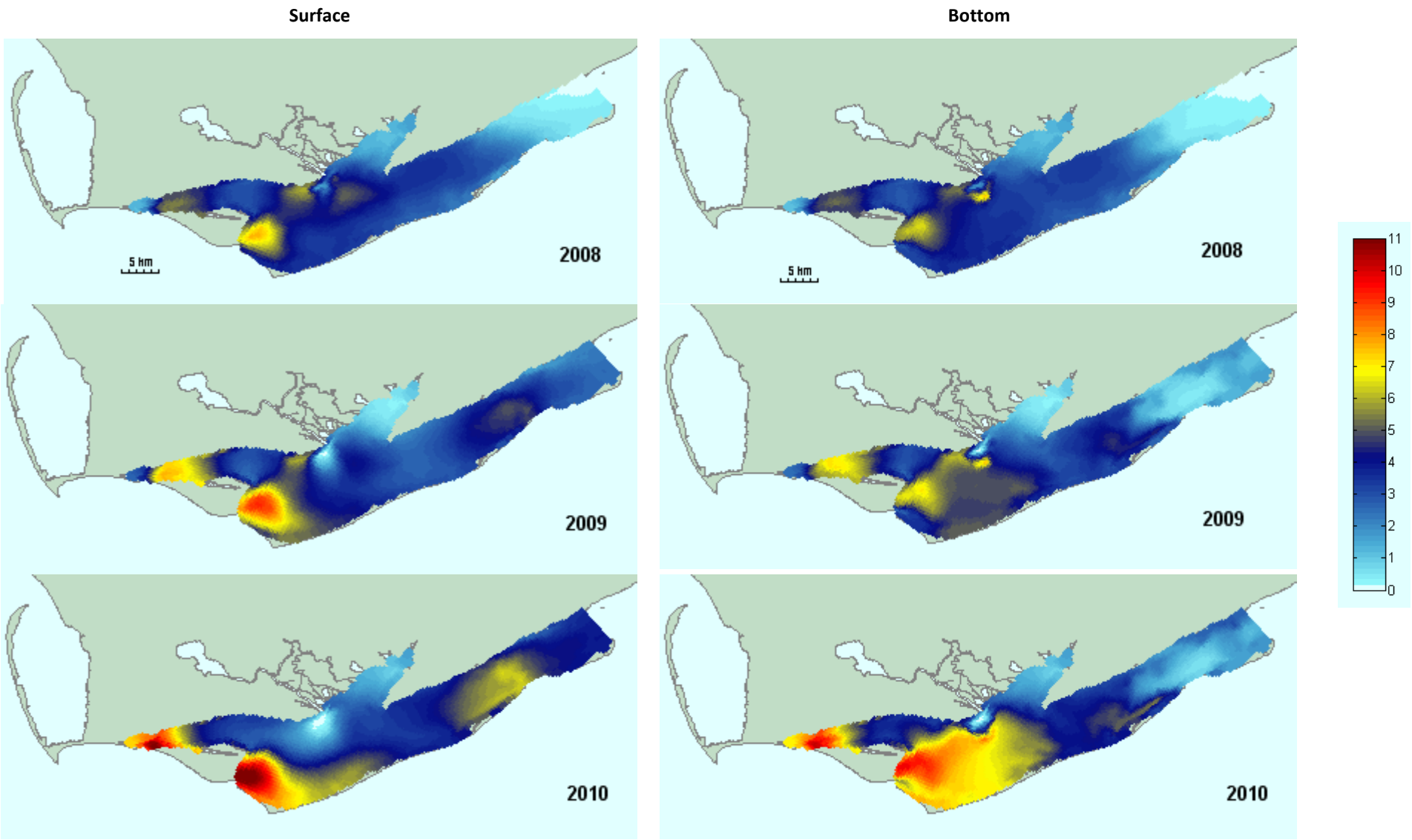

Figure 24. Salinity Monthly Standard Deviation - January

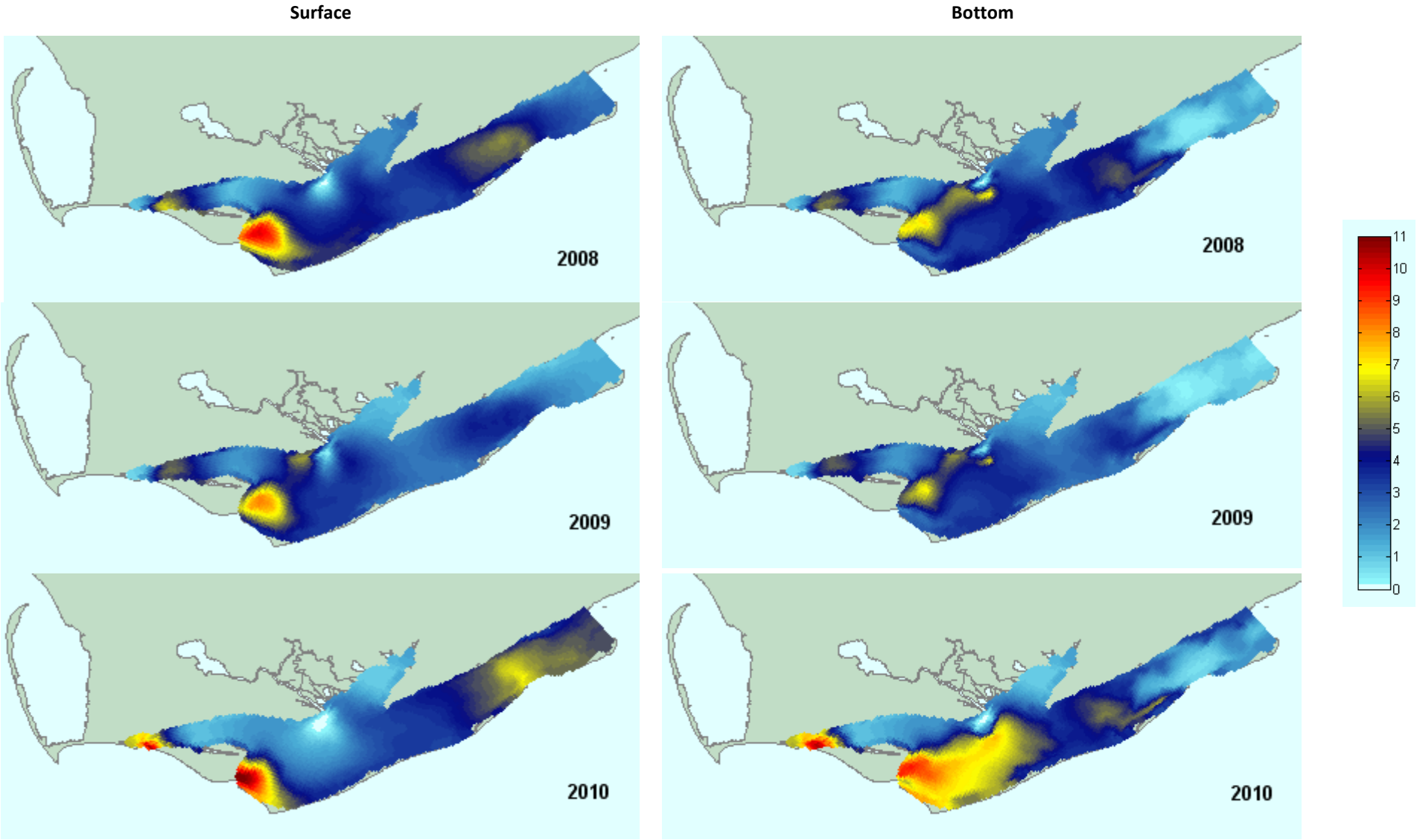

Figure 24 (contd). Salinity Monthly Standard Deviation - February

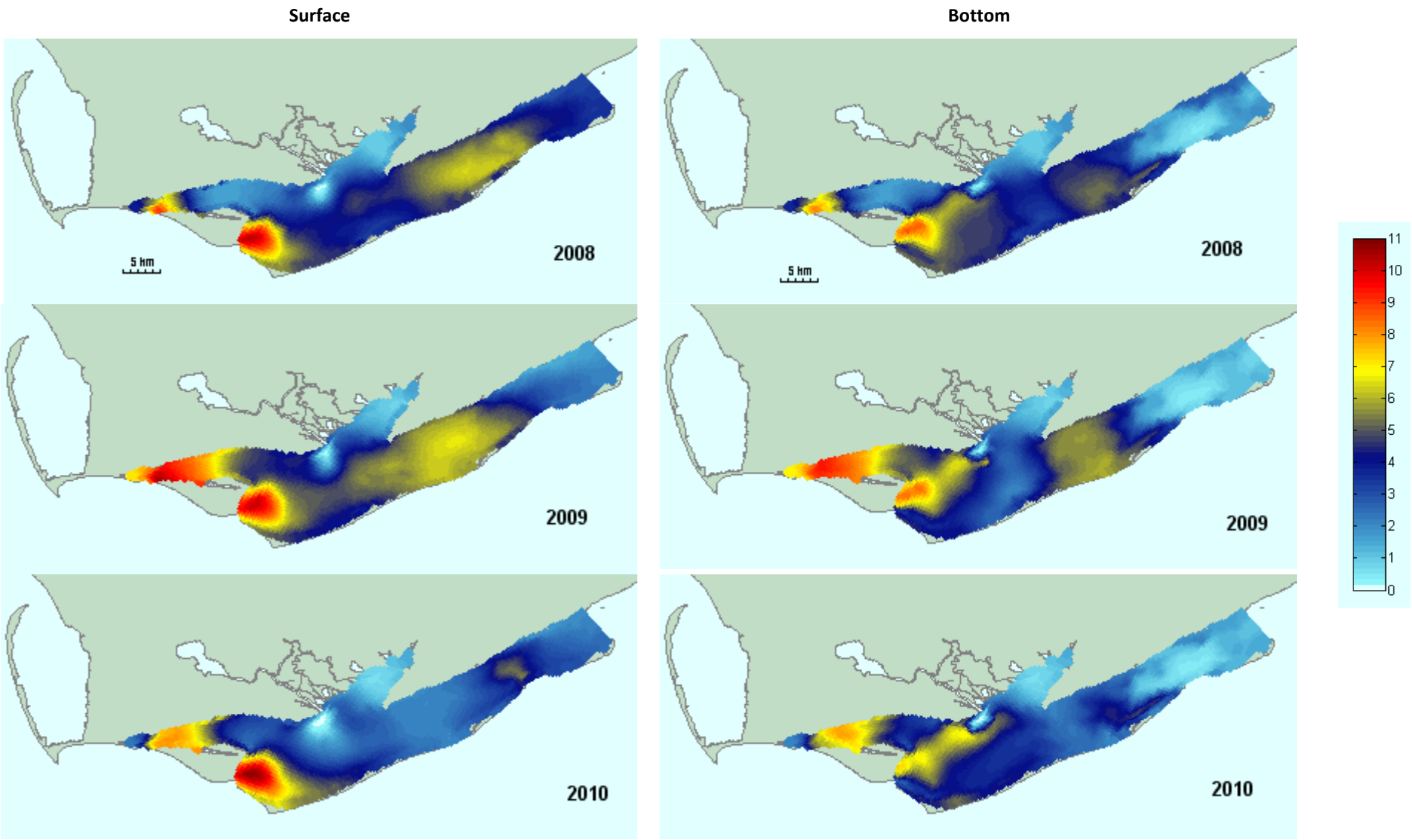

Figure 24 (contd). Salinity Monthly Standard Deviation – March

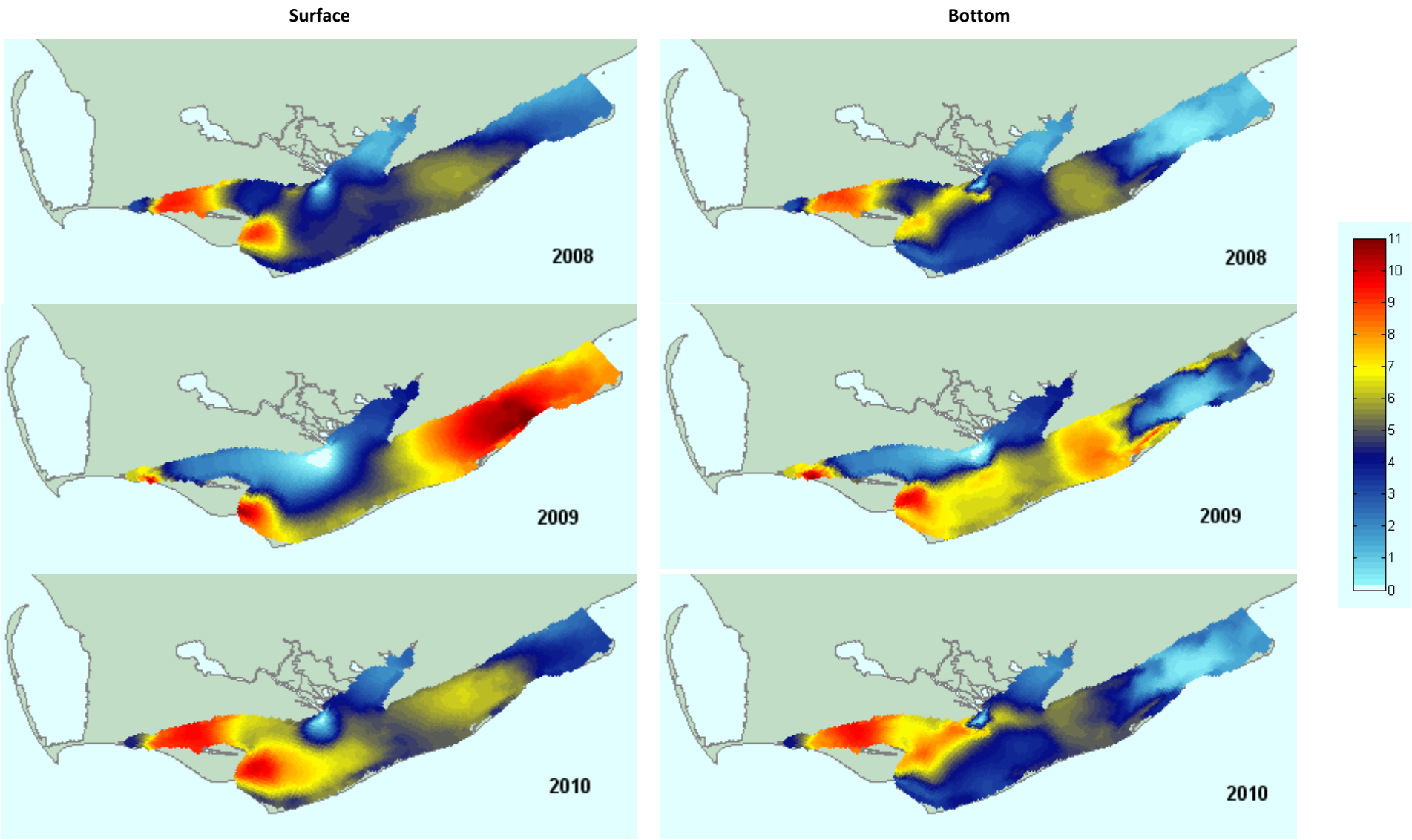

Figure 24 (contd). Salinity Monthly Standard Deviation – April

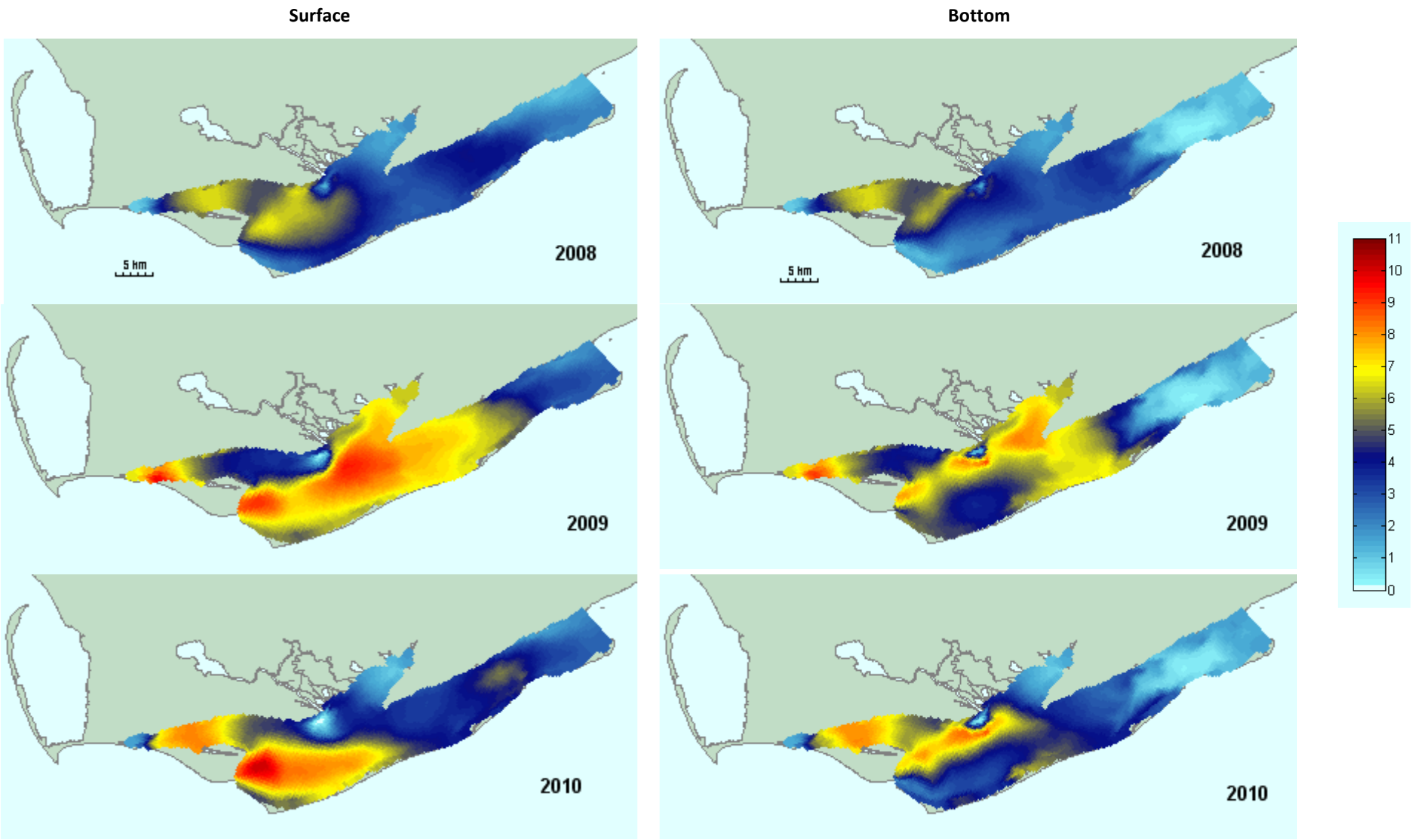

Figure 24 (contd). Salinity Monthly Standard Deviation - May

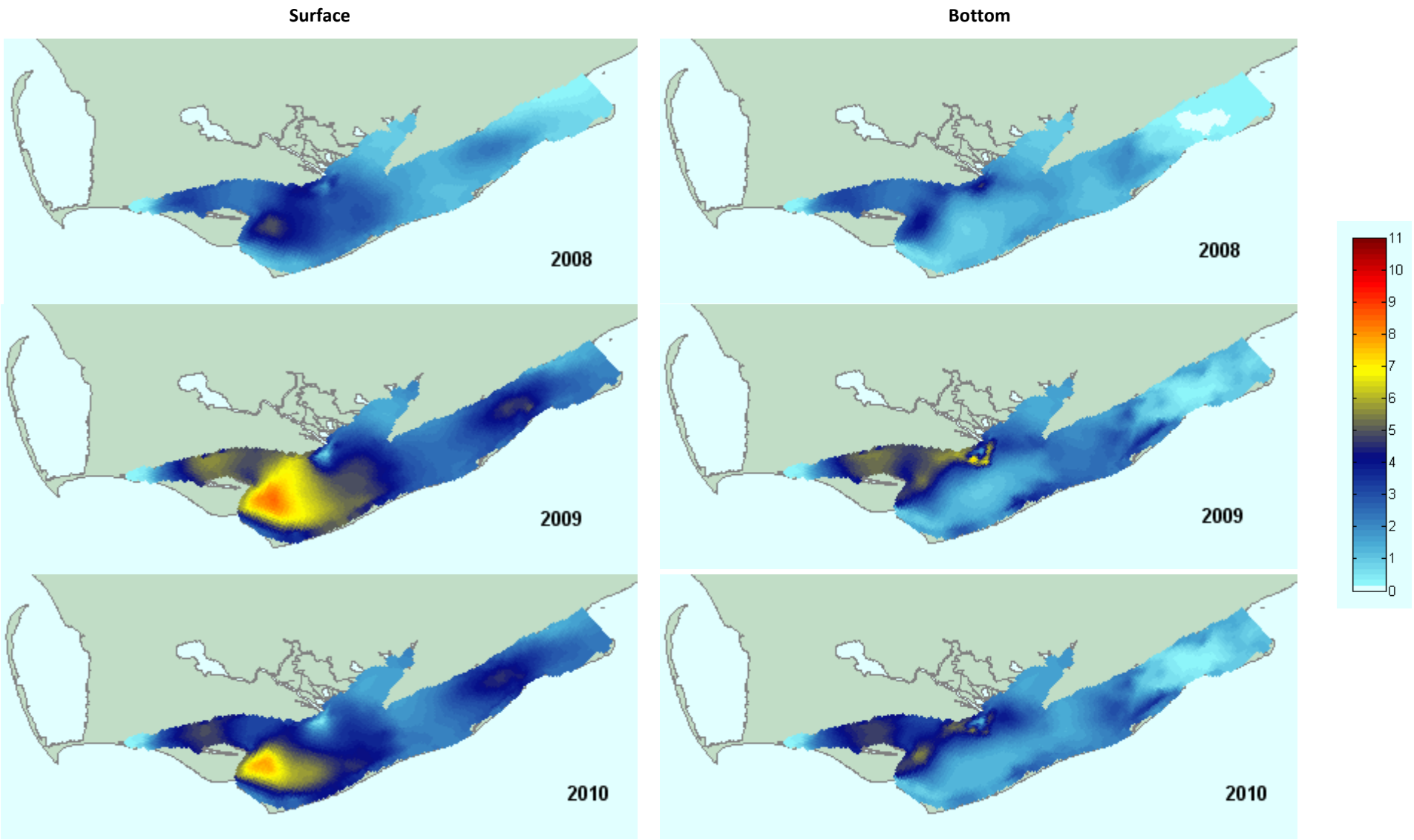

Figure 24 (contd). Salinity Monthly Standard Deviation – June

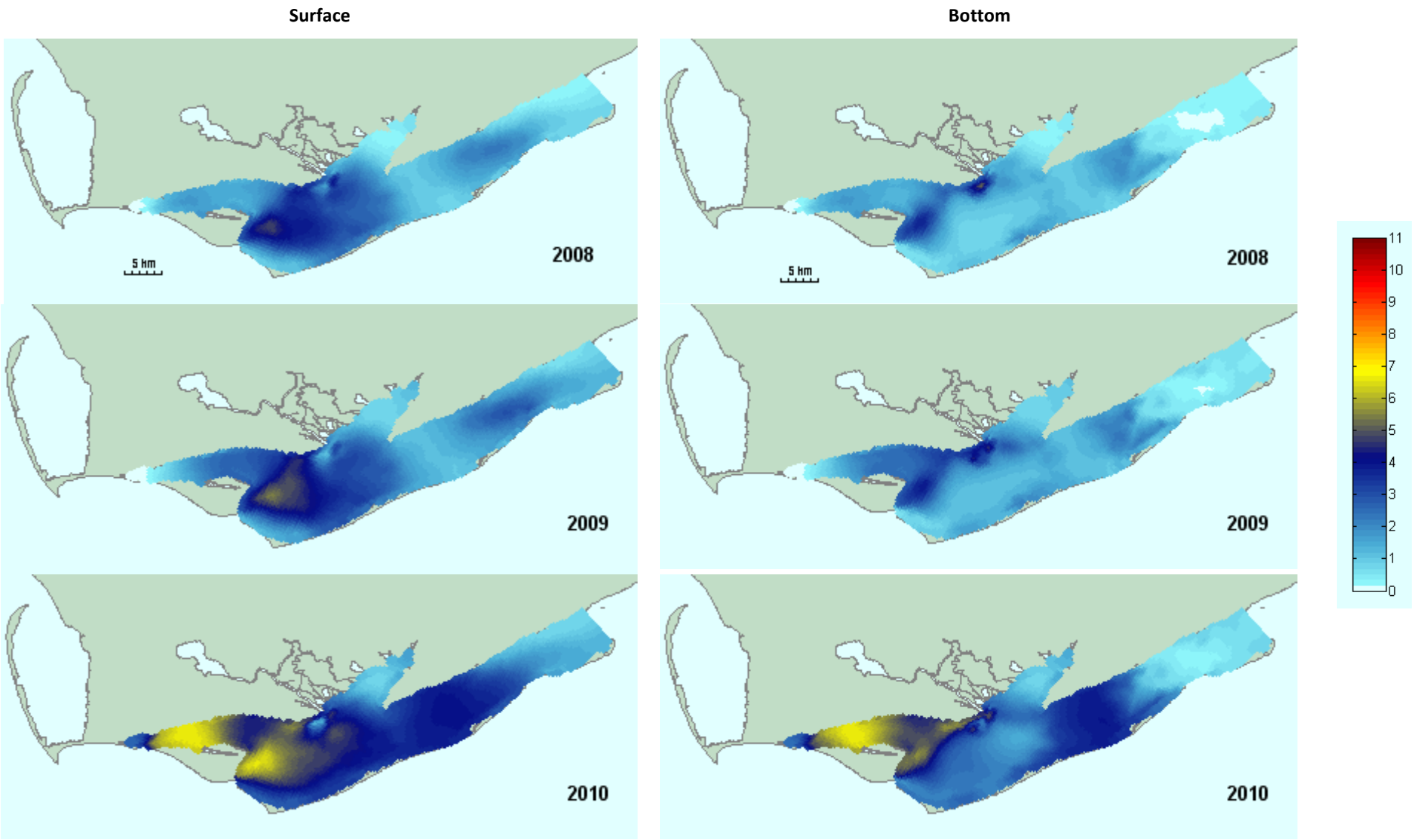

Figure 24 (contd). Salinity Monthly Standard Deviation – July

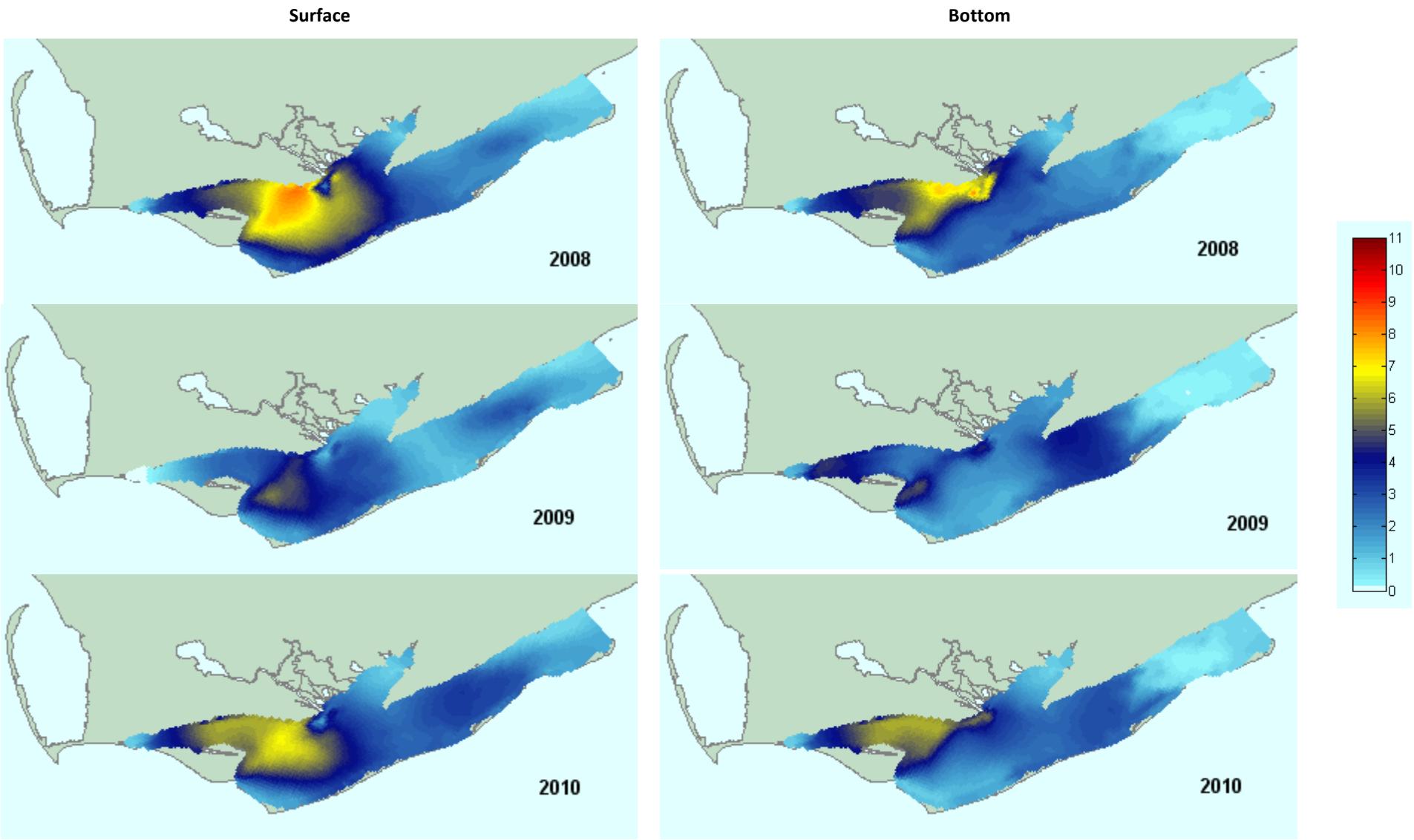

Figure 24 (contd). Salinity Monthly Standard Deviation - August

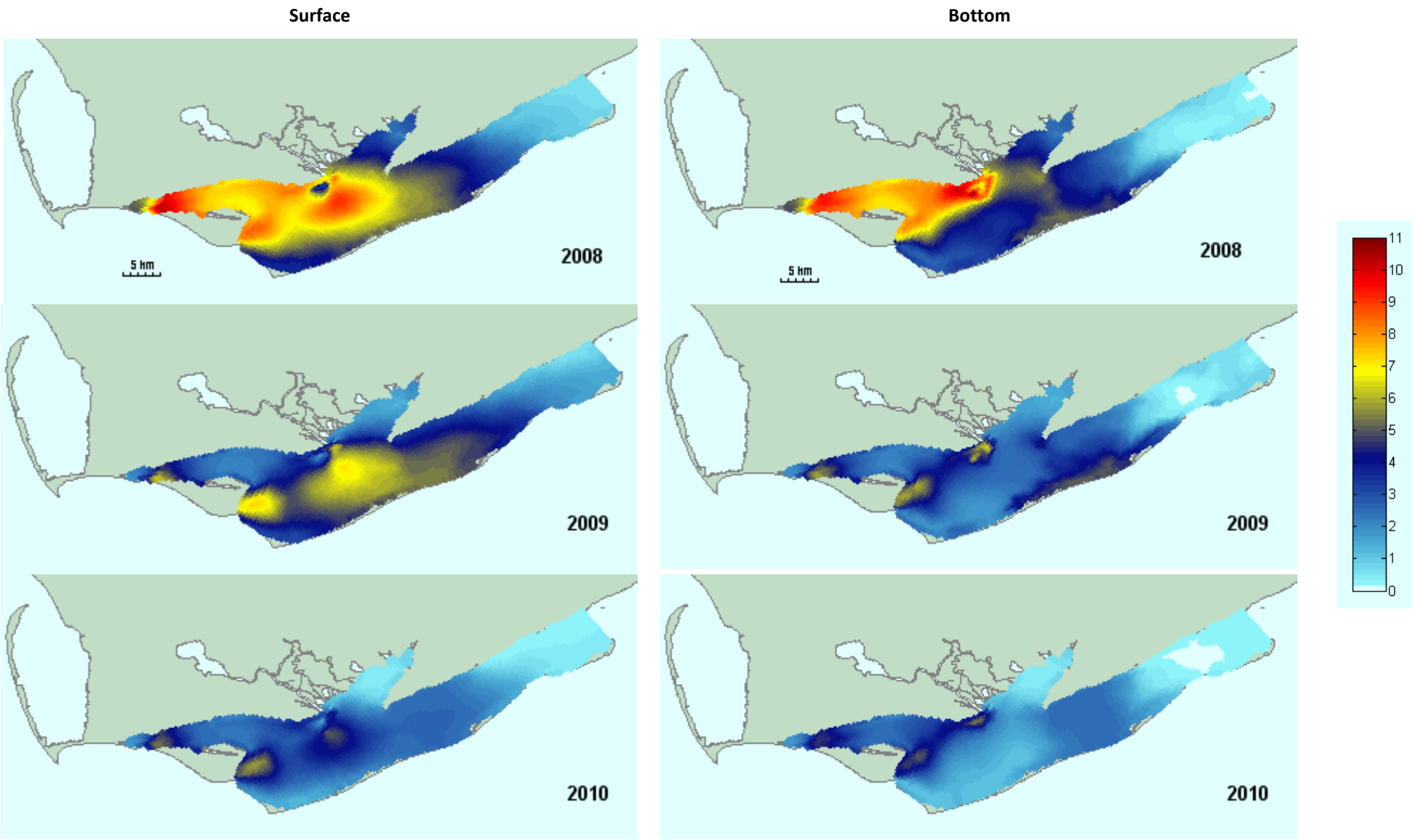

Figure 24 (contd). Salinity Monthly Standard Deviation - September

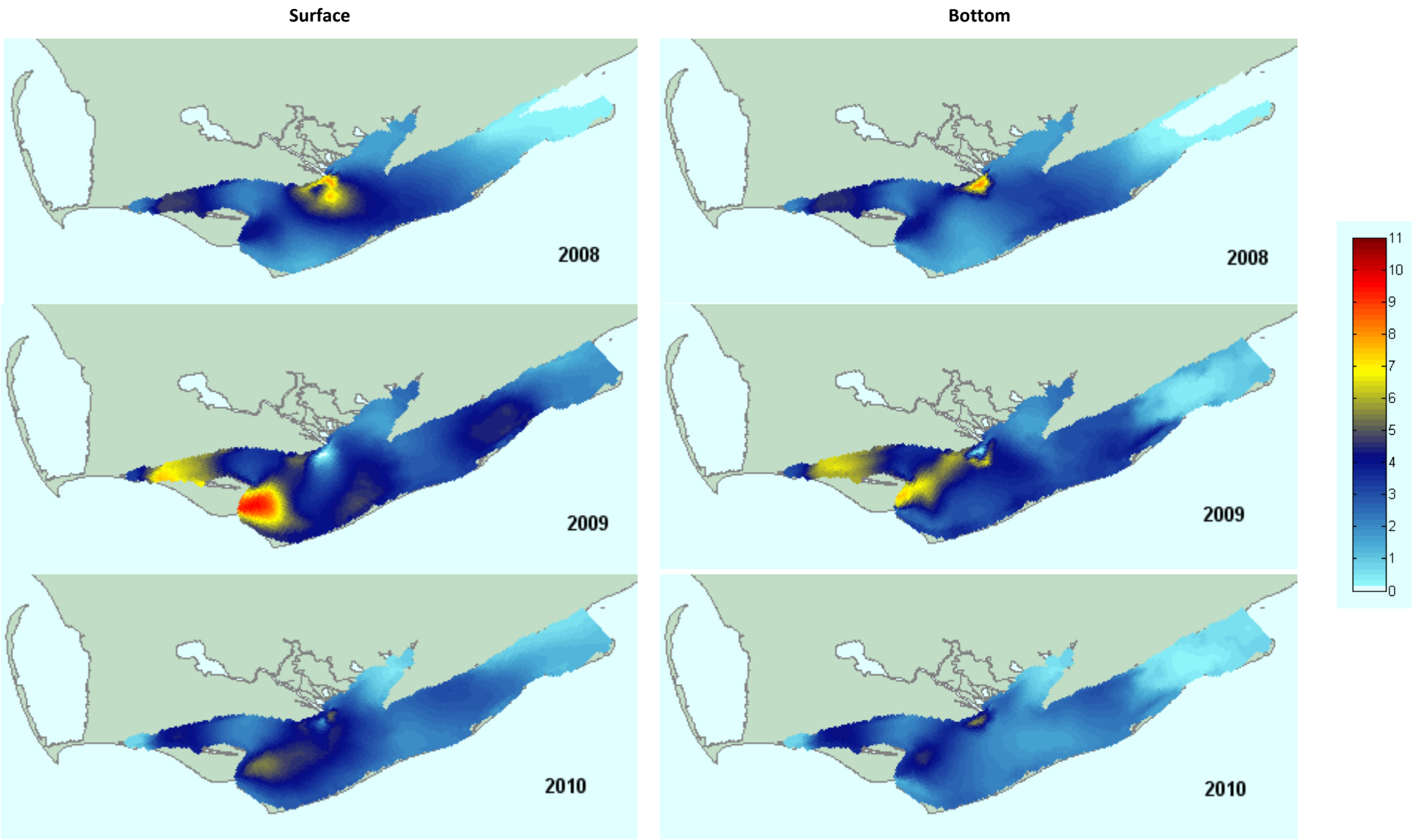

Figure 24 (contd). Salinity Monthly Standard Deviation - October

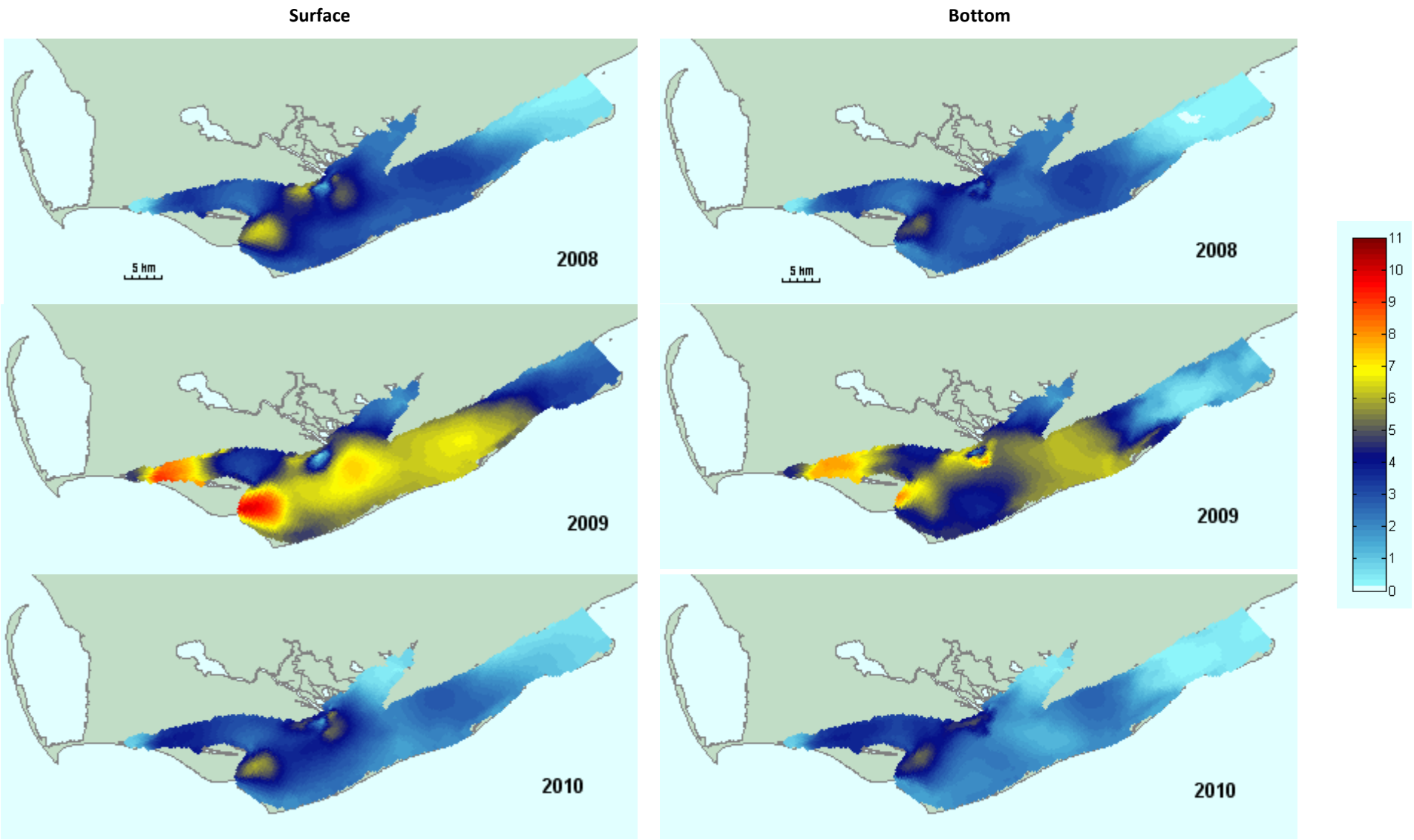

Figure 24 (contd). Salinity Monthly Standard Deviation - November

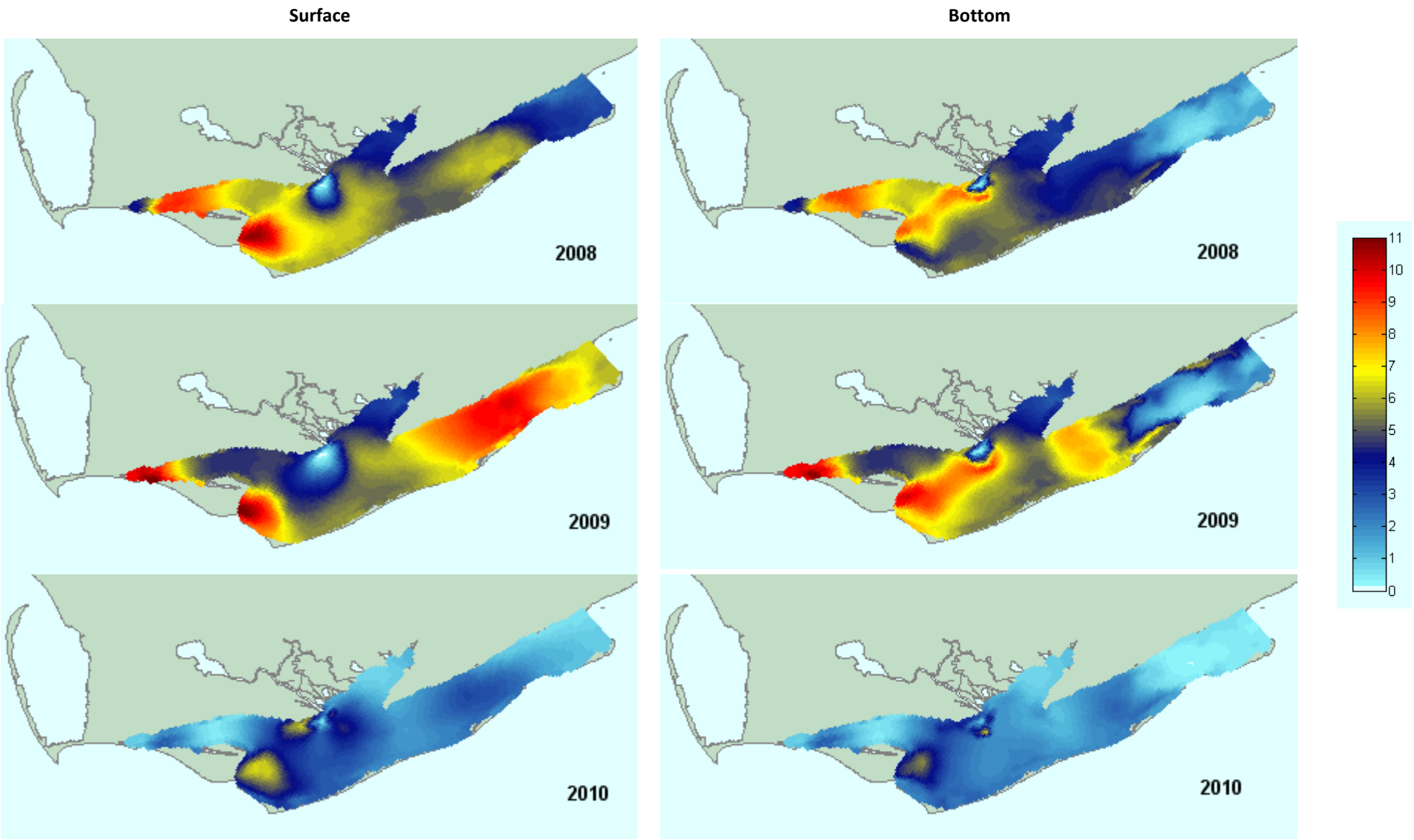

Figure 24 (contd). Salinity Monthly Standard Deviation - December

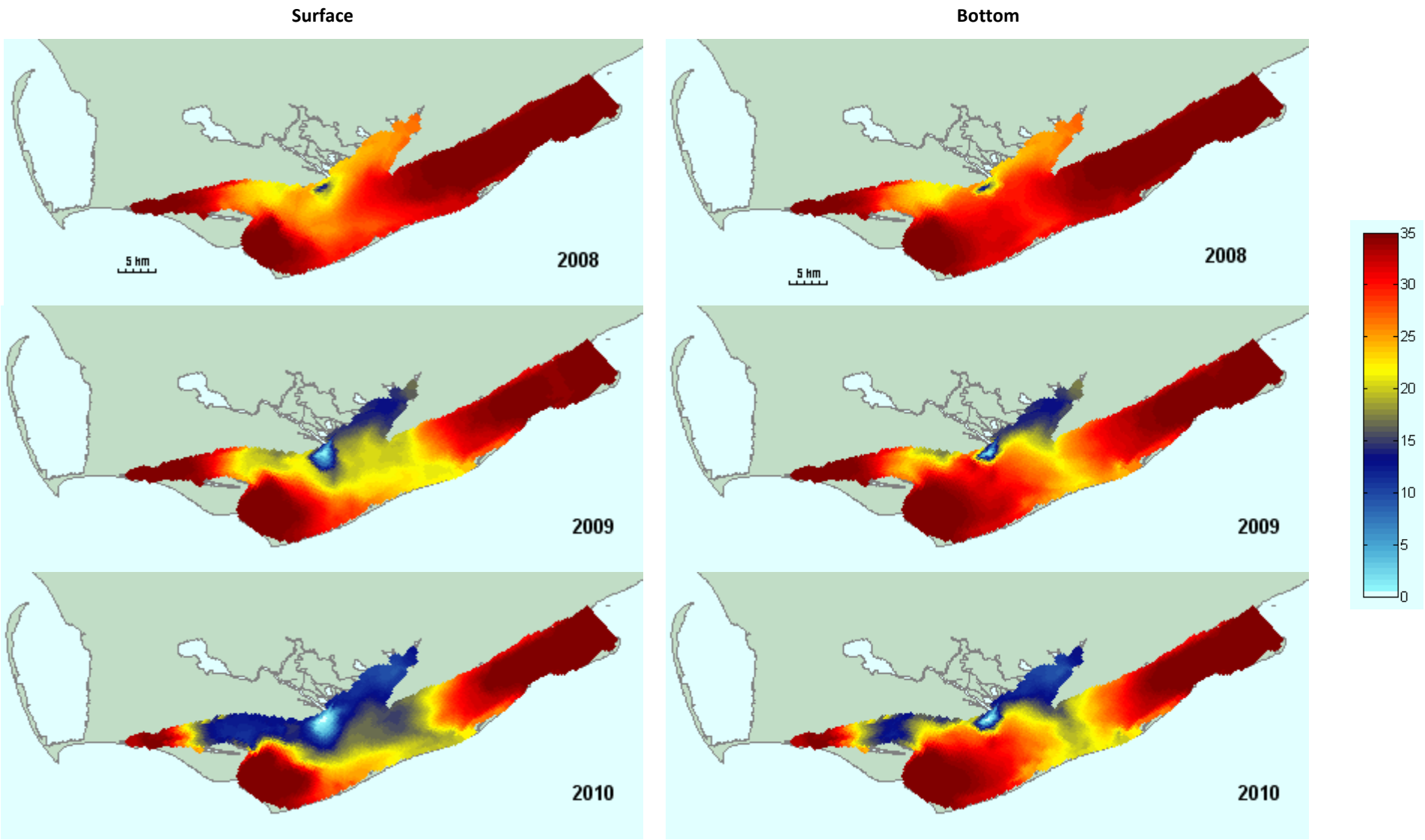

Figure 25. Salinity Monthly Maxima – January

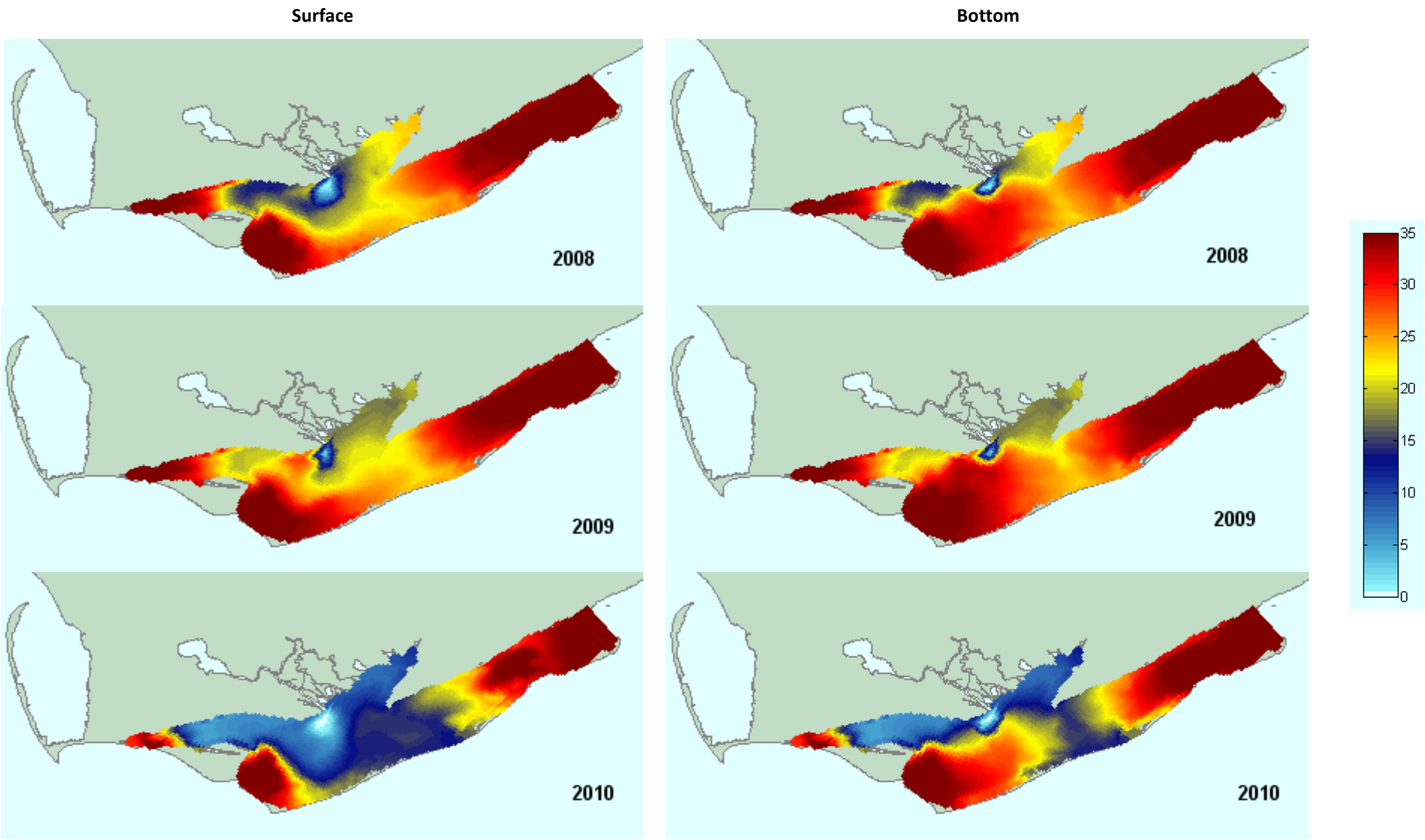

Figure 25 (contd). Salinity Monthly Maxima – February

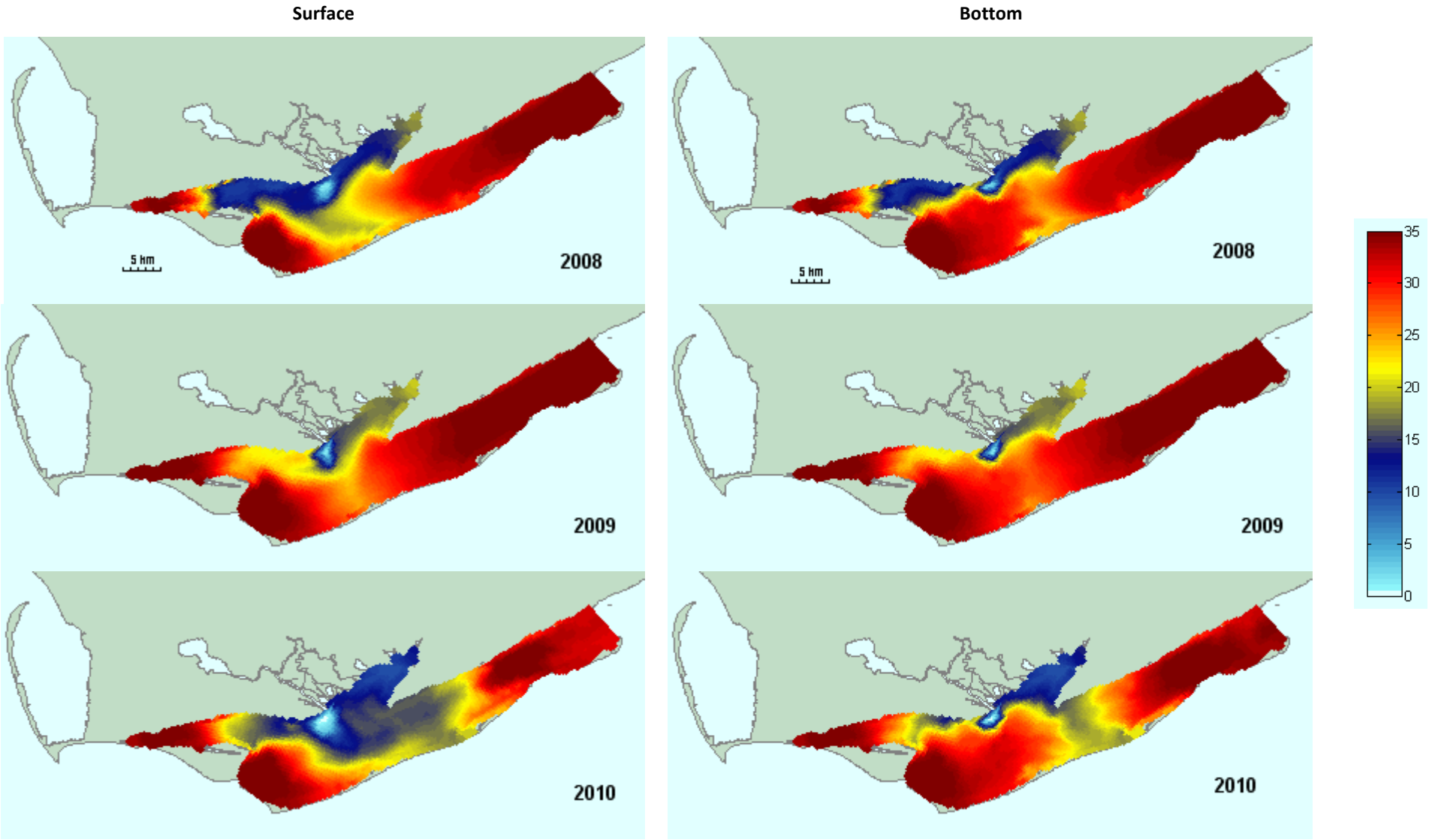

Figure 25 (contd). Salinity Monthly Maxima – March

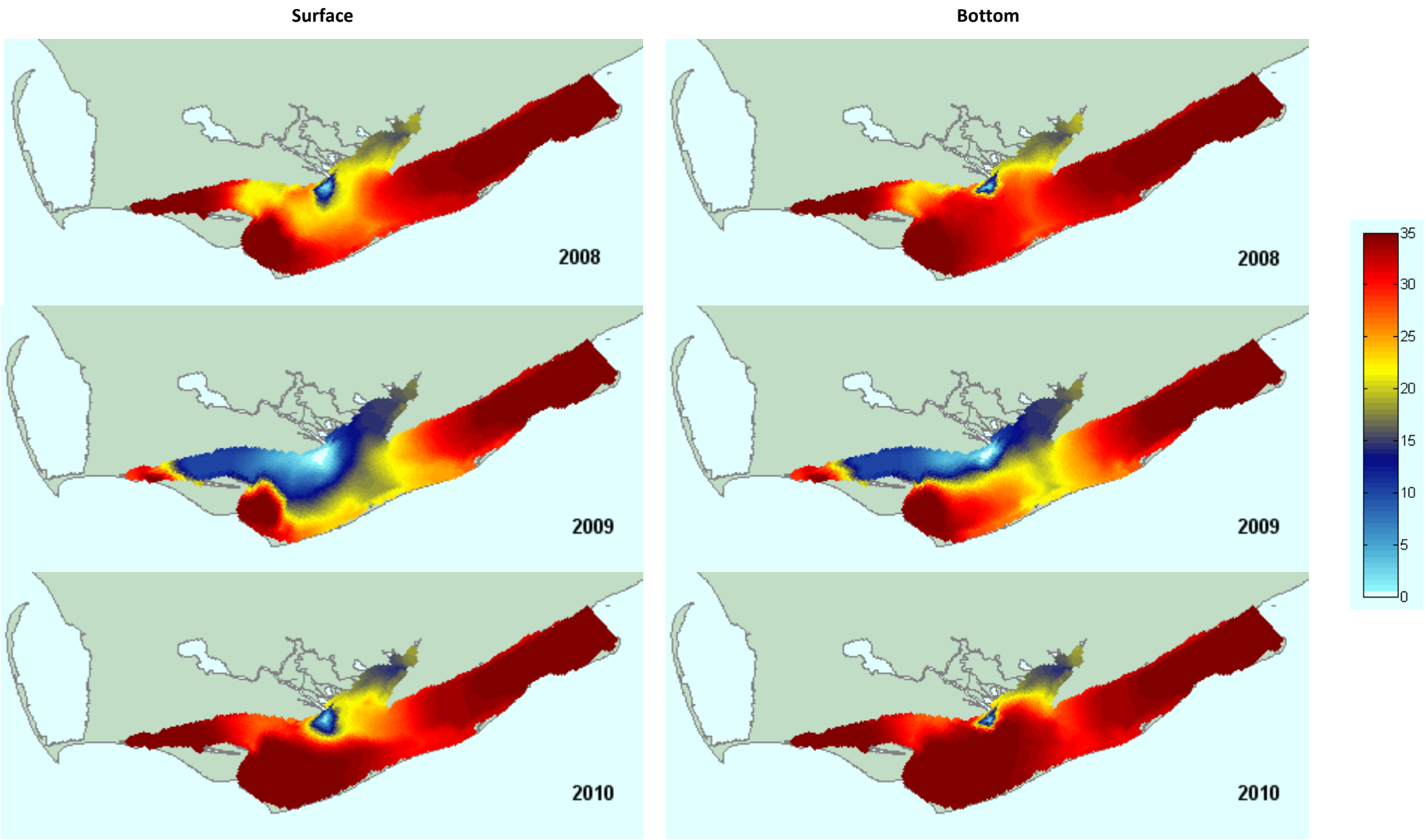

Figure 25 (contd). Salinity Monthly Maxima – April

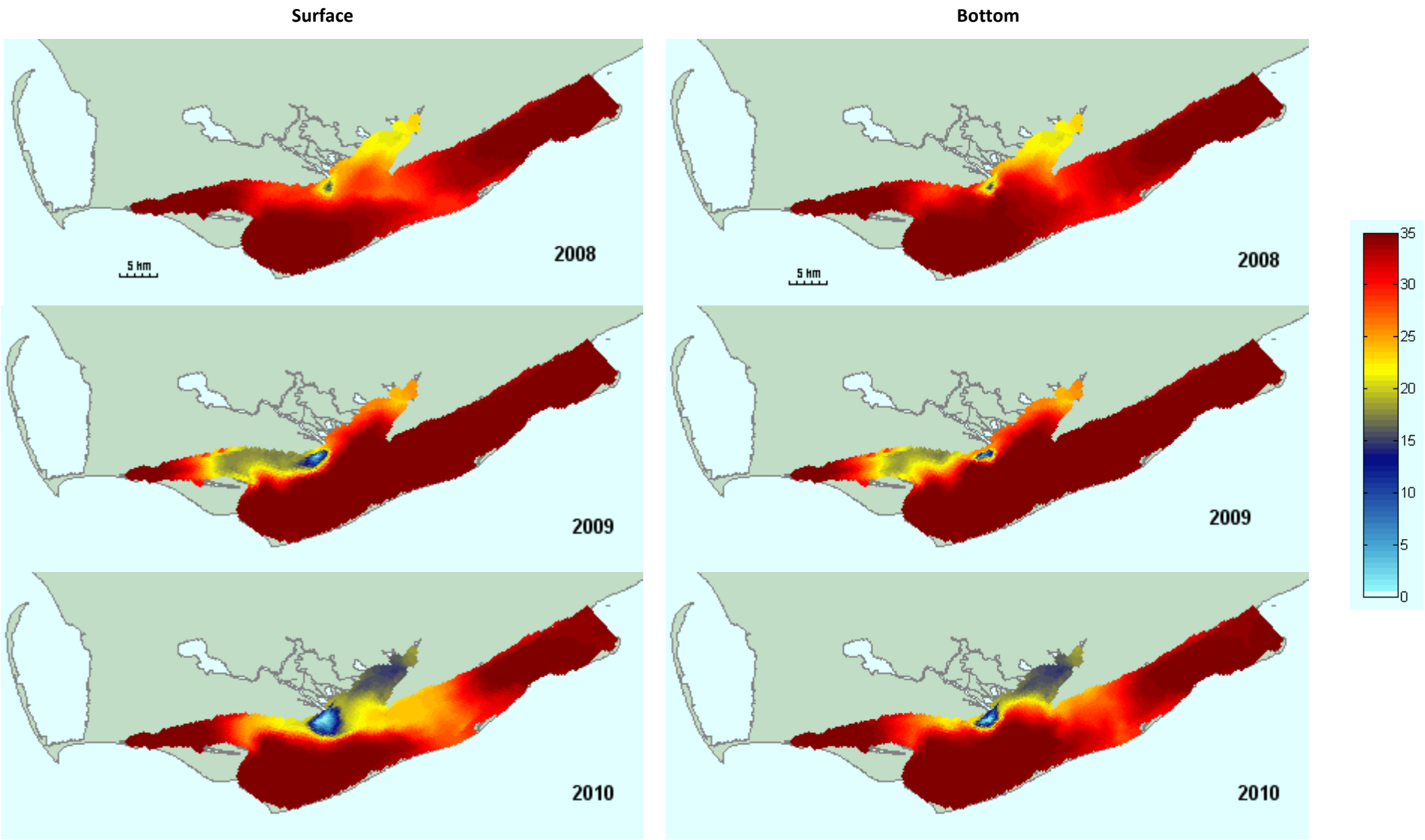

Figure 25 (contd). Salinity Monthly Maxima – May

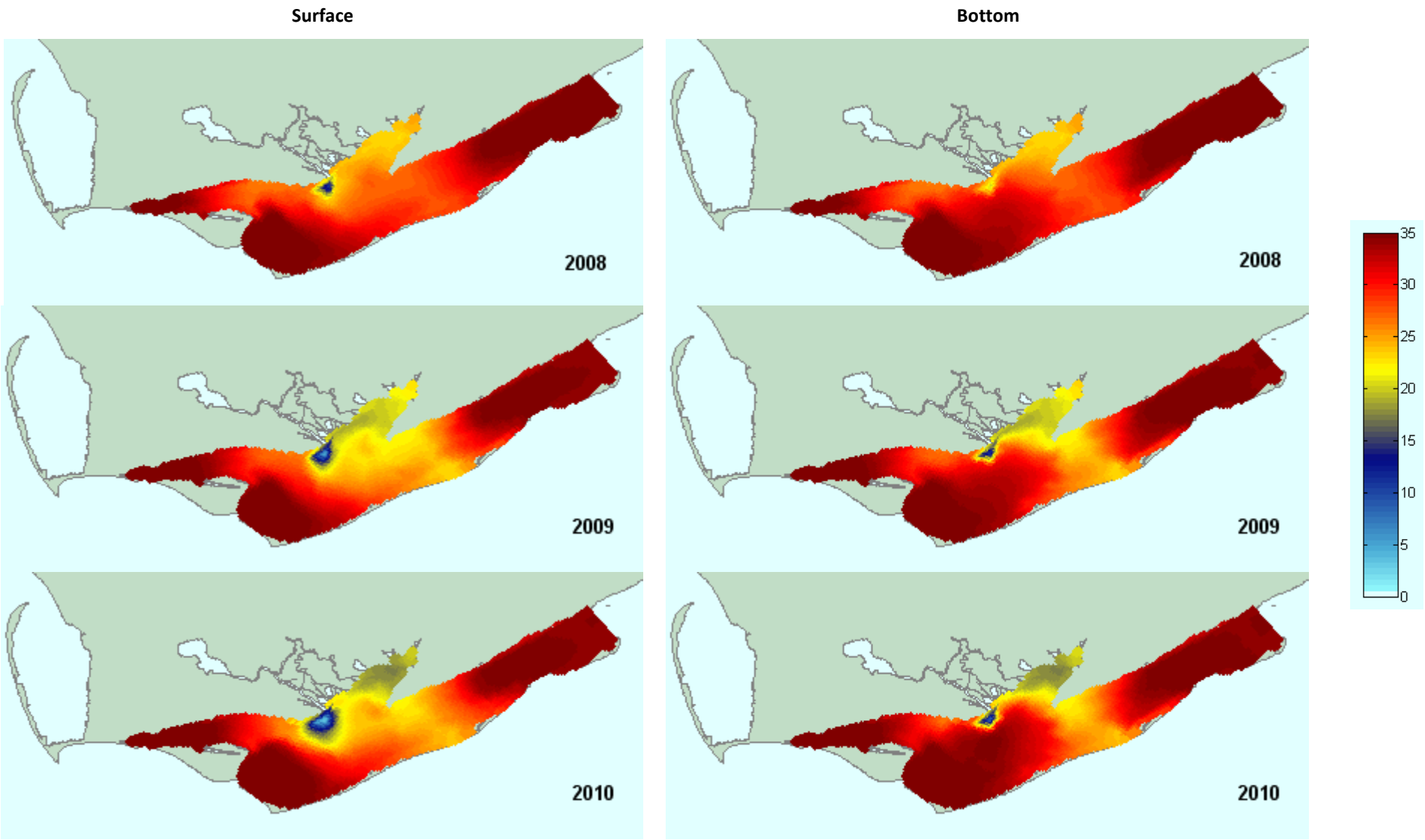

Figure 25 (contd). Salinity Monthly Maxima – June

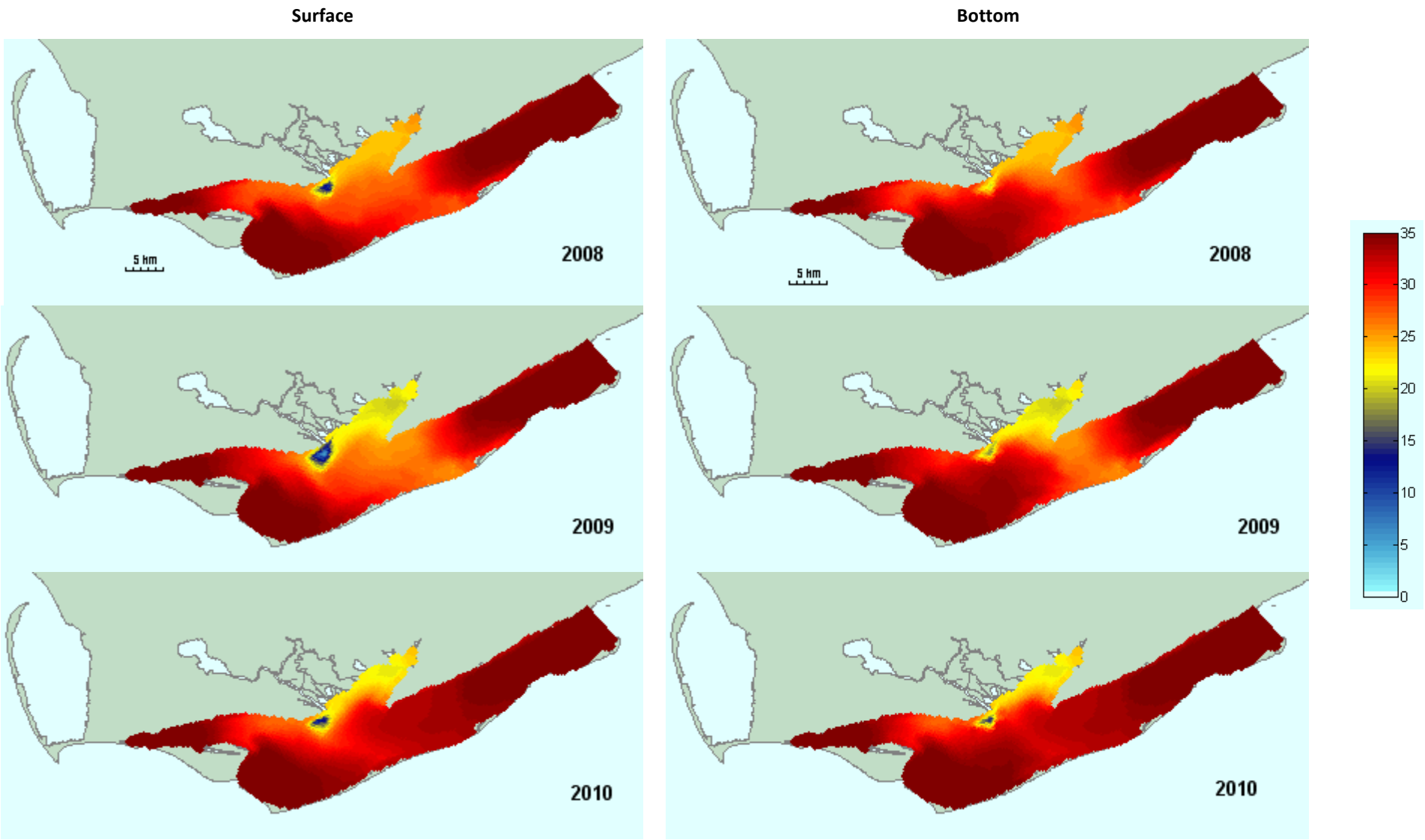

Figure 25 (contd). Salinity Monthly Maxima – July

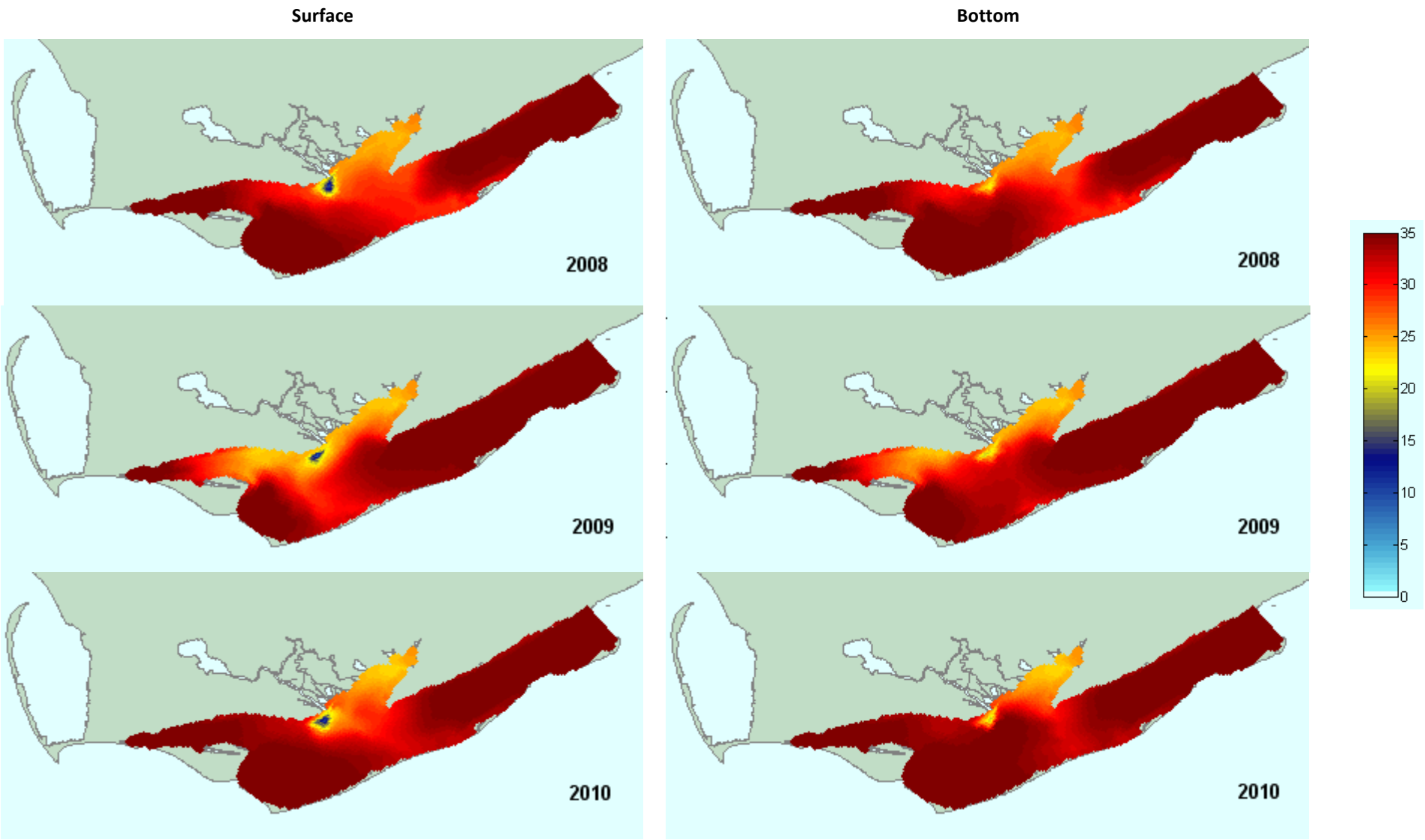

Figure 25 (contd). Salinity Monthly Maxima – August

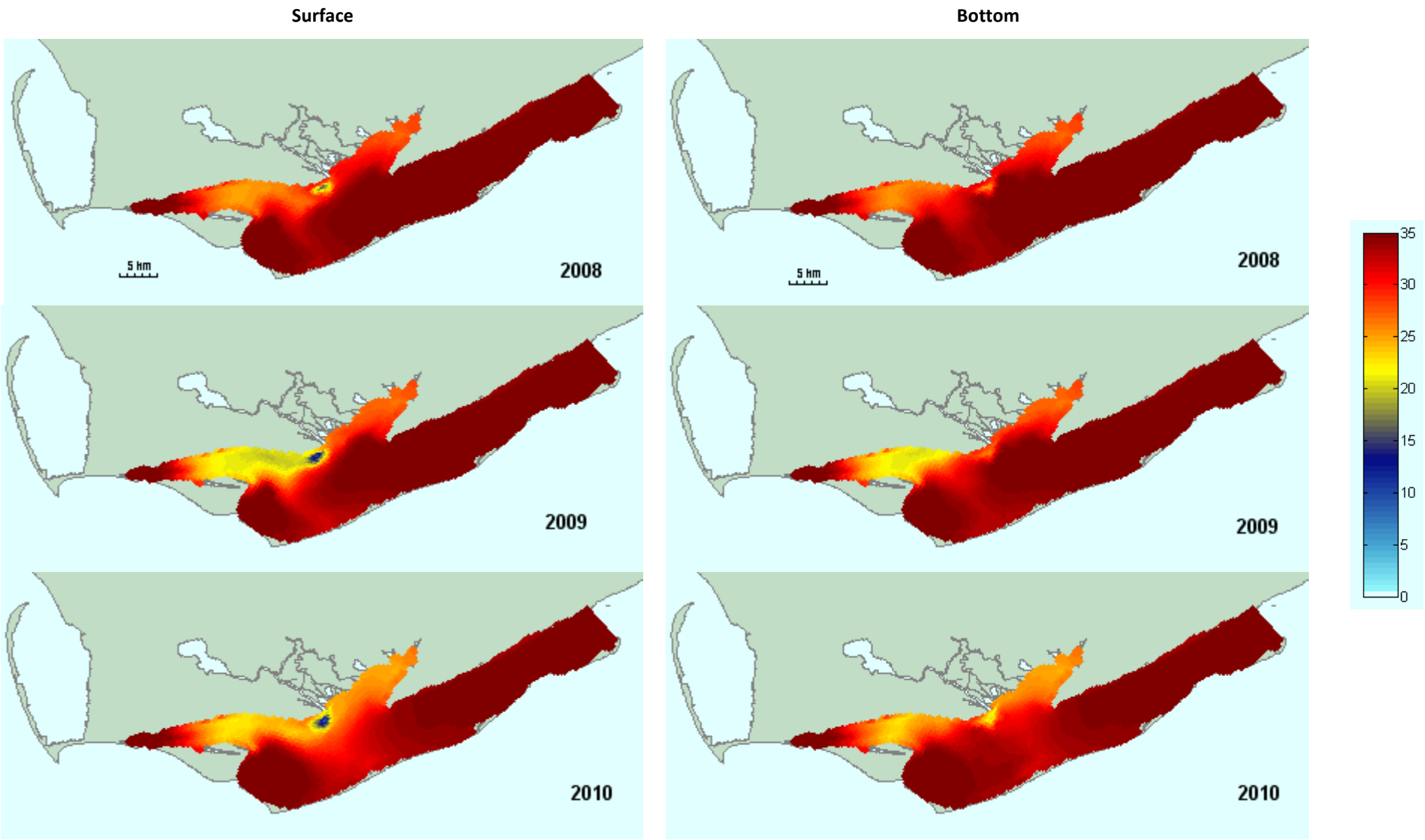

Figure 25 (contd). Salinity Monthly Maxima – September

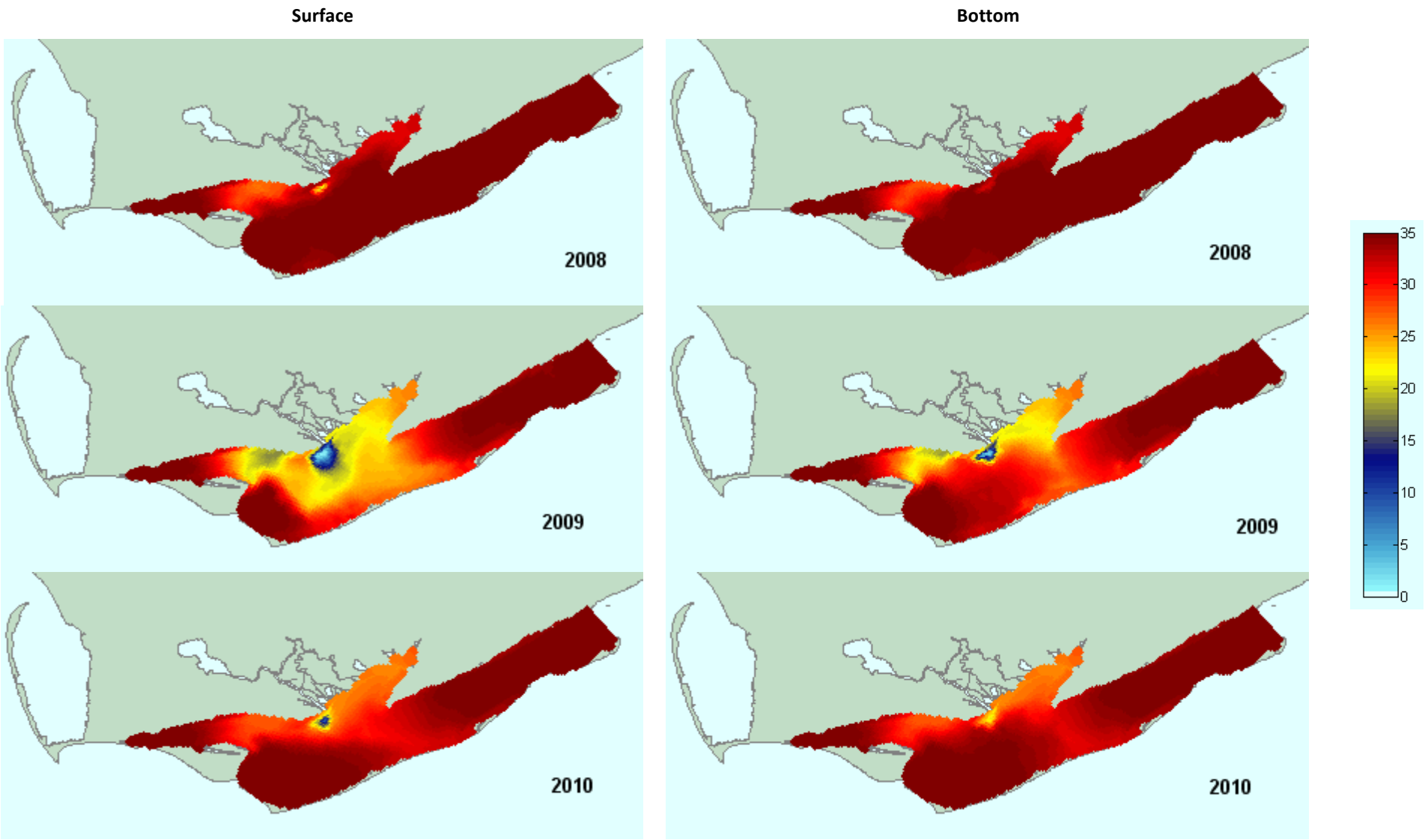

Figure 25 (contd). Salinity Monthly Maxima – October

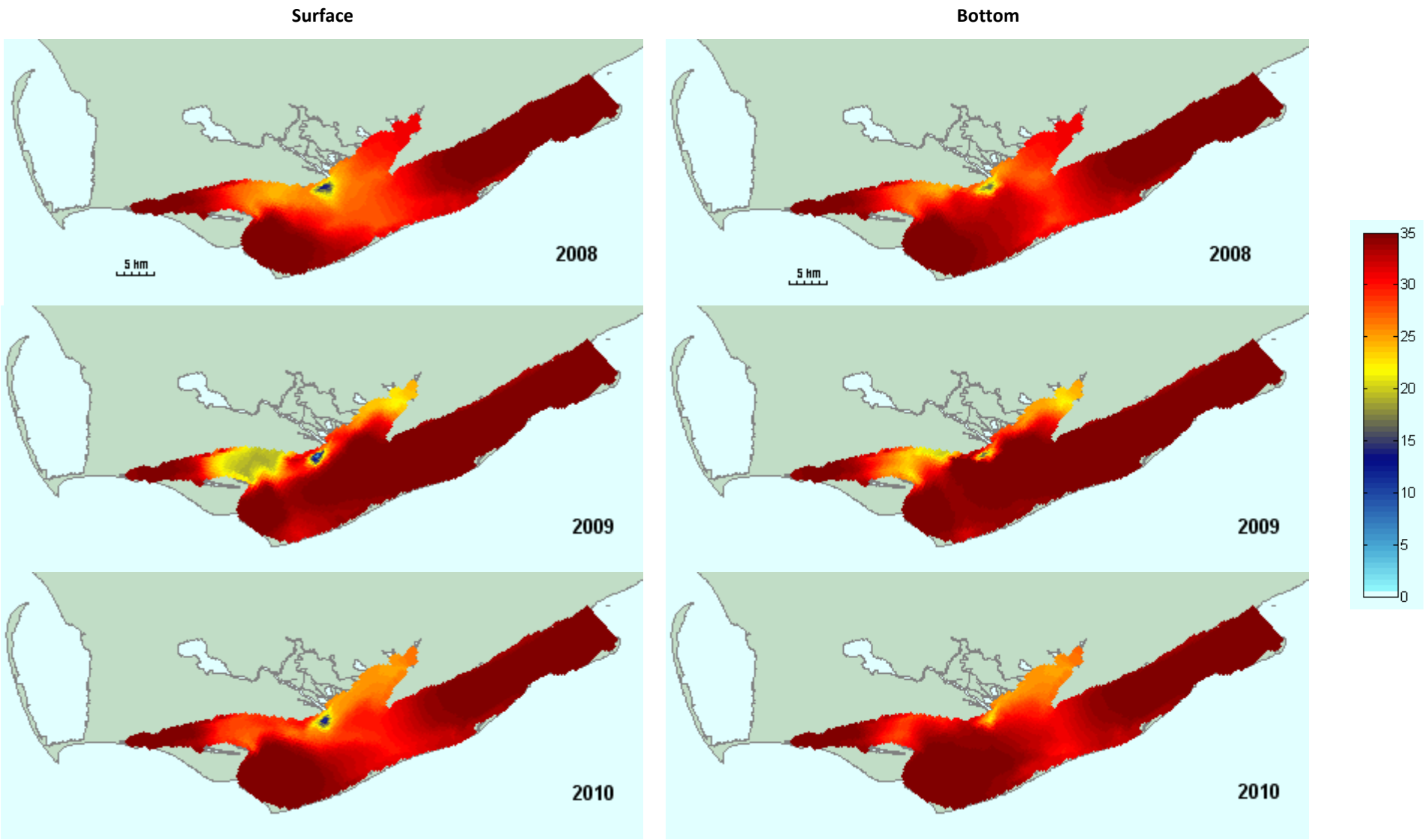

Figure 25 (contd). Salinity Monthly Maxima – November

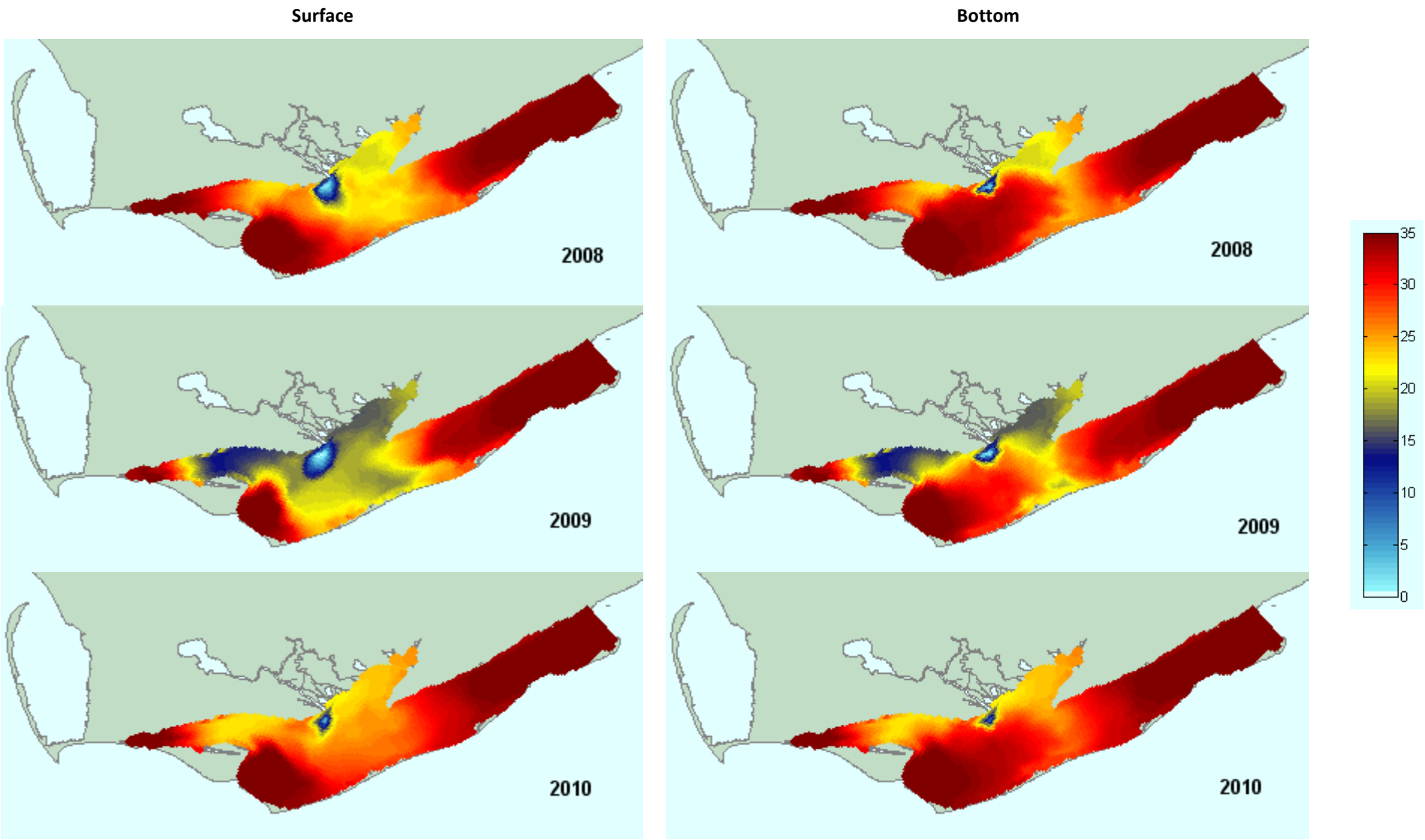

Figure 25 (contd). Salinity Monthly Maxima – December

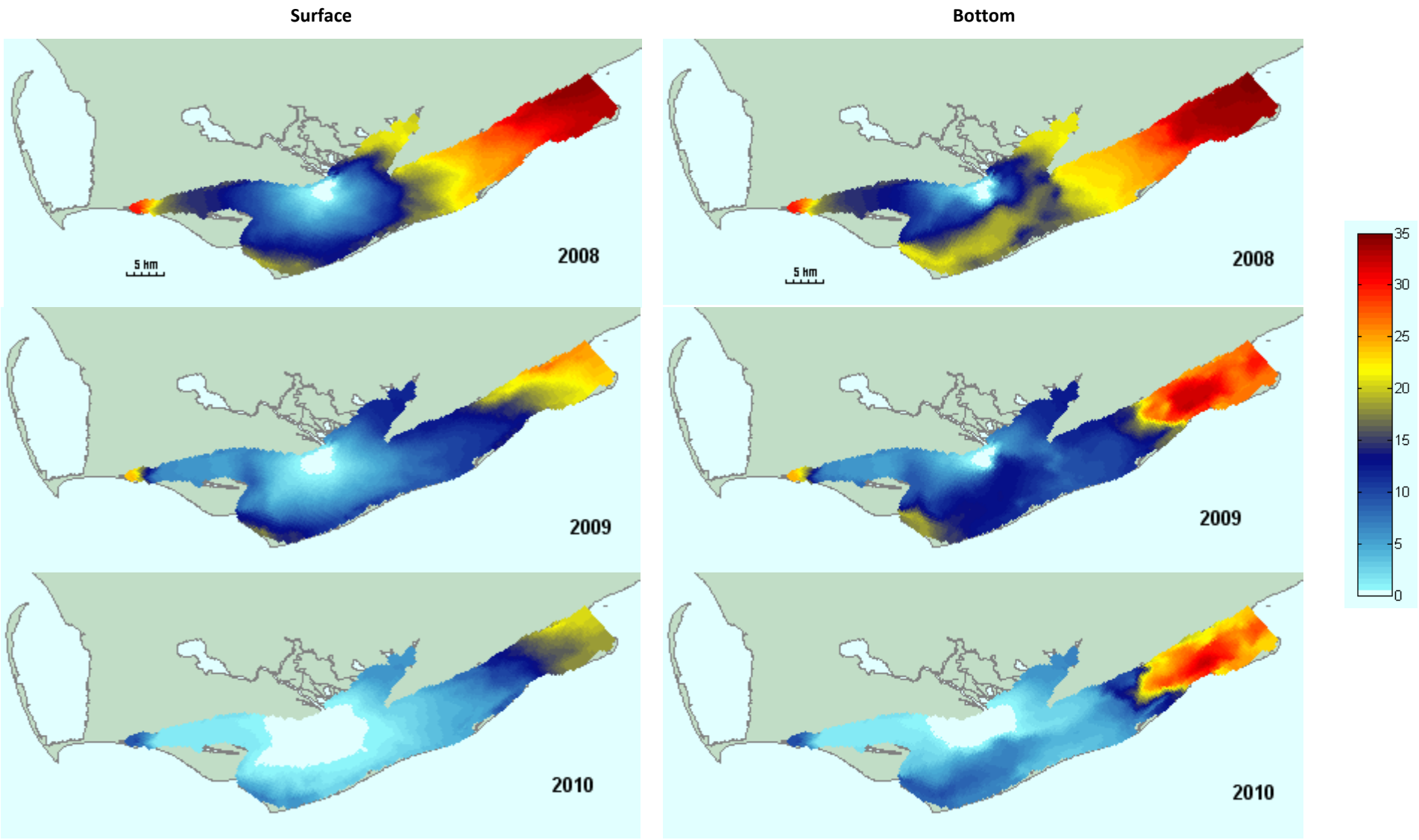

Figure 26. Salinity Monthly Minima – January

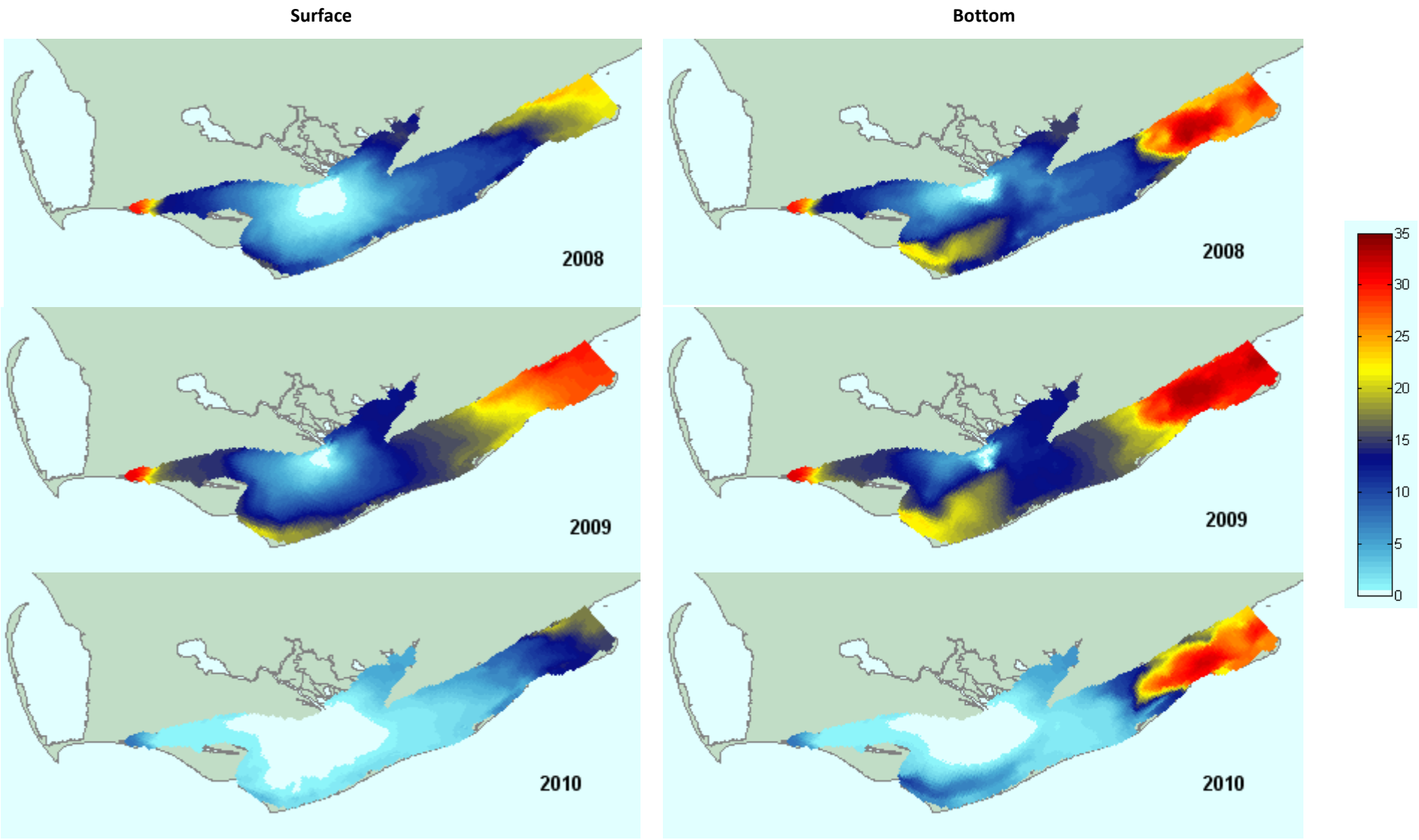

Figure 26 (contd). Salinity Monthly Minima – February

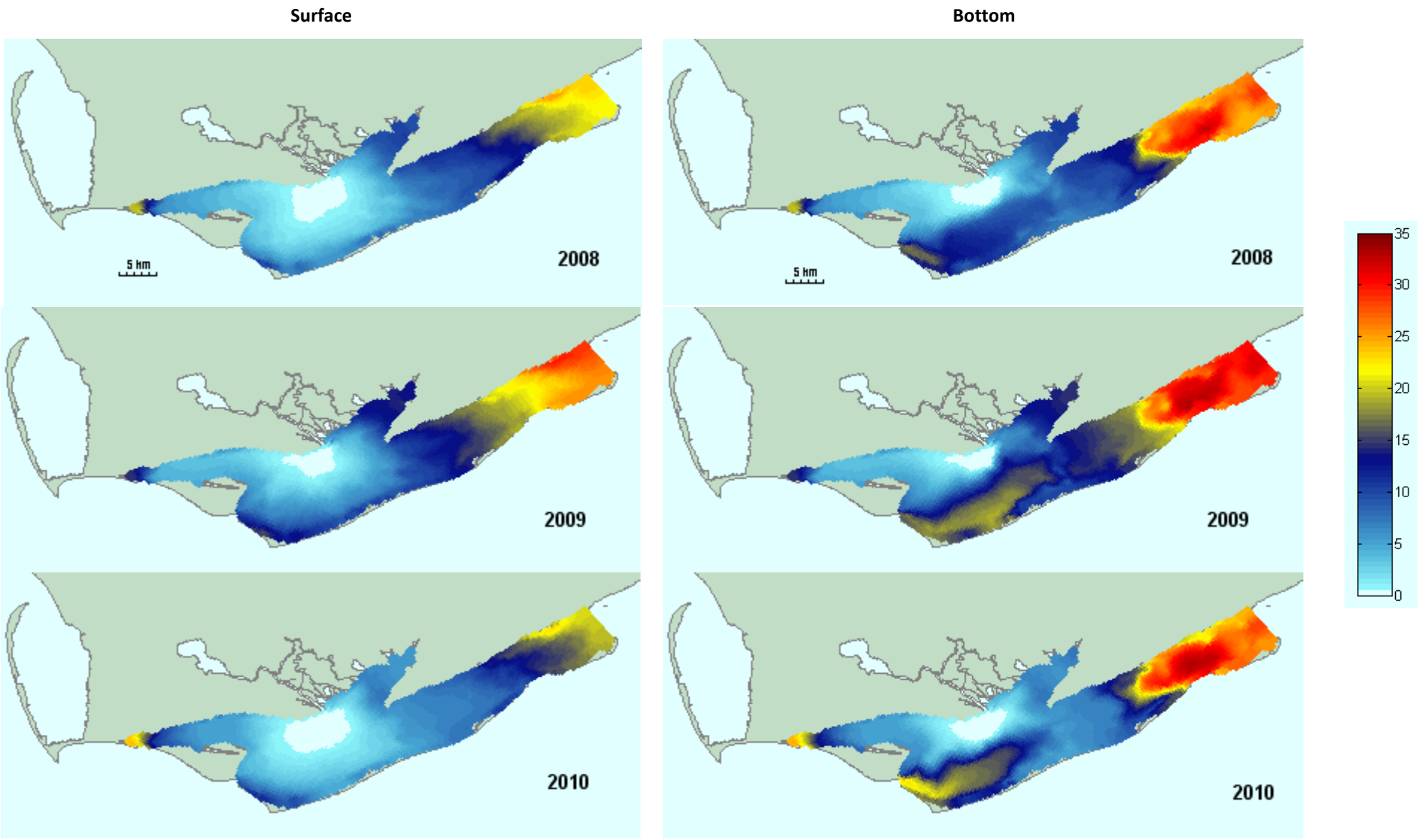

Figure 26 (contd). Salinity Monthly Minima – March

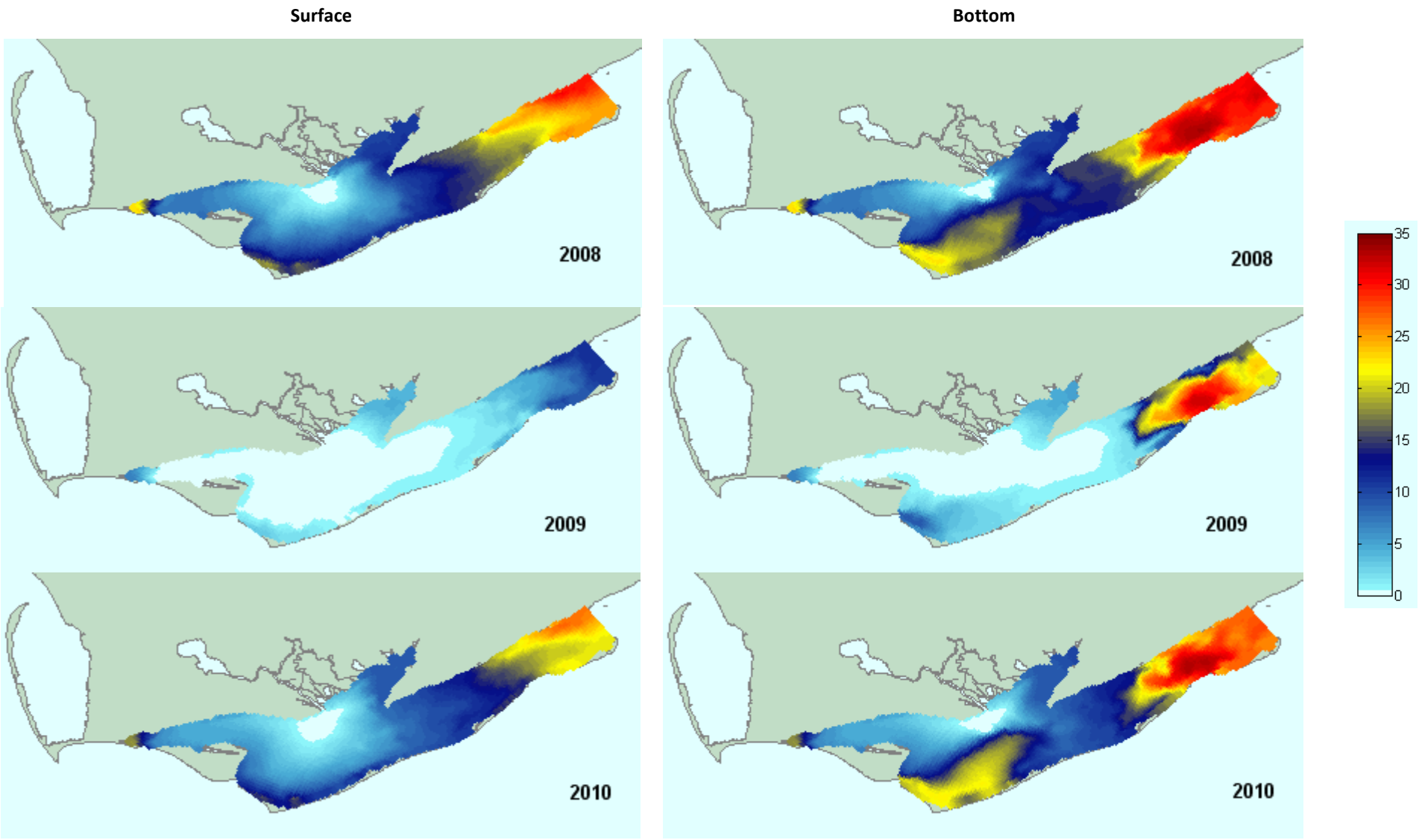

Figure 26 (contd). Salinity Monthly Minima – April

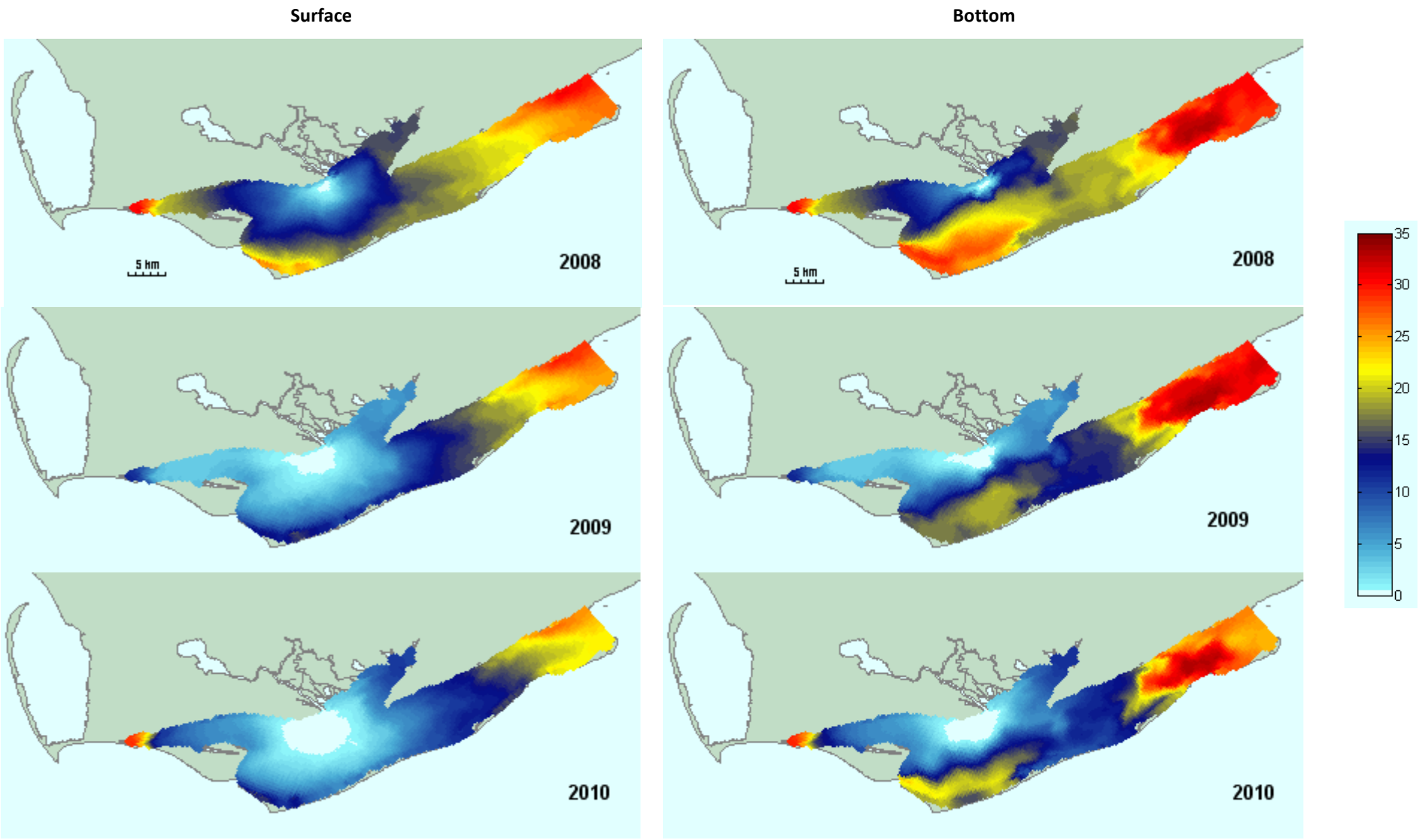

Figure 26 (contd). Salinity Monthly Minima – May

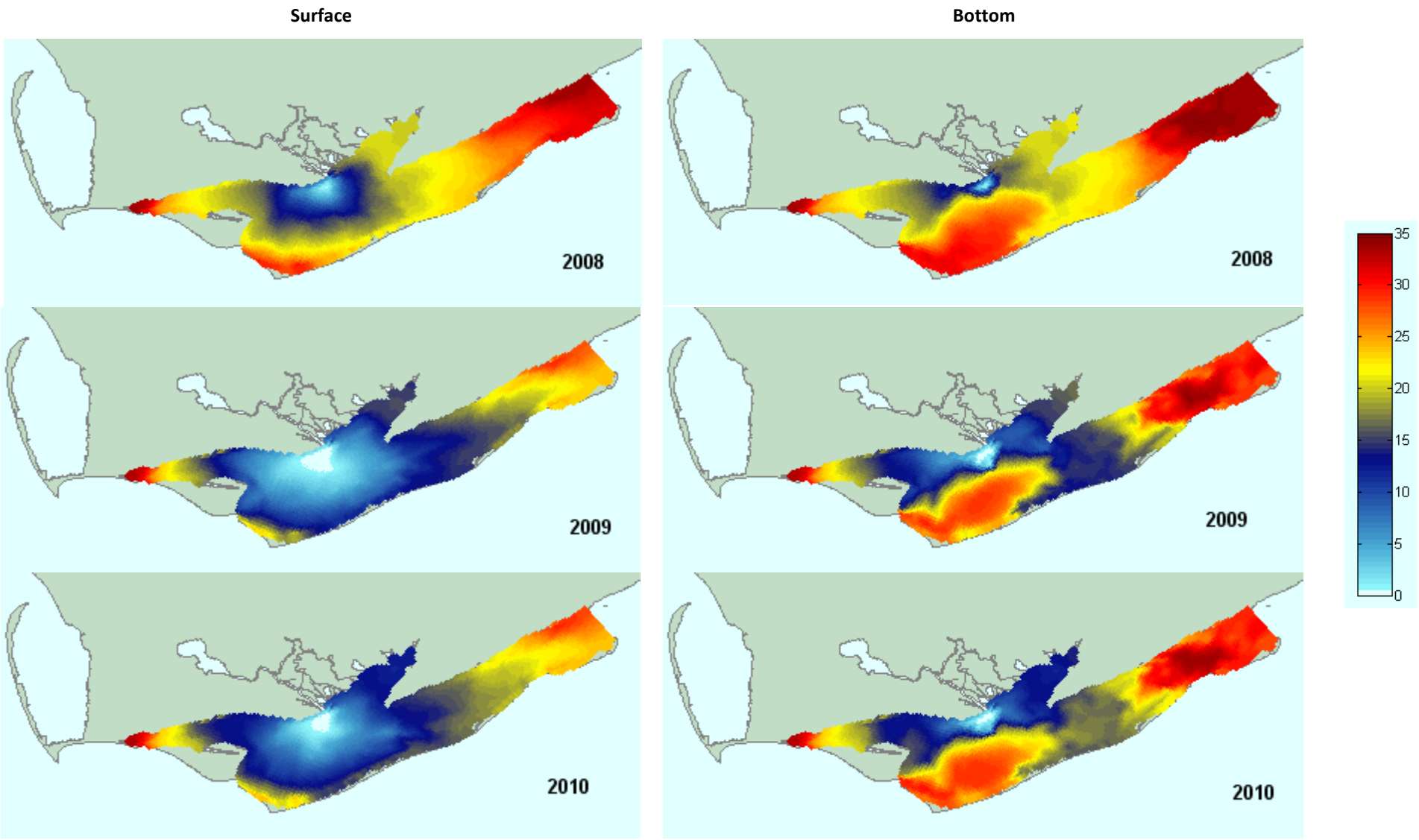

Figure 26 (contd). Salinity Monthly Minima – June

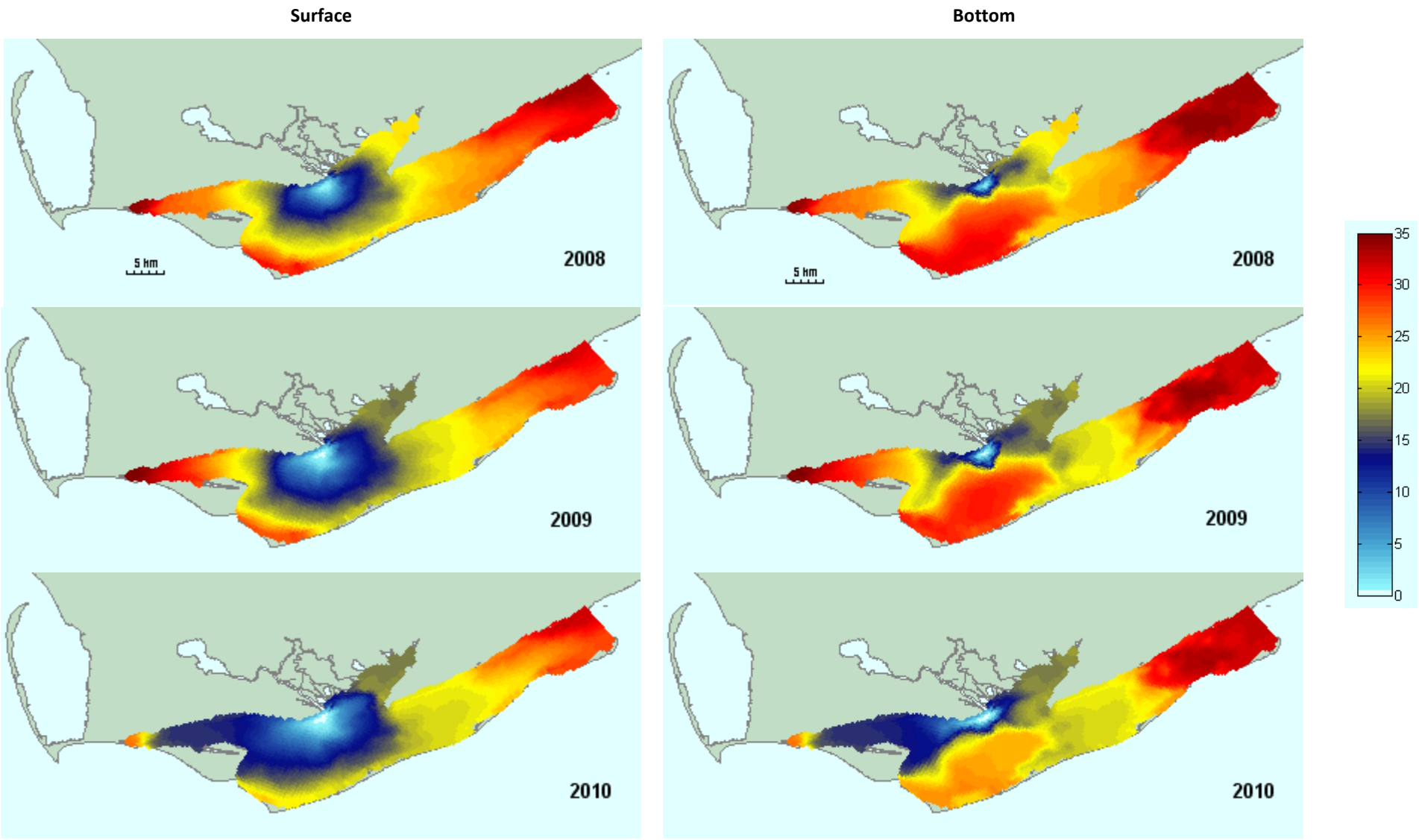

Figure 26 (contd). Salinity Monthly Minima – July

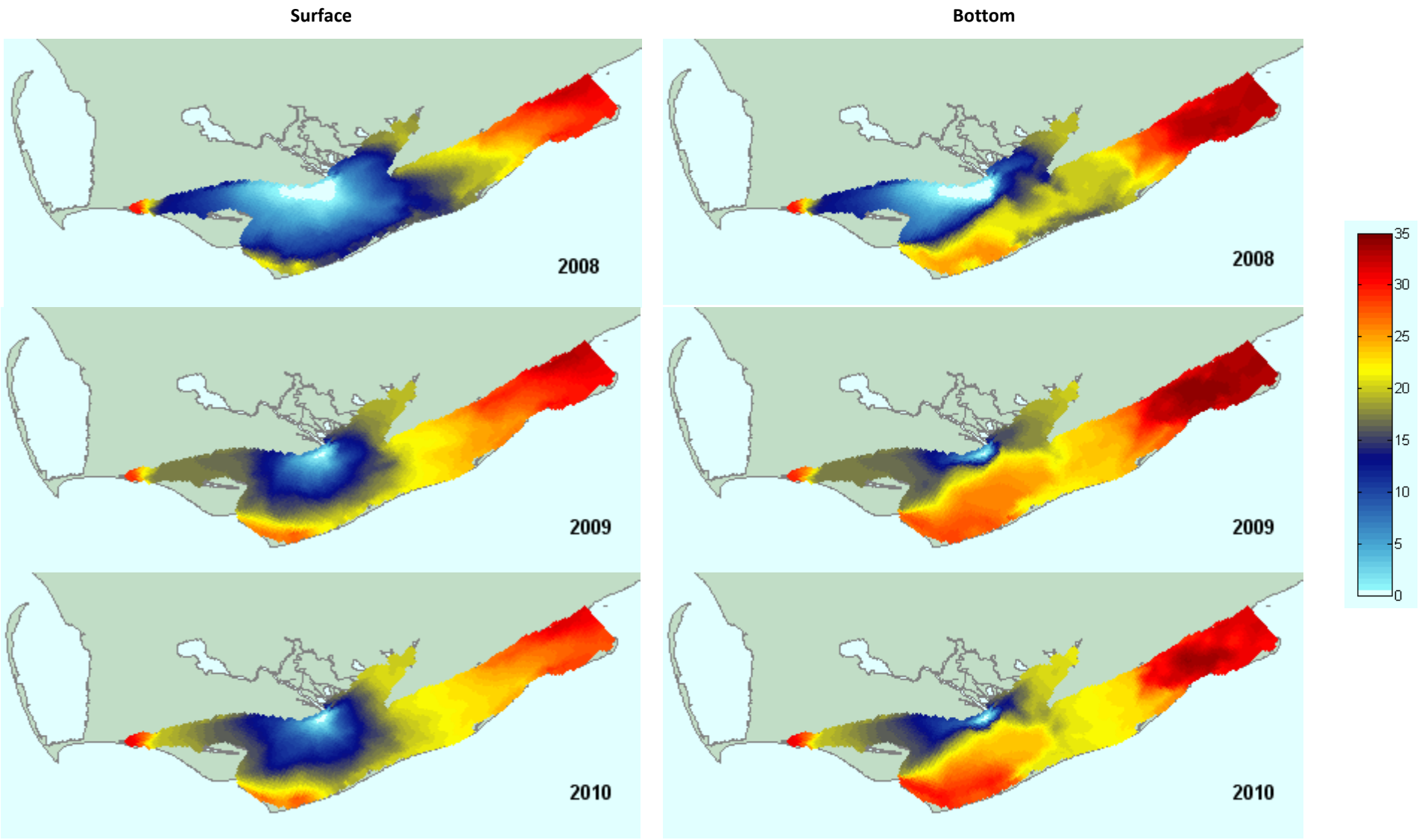

Figure 26 (contd). Salinity Monthly Minima – August

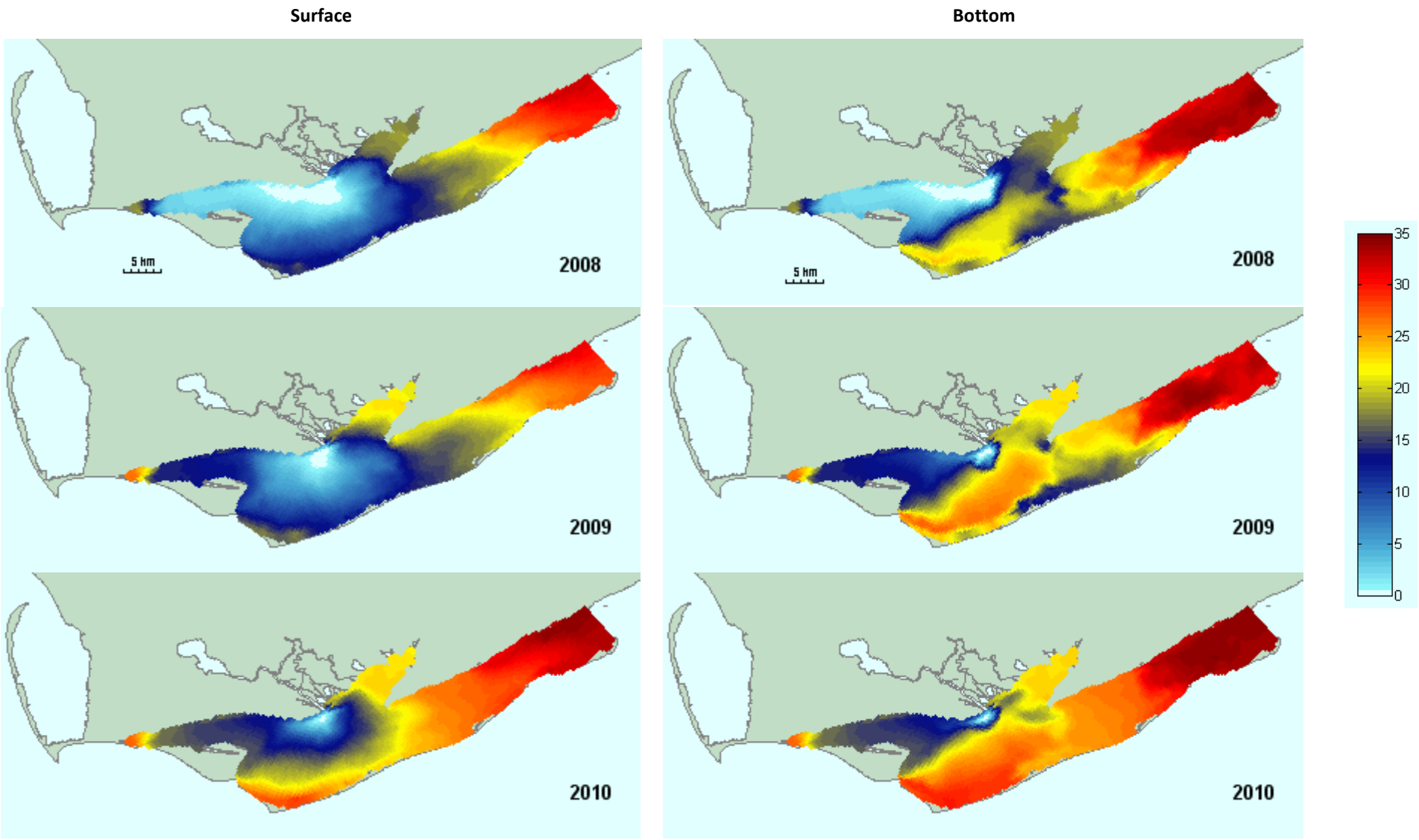

Figure 26 (contd). Salinity Monthly Minima – September

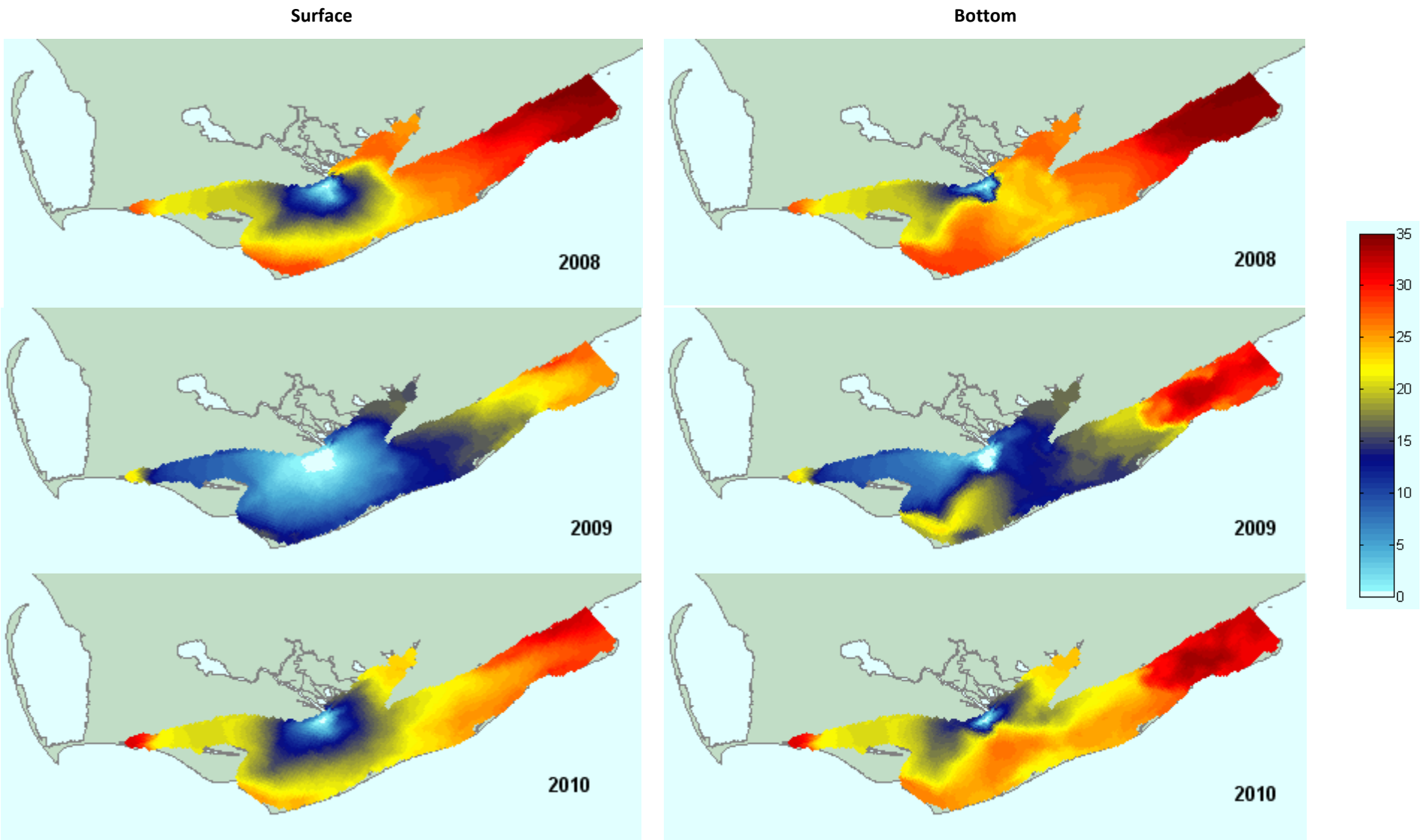

Figure 26 (contd). Salinity Monthly Minima – October

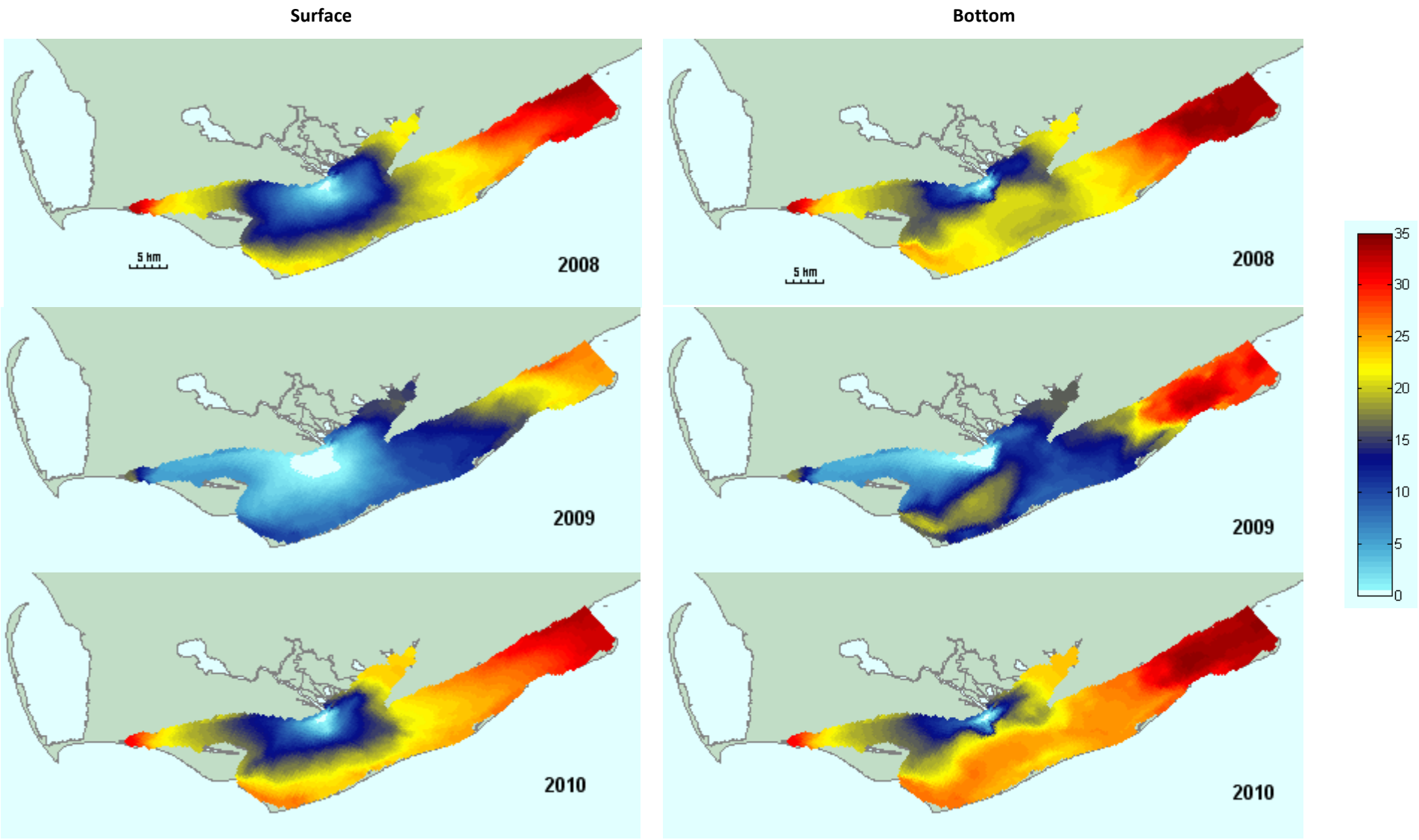

Figure 26 (contd). Salinity Monthly Minima – November

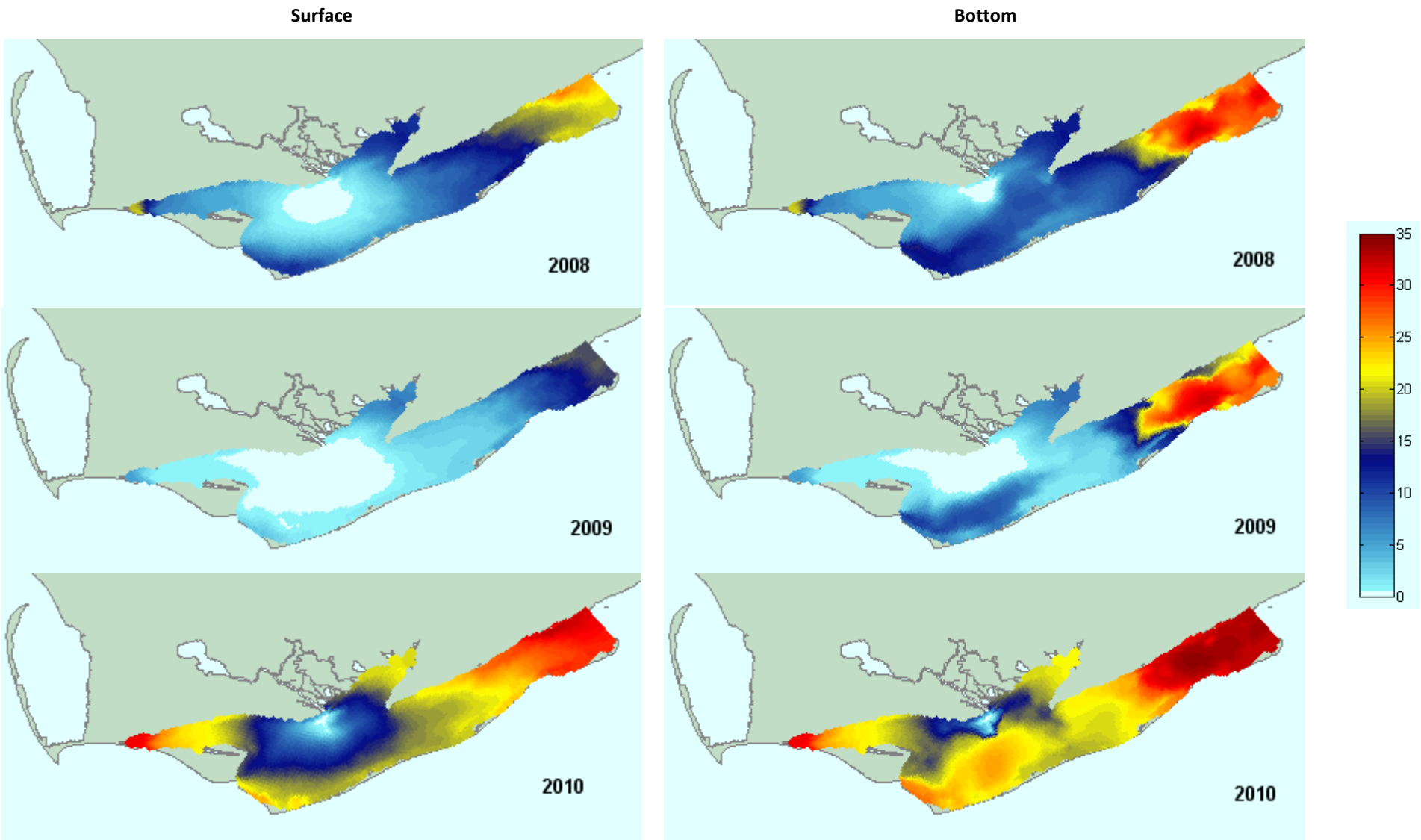

Figure 26 (contd). Salinity Monthly Minima – December

Information Transfer Program Introduction

None.

USGS Summer Intern Program

None.

Student Support					
Category	**Section 104 Base Grant**	**Section 104 NCGP Award**	**NIWR-USGS Internship**	**Supplemental Awards**	**Total**
Undergraduate	0	0	0	0	0
Masters	0	0	0	0	0
Ph.D.	3	2	0	0	5
Post-Doc.	0	0	0	0	0
Total	3	2	0	0	5

Notable Awards and Achievements

Notable awards or achievements achieved under this project #2011GA275B. Paper “Forgetting the Flood? Changes in Flood risk Perceptions over Time” selected to represent UGA Department of Agricultural and Applied Economics for E. Broadus Browne Research Awards for Outstanding Graduate Research, College of Agriculture and Environmental Sciences, University of Georgia, March 27, 2012.

PhD student Ajita Atreya recipient of the Best 2012 PhD Student Award by the Department of Agricultural and Applied Economics, University of Georgia

Selected to represent UGA Department of Agricultural and Applied Economics for E. Broadus Browne Research Awards for Outstanding Graduate Research, College of Agriculture and Environmental Sciences, University of Georgia, March 27, 2012.

Notable awards or achievements achieved under this project #2011GA287B.

Kellock, K. and R.B. Bringolf. Assessment of endocrine disruption in fish and estrogenic potency of waters in Georgia. Presented at the 2011 Georgia Water Resources Conference, Athens, GA, April 11–13, 2011. Awarded Best Student Presentation.

Publications from Prior Years